

AD/A-001 665

T-BURNER TESTING OF METALLIZED SOLID  
PROPELLANTS

F. E. C. Culick

California Institute of Technology

Prepared for:

Air Force Rocket Propulsion Laboratory

October 1974

DISTRIBUTED BY:

**NTIS**

National Technical Information Service  
U. S. DEPARTMENT OF COMMERCE

When U. S. Government drawings, specifications, or other data are used for any purpose other than a definitely related Government procurement operation, the Government thereby incurs no responsibility nor any obligation whatsoever, and the fact that the Government may have formulated, furnished, or in any way supplied the said drawings, specifications, or other data, is not to be regarded by implication or otherwise, or in any manner licensing the holder or any other person or corporation, or conveying rights or permission to manufacture, use, or sell any patented invention that may in any way be related thereto.

ACCESSION for	
NTIS	White Stamps
DDC	Bot. Stamps
UNANNOUNCED	
JUSTIFICATION	
BY	
DISTRIBUTION AVAILABILITY CODE	
Doc.	Avail. 2 - 4 21 1961

A

This technical report has been reviewed by:

Wilbur C. Andrepont  
Chief, Combustion Group

and approved by:

*Paul J. Daily*

Paul J. Daily, Colonel, USAF  
Chief, Technology Division

UNCLASSIFIED

SECURITY CLASSIFICATION OF THIS PAGE (When Data Entered)

REPORT DOCUMENTATION PAGE		READ INSTRUCTIONS BEFORE COMPLETING FORM
1. REPORT NUMBER AFRPL-TR-74-28	2. GOVT ACCESSION NO.	3. RECIPIENT'S CATALOG NUMBER <b>AD/A-001665</b>
4. TITLE (and Subtitle) T-Burner Testing of Metallized Solid Propellants		5. TYPE OF REPORT & PERIOD COVERED Final; 1 oct. 1973-31 aug. '74
		6. PERFORMING ORG. REPORT NUMBER
7. AUTHOR(s) F. E. C. Culick (editor)		8. CONTRACT OR GRANT NUMBER(s) F04611-74-C-0005
9. PERFORMING ORGANIZATION NAME AND ADDRESS California Institute of Technology Pasadena, California 91125		10. PROGRAM ELEMENT, PROJECT, TASK AREA & WORK UNIT NUMBERS
11. CONTROLLING OFFICE NAME AND ADDRESS Air Force Rocket Propulsion Laboratory (DYSC) Edwards, California 93523		12. REPORT DATE October 1974
14. MONITORING AGENCY NAME & ADDRESS; if different from Controlling Office same		13. NUMBER OF PAGES 274
		15. SECURITY CLASS. (of this report) unclassified
		15a. DECLASSIFICATION/DOWNGRADING SCHEDULE n. a.
16. DISTRIBUTION STATEMENT (of this Report) "Approved for Public Release -- Distribution Unlimited"		
17. DISTRIBUTION STATEMENT (of the abstract entered in Block 20, if different from Report)		
18. SUPPLEMENTARY NOTES  Reproduced by NATIONAL TECHNICAL INFORMATION SERVICE U S Department of Commerce Springfield VA 22151		
19. KEY WORDS (Continue on reverse side if necessary and identify by block number)  combustion instability; T-burners; combustion of solid propellants		
20. ABSTRACT (Continue on reverse side if necessary and identify by block number)  The purpose of this report is primarily to summarize recent work on the use of T-burners for testing of metallized solid propellants. Portions of the report were received from contributors associated with eight organizations: Aerojet Solid Propulsion Co., Sacramento, California; Air Force Rocket Propulsion Laboratory, Edwards, California; Brigham Young University, Provo, Utah; California Institute of Technology, Pasadena, California; Hercules, Inc., Magna, Utah; Lockheed Propulsion Co., Redlands, California; Naval Weapons Center, China Lake, California; Thiokol Chemical Chemical Co., Wasatch Div.		

FORM 1 JAN 73 1473

EDITION OF 1 NOV 65 IS OBSOLETE

UNCLASSIFIED

SECURITY CLASSIFICATION OF THIS PAGE (When Data Entered)

**UNCLASSIFIED**

SECURITY CLASSIFICATION OF THIS PAGE(When Data Entered)

**Block 20: Abstract**

**Brigham City, Utah.**

Emphasis is placed on the construction and use of T-burners for test methods based on pulsing, varying the area of propellant surface, or a combination. Detailed discussions are given of current practice followed in performing tests, collecting data, and analyzing experimental results.

Summaries of analyses presently used are included, and the applications to interpreting data taken with T-burners are discussed. Some results of a statistical analysis of tests made in several laboratories, using the same propellant, are included.

The ways in which T-burners may be used in research and development programs are described. In particular, a brief description is given of the data which can be obtained and how they are applied to problems of motor stability.

**UNCLASSIFIED**

SECURITY CLASSIFICATION OF THIS PAGE(When Data Entered)

1a

## FOREWORD

In 1969, the Committee on Standardization of Combustion Instability Measurements in the T-Burner, an ad hoc committee organized by the ICRPG Working Group on Solid Propellant Combustion, produced the "T-Burner Manual" (C. P. I. A. Publication No. 191). That report was restricted to experience gained in testing propellants not containing a metal. During the last few years, considerable use has been made of the T-burner for testing metallized propellants. It is the first purpose of this report to summarize much of that work, and to recommend as far as possible standard procedures.

The present effort is considerably more ambitious than the earlier work. Representatives of seven organizations have participated in planning the report, writing, and proof-reading the several drafts. Prior to preparation of the final draft, a two-day workshop was held. The following people contributed written portions of the report:

M. W. Beckstead	Hercules, Inc.
R. L. Coates	Brigham Young University
J. E. Crump	Naval Weapons Center
F. E. C. Culick	California Institute of Technology
R. L. Derr	Naval Weapons Center
P. L. Micheli	Aerojet Solid Propulsion Co.
C. M. Muhlfeith	Thiokol Chemical Corp.
E. W. Price	Naval Weapons Center
R. Schoner	Air Force Rocket Propulsion Laboratory

Mr. W. C. Andrepont of the Air Force Rocket Propulsion Laboratory served as contract monitor for the work and contributed many useful comments throughout the duration of the work.

The T-burner remains the best available device for making laboratory measurements of the response of a burning solid propellant to sinusoidal oscillations in the near flow field. Besides its place in research, it has been used quite extensively for qualitative testing to screen propellants in development work and to check the behavior of different batches of the same propellant. The experience gained in those various

applications forms the basis of this report.

Study of the T-burner itself continues, however; many questions relating to some aspects of observed behavior, and to detailed interpretation of data, have not been satisfactorily answered. Some of the conclusions reached in this report may therefore be found wanting at a later date. Care has been taken to note all questionable items. Procedures are labelled as recommendations only if they rest on generally recognized firm grounds.

It has not been possible to include all the detailed information necessary to construct and operate a T-burner. Reference is frequently made to work discussed in recent reports which are easily obtained. In addition to the first "T-Burner Manual," those reports, cited at the end of the Introduction, constitute a minimal reference list.

The report is intended to be more than a manual, or guide to operating experimental apparatus. Summaries of current analytical techniques are included in the Appendices, and appealed to in the text. These are useful both for interpreting experimental data and for showing how results obtained with a T-burner can be used in studying the stability of motors. Section 6 of the text describes this subject briefly.

I am indebted to all those listed above for their contributions, their help, and their cooperation. I wish especially to thank Dr. R. L. Derr, who aided greatly in an early re-organization and re-writing of large portions of the report, and very carefully read the entire work.

Finally, I want to express my gratitude to Mr. F. T. Linton who did all the art work for the report, and particularly to Mrs. R. Duffy who patiently and carefully did all the typing for the many drafts.

F. E. C. Culick

## TABLE OF CONTENTS

<u>Section</u>	<u>Page</u>
1. INTRODUCTION .....	1
1.1 Background and Purpose .....	1
1.2 General Description of Testing with T-Burners .....	3
1.3 A Précis of This Report .....	6
References .....	7
2. SUMMARY DESCRIPTION OF ANALYTICAL TECHNIQUES IN COMBUSTION INSTABILITY .....	9
2.1 General Remarks on Current Analysis .....	9
2.2 One-Dimensional Linear Analysis .....	15
2.3 Three-Dimensional Linear Analysis .....	18
2.3.1 Calculation of the Complex Wavenumber .....	19
2.3.2 Calculation of the Balance of Acoustic Energy .....	20
2.3.3 Comparison of the Two Calculations .....	22
2.4 Nonlinear Analysis .....	23
2.4.1 Approximate Nonlinear Analysis .....	23
2.4.2 Numerical Nonlinear Analysis .....	24
2.5 Calculation of the Acoustic Modes .....	27
2.6 Some Remarks on the Data Required for Analysis of Motors and T-Burners .....	27
2.6.1 Response and Admittance Functions .....	28
2.6.2 Dissipation of Acoustic Energy Due to Particulate Matter .....	31
2.6.3 The Influence of Exhaust Nozzles and Vents .....	32
References .....	33
3. TEST METHODS .....	36
3.1 General Description of Different Test Methods .....	36
3.1.1 Pulsed During Burning/After Burning (DB/AB) Method .....	36
3.1.2 Variable Area T-Burner (VATB) Method .....	37
3.1.3 Pulsed - Variable Area T-Burner (Pulsed- VATB) Method .....	38
3.2 Applications of the One-Dimensional Analysis to T-Burner Testing .....	38
3.2.1 Description of Methods in Terms of the One-Dimensional Analysis .....	38
3.2.1.1 Pulsed During Burning/After Burning (DB/AB) Method .....	39
3.2.1.2 Variable-Area T-Burner (VATB) Method .....	41
3.2.2 Application of the T-Burner to Obtain Qualitative Data .....	45
3.2.2.1 Pulsed During Burning/After Burning (DB/AB) Method .....	46
3.2.2.2 Variable-Area T-Burner Method .....	47
3.2.3 Application of the T-Burner to Obtain Quantitative Data .....	47
3.2.3.1 Pulsed During Burning/After Burning (DB/AB) Method .....	47

<u>Section</u>	<u>Page</u>
3.2.3.2 Variable-Area T-Burner Method.....	47
3.3 Pulsed During Burning/After Burnout (DB/AB) Method.....	48
3.3.1 Hardware Configuration.....	48
3.3.1.1 T-Burner Chambers.....	48
3.3.1.2 Surge Tank.....	50
3.3.1.3 Ignition System.....	53
3.3.1.4 Pulser.....	53
3.3.1.5 Transducer and Pulser Location.....	57
3.3.2 Propellant Grain Configurations.....	58
3.3.2.1 Disc, Cylinder, and Cup Grains.....	58
3.3.2.2 Methods of Mounting the Propellant Grains.....	59
3.3.3 Test Procedures.....	59
3.3.3.1 Recommended Test Series.....	62
3.3.3.2 Preparation of Instrumentation and Hardware.....	65
3.3.4 Operational Limitations.....	66
3.3.5 An Example of Raw Data.....	67
3.4 Variable Area T-Burner (VATB) Method.....	67
3.4.1 Hardware Configuration.....	67
3.4.1.1 T-Burner Chambers.....	67
3.4.1.2 Surge Tank Versus Sonic Orifice.....	71
3.4.1.3 Suppressors.....	74
3.4.1.4 Ignition System.....	79
3.4.1.5 Pulsers.....	82
3.4.1.6 Transducer Location.....	82
3.4.2 Propellant Grain Configurations.....	84
3.4.2.1 Cups Versus Cylindrical Grains.....	84
3.4.2.2 Recessed Versus Protruding Grains...	85
3.4.3 Test Procedures.....	86
3.4.3.1 Recommended Test Series.....	86
3.4.4 Operational Limitations.....	87
3.4.4.1 Pressure, Frequency, and Temperature.....	87
3.4.4.2 Propellant Grains.....	88
3.4.5 An Example of Experimental Results.....	89
References.....	91
4. INSTRUMENTATION AND DATA ACQUISITION.....	93
4.1 General Description of Instrumentation.....	93
4.2 Pressure Transducers.....	97
4.3 Oscillograph Records.....	97
4.4 Filtering.....	98
4.5 Magnetic Recording and Spectral Analysis.....	98
4.6 Instrumentation for Suppression Devices.....	99
4.7 Peak Follower Circuit (PFC).....	99
References.....	100

<u>Section</u>	<u>Page</u>
5. ANALYSIS AND REDUCTION OF DATA.....	102
5.1 Methods for Reducing Data .....	102
5.1.1 Pulsed DB/AB Method.....	102
5.1.1.1 Measurement from the Pulsed DB/AB Test Records .....	102
5.1.1.2 Methods of Reducing Pulsed DB/AB Data .....	103
5.1.1.3 Some Examples of Experimental Results .....	110
5.1.2 Variable Area T-Burner Method .....	112
5.1.2.1 Measurement from the VATB Test Records .....	112
5.1.2.2 Methods of Reducing VATB Data.....	117
5.1.2.3 Some Examples of Experimental Results .....	117
5.1.3 Digital Data Reduction.....	122
5.2 Preliminary and Qualitative Evaluation of Data.....	125
5.2.1 Acceptance Criteria for VATB Data.....	125
5.2.2 Acceptance Criteria for Pulsed DB/AB and Pulsed VATB Data .....	126
5.2.3 Presence of Higher Modes in T-Burners.....	126
5.2.3.1 Harmonic Excitation due to Pulsing....	127
5.2.3.2 Harmonic Content in the VATB.....	127
5.2.3.3 Other Sources .....	128
5.3 Reproducibility and Data Scatter.....	128
5.3.1 Data Scatter Due to Geometric Effects .....	129
5.3.2 Measurement Uncertainties .....	131
5.3.2.1 Guidelines for Determining Measure- ment Uncertainties.....	131
5.3.2.2 Some Examples .....	134
5.4 Methods for Obtaining the Response Functions and Particle Damping from Experimental Data.....	134
5.4.1 Assumptions and Approximations.....	134
5.4.2 Direct Methods for Obtaining the Response Functions and Particle Damping .....	135
5.4.2.1 Values Obtained from DB/AB Data ....	136
5.4.2.2 Values Obtained from VATB and Pulsed VATB Data .....	136
5.4.3 Statistical Analysis of Data.....	139
5.4.4 Velocity Coupling .....	145
5.5 Nonlinear Analysis of Data .....	150
References .....	151
6. TEST PROGRAMS AND APPLICATION TO STABILITY OF MOTORS .....	153
6.1 Test Programs .....	153
6.1.1 Comparison of Propellants .....	153
6.1.2 Characterizing a Single Propellant.....	156
6.1.3 Tests for Application to Motor Stability .....	162

<u>Section</u>	<u>Page</u>
6.2 Application of T-Burner Data to Problems of Stability in Motors.....	163
References.....	169
7. CONCLUDING REMARKS.....	171
7.1 Analysis of the T-Burner and the Assumption of One-Dimensional Flow.....	172
7.1.1 Nonisentropic Oscillations of the Combustion Zone (Pressure-Coupled).....	172
7.1.2 Boundary Layer - Combustion Zone Interactions.....	173
7.1.3 Flow-Turning of the Mass-Addition at the Sidewalls.....	174
7.1.4 Flow Adjoining Channel Wall Discontinuities.....	174
7.1.5 Vent Outflow.....	175
7.1.6 Flow Immediately Following Pulses.....	175
7.1.7 Distributed Combustion.....	175
7.2 Nonreproducibility.....	176
7.3 Some Problems Associated with the Reduction of Data.....	176
7.3.1 Nonlinear Growth and Decay.....	177
7.3.2 Extrapolation of the Variable-Area T-Burner Results to Zero Area Ratio.....	177
7.3.3 Reconciliation of Results of Different Test Methods.....	178
7.3.4 Correlation of Particle Damping.....	179
7.4 Nonlinear Behavior.....	179
7.4.1 Gasdynamic Nonlinearities; Mode Coupling..	180
7.4.2 Nonlinearities Associated with Combustion Processes.....	180
7.5 Assumptions Concerning the Mode Shapes.....	181
7.5.1 Heat Transfer.....	182
7.5.2 Strong Acoustic Sources and Sinks.....	182
7.5.3 Rate of Change of Oscillation Amplitude....	182
7.6 Influences of the Mean Flow.....	183
7.6.1 Assumption of Spacewise Uniformity of Combustion Response.....	183
7.6.2 Aluminum Oxide Droplet Size.....	183
7.6.3 Comparison of During Burning and After Burnout Pulses.....	184
References.....	185

#### APPENDICES

Appendix A. Nomenclature.....	187
Appendix B. Statistical Analysis of Data.....	192
References.....	196
Appendix C. Calculation of the Acoustic Modes for a T-Burner.....	197
C.1 One-Dimensional Analysis of the Acoustic Modes... ..	197
C.2 Numerical Calculations of the Acoustic Modes.....	207
References.....	212

<u>Section</u>	<u>Page</u>
Appendix D. Approximate Formulas for Particle Damping and Surface Losses.....	213
D.1 Attenuation of Acoustic Energy by Particle/Gas Interactions.....	214
D.2 Linear Viscous Losses on an Inert Surface.....	217
References.....	220
Appendix E. One-Dimensional Stability Analysis.....	221
References.....	232
Appendix F. Three-Dimensional Stability Analysis.....	233
F.1 Calculation of the Complex Wavenumber.....	233
F.2 Construction of the Balance of Acoustic Energy.....	236
References.....	239
Appendix G. Remarks on the Problem of the Vent.....	240
G.1 Analysis.....	240
G.2 Experimental Results.....	246
References.....	258

## LIST OF FIGURES

<u>Figure</u>	<u>Page</u>
1.2-1	Sketches of Typical T-Burners ..... 4
2.1-1	Schematic Representation of the Contributions to Combustion Instability in Solid Propellant Rocket Motors ..... 10
2.4-1	Typical Record of an Unstable Pressure Oscillation in a Variable Area T-Burner (Ref. 2-18) ..... 25
2.4-2	Spectral Analysis of the Record Shown in Figure 2.4-1 (Ref. 2-18) ..... 26
3.2-1	Graphical Examples of the Correlation of T-Burner Data ..... 43
3.3-1	Typical T-Burner Hardware for Pulsed DB/AB Testing ... 49
3.3-2	Observed Frequency versus Length of T - Burner. Data Are for a Metallized Composite-Modified Double-Base Propellant (Data Supplied by Naval Weapons Center)..... 51
3.3-3	Typical Surge Tank System for Pulsed DB/AB Testing .... 52
3.3-4	Pressure Amplitudes Generated by MK 2 Squibs, ANB 3066 Propellant at 500 psia ..... 55
3.3-5	Schematic Drawing of a Piston Pulser (Ref. 3-14) ..... 56
3.3-6	End Disc Mounting for Pulsed DB/AB Testing (Ref. 3-11) .. 60
3.3-7	Mounting Cylindrical Grains for Flush Conditions During and After Burning ..... 61
3.3-8	A Typical Test Record Obtained from a DB/AB Test ..... 63
3.4-1	Hardware for VATB Tests Using Protruding Grains (Ref. 3-4) ..... 69
3.4-2	Hardware for Pulsed VATB Tests Using Recessed Tapered Grains (Ref. 3-6) ..... 70
3.4-3	Surge Tank for VATB Apparatus with a Paddle Suppressor (Ref. 3-4) ..... 75
3.4-4	Details of a Surge Tank for VATB Apparatus (Ref. 3-14) .. 76

<u>Figure</u>		<u>Page</u>
3.4-5	A Typical Paddle Suppressor (Ref. 3-6).....	77
3.4-6	A Typical Helmholtz Resonator Used as a Suppressor (Ref. 3-5).....	78
3.4-7	Bag Igniters Used in VATB Testing (Ref. 3-6).....	81
3.4-8	Hardware Used in Pulsing a 2.9" T-Burner (Ref. 3-6)...	83
3.4-9	Reproduction of a VATB Test Record (Ref. 3-5).....	90
4.1-1	Block Diagram of Basic Instrumentation.....	94
4.1-2	An Example of Instrumentation Used in Testing Metal- lized Propellants (Ref. 4-9).....	95
5.1-1	Sketch of a Pulsed DB/AB Test Record for Defining Measured Quantities.....	104
5.1-2	Diagrams Showing Measurement of Pressure Amplitude and Frequency.....	105
5.1-3	Least Squares Fit (Eq. 5.1.1) to Experimental Data....	108
5.1-4	Illustration of Third Order Polynomial Fit to Data for $\tau_2$ versus TABO (Ref. 5-1).....	109
5.1-5	Values of $\alpha_1$ for Pulses During Burning as a Function of Pressure Amplitude for a Typical Test Series (Ref.5-1)..	111
5.1-6	Values of $\alpha_2$ for Pulses After Burnout as a Function of TABO for $\Delta p = 4$ (Ref. 5-1).....	113
5.1-7	Variation of $\alpha_d$ and $\alpha_c$ with Pressure Amplitude for ANB 3066 Propellant: $f \approx 820$ Hz, $\bar{p} \approx 500$ psia (Ref. 5-1).....	114
5.1-8	Example of Data Reduction.....	115
5.1-9	Nomenclature for Different Grain Configurations.....	119
5.1-10	Reproduction of Portions of a Typical Pressure Record from a VATB Test (Ref. 5-2).....	120
5.1-11	Plot of the Growth Period Shown in Figure 5.1-10 (Ref. 5-2).....	121
5.1-12	Typical VATB Data for ANB 3066; $f \approx 300$ Hz, $\bar{p} \approx 500$ psia (Ref. 5-2).....	123

<u>Figure</u>		<u>Page</u>
5.1-13	Typical Data Taken with Pulsed VATB Tests for ANB 3066; $f \approx 800$ Hz, $p \approx 500$ psia (Ref. 5-3).....	124
5.3-1	The Influence of Geometry According to the One-Dimensional Analysis (Ref. 5-3).....	130
5.3-2	Calculated Estimate of the Change in the Growth Constant Due to Changing Area Ratio for a Cylindrical Test Sample. ANB 3066 propellant; $f \approx 800$ Hz, $p \approx 500$ psia .....	132
C-1	Configurations and Definitions of Geometric Variables..	198
C-2	Natural Frequency of the Fundamental Mode with Propellant Grains at the Ends of a T-Burner ( $\beta_0 = 0$ ).....	201
C-3	Natural Frequency of the Fundamental Mode with Propellant Grains Displaced from the Ends of a T-Burner ( $\beta_0 = 0.25$ ).....	202
C-4	Fundamental Mode Shape for Recessed and Protruding Grains Located at the Ends of a T-Burner ( $\beta_0 = 0$ ).....	203
C-5	Fundamental Mode Shapes for Recessed and Protruding Grains Displaced from the Ends of a T-Burner ( $\beta_0 = 0.25$ ).....	204
C-6	$C_l^0$ versus $\beta$ for Recessed and Protruding Grains; Fundamental Mode ( $\beta_0 = 0$ ).....	205
C-7	$C_l^0$ versus $\beta$ for Recessed and Protruding Grains; Fundamental Mode ( $\beta_0 = 0.25$ ).....	206
C-8	$e_l^2$ versus $\beta$ for Recessed and Protruding Grains; Fundamental Mode ( $\beta_0 = 0$ ).....	208
C-9	$e_l^2$ versus $\beta$ for Recessed and Protruding Grains; Fundamental Mode ( $\beta_0 = 0.25$ ).....	209
C-10	$g_l$ versus $\beta$ for Recessed and Protruding Grains; Fundamental Mode ( $\beta_0 = 0$ ).....	210
C-11	$C_l$ versus $\beta$ for Recessed and Protruding Grains; Fundamental Mode ( $\beta_0 = 0$ ).....	211

<u>Figure</u>		<u>Page</u>
G-1	Sketches of Two Interpretations of the Influence of a Center Vent.....	245
G-2	Configuration of a T-Burner for Studies of the Influence of the Vent.....	247
G-3	A Quarter-Wave Burner and a T-Burner with Displaced Grains.....	250
G-4	Comparison of Test Data for the Vent with Calculations Using Several Combinations of VF and FT.....	253
G-5	Comparison of Experimental Results and Calculations for a Smokeless Propellant Tested in the T-Burner Shown in Figure G-3(b).....	255

LIST OF TABLES

<u>Table</u>		<u>Page</u>
3.2-1	Definitions of Parameters Contained in Eqs. (3.2.1) and (3.2.2).....	40
3.3-1	Squibs Used in Pulsed T-Burners.....	54
3.4-1	T-Burner Chamber Diameters.....	68
3.4-2	Characteristics of Suppressors.....	79
3.4-3	Typical Formulation of Pyrotechnic Paste (Ref. 3-4)...	80
4.1-1	Typical Instruments Used in T-Burner Facilities.....	96
5.1-1	Computations for VATB Data.....	118
5.1-2	Pulsed/Variable Area Data.....	122
5.3-1	Measurement Uncertainties for T-Burner Data.....	133
5.4-1	Definitions of Quantities Used in Statistical Analysis...	142
5.4-2	Experimental Data Taken in a Pulsed Variable-Area T-Burner with Cylindrical Grain (Ref. 5-3).....	143
5.4-3	Table of Residuals for the Data of Table 5.4-1. The Dependent Variable is $\alpha - \alpha_m$ .....	144
5.4-4	Effect of Velocity Coupling on Data Analysis.....	149
B-1	Compilation of T-Burner Data (Refs. B-1 and B-2).....	193
G-1	Experimental Values of the Response Function.....	254
G-2	Statistical Comparison of Theory and Data.....	256

## 1. INTRODUCTION

### 1.1 Background and Purpose

Several years ago, a manual (ref. 1-1) for the use of T-burners was prepared by a committee of the ICRPG Working Group on Solid Propellant Combustion. The purpose of that work was to summarize the experiences of the various investigators who had used the device, and to specify, as far as possible, standards for the apparatus, test conditions, and methods of data reduction. However, owing to the lack of data for testing with metallized propellants, the manual was restricted to work with un-metallized propellants.

Since the publication of ref. 1-1, a considerable amount of effort has been devoted to studying the unsteady burning of metallized propellants. The T-burner remains as the only test device to yield data for the unsteady burning of solid propellants over broad ranges of frequency and pressure. There are many problems associated with the T-burner, particularly when used to test metallized propellants. Nevertheless, it is the simplest configuration available if one is restricted to observing the spontaneous growth of oscillations or the decay following a pulse. Indeed, much of the experience gained with T-burners is applicable to more complicated configurations used for propelling vehicles.

Broadly, there are two main uses of the T-burner; as a means of comparing qualitatively the behavior of different propellants, and as a test device for measuring quantitatively the response of a burning propellant to unsteady motions. The bulk of this report is devoted to the more difficult problem of obtaining quantitative information; the procedures for making qualitative observations are necessarily covered as well. Almost all of the material is presented within the context of testing metallized propellants. The techniques of testing un-metallized propellants have not significantly changed since the publication of ref. 1-1.

In passing, it should be noted that ideally one would like to obtain the response of a burning surface to steady oscillations having fixed amplitude and frequency. As the T-burner is presently used, and described here, the ideal situation is not realized. The response is obtained always under conditions when the amplitudes of oscillations are growing or decaying. Subsequent use of the data then implies certain assumptions --

particularly that the behavior is linear, and that the response is sensibly independent of the rate of change of amplitude. Measurements in the presence of steady oscillations require either that some sort of device like a classical impedance tube be used, or that the fluctuations of the mass flow leaving the burning surface be measured directly. Experimental techniques are not presently available for realizing either alternative.

The experimental and analytical difficulties peculiar to testing with metallized propellant arise principally from the presence of particulate matter in the combustion products. This is a source of rather large dissipation of acoustic energy, thereby reducing the tendency for instability of waves. One way of compensating so as to obtain spontaneous instabilities is to use larger test grain, extending along the lateral boundary. Another way of obtaining data is to introduce pulses and observe the decay of waves. These test techniques are referred to, respectively, as the "variable-area method" and the "pulsed method." A combination of these methods appears to be the best way of obtaining quantitative results.

A primary purpose of this report is to summarize experience gained, in the past several years, by workers in several laboratories using the T-burner and testing methods referred to above. The experimental equipment is described in detail; recommended test procedures are given; and methods of analysis and data reduction are covered in detail. An important factor in the developments reported here is that a large amount of data has been obtained for a single propellant (ANB 3066) using all the test techniques, and in several different laboratories (refs. 1-2 to 1-7). Therefore, it has been possible to study the experimental aspects quite thoroughly, and to apply statistical techniques of data analysis.

Even with the substantial progress made since the first manual on T-burners was written, it is not possible to set down firmly established procedures. Many issues and problems are far from settled, but in view of the importance of the T-burner as an aid to treating the practical problem of combustion instability in motors, it is useful to bring together, in one volume, what is presently known. The remaining difficulties,

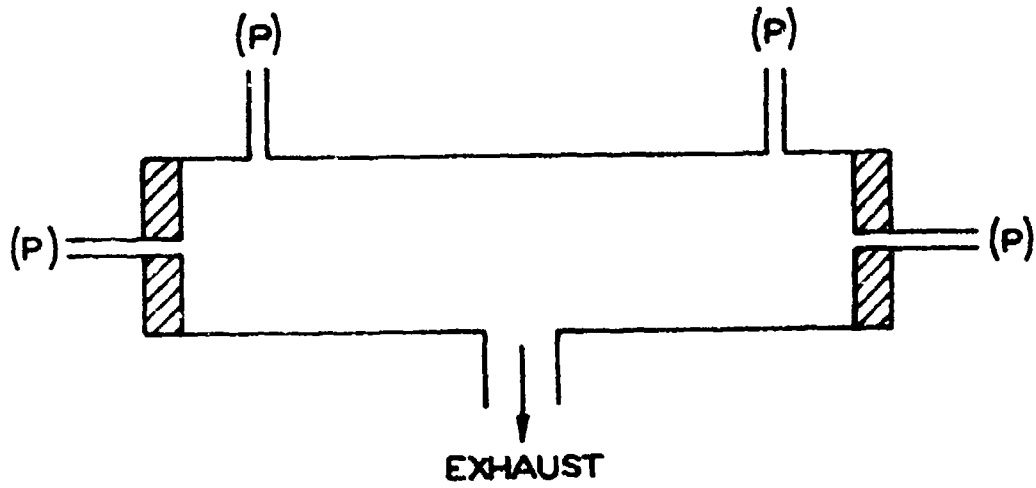
uncertainties, and limitations are carefully covered as they arise in subsequent discussion, and are summarized in the last section.

## 1.2 General Description of Testing with T-Burners

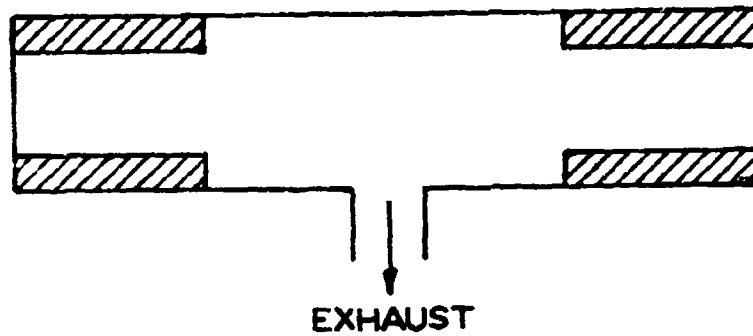
The T-burner is basically the same now as described in ref. 1-1. It consists of a straight tube, having diameter usually in the range  $1\frac{1}{2}$  in. to 5 in., with a vent in the center. Some T-burners having larger or smaller diameters have been used, but for the frequency range covering a few hundred to several thousand Hertz, diameters within the above limits give satisfactory results. Propellant grains are almost always mounted at the ends, but in addition there may be samples placed along the lateral boundary (Figure 1.2-1). The primary purpose of this configuration is to produce relatively low losses of acoustic energy, so that small disturbances will be unstable. If the driving by the propellant is sufficiently strong, then an acoustic instability will occur. Usually, the lowest longitudinal mode is excited spontaneously, with frequency approximately equal to the average speed of sound divided by twice the length,  $\bar{a}/2L$ . The techniques described in ref. 1-1 were based on observation of the growth and decay rates, or by comparing growth rates for different areas of burning surface. The most serious problem is determination of the losses in the system.

It has already been noted that when metallized propellants are tested, the increased losses associated with the particulate matter forces development of more elaborate test procedures. As a result, it becomes more difficult to obtain good reproducible data, and the interpretation of test records is much more complicated. Details of the apparatus and test procedures are covered later; here, only a brief introductory description will be given.

The method of testing with variable area of burning surface is based on the idea that the growth rate of unstable motions is (approximately, at least) proportional to the area of burning surface. The coefficient of proportionality is directly related to the response function for the surface. Tests are made for different areas of surface. Then a plot of the observed growth rates versus area will be, in an ideal case, a straight line whose slope will be related to the response function. The



(a) Simple end burner for pulse testing; (P) denotes typical locations of pulsers or pressure transducers.



(b) A T-burner with cylindrical grains for variable-area testing.

Figure 1.2-1 Sketches of Typical T-Burners

intercept, i. e., the value of the growth constant for vanishingly small area, should be related to the losses in the system. Roughly, the observed behavior is consistent with this picture, but the results are greatly more complicated in detail, and present serious problems of interpretation.

For example, the use of grains extending along the lateral boundary means that during all but a very small portion of the firing, the grain either protrudes from the wall or is recessed. The influence of this geometrical change must be accounted for in the interpretation of data. In order to obtain good definition of the curve, growth rate versus area, some firings must be done with rather large areas, large enough that waves may grow immediately out of the ignition transient, and the data for the growth period may be poor or unusable.

Consequently, it has become standard practice in several laboratories to incorporate in the burner a device which will suppress the instability until the flow field has reached steady state. For example, the use of a paddle, obstructing the cross-section area at the center of the burner, has been very successful. When the paddle is withdrawn, the oscillation, if unstable, will grow. It is also possible to withdraw and insert the paddle several times (generally no more than three) during a firing, thereby yielding more data per firing.

The second primary method of testing metallized propellants makes use of pulses injected at one of several possible locations (as indicated in Figure 1.2-1(a)) with either small explosive charges, or by using the piston-pulser described in §3.4.1.5. The use of pulses has long been common for qualitative assessment of liquid rocket engines, but extensive application to T-burners is quite recent. In the work described later, the basis is the idea that the decay rate following a pulse during a firing is proportional to the difference between the rate of energy gain (due mainly to the combustion processes) and the rate of energy loss. Then if a pulse is introduced after burnout, the rate of decay reflects the rate of energy loss in the system. Ideally, then, combination of the two measurements will produce quantitative results for the rate of energy gain, or the response function, associated with the combustion processes. In practice, reproducible accurate data are difficult to obtain.

For reasons which will be elaborated upon later, §3.4 and §5, a combi-

nation of the variable-area and pulsing techniques appears very attractive, and may well be the best procedure for obtaining quantitative information. On the other hand, for comparing the qualitative behavior of propellants, both techniques have been successfully used separately. Pulsed testing offers the advantage of obtaining directly an assessment of the influence of particles on energy losses.

### 1.3 A Précis of This Report

The technical description of the T-burner is conveniently divided into four parts: analysis of the device, test methods, instrumentation and data acquisition, and data analysis and interpretation. These four subjects are covered in the succeeding four sections of the report.

In §2, the methods of analysis are described and a few important results quoted. The purpose is mainly to provide sufficient information that the reader may be aware of what is available, and to introduce the basis for later discussion of the interpretation of data. The connections between the analyses of T-burners and motors is briefly covered. More comprehensive discussions of the details of the analyses appear in Appendices C - F. The sections on analysis are not prerequisite to the other parts of the report and may be overlooked by those concerned principally with the construction and use of T-burners.

The methods of testing are covered in §3. It would perhaps be helpful to the reader unacquainted with the subject to examine first the previous report on testing with T-burners, ref. 1-1. The treatment of the experimental procedures given here is quite lengthy and detailed. Many of the items discussed arise because of the difficulties associated with testing metallized propellants. Hence, it is well to understand first those aspects which are important to testing un-metallized propellants.

A thorough discussion of the instrumentation used, and the various methods of data acquisition, are given in §4. Owing to the problem of reproducibility and rather large uncertainties in the data, the analysis and interpretation of data have become a very important part of the experimental work. This subject is treated in §5. Especially, it should be noted that because a great many measurements have been made, it has become possible -- indeed, necessary -- to use statistical methods of

analyzing data. The subject is summarized in §5.4.3 and covered in greater detail in Appendix B. Another feature which has received increasing attention in the last several years is nonlinear behavior. Among others, the discussion in §5 touches upon the questions of harmonic content and limiting amplitudes of pressure traces.

Section 6 is intended to be particularly interesting to those concerned with program management and the practical use of T-burners. The discussion of §6.1 covers various aspects of planning test programs for T-burners, both for research and in connection with motor development. In §6.2, the use of data taken with T-burners to study and predict the stability of motors is covered.

Throughout the body of the manual, various difficulties and unresolved problems are mentioned as they arise. In §7, many of these are summarized for convenient reference. That section is intended to provide a brief survey of problems which, for the most part, are not related so much to practical operation of the T-burner as to fundamental aspects. The discussion should serve as a caution to the careful user, and as an outline of matters which merit close attention.

#### REFERENCES

- 1-1 "T-Burner Manual." CPIA Publication No. 191, CPIA, Silver Spring, Maryland (November 1969).
- 1-2 Derr, R. L. "Development and Evaluation of the Variable Area T-Burner," AFRPL-TR-72-97, Lockheed Propulsion Co., Redlands, California (February 1973).
- 1-3 Beckstead, M. W., Bennion, D. U., Butcher, A. G., and Peterson, N. L. "Variable Area T-Burner Investigation," AFRPL-TR-72-85, Hercules, Inc., Magna, Utah (December 1972).
- 1-4 Peterson, J. A., Muhlfeith, C. M., and Sayer, L. H. "Final Report: Pressure Oscillation Investigation for Minuteman III," AFRPL-TR-72-98, Thiokol Chemical Corp., Wasatch Division, Brigham City, Utah (January 1973).
- 1-5 Evaluation of Pulse T-Burner for Metallized Propellants, AFRPL-TR-72-54: Vol. I, "Experimental Procedures for the T-Burner," Micheli, P. L.; Vol. II, "Stability Analysis," Micheli, P. L.; Vol. III, "Piston Pulser Development," Lovine, R. L. Aerojet Solid Propulsion Co., Sacramento, Calif. (January 1973).

- 1-6 Crump, J. "Oscillatory Combustion Experimentation and Analysis," AFRPL-TR-72-99, Naval Weapons Center, China Lake, California (February 1973).
- 1-7 Gould, R. D. and Penny, P. D. "An Experimental Investigation of the Burning Rate of Propellant ANB 3066 under Oscillatory Pressure and Oscillatory Velocity Conditions," AFRPL-TR-73-95, Rocket Propulsion Establishment, Westcott, Aylesbury, Buckinghamshire, United Kingdom (November 1973).

## 2. SUMMARY DESCRIPTION OF ANALYTICAL TECHNIQUES IN COMBUSTION INSTABILITY

### 2.1 General Remarks on Current Analyses

Perhaps the most important point to appreciate is that analytical work on combustion instability in general, and on T-burners in particular, provides basically a framework for treating observations and measurements. The physical situations are so complicated as to preclude a complete theoretical analysis starting from first principles and ending with precise values for the growth rates and limiting amplitudes of unstable oscillations in a motor. The treatment of these problems requires an intimate coordination of both analytical and experimental techniques.

A second important point is that effort expended upon the T-burner is not so restricted as one might superficially assume. The T-burner is, after all, just a special kind of rocket motor. Thus, the same analyses apply to both T-burners and full-scale motors. Because tests in T-burners are relatively inexpensive, and data under widely varying conditions are quite easily obtained, the device affords a very convenient means for checking certain features of analytical results.

The coverage of analytical work in this report is necessarily restricted to those parts which are most directly applicable to T-burners, with particular attention paid to problems arising in testing aluminized propellants. However, to provide a context and to show explicitly the relation of work on T-burners to the problem of combustion instability in motors, it is helpful to consider briefly the general situation. Figure 2.1-1, adapted from ref. 2-1, is intended to show how the problem is broken into various pieces in order to isolate special analytical and experimental problems. The overall formal framework is provided by analysis of the gasdynamics for the chamber. Important contributions which distinguish this situation appear either as source terms for the gasdynamics or as boundary conditions. These include the following.

- (1) residual combustion and the influence of particulate matter within the volume;
- (2) the consequences of transient motions of the propellant grain;
- (3) the action of the exhaust nozzle on unsteady motions in the chamber;

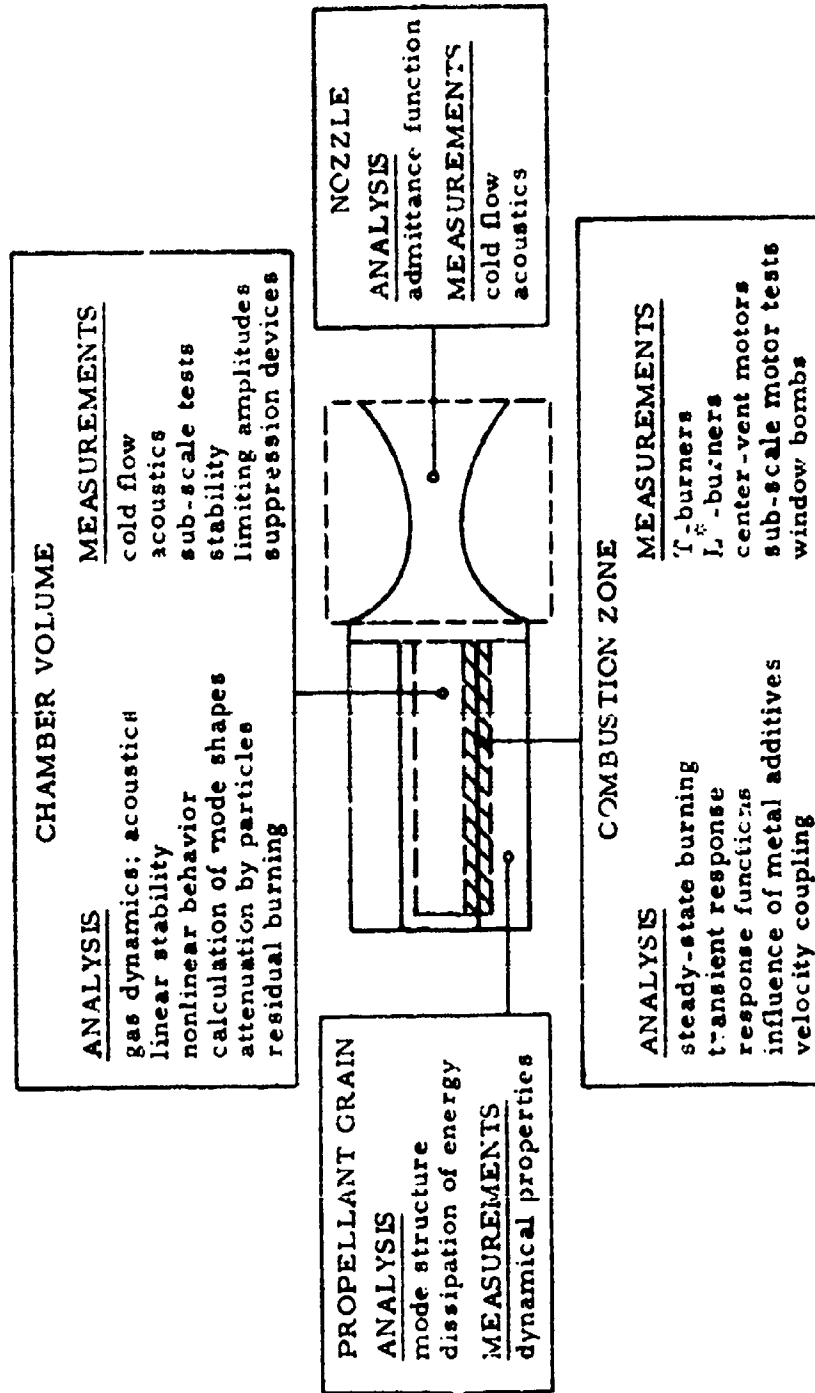


Figure 2-1. Schematic Representation of the Various Contributions to Combustion Instability in a Solid Propellant Rocket Motor.

- (4) interactions between the combustion processes at the burning surfaces and motions in the chamber; in general, the combustion processes are sensitive to both pressure and velocity fluctuations.

The last three are conveniently treated as boundary conditions.

The amount of energy dissipated by vibratory motions of the sample grains is negligible and can therefore be neglected. Corresponding to the exhaust nozzle in a rocket motor is the center vent of the T-burner. The influence of the vent has lately been the subject of considerable controversy and research. Until quite recently, it had generally been assumed that the center vent had no effect on the fundamental mode of a T-burner, but this so far has not been satisfactorily justified by definitive measurements (see discussions in §2.6.3 and Appendix G). So far as predictions of motor stability are concerned, the primary purpose of the T-burner is to provide numerical values for the interactions between harmonic disturbances and the surface combustion processes. The interactions are conveniently represented as response functions defined below in §2.6; these are frequency responses for a burning surface. It is primarily because of these interactions, which convert a small fraction of the energy released in chemical reactions to mechanical energy of fluid motions, that instabilities occur. For analysis of the stability characteristic of a motor, the response functions must be known; but because it is not possible to compute these quantities, measured values are required, and hence the interest in T-burners. It should be noted that important information related to particle damping can also be obtained from measurements taken with T-burners.

The response functions cannot presently be measured directly; in principle, this would be possible if one could measure (say, by optical means) the fluctuations of the gases departing the burning surface. Consequently, it is necessary to extract the desired information from measurements of the unsteady pressure in the burner. Put most simply, the purpose of analysis is the following.

With the developments described in §§2.2-2.5, one finds a formula for the growth constant  $\alpha$ ; this appears in the linear analysis as the constant in the exponential growth of the pressure amplitude. That is, a

small initial disturbance of pressure increases in time as  $\exp(\alpha t)$ . The formula for  $\alpha$  depends on the gasdynamics and all other contributions listed above, including the response function. The idea then is to measure  $\alpha$  and assume that all other quantities except the response function are known by some means or other. Then one can use the formula to compute the response function. There are two sources of uncertainty: the data for  $\alpha$  exhibit considerable experimental scatter, and the other quantities are not known accurately. For example, the influence of the center vent is in doubt, and because particle sizes are not well known, the dissipation of energy by the particulate matter is also not known accurately. The strategy followed is to analyze the gasdynamics as completely as possible, and conduct separate experiments to try to determine other contributions to the growth rate.

The analyses may, in the first instance, be divided into two classes, linear and nonlinear. By far the most effort has been expended on linear analysis, although nonlinear behavior is a subject of increasing effort. Most of the work in interpretation of T-burner data (55) has been based on the linear analyses described in §§2.2 and 2.3. An approximate nonlinear analysis, described in §2.4, has been used (§5.5) to try to gain understanding of those processes which determine the limiting amplitudes of oscillations. Although the results to date must be regarded as more exploratory than definitive, this problem in the long range has great practical importance, for in real motors one is really concerned with the amplitudes of oscillation. In some cases, unstable motions of sufficiently small amplitude can be tolerated.

The primary purpose of this report is to provide the information necessary to use the T-burner effectively as an experimental device. Consequently, analytical developments occupy a lesser position. For this reason, the details of all calculations are included as appendices. Sections 2.2-2.5 serve only to describe the analyses which have been used, and to cite the important formulas used for the interpretation of data.

All analyses begin with the general conservation equations for unsteady fluid motion. In order to construct manageable problems, several simplifying approximations must be introduced and are common to all the treatments summarized here. The conservation equations are, of course, highly nonlinear, and the first task is to produce simpler equations by

making use of small parameters to expand the thermodynamic and flow variables. In solid propellant rockets and T-burners, there are in the first instance two such quantities; the Mach number of the average flow, and the Mach number of the acoustic field. The second is proportional to, and hence serves as a measure of, the amplitude of the pressure oscillations.

It is an excellent approximation for T-burners that the Mach number of the average flow is much less than unity; generally, it is less than .01 over the entire chamber volume, except possibly for a very small region in the vicinity of the vent. The acoustic Mach number varies from nearly zero in the initial part of the growth of an unstable wave, to as large as .2 - .3 or more when the waves have reached limiting amplitude.

All computations of unsteady motions in combustion chambers are based on the idea that combustion and flow constitute deviations from classical acoustics. Thus, the zeroth approximation is that the waves in chamber are classical acoustic modes, described by the equations of linear classical acoustics; the equations for the acoustic velocity and pressure in three dimensions are:

$$\bar{\rho} \frac{\partial \vec{u}'}{\partial t} + \nabla p' = 0 \quad (2.1.1)$$

$$\frac{\partial p'}{\partial t} + \nabla \bar{\rho} \cdot \vec{u}' = 0 \quad (2.1.2)$$

For a chamber enclosed by rigid walls, the velocity normal to the boundary must vanish, so according to (2.1.1), the normal component of the pressure gradient is zero:

$$\bar{\rho} \hat{n} \cdot \frac{\partial \vec{u}'}{\partial t} = \bar{\rho} \frac{\partial}{\partial t} (\hat{n} \cdot \vec{u}') = \hat{n} \cdot \nabla p' = 0 \quad (2.1.3)$$

In combustion chambers, there is necessarily a mean flow. If the average Mach number is assumed to be small, and the acoustic Mach number is assumed to be smaller yet\* (in a sense which is considered briefly in Appendices E and F, but elaborated upon more thoroughly in

---

\* It is important to note that linear behavior (i. e., exponential growth of the amplitude) is often observed at amplitudes much greater than the limit suggested by this criterion. The reason for this apparent inconsistency may be connected with nonlinear behavior, although this has not been proven.

the references cited there), then eqs. (2.1.1) - (2.1.3) are augmented by terms on the right hand sides which are linear in both the Mach numbers. That is, all of the inhomogeneous terms are proportional to the average Mach number, and to the acoustic Mach number.

The important feature is that, providing the combustion processes are linearized, the governing equations remain linear, even though all physical processes may be accounted for\*. This system of equations can be used as the basis for calculations of linear stability. The idea is that an arbitrary disturbance within the chamber can be represented as a superposition of its Fourier components, i. e., as a superposition of the normal modes of the chamber. In order that the disturbance should be stable, all of its components must be stable. Hence, it is sufficient to study the linear stability of the normal modes of the chamber.

By this argument, the problem of linear stability comes down to a calculation of the stability of harmonic motions, for by definition, the normal modes vary harmonically in time. The actual modes in the chamber are distorted by the action of combustion processes and the mean flow, but it happens that within the approximations just described, it is sufficient to know only the unperturbed classical modes for a closed chamber. The formal and practical simplifications arising from this fact are very great.

In all the analytical work, the first task is to determine the unperturbed acoustic modes. Two calculations are noted here. For the T-burner with grains extending along the lateral boundary, the variations of cross-section area can be accommodated by the one-dimensional analysis (§2.2 and Appendix C.1). If the computation capability is available -- virtually a necessity to do stability calculations for a full-scale motor -- the numerical computation mentioned in Appendix C.2 is likely to be more efficient for extensive applications.

Linear analyses produce formulas for the growth constant  $\alpha$  of a small disturbance. The disturbance then has amplitude which varies as  $\exp(\alpha t)$  in time. In all cases,  $\alpha$  is given as a sum of integrals, each con-

---

\* Certain nonlinear features of velocity coupling, for example, rectification, can be partially accommodated within such a formulation.

taining the unperturbed mode shape as a factor in the integrand. The interpretations of data discussed in this report are all based on formulas of that sort.

The nonlinear analysis described in § 2.4 also requires that the unperturbed acoustic modes be known. Indeed, it is generally true that if only effects which are linear in the average Mach number are retained, then the unsteady behavior can be calculated without knowing how the classical modes are distorted.

One of the major sources of difficulty is the influence of viscous forces. Two simple results have been very useful: the linear attenuation by the acoustic boundary layer on a rigid wall, and the attenuation due to relative motions of particulate matter and gas. But problems such as the three-dimensional unsteady viscous flow at the center exhaust vent and in the vicinity of lips or recessed ledges remain unsolved, both analytically and experimentally. There are other viscous effects (generically referred to as "flow-turning") associated with the flow entering the chamber from the burning surfaces on the lateral boundary. These arise from the physical process in which the incoming flow acquires acoustic energy. The detailed problem has not been solved, but the one-dimensional analysis provides an approximate representation.

## 2.2 One-Dimensional Linear Analysis

The primary practical reason for carrying out analyses of the T-burner is to provide formulas for interpreting data. Various analyses differ depending on what aspects are emphasized. There are two important features which are explicitly and easily accounted for in the one-dimensional calculation: abrupt changes of cross-sectional area, and acoustic/mean flow interactions associated with the flow entering along the lateral boundary. These can be handled in an extension of a classical three-dimensional analysis only by including viscous forces and treating essentially a problem of boundary layer theory. In the one-dimensional analysis, the flow through the lateral boundary is represented by sources of mass, momentum, and energy. The calculations described in this section provide approximate means of estimating the boundary processes.

To a first approximation, the normal modes of a T-burner are those of an organ pipe closed at both ends; the pressure varies as

$\cos(k_l z)$  along the tube ( $z = 0$  at one end) and the eigenvalues, the wavenumbers for the normal modes, are  $k_l = l\pi/L$ . If  $\bar{a}$  is the speed of sound, then the natural or resonant frequencies are  $\omega_l = \bar{a}k_l$ .

Two influences must be taken into account to give results for the acoustic modes which are sufficiently accurate for most practical purposes: geometrical deviations from the straight tube, and the effects of combustion on the speed of sound. The second really just means using the correct speed of sound for the combustion products, including the particulate matter. In almost all work reported to date, the speed of sound has been assumed uniform. A simple correction for a non-uniform value has been given in ref. 2-2. In Appendix E, the way in which the influence of particulate matter is accounted for is discussed, and explicit formulas are given in Appendix D. Computation of the mode shapes and frequencies for a chamber having abrupt changes of area is also discussed in Appendix C. Eventually, the frequencies must be found by numerically solving a transcendental equation. A few examples are included there.

The quantity which is most useful for interpreting experimental data is the growth constant  $\alpha$ . Two ways of computing  $\alpha$  are discussed in the Appendices; by calculation of the complex wavenumber and by constructing the equation for the balance of acoustic energy: both calculations of course begin with the general conservation equations. The imaginary part of the complex wavenumber is proportional to the growth constant, which is one-half of the fractional rate of change of time-averaged acoustic energy in the chamber,

$$\alpha = \frac{1}{2E} \frac{dE}{dt} \quad (2.2.1)$$

It is a very nice feature of linear systems that the formula for the growth constant has the form of a sum of contributions; and some represent losses. When the losses equal the gains,  $\alpha$  vanishes and the disturbance is neutrally stable.

Equation (E.33) of Appendix E is the general one-dimensional result for  $\alpha$ ; if the mean velocity  $\bar{u}_b$  of the gases leaving the surface is assumed to be independent of position on the burning surface, that equation becomes:

$$\alpha = -\frac{\bar{Y}P_o}{2E_t^2} \left\{ \left[ \hat{p}_t \left( \hat{u}_b(r) + \frac{\bar{u}_b \hat{p}_t}{\rho a} \right) S_c \right]_0^L - \bar{u}_b \int_0^L \hat{p}_t \int \left[ \frac{\dot{m}_b}{\bar{m}_b} + \frac{\Delta \hat{T}}{T_o} \right]^{(r)} dqdz \right\}$$

combustion and exhaust nozzle

$$- \frac{\bar{u}_b}{2E_t^2} \int_0^L \frac{1}{k_t} \left( \frac{d\hat{p}_t}{dz} \right)^2 \int dqdz \quad (2.2.2)$$

mean flow/acoustics interactions ("flow-turning")

$$+ \frac{a^2}{2x_t E_t^2} \left\{ \int_0^L \delta F_p^{(i)} \frac{d\hat{p}_t}{dz} S_c dz + x_t \frac{\bar{R}}{\bar{C}_v} \int_0^L \delta \hat{Q}_p^{(r)} \hat{p}_t S_c dz - \int_0^L \delta \hat{u}_p^{(i)} \frac{d\hat{p}_t}{dz} \int \bar{m}_b(p) dqdz \right\}$$

contributions from particulate matter

Note that residual combustion within the chamber has been ignored.

Details are given in Appendix E for the application of Eq. (2.2.2) to T-burners. Combination of (E.47), (E.51), and (2.2.2) gives

$$\alpha = \frac{\bar{u}_b}{K_t} \frac{1}{e_t^2} \left\{ \left[ \frac{S_{bc1}}{S_{co}} + \cos^2(\beta K_t) \frac{S_{bc2}}{S_{co}} \right] B_e + C_t \frac{S_{bs}}{S_{co}} B_s \right\} + \alpha_m + \alpha_d \quad (2.2.3)$$

where  $\alpha_d$  represents the influence of all losses, and

$$\alpha_m = - \frac{\bar{u}_b}{L} \frac{S_{bs}}{S_{co}} \frac{g_t}{e_t^2} (FT) + 2 \frac{\bar{u}_b}{L} \frac{S_b}{S_{co}} (C_t^o)^2 (VF) \quad (2.2.4)$$

This formula contains all the formal mean flow/acoustics interactions associated with "flow turning" in the one-dimensional approximation\*. The first part is the loss accompanying flow inward at the lateral burning surface, and the second is the formal result representing a gain of energy at the center vent. An extended discussion of the influence of the vent is given in Appendix G. The losses represented by  $\alpha_d$  are principally those associated with the particulate matter when metallized propellants are tested. Elementary calculations of the particle damping and wall losses are given in Appendix D.

\*The factors (FT) and (VF) are not part of the theoretical prediction. They are inserted to conform with the use of this formula to interpret data. The values of (FT) and (VF) are then either fixed, or allowed to float. See particularly §6.2.

The influence of the surface combustion processes are represented by the bracketed terms in Eq. (2.2.3). Velocity coupling has been neglected. The symbols B stand for the combination  $A_b^{(r)} + \bar{u}_b/\bar{a}$ , where  $A_b^{(r)}$  is the real part of the admittance function, proportional to the ratio of the fluctuation of velocity of the gases leaving the surface, to an impressed fluctuation of pressure. Subscript ( )<sub>e</sub> denotes end burning surfaces (i. e., burnt gases issue parallel to the surface), and subscript ( )<sub>s</sub> stands for side or lateral surfaces. It is assumed that the quantities B are constant over the surfaces with which they are associated. Application of Eq. (2.2.3) to interpretation of data is discussed in §§ 3 and 5.

Equation (2.2.3) simplifies considerably for some configurations which have been used. In particular, pulsed T-burners often have only grains at the ends, so  $S_{bs} = S_{be} = 0$ . If all losses and whatever influence the vent may have are included in  $\alpha_d$ , then (2.2.3) may be written

$$\alpha = \alpha_c \frac{S_{be}}{S_{co}} + \alpha_d \quad (2.2.5)$$

Now, because the chamber is uniform,  $\omega_l/K_l \epsilon_l^2 = 2\bar{a}/L$  (see Appendix E), and  $\alpha_c$  in the above equation is

$$\alpha_c = 2 \frac{\bar{a}}{L} \left( A_b^{(r)} + \bar{u}_b/\bar{a} \right) \quad (2.2.6)$$

This definition of  $\alpha_c$  conforms with the common usage in discussions of pulsed T-burners (§ 3.3).

### 2.3 Three-dimensional Linear Analysis

There are principally two kinds of analyses which have been used to study the linear stability of three-dimensional motions. The formulas produced for the growth constant  $\alpha$  are identical in most respects, but neither analysis contains certain contributions -- notably the "flow-turning" effect -- which are found in the one-dimensional analysis (§2.2 and Appendix E). The reason for this is that the "flow-turning" is a process which in the real flow occurs in a boundary region and necessarily involves viscous forces; that is why it appears as a mechanism for attenuating acoustic energy. The one-dimensional analysis provides an approximate means of computing the loss. Only if viscous effects are taken into account will a three-dimensional analysis contain this contribution.

No solutions for three-dimensional viscous flows are available for the problems of interest here. All viscous effects have been appended to the results of analyses which have involved essentially perturbations of a classical inviscid analysis. Not only must the flow-turning effect be added after the fact but, better known, so is the loss due to viscous stresses and heat transfer acting in the acoustic boundary layer on an inert wall.

For most purposes in work with T-burners, a one-dimensional analysis of the sort described in Appendix E and §2.2 suffices, although it may prove desirable to compute the acoustic modes by using numerical analysis (§2.5 and Appendix C.2). The reasons for including a description of three-dimensional analysis here is to make more apparent the connection between T-burners and full-scale motors, and to clarify the origin of a controversy concerning the subsonic vent, which has appeared in the literature. As for the one-dimensional analysis, details are not included; a more complete description is given in Appendix E.

2.3.1 Calculation of the Complex Wavenumber. This analysis (refs. 2-4, 2-6, 2-7) is developed in the same way as the one-dimensional analysis. The main differences are that three-dimensional motions are treated, and the source terms representing the flow in at the lateral boundaries are missing. Of course, certain features of the inward flow are contained in boundary conditions set on the three-dimensional solutions, but the processes occurring in viscous boundary layers are absent.

The normal modes, to first approximation, are those for a chamber having the same shape as the motor or T-burner, but enclosed by rigid walls. A sonic exhaust nozzle is closed by a rigid surface placed at the entrance plane; a subsonic vent should be treated as an open orifice or exhaust tube with the boundary condition that the pressure is constant over the exit plane.

Computation of the natural modes and frequencies must be done in general numerically (Appendix C.2). The correct speed of sound to use is that for the gas/particle mixture, as shown by the formulation described in Appendices E and F.

The differential conservation equations are combined to give an inhomogeneous wave equation with inhomogeneous boundary conditions. By comparison with the unperturbed problem for the chamber without

combustion and flow, one can eventually deduce a formula for the complex wavenumber, of which the real part is the growth or decay constant, defined as above in Eq. (2.2.1). The formula for  $\alpha$  can be found from Eq. (F.17) in Appendix F; it will not be repeated here because it has essentially the same form as Eq. (2.2.2), which has been used more widely for interpreting the results of T-burner tests.

2.3.2 Calculation of the Balance of Acoustic Energy. The first study of three-dimensional motions (ref. 2-3) was based on this kind of analysis. Application to T-burners was subsequently discussed in ref. 2-8, but, as noted above, the viscous processes associated with the inward flow on lateral burning surfaces are absent. The original formulation, and more recent application to T-burners (refs. 2-9, 2-10), involves the assumption that the flow field is inviscid.

Of course, it is necessary to begin in any case with the conservation laws. The approach taken in ref. 2-3 is to treat them in integral form and construct a relation for the balance of energy within the chamber. What one is really interested in for questions of stability is the acoustic energy, the energy associated with the unsteady flow field; cf. Eq. (2.2.1). However, the authors of ref. 2-3 chose to work with the total energy. This has the consequence, demonstrated in refs. 2-4 and 2-7, that the influences of processes within the volume (e. g. attenuation by particulate matter and energy released by residual combustion) cannot be accounted for. The reason for this unfortunate feature is that in the balance of total energy in the volume, the energy change of the unsteady field is compensated by an equal change in the energy of the steady field. The quantity one needs for the stability analysis (e. g.  $\alpha_p$  associated with the particles) is lost in the bookkeeping.

For a linear stability analysis, one can simply add to the formula for  $\alpha$  whatever contributions are required. This is the way particle damping has been included in the calculations reported in refs. 2-8 to 2-10. One must be able, of course, to compute independently the fractional rate of change of acoustic energy associated with any process of interest. That this is not always an obvious computation is shown by the example of particle damping covered in Appendix D.

A brief description of the analysis given in ref. 2-3 is provided in Appendix F. The formula for  $\alpha$  can eventually be put in the form (F. 24):

$$\alpha = - \frac{\bar{p} \bar{a}^2}{2E_N} \oint \left[ \hat{p} \hat{u}^{(r)} + \bar{u} \frac{\hat{p}^2}{\rho \bar{a}} + \bar{\rho} (\bar{u} \cdot \hat{u}) \hat{u} \right] \cdot \hat{n} dS + \alpha_m + \alpha_d \quad (2.3.1)$$

This differs from the formulas given in refs. 2-4, 2-6, and 2-7 by the added term  $(\bar{u} \cdot \hat{u}) \hat{u}$ . Before examining that term more closely, note first that the other two terms are precisely those encountered in the formula for the complex wavenumber. Compare, for example, the first group of terms in Eq. (E. 33) and the integral representing the combustion coupling in Eq. (F. 17). With the definition (E. 34) of the admittance function, one can write

$$- \left[ \hat{u}^{(r)} \cdot \hat{n} + \frac{\hat{p}}{\rho \bar{a}} \bar{u} \cdot \hat{n} \right] = \frac{\hat{p} \bar{a}}{\bar{\rho} P_0} A_b^{(r)} + \frac{\hat{p}}{\rho \bar{a}} \bar{M}_b = \frac{\hat{p} \bar{a}}{\bar{\rho} P_0} (A_b^{(r)} + \bar{M}_b) \quad (2.3.2)^*$$

Thus, (2.3.1) can be written

$$\alpha = \frac{\bar{a}}{2E_N} \oint \hat{p}^2 (A_b^{(r)} + \bar{M}_b) dS - \frac{(\bar{\rho} \bar{a})^2}{2E_N} \oint (\bar{u} \cdot \hat{u}) \hat{u} \cdot \hat{n} dS + \alpha_m + \alpha_d \quad (2.3.3)$$

The first integral in (2.3.3) extends over the entire boundary surface, and therefore covers not only all burning surfaces but also the entrance planes of subsonic vents and choked exhaust nozzles. The last will not be considered here.

With some re-writing, the first integral of (2.3.3) applied to the burning surface will reproduce the terms containing  $B_g$  and  $B_e$  in Eq. (2.2.3). For the fundamental mode, the amplitude  $\hat{p}$  of the pressure vanishes at the center of the burner, so the contribution from this integral is very small over the entrance plane of a center vent; it is conventionally dropped as being negligible. Let  $\alpha_b$  denote all the contributions from the burning surfaces, so (2.3.3) becomes

---

\* The minus sign arises because  $\hat{u}^{(r)} \cdot \hat{n}$  is positive outward from the boundary, whereas  $\hat{u}_b^{(r)}$  in the definition of  $A_b^{(r)}$  is positive inward. Note also that  $\bar{M}_b$  is defined as  $\bar{u}_b / \bar{a}$  where  $\bar{a}$  is the average speed of sound in the chamber.

$$\alpha = \alpha_b + \alpha_m + \alpha_d - \frac{\bar{p} \bar{a}^2}{2E_N} \oint (\bar{\mathbf{u}} \cdot \hat{\mathbf{u}}) \hat{\mathbf{u}} \cdot \hat{\mathbf{n}} dS \quad (2.3.4)$$

In the analyses of refs. 2-4 to 2-7, the last integral in this equation also appeared, but was dropped for the following reason. On all burning surfaces the mean flow velocity is normal to the surface, so  $\bar{\mathbf{u}} \cdot \hat{\mathbf{u}} = \bar{u}_b \hat{u}_b$ , and the integrand is  $\bar{u}_b (\hat{u}_b)^2$ . But  $\hat{u}_b$  is of the order of the average Mach number (see §2.6). This term is therefore of the order of the cube of the Mach number and is negligibly small for those surfaces. It should be recalled (Appendix F) that only terms of first order in the Mach number can be retained if the formula (2.3.1) is used. In refs. 2-4 through 2-7 it has been assumed also that the value of this integral over the center vent is negligibly small. However, in refs. 2-9 and 2-10, an argument has been made that the integral is of the order of the Mach number, and hence is significant for the center vent. These contrary views, plus a formal result for the "flow-turning" term ( $\alpha_m$ ), constitute the basis for certain questions related to the center vent. These questions are pursued further in Appendix G, where various explicit forms for the growth constant  $\alpha$  are given.

2.3.3 Comparison of the Two Calculations. The most important point to be made is that for linear problems the formal results obtained from the two approaches just described must be identical. This is not immediately obvious because the authors of ref. 2-3 chose to work with the total energy. If one forms the integral balance of acoustic energy only, then, as shown in refs. 2-4 and 2-7, the identity of the results is readily established. Arguments concerned with the magnitudes of particular contributions and their interpretation are quite distinct from the formal results.

In order to construct the equation for the balance of acoustic energy, one must carry through the same operations with the differential equations (i. e., the expansions in small parameters) as for the computation of the complex wavenumber (see the comments on pp. 2-4 and 2-5). The most attractive feature of working with the balance for acoustic energy is that it appears to be less obscure and formal. Indeed, the fact that twice the imaginary part of the wavenumber multiplied by the speed of sound must equal the fractional rate of change of energy -- Eq. (2.2.1)

-- is not immediately obvious.

The new terms which were found in the one-dimensional analysis must in either case be somehow "patched" onto the three-dimensional result. It is perhaps worth noting that the one-dimensional analysis was originally carried out by using a calculation of the complex wavenumber. The formulas for the one- and three-dimensional wavenumbers were used as the vehicle for incorporating the one-dimensional results -- i. e., the approximations to boundary layer processes -- in the three-dimensional result. It is possible (see ref. 2-7) to construct a three-dimensional analysis with source terms on the surfaces, which will eventually combine all known linear results in a single analysis.

Perhaps the greatest advantage of working directly with the differential equations is that it has been possible to develop an approximate nonlinear analysis. This is described briefly in the following sections. The relationship (2.1.1) between the fractional rate of change of acoustic energy and the exponential rate constant is strictly a feature of linear behavior. It is likely, therefore, to be very difficult (if not impossible) to extend usefully to nonlinear behavior, an analysis founded only on the balance of acoustic energy.

#### 2.4 Nonlinear Analysis

Acoustic pressure oscillations in both rocket motors and T-burners normally reach a limiting amplitude after a period of growth. To reach a limiting amplitude requires a nonlinear mechanism, a process that depends nonlinearly on the amplitude. Although some theoretical and experimental studies have been performed, the precise mechanisms that lead to amplitude limiting have not yet been clearly defined. At the present time there are two ways of examining nonlinear behavior analytically: by an approximate analysis, refs. 2-11 and 2-12; or by applying a numerical calculation, refs. 2-13 to 2-17. To the present, very little quantitative nonlinear analysis has been done for T-burners, so the subject will be treated only briefly in this report.

2.4.1 Approximate Nonlinear Analysis. The approximate analysis discussed in refs. 2-11 and 2-12 was very strongly conditioned by the methods of linear analysis described in §2.2 and §2.3.1, and motivated

by the behavior observed in T-burners. The analysis was guided by the observation that very often it appears that the unstable oscillation consists essentially of a single mode having a well-defined frequency but amplitude changing in time. Figure 2.4-1 is an actual record taken from ref. 2-18. The harmonic variation of the pressure appears to be relatively clean with no overtones. Figure 2.4-2 shows the result of a harmonic analysis of the record reproduced in 2.4-1(a). Evidently, the proportion of oscillations at the higher frequencies is not necessarily negligible.

In ref. 2-12 the pressure field is represented essentially as a Fourier expansion in the normal modes in an attempt to simulate the harmonic content seen in T-burner records. The amplitudes and phases are time dependent, and must be determined. The problem is eventually reduced to solving a set of nonlinear equations representing a set of coupled nonlinear harmonic oscillators. A simplified method of solution has been worked out, and results can be obtained quite inexpensively. No detailed treatment of the behavior in T-burners is presently available. Preliminary comparison (ref. 2-19) with some exact solutions for special cases of instability in motors shows that the analysis may be acceptably accurate and eventually very useful. The main advantages of the approximate analysis, as compared with numerical analyses, is that it is vastly cheaper and can be more readily applied to three-dimensional problems.

These remarks on the approximate analysis are included here because of the potential value of this approach. To date, useful results are quite limited. Ultimately, the real value lies not so much in interpreting nonlinear behavior in T-burners as in understanding nonlinear processes in a more general way for application to motors.

2.4.2 Numerical Nonlinear Analysis. All the numerical solutions (refs. 2-13 to 2-17) are for one-dimensional problems, so the results must be compared with the analysis described in §2.2. The same sets of conservation equations are used. Only in refs. 2-13 and 2-14 have the influences of particulate matter been accounted for. Because the motions of the particles were calculated as part of the solution, the equations were not combined in the manner described in §2.2.

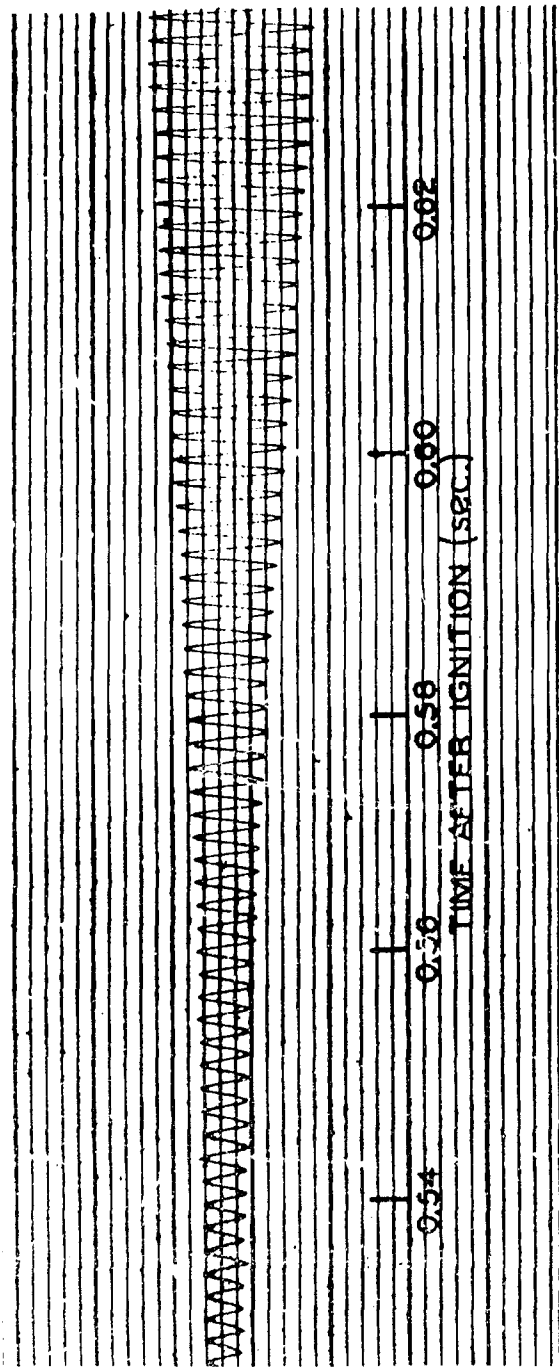


Figure 2.4-1 Typical Record of an Unstable Pressure Oscillation in a Variable Area T-Burner (ref. 2-18)

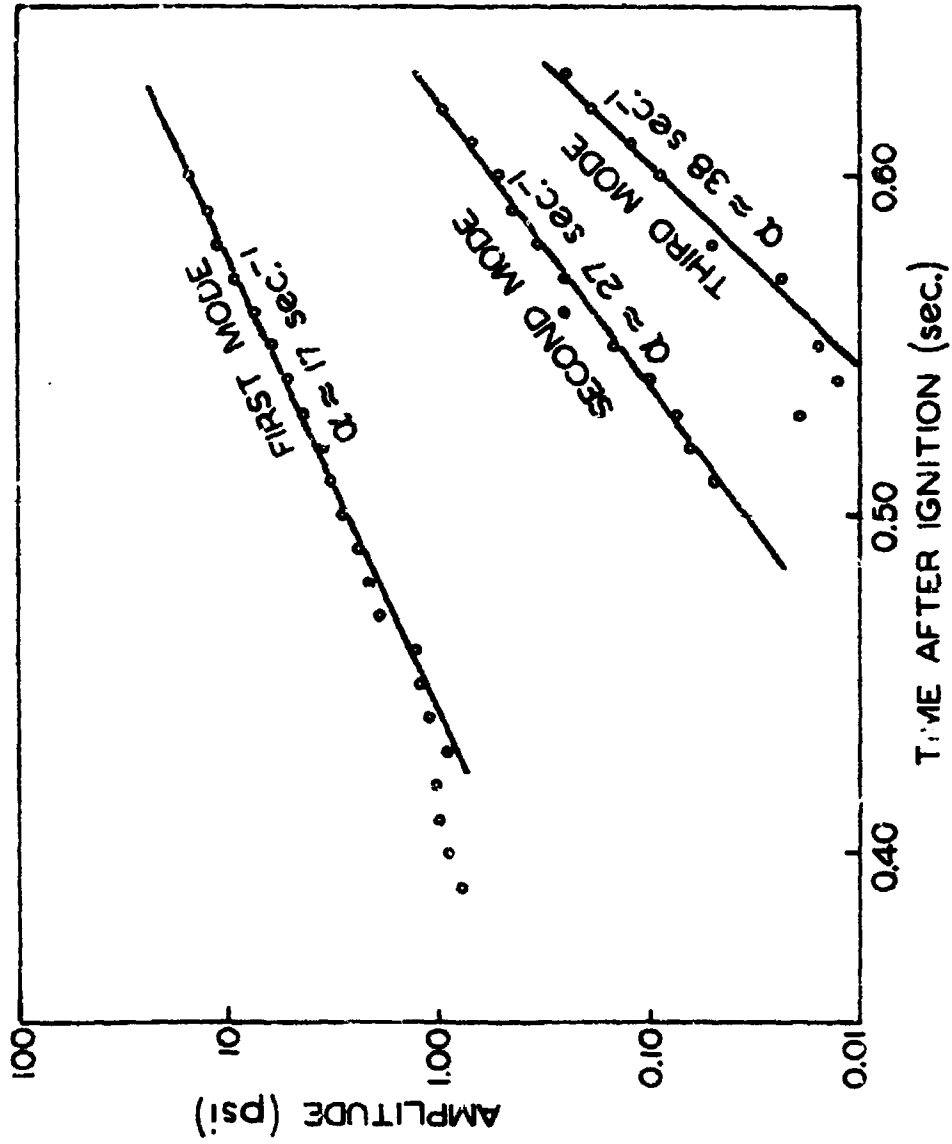


Figure 2.4-2 Spectral Analysis of the Record Shown in Figure 2.4-1  
(ref. 2-18)

A crucial part of the problem which has been properly included in refs. 2-13 to 2-16 is the transient behavior of the combustion response. Although it is possible to use only a crude model for coupling (see §2.6.1), it is necessary to represent the combustion processes by a frequency response which shows a peak, generally in the range of several hundred to perhaps two thousand Hertz. Another aspect is nonlinear behavior of the combustion response, which has been shown in ref. 2-14 to be very important under many circumstances.

Some numerical calculations have been done for T-burners in ref. 2-17; because the frequency dependence of the combustion response was ignored, the results are of limited value for comparison with experimental data. The computations do, however, provide some information in respect to the limitations of linear calculations. The analyses reported in refs. 2-14 to 2-16 can be extended to T-burners without fundamental complications.

#### 2.5 Calculation of the Acoustic Modes

It is clear from the discussions of §§ 2.2, 2.3, and Appendices E and F that to obtain numerical results for linear stability, one must have complete knowledge of the unperturbed acoustic modes. These are the normal (harmonic) modes of oscillation in a chamber having the same geometry as the T-burner, or motor, but in the absence of combustion and flow.

For simple geometries -- straight circular cylinders, for example -- the normal modes are easily computed. More difficult, but still amenable to analysis, are the longitudinal modes in a straight tube having nonuniform cross-sectional area. All other cases can be treated only numerically. Numerical calculations of the acoustic modes, and the analysis for one-dimensional modes, are discussed in Appendix C.

#### 2.6 Some Remarks on the Data Required for Analysis of Motors and

##### T-Burners

The T-burner has already been established as a useful device for quantitative testing of un-metallized propellants (ref. 2-2) and for qualitative testing of metallized propellants (ref. 2- ). But in order to perform a stability analysis of motors using metallized propellants, a considerable amount of quantitative information is required (refs. 2-20 to 2-22). The most pressing items are the response of surface combustion to an un-

steady flow field, and the losses associated with the particles in the combustion products. At the present time, it is not possible to compute a priori the combustion response for real propellants. Experimental determination is necessary. Currently, only the T-burner can provide this information.

However, to obtain quantitative results for the combustion response from T-burner firings, it is necessary to have not only an analytical framework within which data may be interpreted, but also certain other information which probably must be determined experimentally. The most important problems are the dissipation of energy due to particulate matter and the influence of the center vent or exhaust nozzle. Indeed, much of the need for the present report arises from difficulties associated with those two items.

It happens also that for predicting the stability of small disturbances in a motor, the losses due to particulate damping and the exhaust nozzle are two of the three dominant stabilizing mechanisms. The third -- which one must assume can be computed accurately -- is the "flow-turning" effect discussed in Appendix E. The point is, that the intensive attention given these questions in relation to T-burners, also produces very necessary information for the treatment of full-scale motors.

2.6.1 Response and Admittance Functions. There are two functions commonly used to describe the effect of small amplitude harmonic pressure fluctuations on the burning of a propellant; the response function  $R_b$  and the admittance function  $A_b$ :

$$R_b = \frac{\hat{m}_b / \bar{m}_b}{\hat{p} / p_0} \quad (2.6.1)$$

$$A_b = \frac{\hat{u}_b / \bar{a}}{\hat{p} / \bar{\gamma} p_0} \quad (2.6.2)$$

Note that a factor  $\bar{\gamma}$  appears in  $A_b$  but not in  $R_b$ , although in some discussions  $\bar{\gamma}$  is incorporated in  $R_b$ . As defined here,  $R_b$  equals  $n$ , the index in the burning rate law,  $r \propto p^n$ , for slow variations (i. e., at low frequencies).

The functions  $R_b$  and  $A_b$  defined here are for pressure coupling

only. Corresponding functions can be defined for velocity coupling to represent the influences of fluctuations of velocity parallel to the surface. The subject of velocity coupling is much more complicated and, while fundamentally important to many cases of instabilities, is very poorly understood. Most of this report will be concerned with pressure coupling only, but especially for long lateral grains in a variable area T-burner, the presence of velocity coupling should not be ignored. A discussion is given later in § 5.4.4.

It is an implicit assumption that the dynamical behavior of burning surfaces can be characterized by a response function which is essentially a property of the propellant. For a given propellant,  $R_b$  and  $A_b$  depend on frequency, pressure, and the temperature of the solid. All these variables can be controlled for T-burner testing. For practical purposes, one must then assume that the numerical values obtained in the laboratory can be applied to a motor. Probably the most important features which are different are the radiation flux incident upon the surface, and the total mass flux past the surface, both being usually larger in a motor.

The significance of velocity coupling is also related to the assumption noted. It is known that when the velocity parallel to the surface is unsteady, the response of surface combustion depends on both the steady and unsteady components of velocity. Consequently, the dynamical behavior will depend on the local environment in the motor. Laboratory testing to obtain the necessary information is then a much more difficult task.

It is mainly as a convenience that the response and admittance functions are introduced. Because the mass fluctuation ( $\hat{m}_b$ ) and velocity fluctuation ( $\hat{u}_b$ ) are not in general in phase with the pressure fluctuation,  $R_b$  and  $A_b$  are complex functions of frequency. The rate at which work is done (per unit area of surface) by the combustion processes on the acoustic waves in the chamber, is equal to the product the pressure fluctuation and component of velocity fluctuation in phase with the pressure:

$$\begin{aligned} \text{rate of doing work} \\ \text{per unit area} \end{aligned} = \hat{u}_b(r) \hat{p} = \frac{p_o \bar{a}}{\gamma} A_b(r) \left( \frac{\hat{p}}{p_o} \right)^2. \quad (2.6.3)$$

Consequently, the driving due to the burning surface is proportional to

the real part of the admittance function. Owing to interactions between the acoustic and mean flow fields, an additional term  $\bar{M}_b \equiv \bar{u}_b/\bar{a}$  arises, and as shown by the formulas deduced in Appendix E, the driving by surface combustion is proportional to  $A_b^{(r)} + \bar{M}_b$ . It is this combination which one wishes to obtain from T-burner data, and which is required for stability analysis of motors.

The mass flux and velocity are related by the definition  $m_b = \rho_g u_b$ . Thus, the admittance and response functions are not independent. A very simple calculation, outlined in Appendix E, leads to the identity

$$A_b + \frac{\bar{u}_b}{\bar{a}} = \bar{\gamma} \frac{\bar{u}_b}{\bar{a}} \left( R_b + \frac{\Delta\hat{T}/T_o}{\hat{p}/p_o} \right) \quad (2.6.4)$$

The temperature fluctuation  $\Delta\hat{T}$  is the difference between the actual temperature fluctuation at the edge of the combustion zone, and the isentropic temperature fluctuation accompanying the pressure fluctuation  $\hat{p}$ . Thus,  $\Delta\hat{T}$  is the non-isentropic part of the temperature fluctuation. An analysis producing  $R_b$ , such as those giving the formula (2.6.6) below, will also give a formula for  $\Delta\hat{T}$ . Because it is the combination (2.6.3) which appears in the stability analysis, it is convenient to use a single symbol. The real part is denoted in this work by  $B_e$  or  $B_s$ .

$$B_e = \left( A_b^{(r)} + \frac{\bar{u}_b}{\bar{a}} \right)_e \quad (\text{end-burning surfaces})$$

$$B_s = \left( A_b^{(r)} + \frac{\bar{u}_b}{\bar{a}} \right)_s \quad (\text{lateral or side-burning surfaces}) \quad (2.6.5)$$

A yet finer level of interpretation of data consists in correlating the measured values of  $R_b$  with a model. To the present, this has been attempted only for the model to which essentially all linear calculations reduce (ref. 2-23). The response function is then given by the relatively simple formula

$$R_b = n \frac{AB}{\lambda + \frac{A}{\lambda} - (A+1) + AB} \quad (2.6.6)$$

Here,  $n$  is again the pressure index and  $A$  and  $B$  are parameters\* depend-

---

\*The parameter  $B$  in (2.6.6) is of course not the same  $B$  defined by (2.6.5). No confusion should result because the formula (2.6.6) for the response function will not be used in this report.

ing on the chemical and physical properties of the propellant. The quantity  $\lambda$  is a complex function of the dimensionless frequency,  $\omega\kappa/\bar{r}^2$ . Plots of the real and imaginary parts of (2.6.4) may be found in many of the references cited (e. g. 2-1);  $R_D^{(r)}$  shows the qualitative behavior described above: In particular, there is a rather broad band of enhanced amplification. It is this function which has been used to represent the linear transient behavior in the calculations reported in refs. 2-13 to 2-16. Moreover, the only nonlinear calculations -- also discussed in those works -- rest essentially on the same basic assumptions.

While some attempts (refs. 2-24 and 2-25, for example) have been made to deduce the values of A and B from T-burner data, the problem will not be discussed in this report. Obviously, rather extensive measurements are required over wide ranges of both frequency and pressure. The formula (2.6.4) does not include the influence of a metal in the propellant, except for changes in the thermodynamic properties. No analysis of the influence of a metal additive on combustion processes has been done. Consequently, the value of trying to determine the parameters A and B is questionable.

#### 2.6.2 Dissipation of Acoustic Energy Due to Particulate Matter.

Two major sources of energy loss for unsteady motions in a solid propellant rocket motor are the exhaust nozzle and particles suspended in the gases. While the exhaust nozzle affects mainly longitudinal modes, the damping due to the particles tends to stabilize all modes. The attenuation varies strongly with frequency, and for a given particle size there is a frequency for which the attenuation is a maximum. For the particle sizes produced in motors, the optimum frequency is usually greater than, roughly, a kilohertz.

In T-burners, the energy losses associated with viscous forces and heat conduction at the lateral boundary may be important, but it appears that for metallized propellants these are dominated by particle damping. A second major source of loss -- at least for the even modes -- is the center vent, discussed in the following section. As implied several times in earlier discussion, the contribution to the growth constant  $\alpha$  from particle damping is sufficient that it must be known quite accurately to determine quantitatively the influence of the combustion processes.

Even if the T-burner is used for qualitative assessment of the behavior of propellants, at least a limited knowledge of particle damping must be available. It may be, for example, that different propellants produce different results in T-burner firings because the condensed products of combustion are different. An important advantage of testing with pulsed T-burners is that a more direct determination of particle damping can be obtained.

For these reasons, there has been and still is considerable concern with particle damping. Unfortunately, there are some serious uncertainties which are far from being satisfactorily clarified. The total weight fraction ( $C_m$ ) of particulate matter can be determined quite accurately from the composition of the propellant, but neither the size distribution nor the average size is well known. There is some basis for making rough assumptions about the size distributions, and some experimental information is available (see, for example, the recent work reported in refs. 2-26 to 2-28). But for the most part, the influence of the particles is interpreted in terms of a single average diameter,  $\bar{D}$ . It is then sufficient to use the simplest representations of particle damping, discussed in Appendix D. That practice will be followed throughout this report.

Much of the work which has been done on the problem of particle damping in T-burners is also relevant to the stability of motions in motors. However, one must bear in mind that for several reasons, the sizes of particles produced can be significantly different in different geometries. For example, both the average and oscillating flows may influence the behavior of the aluminum on the propellant surface. Residual combustion and/or agglomeration may affect the particle sizes in the gas phase. These problems are important, but remain unsolved.

2.6.3 The Influence of Exhaust Nozzles and Vents. Because the T-burners operate with a center nozzle or vent, work which has been done on sonic exhaust nozzles for motors (e. g. refs. 2-27 and 2-28) is inapplicable. Moreover, because the center vent is generally not choked, the problem of its influence on unsteady motions is difficult. Three extreme cases have arisen: that the vent may cause a gain of acoustic energy for the fundamental and odd modes, a formal result of the one-

dimensional analysis (ref. 2-5); that the vent may produce a substantial loss, in particular for the fundamental mode (ref. 2-9); and, what until fairly recently had been assumed without question, the vent has no effect on the fundamental and all odd harmonics.

These divergent possibilities are the substance of the problem associated with the treatment of the center vent. A more complete discussion will be found in Appendix G. It is an important question, because the values of the response function deduced from data depend directly on what contribution to the losses (or gains) is assigned to the vent. One definite statement can be made: there is no doubt that the center vent in any case is a source of significant energy loss for the even modes. The reason for this is that the pressure fluctuation at the vent is then large, and even in the absence of mean flow, radiation of energy from the vent is significant.

It must be emphasized that the corresponding problem of the exhaust nozzle for a motor is quite different and better understood. Calculations appear to give reasonably good results, at least for longitudinal modes. The reasons for difficulty with the center vent in a T-burner are that the flow is subsonic, and the average flow must turn into the direction normal to the direction of most of the acoustical motions.

#### REFERENCES

- 2-1 Culick, F. E. C. "Research on Combustion Instability and Application to Solid Propellant Rocket Motors," AIAA Paper 71-753, AIAA/SAE 7th Propulsion Joint Specialists Conference (June 1971).
- 2-2 "T-Burner Manual," CPIA Publication No. 191, CPIA, Silver Spring, Maryland (November 1969).
- 2-3 Cantrell, R. H. and Hart, R. W. "Interaction between Sound and Flow in Acoustic Cavities: Mass, Momentum, and Energy Considerations," J. Acoust. Soc. Amer., V. 36, no. 4 (April 1964), pp. 697-706.
- 2-4 Culick, F. E. C. "Interaction Between the Flow Field, Combustion and Wave Motions in Rocket Motors," NWC TP 5349, Naval Weapons Center, China Lake, Calif. (June 1972).
- 2-5 Culick, F. E. C. "The Stability of One-Dimensional Motions in a Rocket Motor," Combustion Science and Technology, V. 7, no. 4 (1973), pp. 165-175.

- 2-6 Culick, F. E. C. "Acoustic Oscillations in Solid Propellant Rocket Chambers," Astronautica Acta, V. 12, no. 2 (1966), pp. 113-126.
- 2-7 Culick, F. E. C. "Stability of Three-Dimensional Motions in a Combustion Chamber," to be published in Combustion Science and Technology (1974).
- 2-8 Hart, R. W. and McClure, F. T. "Theory of Acoustic Instability in Solid-Propellant Rocket Combustion," 10th Symposium (International) on Combustion, The Combustion Institute (1965), pp. 1047-1065.
- 2-9 Horton, M. D. and Coates, R. L. "T-Burner Experiments Compared with Theory," J. Spacecraft and Rockets, V. 11, no. 1 (January 1974), pp. 48-51.
- 2-10 Coates, R. L. and Horton, M. D. Private communication to F. E. C. Culick (1974).
- 2-11 Culick, F. E. C. "Nonlinear Growth and Limiting Amplitude of Acoustic Waves in Combustion Chambers," Combustion Science and Technology, V. 3, no. 1 (April 1971), pp. 1-16.
- 2-12 Culick, F. E. C. "Nonlinear Behavior of Acoustic Waves in Combustion Chambers," 10th JANNAF Combustion Meeting (Aug. 1973).
- 2-13 Levine, J. N. and Culick, F. E. C. "Numerical Analysis of Nonlinear Longitudinal Combustion Instability in Metallized Solid Rocket Motors," 9th JANNAF Combustion Meeting (Sept. 1972).
- 2-14 Levine, J. N. and Culick, F. E. C. "Nonlinear Longitudinal Combustion Instability in Solid Rocket Motors," 10th JANNAF Combustion Meeting (August 1973).
- 2-15 Kooker, D. E. and Zinn, B. T. "Numerical Solution of Axial Instabilities in Solid Propellant Rocket Motors," 10th JANNAF Combustion Meeting (August 1973).
- 2-16 Kooker, D. E. and Zinn, B. T. "Triggering Axial Instabilities in Solid Rockets: Numerical Predictions," AIAA Paper No. 73-1298, AIAA/SAE 9th Propulsion Joint Specialist Conference (Nov. 1973).
- 2-17 Coates, R. L., Kerzner, H., and Peterson, J. A. "Numerical Analysis of Solid Propellant Combustion Instability in T-Burners," AIAA Paper No. 73-1299, AIAA/SAE 9th Propulsion Joint Specialist Conference (November 1973).
- 2-18 Hercules, Inc. "Final Report for Subtask 2, T-Burner Analysis, of Task 5, Pressure Oscillation Study, Engineering Support on the Minuteman M-57A1 Rocket Motor," Report MTO-1124-55 (September 1971).

- 2-19 Culick, F. E. C and Levine, J. N. "Comparison of Approximate and Numerical Analyses of Nonlinear Combustion Instability," AIAA Paper No. 74-201, AIAA 12th Aerospace Sciences Meeting (February 1974).
- 2-20 Price, E. W. "Application of Combustion Instability Research," NWC TP 5603, Naval Weapons Center, China Lake, California (January 1974).
- 2-21 Culick, F. E. C. "Research on Combustion Instability and Application to Solid Propellant Rocket Motors," AIAA Paper No. 71-753, AIAA/SAE 7th Propulsion Joint Specialist Conference (June 1971).
- 2-22 Culick, F. E. C. "Research on Combustion Instability and Application to Solid Propellant Rocket Motors, II" AIAA Paper No. 72-1049, AIAA/SAE 8th Joint Propulsion Specialist Conference (November 1972).
- 2-23 Culick, F. E. C. "A Review of Calculations for Unsteady Burning of a Solid Propellant," AIAA J., V. 6, no. 12 (December 1968), pp. 2241-2255.
- 2-24 Beckstead, M. W. and Culick, F. E. C. "A Comparison of Analysis and Experiment for Solid Propellant Combustion Instability," AIAA J., V. 9, no. 1 (January 1971), pp. 147-154.
- 2-25 Brown, R. S., Muzzy, R. J., and Steinle, M. E. "Surface Reaction Effects on the Acoustic Response of Composite Solid Propellants," AIAA J., V. 6, no. 3 (March 1968), pp. 479-488.
- 2-26 Derr, R. L., Churchill, H. L., and Fleming, R. W. "Aluminum Behavior Near the Burning Surface of a Composite Propellant," 10th JANNAF Combustion Meeting (August 1973).
- 2-27 Eisel, J. L., Price, E. W., Stine, C. E., and Brown, B. G., "Pressure and Velocity Dependence of  $Al_2O_3$  Particles Produced During Solid Propellant Combustion," 10th JANNAF Combustion Meeting (August 1973).
- 2-28 Kraeutle, K. J. "The Analysis of Combustion Residues of Aluminized Propellants and Its Significance for the Study of Acoustic Damping," 10th JANNAF Combustion Meeting (August 1973).
- 2-29 Crump, J. E., Price, E. W., Mathes, H. B., and Dehority, G. L. "Oscillatory Combustion Experimentation and Analysis Work in Support of an Air Force Program, 1971-72," NWC-TP-5630 or AFRPL-TR-73-108 (June 1974), Naval Weapons Center, China Lake, Calif.

### 3. TEST METHODS

In this section, the different methods for T-burner testing are described in detail. The one-dimensional analysis, described in §2, is discussed and applied to these different methods to show how they can be used (1) for qualitative testing to determine the relative stability properties of propellants; and (2) for quantitative testing to determine the response parameters and damping required for the motor stability analysis described in §2.6.

The apparatus necessary to conduct T-burner tests is discussed in terms of the different methods. It is not recommended that the user of this report select a T-burner method and focus attention on subsections devoted to that method alone. Rather, a careful reading of this entire section is suggested so as to gain insight into the problems that can be encountered in T-burner testing with aluminized propellants. It is also recommended that the T-burner manual for un-aluminized propellants (ref. 3-1) be obtained for convenient reference while reading this section.

#### 3.1 General Description of Different Test Methods

With heavily aluminized propellants, the acoustic damping resulting from  $Al_2O_3$  product droplets is so high that spontaneous or self-excited oscillations will not occur in the T-burner unless relatively large burn surface area (sufficient for the combustion response to overcome the high damping) is used. Accordingly, the growth/decay method described in ref. 3-1 for non-aluminized propellants having an end disc configuration cannot be relied upon for the testing of aluminized propellants.

Two basic test approaches have been employed to study aluminized propellants in the T-burner. One is to pulse the T-burner with an auxiliary charge (pulser) and measure the decay rate of the resulting pressure oscillations; the other is to use sufficiently large propellant samples to induce spontaneous oscillations. In the latter case, the growth rate of pressure oscillations is measured. Based on these test approaches, three T-burner test methods have evolved.

3.1.1 Pulsed During Burning/After Burning (DB/AB) Method. In this method, auxiliary charges (pulses) are fired during burning and immediately after the propellant burnout (ref. 3-2). A direct analogy can be

drawn between the operation of the pulsed DB/AB method and the standard growth/decay method employed for non-aluminized propellant testing (ref. 3-1).

For non-aluminized propellants, acoustic energy gains normally exceed acoustic energy losses during propellant burning. Thus, spontaneous oscillation growth will occur followed by an oscillation decay when the propellant burns out. The net acoustic gains are measured from the growth of oscillations during burning and the acoustic losses are measured from the decay of oscillations at burnout. The difference between the growth and decay rates is indicative of the combustion response.

Similar data are obtained from the pulsed DB/AB method. The first pulse, during burning, corresponds to the growth period in the growth/decay method; and the second pulse, immediately after propellant burnout (when the burner is presumably still filled with a normal distribution of  $Al_2O_3$  droplets), corresponds to the decay period in the growth/decay method. For the pulsed DB/AB method, the difference between the decay rates measured during and after burning is indicative of the combustion response.

3.1.2 Variable-Area T-Burner (VATB) Method. In this method, propellant samples are used having sufficiently large burn area to provide spontaneous pressure oscillations in the T-burner (refs. 3-3 to 3-6). Tests are conducted with different propellant surface areas and the net acoustic energy gains are measured from the rate of oscillation growth. If the rate of oscillation growth is plotted as a function of propellant burn area at the time of oscillation growth, the slope of the curve is indicative of combustion response and the extrapolated intercept at zero burn area is indicative of acoustic energy losses (or damping) in the T-burner. This method of T-burner testing is described in ref. 3-1 as an alternate to the growth/decay method for non-aluminized propellants.

For testing of non-aluminized propellants, end discs of propellants can be used. The sample area on each end of the burner ranges from the value of the burner cross-sectional area down to the lowest value for which oscillations occur spontaneously in the T-burner. For testing of highly aluminized propellants, however, samples having burn area larger than the cross-sectional area of the burner are required for spon-

taneous oscillations. Thus, cylindrical or cup-shaped propellant samples are normally required for the VATB method when aluminized propellants are tested.

### 3.1.3 Pulsed - Variable Area T-Burner (Pulsed-VATB) Method.

This method is essentially the same as the VATB method. However, here tests are conducted with propellant samples having a burn area less than that required for spontaneous oscillations in the T-burner. For these test conditions, the T-burner is pulsed during burning and the net acoustic energy losses during burning are measured from the rate of oscillation decay. These decay rate data are plotted as a function of sample burning area; the combustion response and the T-burner damping are inferred from these data as described for the VATB method.

Because analysis of data from the VATB and pulsed-VATB method are the same, these methods will be described under the general heading of VATB Method in most discussions that follow. In practice, data from both of these methods are combined and analyzed to obtain instability characteristics for an aluminized propellant. The important advantage gained from using both techniques is that a greater range of burning surface area is covered. This produces better quantitative results, as later discussions will show.

## 3.2 Applications of the One-Dimensional Analysis to T-Burner Testing

3.2.1 Description of Methods in Terms of the One-Dimensional Analysis. The net acoustic energy gains (or losses) associated with linear combustion pressure oscillations in a T-burner are represented by a growth constant  $\alpha$ . A formula for  $\alpha$  is derived in Appendix E and has been quoted above as Eq. (2.2.3).\*

$$\alpha = \left\{ \left( \frac{\omega}{K_t e_t} \right) \left[ \frac{S_{be1}}{S_{co}} + \cos^2(\beta K_t) \frac{S_{be2}}{S_{co}} \right] \right\} B_e + \left\{ \left( \frac{\omega}{K_t e_t} \right) (C_t) \left( \frac{S_{bs}}{S_{co}} \right) \right\} B_s + \alpha_m + \alpha_d$$

acoustic driving from end-  
burning surfaces

acoustic burning from side-  
burning surfaces

(3.2.1)

\* An additional contribution from velocity coupling will be discussed in §5.4.4; see Eq. (5.4.6).

$$\alpha_m = -\frac{\bar{u}_b}{L} \frac{S_{bs}}{S_{co}} \frac{g_t}{c_t^2} (FT) + 2 \frac{\bar{u}_b}{L} \frac{S_b}{S_{co}} (C_t^0)^2 (VF) \quad (3.2.2)$$

The parameters shown in this equation are defined in Table 3.2-1. The first term in  $\alpha_m$  arises from losses associated with the flow in at the lateral burning surface, and the second term arises from the vent. The vent factor, VF, is introduced to account for present uncertainties in the T-burner acoustic analysis (see Appendix G). The factor FT is shown because in some treatments of the data it has been included as a floating parameter; see §6.2. Here and elsewhere, the Mach number is by definition the ratio of the speed of gases leaving the burning surface, and the average speed of sound in the mixture:  $\bar{M}_b = \bar{u}_b / \bar{a}$ .

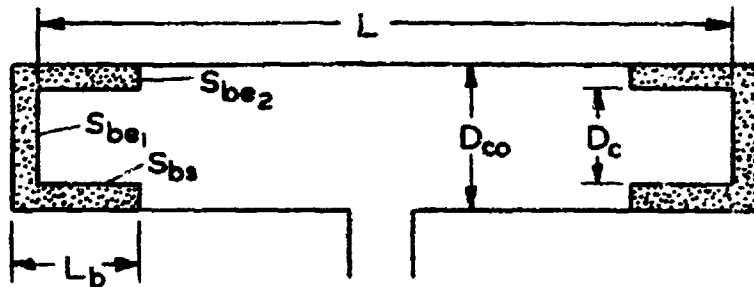
Three quantities in this equation characterize the stability properties of an aluminized propellant used in a T-burner:  $B_e$ ,  $B_s$ , response functions for pressure coupling; and  $\alpha_d$ , the net acoustic damping, mainly due to condensed material suspended in the gas. A fourth parameter, characterizing the response to velocity coupling, will be introduced in §6.2. The response functions provide a measure of the damping characteristics of the propellant, and the net acoustic damping provides a measure of the aluminum oxide droplet size created by the burning propellant. In addition, the quantities FT and VF shown in Eq. (3.2.2) might be regarded as parameters; the values deduced from the one-dimensional computations must be approximate at best.

If the acoustic energy gains associated with end- and side-burning surfaces could be measured during the growth of oscillations in a T-burner, calculation of the two response functions would be a simple matter. Unfortunately, a method for direct measurement of these quantities is not known. T-burner data consist of net acoustic energy gains during growth of oscillation amplitude or net losses during decay of oscillations. The different T-burner methods represent different approaches that have been followed to infer the parameters of interest from these net acoustic energy measurements. In the following, the pulsed (DB/AB) and VATB methods are described in terms of Eq. (3.2.1).

#### 3.2.1.1 Pulsed during burning/after burning (DB/AB) method.

For this method, the net acoustic energy decay rates during and after burning are measured. For the case of propellant discs located at

Table 3.2.1 Definition of Parameters Contained in Eqs. (3.2.1) and (3.2.2)



symbol	definition
1. parameters determined from correlation of T-burner data	
$B_e$	response function for end-burning surfaces (Eq. E-36 of Appendix E)
$B_s$	response function for side-burning surfaces (Eq. E-37 of Appendix E)
$\alpha_d$	net acoustic damping in the T-burner
2. acoustic energy quantities measured in a T-burner test	
$\alpha$	net growth (or decay) constant for pressure oscillations (§5.1)
$\omega$	angular frequency of pressure oscillations (§5.1)
3. parameters calculated from the T-burner geometry	
$K_l$	normalized wave number (Eq. C.12 and Fig. C-2 of Appendix C)
$e_l^2$	mean acoustic energy correction factor (Eq. C.14 and Fig. C-8 of Appendix C)
$C_l$	amplitude correction for side-burning surfaces (Eq. C.16 and Fig. C-11 of Appendix C)
$C_l^0$	mode shape correction factor (Eq. C.11 and Fig. C-6 of Appendix C)
$g_l$	flow turning factor (Eq. C.15 and Fig. C-10 of Appendix C)
$\beta$	normalized grain length ( $\beta = 2L_b/L$ )
$S_{be}$	end-burning area ( $S_{be1} = \pi D_c^2/4$ , $S_{be2} = 2(D_{co}^2 - D_c^2)/4$ )
$S_{bs}$	side-burning surface of one grain ( $S_{bs} = \pi D_c L_b$ )
$S_{co}$	cross-sectional area of T-burner chamber ( $\pi D_{co}^2/4$ )
$S_c$	cross-sectional area of grain bore ( $\pi D_c^2/4$ )

each end of the T-burner, the net acoustic energy loss for the pulse during burning is

$$\alpha_1 = 4f \left( \frac{S_{bel}}{S_{co}} \right) B_e + 4f \bar{M}_b \left( \frac{S_{bel}}{S_{co}} \right) VF + \alpha_d. \quad (3.2.3)$$

The net loss for the pulse after burning is

$$\alpha_2 = \alpha_d, \quad (3.2.4)$$

where it is assumed that mean burning and mean flow from the T-burner flow has ceased at the time of the second pulse\*.

If the crucial assumption is made that the magnitude and mechanism of acoustic energy losses represented by  $\alpha_d$  are the same for both pulses, the response function for end-burning surface can be calculated as

$$B_e = \frac{\alpha_1 - \alpha_2}{4f (S_{bel}/S_{co})} - \bar{M}_b (VF). \quad (3.2.5)$$

In a similar manner, the response function for side-burning surfaces can be determined from pulsed (DB/AB) tests using short ( $\beta \ll 1$ ), flush ( $S_{co}/S_c = 1.0$ ) cylinders. Thus,

$$B_s = \frac{\alpha_1 - \alpha_2}{4f (S_{bs}/S_{co})} - \bar{M}_b (VF). \quad (3.2.6)$$

In principle, therefore, the pulsed (DB/AB) method can be employed to measure directly the net acoustic damping in the T-burner,  $\alpha_d$ , and measure data necessary to infer the two response functions  $B_e$  and  $B_s$ .

### 3.2.1.2 Variable-area T-burner (VATB) method.

There are several methods of using Eq. (3.2.1) to interpret VATB test data. These are distinguished by the propellant grain configurations

---

\* Test procedures for determining the optimum time for the second pulse are given in §3.3.3; additional comments pertaining to mean flow conditions are given in §7.

used in the T-burner and the assumed form of  $\alpha_d$ . In one method (refs. 3-1, 3-4, and 3-5), the crucial assumption is made that the magnitude and mechanism of acoustic energy losses represented by  $\alpha_d$  are independent of changes in propellant geometry. In other words,  $\alpha_d$  is assumed constant over the area ratio variations considered in a VATB test series. In the second method (refs. 3-5, 3-6), the dependence of  $\alpha_d$  on changes in frequency is taken into account, but the losses are still assumed constant with area ratio.

In the following, the VATB method is described in terms of different grain geometries with  $\alpha_d$  assumed constant. The method of data analysis where  $\alpha_d$  is treated as a frequency-dependent variable is discussed separately.

(a) cylindrical grains. One propellant grain configuration that can be used in the VATB is the cylinder, where  $S_{be}/S_{co} = 0$  and  $S_{bs}/S_{co} \neq 0$ . In this case, Eq. (3.2.1) can be written as\*

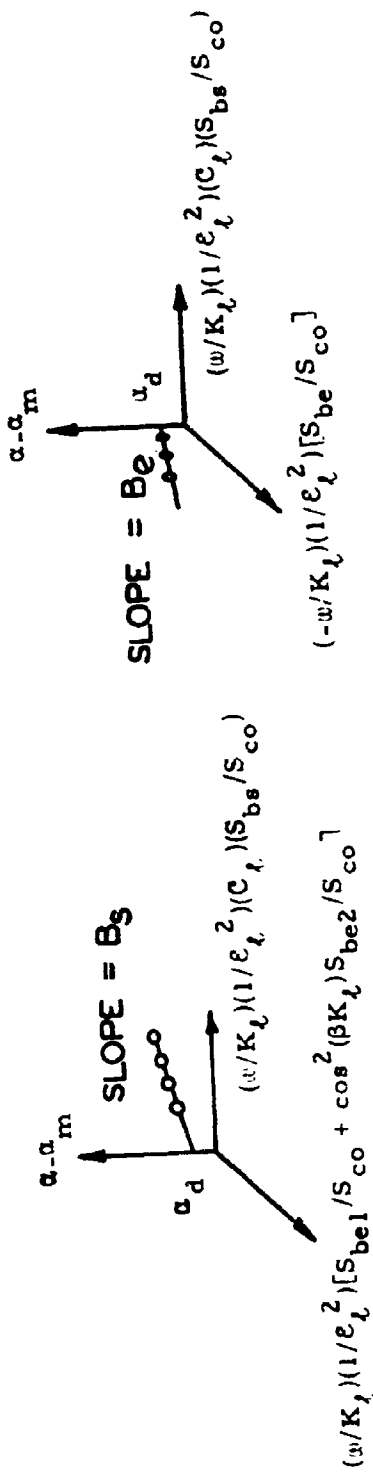
$$\alpha - \alpha_m = \left\{ \left( \frac{\omega}{K_t} \right) \left( \frac{1}{e^2} \right) (C_t) \left( \frac{S_{bs}}{S_{co}} \right) \right\} B_s + \alpha_d \quad (3.2.7)$$

The form of this equation is that of a straight line if  $\alpha_d$  and  $B_s$  are assumed constant. The coordinates are  $(\alpha - \alpha_m)$  versus the bracketed term in front of  $B_s$ ; the slope of the line is  $B_s$ ; and the intercept of the line on the  $(\alpha - \alpha_m)$  axis is  $\alpha_d$ , as shown in Figure 3.2-1(a). Since a VATB test series provides data consisting of the growth constant,  $\alpha$ , for different area ratios,  $S_{bs}/S_{co}$ , these can be plotted on this coordinate system, and both  $B_s$  and  $\alpha_d$  determined by fitting a straight line through the data. It should be noted that a large extrapolation could be necessary to determine  $\alpha_d$  if large area ratios,  $S_{bs}/S_{co}$ , are required for self-excited oscillations in the T-burner. This problem can be eliminated if the T-burner is pulsed at lower area ratios. It can be seen that the use of cylindrical grains alone provides a value for net damping,  $\alpha_d$ , and only one of the important response parameters (viz.,  $B_s$ ).

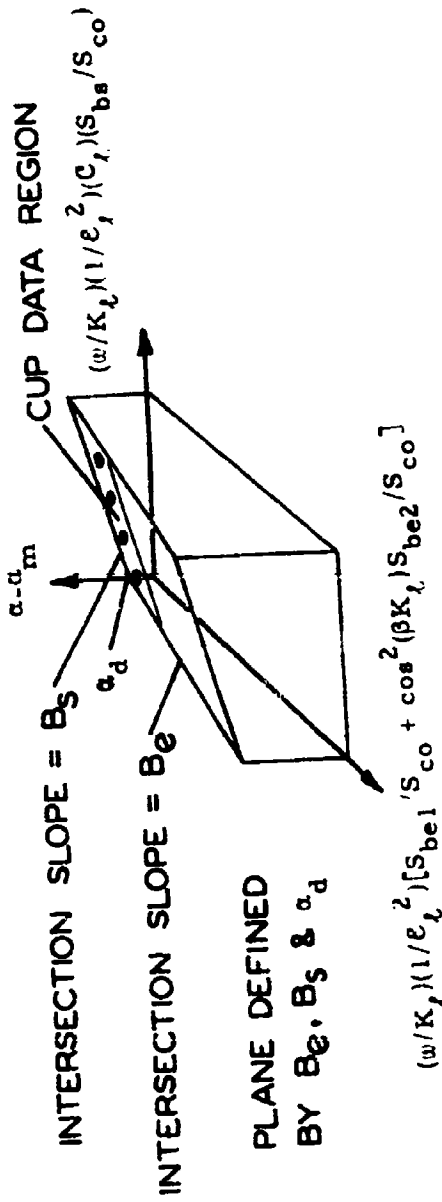
(b) end disc grains. For propellant grains that have end-burning surfaces only (viz., discs), the net acoustic energy gains in the VATB are given as

---

\* FT and VF have been assumed to be known when this approach was used.



(a) CYLINDER DATA ( $S_{be}/S_{co} = 0$ )



(b) END-DISC DATA ( $S_{bs}/S_{co} = 0$ )

Figure 3.2-1 Graphical Examples of the Correlation of T-Burner Data.

$$\alpha - \alpha_m = \left\{ \left( \frac{w}{K_t} \right) \left( \frac{1}{\ell^2} \right) \left( \frac{S_{be1}}{S_{co}} \right) \right\} B_e + \alpha_d \quad (3.2.8)$$

Here, the coordinates for plotting the VATB data are  $(\alpha - \alpha_m)$  and the bracketed term in front of  $B_e$ . The data should fall along a straight line of slope  $B_e$  and the line should intercept the  $(\alpha - \alpha_m)$  axis at  $\alpha_d$ , as shown in Figure 3.2-1(b). Again, it must be assumed that the response parameter (in this case,  $B_e$ ) and  $\alpha_d$  are constants. In general, the use of end discs in VATB testing for metallized propellants will not provide sufficient acoustic energy gains to exceed net damping in the T-burner. As a result, pulse testing must be relied upon for data that would be correlated in this manner. Accordingly, the use of end discs alone in the variable-area method must be categorized under the pulsed variable-area method.

(c) cup grains. For propellant grains that have end- and side-burning surfaces (viz., cups), Eq. (3.2.1) cannot be simplified to permit analysis on a two-dimensional plot. In terms of the plots described for the two previous cases, VATB data resulting from cups can be plotted in three-dimensional space having the coordinates shown in Figure 3.2-1(c). The data should define a plane having slopes

$$B_s \text{ in the } \alpha - \alpha_m \text{ versus } \left( \frac{x}{K_t} \right) \left( \frac{1}{\ell^2} \right) (C_t) \left( \frac{S_{bs}}{S_{co}} \right) \text{ plane,}$$

(3.2.9)

and

$$B_e \text{ in the } \alpha - \alpha_m \text{ versus } \left( \frac{w}{K_t \ell^2} \right) \left[ \frac{S_{be1}}{S_{co}} + \cos^2(\beta K_t) \frac{S_{be2}}{S_{co}} \right] \text{ plane.}$$

Cup grains seem appealing for VATB testing because, theoretically, both the end and side response parameters ( $B_e$  and  $B_s$ ) can be evaluated from a VATB test series. However, it has been found that there is insufficient variation in the end area ratio,  $S_{be}/S_{co}$ , to provide adequate data to define accurately the orientation of the data plane within the  $B_e$  plane.\* Thus, this approach to VATB must be viewed with skepticism until test procedures are improved. This aspect of VATB testing is discussed in §3.2.3.2.

\*Through statistical analysis of 104 VATB datum points, reasonable values of  $B_e$  have been obtained (ref. 3-7). The number of VATB tests required to obtain this set of data is considered prohibitive in terms of cost to determine the response function for a propellant at one pressure and frequency.

(d)  $\alpha_d$  assumed to vary with frequency. If the assumption is made that the net damping in the T-burner is due to particle damping only, the expression for  $\alpha_p$  given in Appendix D as Eq. (D. 24):

$$\alpha_p = -\frac{1}{Z} \left( \frac{C_m}{1+C_m} \right) \left\{ \frac{\omega^2 \tau_d}{1+\omega^2 \tau_d^2} + (\bar{\gamma}-1) \frac{C}{\bar{C}_p} \frac{\omega^2 \tau_t}{1+\omega^2 \tau_t^2} \right\}$$

where

$$\tau_d = \frac{\rho_s \sigma^2}{18\mu} \quad \text{and} \quad \tau_t = \frac{3}{Z} \frac{C}{C_p} Pr \tau_d.$$

The correlation of VATB results in the determination of a mean particle diameter,  $\sigma$ , rather than  $\alpha_d$ . The effect of this substitution is to take into account variations in  $\alpha_d$  due to frequency changes that occur during a VATB test series; such variations in frequency result from changes in the gas/particle speed of sound and mode distortions which are dependent upon the propellant grain geometry. An example of this approach to correlating VATB data is presented in ref. 3-6.

### 3.2.2 Applications of the T-burner to Obtain Qualitative Data.

One important purpose of conducting T-burner tests is to establish the relative stability properties of two propellants. This use of the T-burner has been encountered in several different types of studies.

(a) Quality control of production propellants. When a rocket motor is marginally stable, the T-burner can be used to identify changes in stability behavior arising from changes in the propellant response or damping characteristics. The effect of mix-to-mix as well as lot-to-lot variations on motor stability can be determined with the T-burner at relatively low cost (ref. 3-8).

(b) Systematic variations in propellant ingredients. In the pursuit of propellant additives that minimize propellant response or maximize damping, the T-burner can be used to measure relative changes in these properties for systematic changes in ingredients (refs. 3-9 and 3-10).

(c) Optimum motor conditions for minimizing instability. T-burner tests can be employed to determine the dependence of propellant response on frequency and pressure. More specifically, the pressure and frequency where the response is maximum can be determined. Based

on these data, changes can be made to an unstable motor to minimize the risk of instability.

For quantitative T-burner testing, it is assumed that changes in either one of the response functions,  $B_e$  or  $B_s$ , are indicative of the overall propellant response. As described below, additional assumptions are made regarding the form of the mean flow/acoustic interaction term,  $\alpha_m$ . These assumptions may not be justified for the quantitative determination of the response functions  $B_e$  and  $B_s$ , but for relative comparison of propellant response, no large error is introduced into the results.

### 3.2.2.1 Pulsed during burning/after burning (DB/AB) method.

For this test method, either end disc or cylinder grains can be used at each end of the T-burner with area ratio  $S_b/S_{co}$  approximately unity. Assuming that the mean flow/acoustic interaction term is zero, and noting that  $C_\lambda$  is unity and mode distortion is minimal for short cylinders and end discs, Eq. (3.2.1) is written as

$$\alpha = 4f \frac{S_{be}}{S_{co}} B + \alpha_d, \quad (3.2.10)$$

where  $B \equiv B_e = B_s$ .

The net acoustic loss resulting from the pulse during burning is

$$\alpha_1 = 4f \frac{S_{be}}{S_{co}} B + \alpha_d.$$

The net acoustic loss resulting from the pulse after burning is

$$\alpha_2 = \alpha_d.$$

By assuming that the acoustic damping during burning is equal to that after burning, the propellant response is

$$B = \frac{\alpha_1 - \alpha_2}{4f(S_{be}/S_{co})}. \quad (3.2.11)$$

In practice, the first term on the right hand side of Eq. (3.2.10) is usually referred to as the "combustion alpha" or  $\alpha_c$ . Thus, the alternative response parameter used for comparing the stability properties of different propellants is

$$\alpha_c = \frac{\alpha_1 - \alpha_2}{S_b / S_{co}} \quad (3.2.12)$$

Qualitative tests using the pulsed DB/AB method provide, therefore, a direct measurement of the acoustic damping (approximately the particulate damping) in the T-burner and the response function, B, or the combustion alpha,  $\alpha_c$ , for the propellant. Data of this type may be found in ref. 3-11.

3.2.2.2 Variable-area T-burner method. Qualitative data are obtained from the VATB method by assuming a value for the vent factor, VF, and testing with cylinders of different lengths; the growth alphas are correlated using Eq.(3.2.7) to obtain the response function, B, and the net damping in the T-burner,  $\alpha_d$ . For relating the response function B to the combustion alpha  $\alpha_c$ , the following expression is obtained from Eqs. (3.2.11) and (3.2.12):

$$\alpha_c = 4fB .$$

3.2.3 Application of the T-Burner to Obtain Quantitative Data. The T-burner can be employed to determine the end- and side-burning response parameters ( $B_e$  and  $B_s$ ) for use in the three-dimensional stability analysis, described in §2.3. The approaches of T-burner testing to obtain quantitative data of this type are not markedly different from those outlined in the preceding section for determining qualitative data. The primary difference is in how the one-dimensional theory is used to correlate the data.

3.2.3.1 Pulsed during burning/after burning (DB/AB) method.

In this method, end discs must be used in tests to determine  $B_e$  and cylinders for tests to determine  $B_s$ . The test approach is that described in §3.2.1. It should be noted that the vent factor, VF, must be known before  $B_e$  and  $B_s$  can be evaluated. A discussion of this factor is given in Appendix G.

3.2.3.2 Variable-area T-burner method.

Testing with the VATB method for quantitative data is accomplished as described in §3.2.2. Again, a value for the vent factor, VF, is necessary to use this method. Cylindrical grains can be used to obtain

$B_s$ . Ideally, end discs of varying area ratio,  $S_{del}/S_{co}$ , or cups of varying length can be used to obtain  $B_e$ . Unfortunately, correlation of data to obtain  $B_e$  has not been successful; variable-area testing using end discs is not promising because of the small contribution from the partial end discs. Thus, the VATB method is limited to obtaining  $B_s$  and  $\alpha_d$ . The response function due to end burning surfaces can be obtained from pulsed DB/AB testing.

### 3.3 Pulsed During Burning/After Burning (DB/AB) Method

In this subsection, the pulsed DB/AB method of testing aluminized propellants is described in detail.

3.3.1 Hardware Configuration. The basic hardware for the pulsed DB/AB method is essentially the same as that described in the T-burner manual for un-aluminized propellants (ref. 3-1). In the following, specific features of hardware necessary for testing with the pulsed DB/AB method are discussed. Design details pertaining to T-burners utilized in pulsed DB/AB testing can be found in refs. 3-11, 3-12, and 3-13.

#### 3.3.1.1 T-burner chambers.

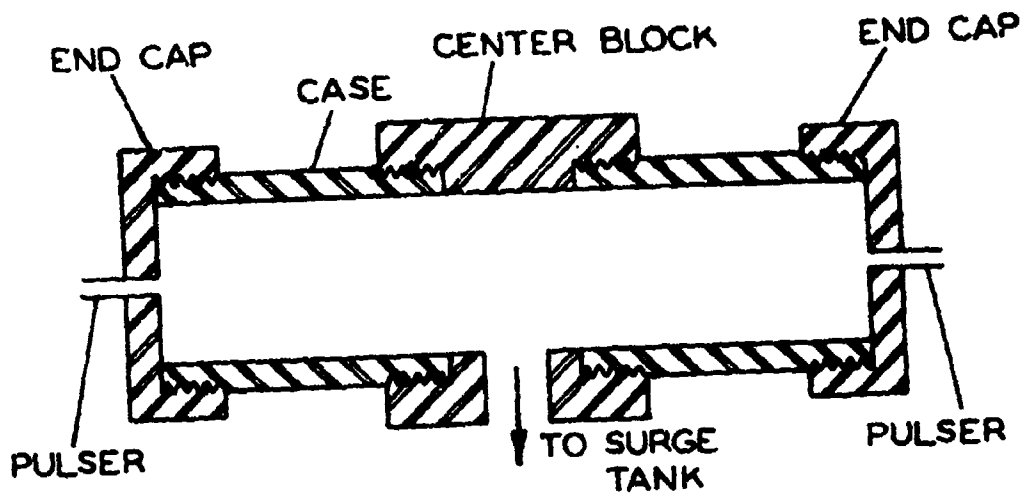
Pulsed DB/AB testing has been done with T-burner chambers having 1.5 in. diameter (refs. 3-11, 3-12, 3-13). A detailed discussion of factors to be considered in selecting the chamber diameter is given in §3.4.1.1. In one configuration, the T-burner chambers are coupled to a center block that contains the T-burner vent as shown in Figure 3.3-1(a). This approach allows variations in T-burner length (for changes in frequency) by leaving the center block mounted in place and replacing the chambers with those having the desired length.

In a second configuration, the T-burner chambers are a single tube with an exhaust tube attached at the vent location, as shown in Figure 3.3-1(b).

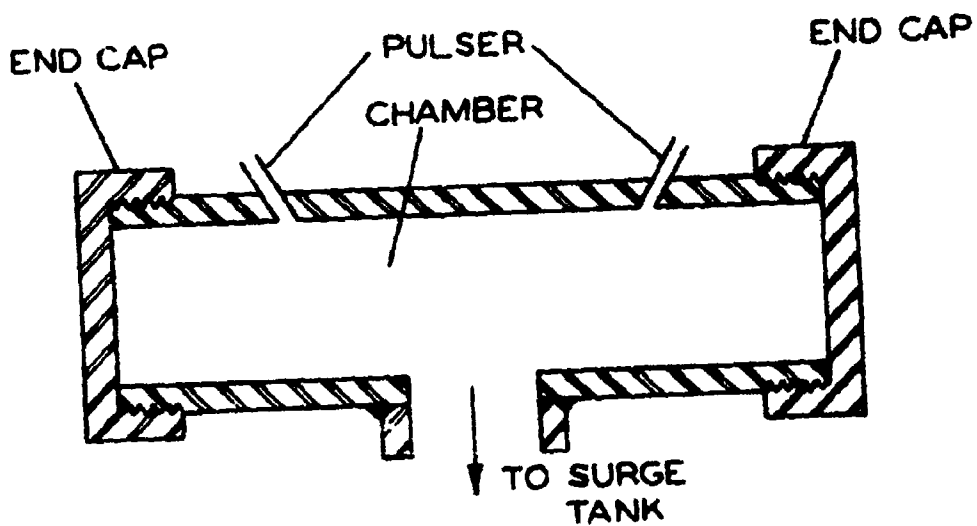
The T-burner test frequency is determined by the length of the T-burner chambers,  $L$ , and the speed of sound of the gas/particle mixture in the T-burner,  $\bar{a}$ :

$$f_o = \bar{a}/2L \quad (\text{Hz}) .$$

Since the speed of sound of the gases in the T-burner is influenced by heat loss to the walls, it cannot be calculated accurately. A plot of ob-



(a)



(b)

Figure 3. 3-1 Typical T-Burner Hardware for Pulsed DB/AB Testing

served frequency versus T-burner length is presented in Figure 3.3-2 to aid in the selection of T-burner lengths when a particular frequency is of interest. Note that this figure is for one propellant and should therefore be used only as a guide. Both the speed of sound itself and the change with length will depend on the composition of the propellant.

Recommendations: Either of the two T-burner chamber configurations shown in Figure 3.3-1 is recommended for pulsed DB/AB testing. The single-tube configuration has a smooth interior wall that does not introduce acoustic losses due to cross-sectional area discontinuities; however, if designed and machined properly, the multiple chamber/center block configuration is not susceptible to these type losses. A chamber diameter of 1.5 in. is recommended for the pulsed DB/AB T-burner.

#### 3.3.1.2 Surge tank.

A surge tank is recommended for pulsed DB/AB testing. The surge tank is normally coupled to the T-burner with a heat exchanger tank between the surge tank and T-burner, as shown in Figure 3.3-3. The heat exchanger reduces the temperature of the combustion products and, therefore, serves to decrease the pressure build up in the overall system by extracting thermal energy from the gases. The heat exchanger can be a small tank packed with a bed of chain.

If pressurizing gases are to be stored in the surge tank between tests, it is recommended that the valve that isolates the surge tank from the T-burner be between the heat exchanger and surge tank, as shown in Figure 3.3-3. In this way, the heat exchanger will trap a large fraction of the aluminum oxide in the exhaust products and minimize wear to the valve seat.

The heat exchanger and surge tank system used at one pulsed DB/AB T-burner installation consists of a 1 cubic ft. chamber packed with 35 lbs. of iron chain for the heat exchanger and a 5.76 cubic ft. chamber for the surge tank. This installation also has a "uniflow" section which is detailed in Figure 3.3-3. The series of cones with 5/8 in. diameter openings permit unrestricted flow from the T-burner to the surge tank system; however, due to the spaced conical arrangement, backflow from the surge tanks to the burner is impeded. This feature eliminated a problem of low frequency burner - tank coupled oscillations

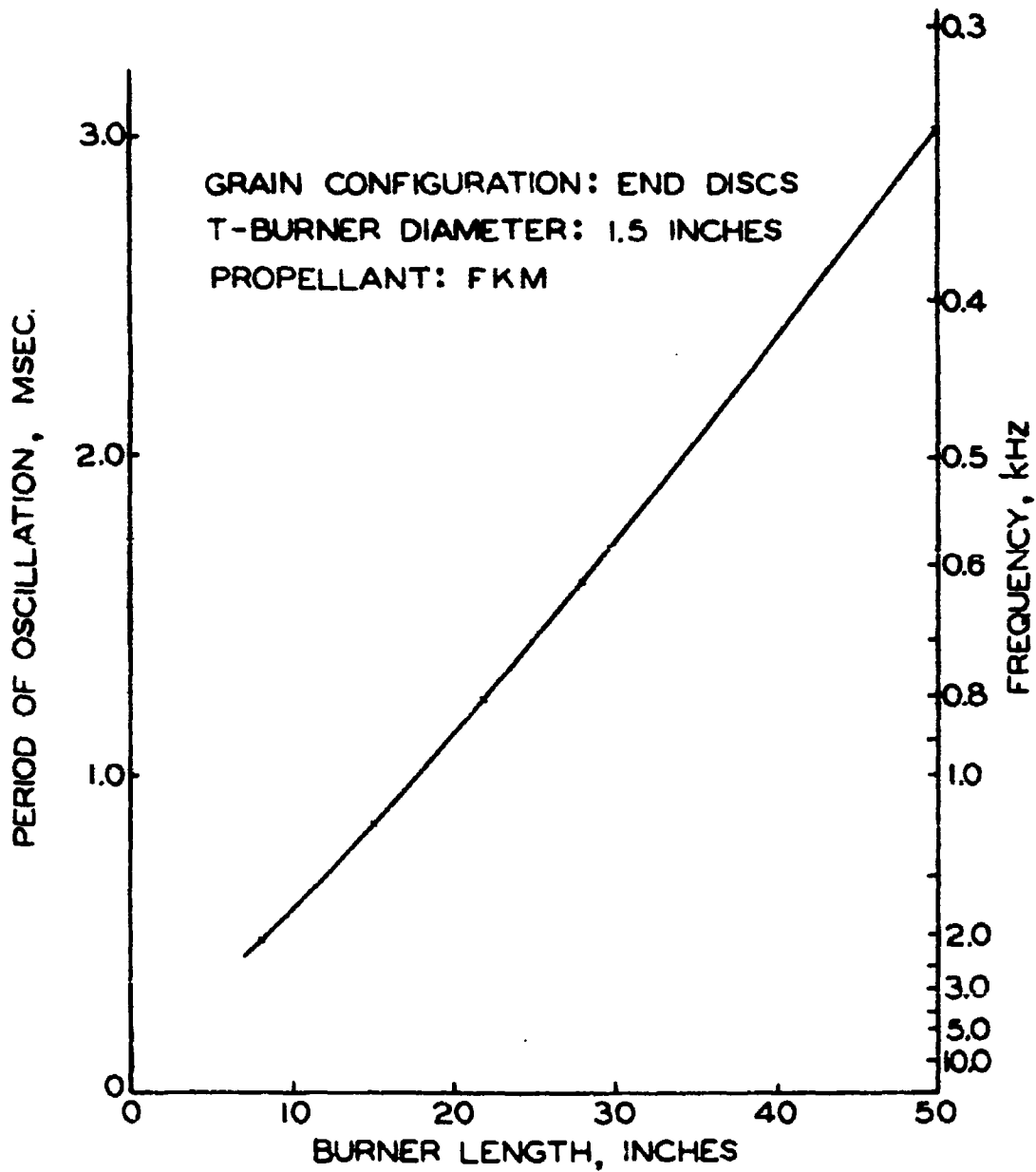


Figure 3.3-2 Observed Frequency Versus Length of T-Burner. Data Are for a Metallized Composite-Modified Double-Base Propellant ( data supplied by Naval Weapons Center)

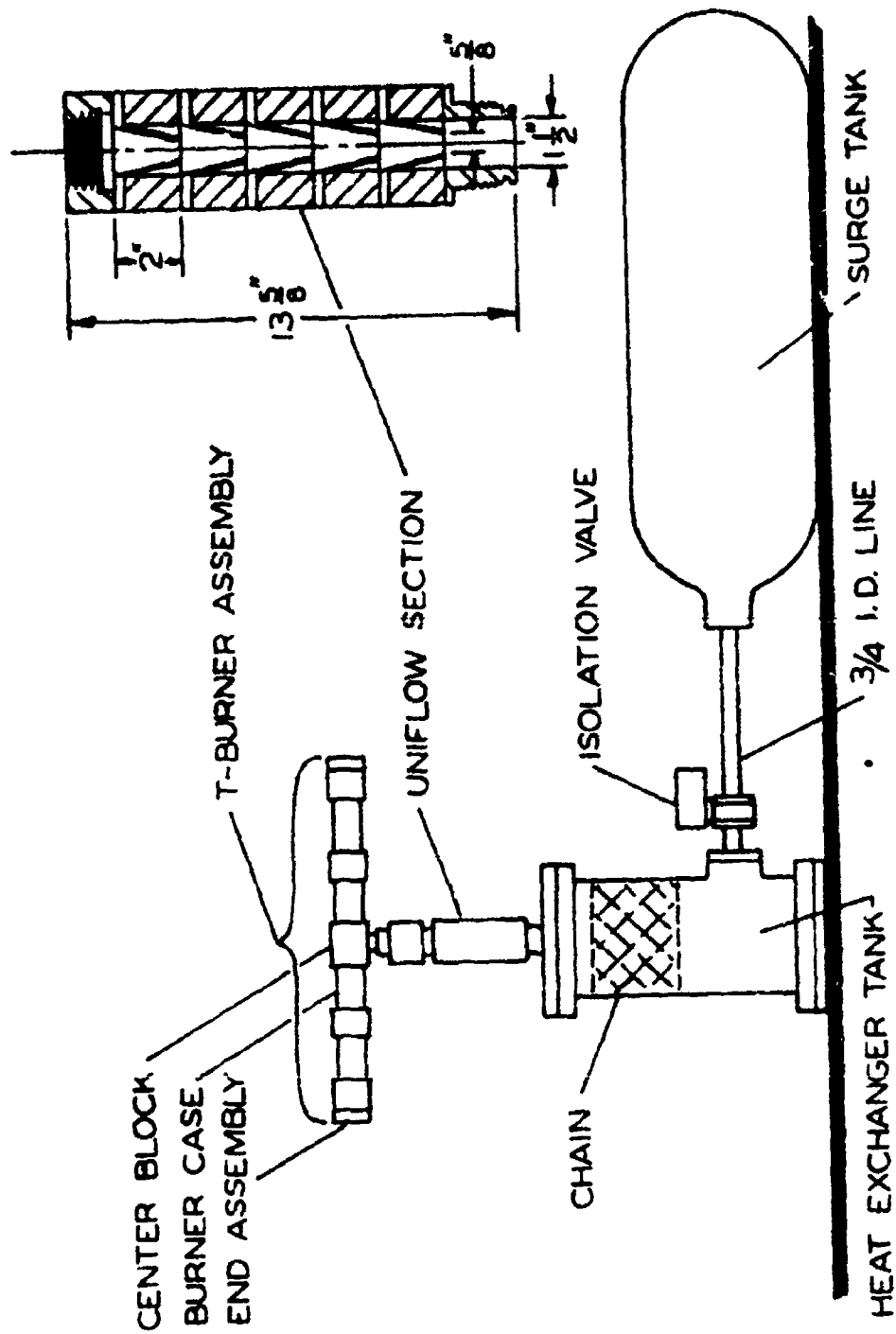


Figure 3. 3-3 Typical Surge Tank System for Pulsed DB/AB Testing

stimulated by the pulse under some burner test conditions.

Additional comments and considerations pertaining to surge tank installations are given in § 3. 4. 1. 2.

#### 3. 3. 1. 3 Ignition System.

The requirements for an igniter in the pulsed DB/AB method are the same as that for the growth/decay method described on pp. 30-32 of ref. 3-1. In one laboratory that utilizes the pulsed DB/AB method, an igniter is used with an ignition aid material coating on the propellant surface. The teardrop igniter consists of a nichrome bridge wire (0.004-in. diameter by 0.200-in. length) attached to No. 32 cotton-covered wires. The igniter assembly is dipped into a pyrotechnic mix to form a teardrop having a nominal weight of 60 mg.

Additional comments pertaining to igniter fabrication and a formulation for pyrotechnic paste are given in Section 3. 4. 1. 3.

#### 3. 3. 1. 4 Pulser.

The pulser used in the pulsed DB/AB method (and pulsed VATB method<sup>\*</sup>) introduces the pressure disturbance that is utilized to measure the acoustic energy losses in the T-burner. Ideally, the pulser should introduce a gas/particle mixture identical to the combustion products that prevail in the T-burner due to propellant burning. In addition, the pulser mass injection rate should be tailored to excite fundamental mode and minimize excitation of the higher modes. Tailoring criteria for pulsers have not been developed; however, experimental studies of harmonic excitation for several different pulsers are presented in ref. 3-5. Brissant pulsers are not desirable because they excite higher modes of oscillation and possibly disturb the behavior of aluminum filigrees and agglomerates loosely attached to the propellant surface.

Two types of pulsers have been tested: squibs and piston pulsers. Table 3. 3-1 shows the different squibs that have been considered.

For the 1.5-in. T-burner, most tests have been done with the Bermite Mk 2 black powder (90 mg) squib. It is reproducible, and creates sufficient strength to allow acceptable pressure amplitudes. The ARC special squib (manufactured by the Northern Flare Division of At-

---

<sup>\*</sup> See § 3. 4. 1. 4 for comments on pulsers used in the pulsed VATB method.

lantic Research Corp. ) uses the same hardware as the Mk 2 but contains 45 mg of FFFG powder and 45 mg of  $\text{BKNO}_3$ . Recently, this squib has been used as a replacement for the Bermite Mk 2.

Table 3.3-1 Squibs Used in Pulsed T-Burners

<u>Manufacturer</u>	<u>Designation</u>	<u>Strength**</u>
Bermite	Mk 1	2 psi
Bermite	Mk 2	4 psi
Atlantic Research Corp. (ARC)	special	7 psi
Holex	1395	20 psi
Holex	6100	40 psi

\*Nominal peak-to-peak amplitude at 500 psi and 800 Hz burner (1.5-in. diameter).

Data indicating the pressure pulse amplitude generated by the Mk 2 pulser are shown in Figure 3.3-4. These data were extracted from pulse decays obtained during burning with ANB 3066 propellant at a nominal pressure of 500 psi in the 1.5-in. diameter NWC T-burner at five different T-burner lengths (frequencies). The plotted pressure amplitudes are the mean values of the peak "usable" pressure amplitudes for five test series; each series consisted of ten or more tests. The data bars indicate one sample deviation about the mean value.

The piston pulser is shown in Figure 3.3-5. This type of pulser is being developed by Aerojet Solid Propellant Co. and is described in detail in ref. 3-14. It consists of a small piston in a cylinder that is coupled to the T-burner chamber. When the piston is driven forward, the gases in the cylinder are introduced into the T-burner and the pressure pulse is created. The piston is driven by a small pyrotechnic charge in the breech when initiated by a squib. The stroke is tailored to provide both the desired mass injection (mean over pressure) and the duration. The piston weight also is used to tailor the firing duration. Soft metal spacers at the end of the breech are used (1) to absorb shock impact from the piston, (2) to alter resonant cavity features of the pulses,

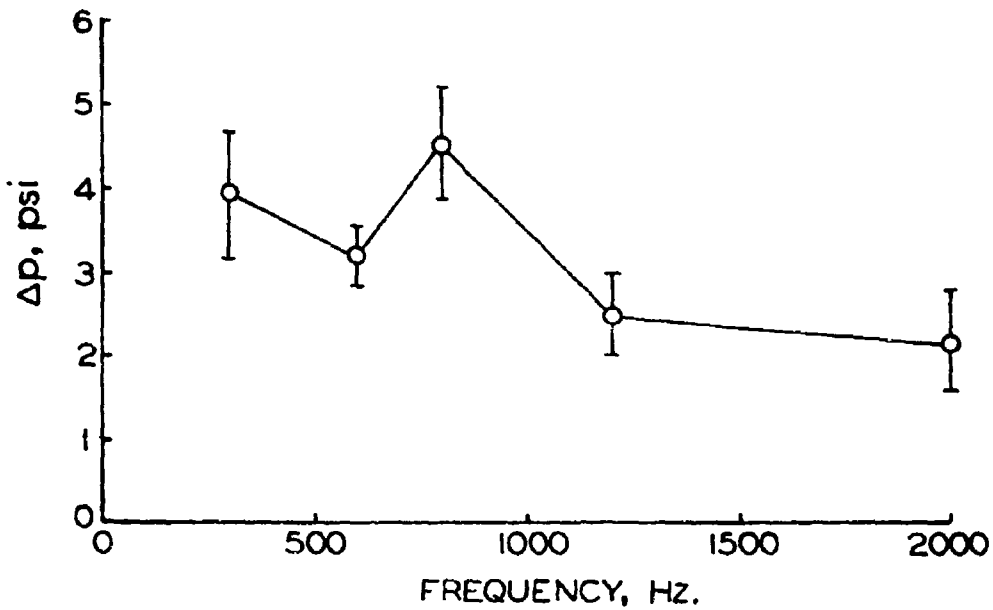


Figure 3. 3-4 Pressure Amplitudes Generated by Mk 2 Squibs, ANB 3066 Propellant at 500 psia. Squibs oriented parallel to the axis and located at the ends (ref. 3-13).

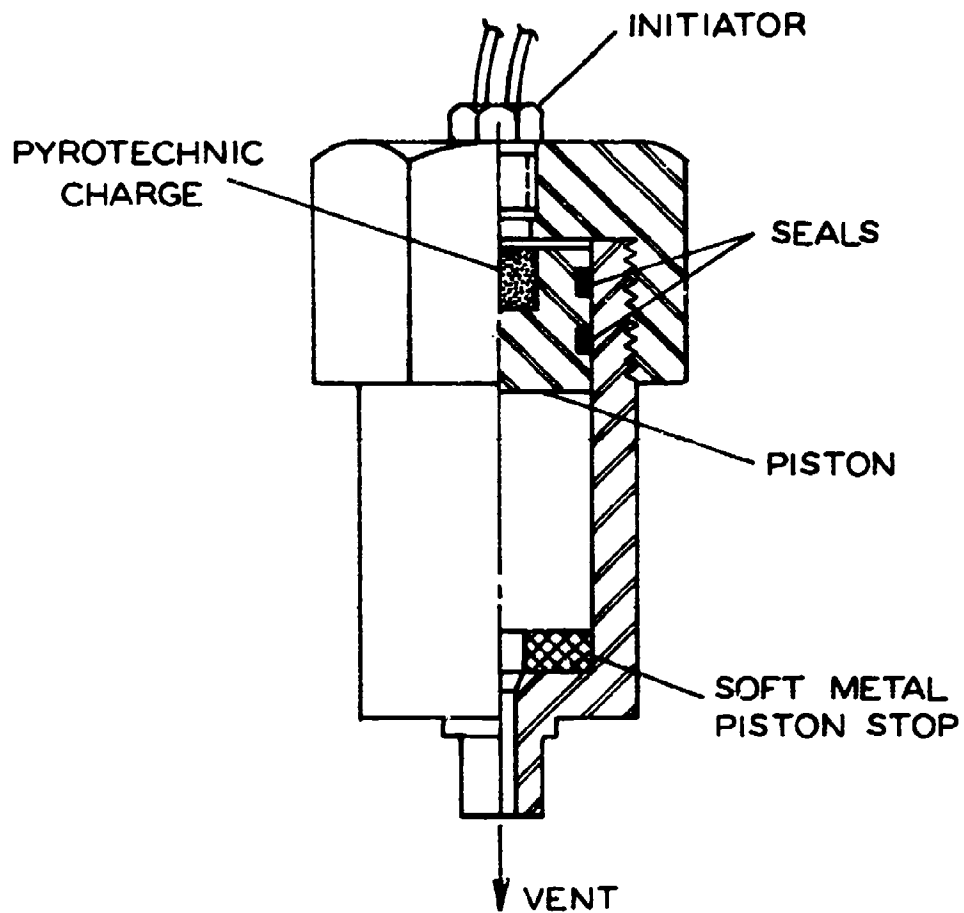


Figure 3. 3-5 Schematic Drawing of a Piston Pulser (ref. 3-14)

and (3) to refine stroke duration if needed. The gases vent through a subsonic orifice.

Recommendations: It is recommended that either the Mk 2 or ARC special squibs be used as pulsers in the pulsed DB/AB T-burner. The piston pulser could become an acceptable replacement for squibs in the future. It is suggested that recent literature on pulsers be examined before making a selection.

#### 3.3.1.5 Transducer and pulser location.

In principle, only one high-frequency transducer is necessary in a T-burner test. This transducer can be mounted at the center of either end cap or along the T-burner chamber wall near either end cap. A second high-frequency transducer at the opposing end provides redundancy of data.

Harmonic content can be obtained from electronic filtering (spectrum analyzer) of the output from a high-frequency transducer mounted near the end of the T-burner chamber. Oscillations in the even longitudinal modes can be measured by mounting a high-frequency pressure transducer at the center of the T-burner (vent location).

Two locations have been used for pulsing the T-burner. Most commonly, the pulsers are located at the center of the end caps, as shown in Figure 3.3-1(a). In the second case, the pulsers are located at the quarter wave points, as shown in Figure 3.3-1(b).

The argument for pulsing at the ends is that the pulser gases enter the chamber symmetric to the axis of the T-burner and rapidly develop into a standing longitudinal wave with minimum distortion due to reflection from the T-burner walls. Arguments for the quarter wave location are (1) this location is at the pressure nodal point for even modes; thus, excitation of even modes is minimized; and (2) this location is downstream from the propellant surface which could be altered by the sweeping action of the pulse gases when they enter.

Recommendation: Either of the pulser locations described above can be employed in pulsed DB/AB testing. Insufficient data exist to establish which approach is optimum. It should be noted that locating the pulsers on the end caps makes it necessary to mount the high-frequency

transducer on the side walls.

### 3.3.2 Propellant Grain Configurations.

#### 3.3.2.1 Disc, cylinder, and cup grains

The pulsed DB/AB method relies upon direct measurement of the decay of waves due to acoustic energy losses in the T-burner immediately after propellant burning, before the combustion products are changed due to venting. It is therefore necessary that the propellant grains burn out simultaneously and have no small slivers which continue to burn during the second pulse. Whereas simultaneous burnout can be achieved by precise machining of the propellant web thickness and simultaneous ignition of the grains, prevention of slivering is achieved by uniformly igniting grains that have uniform web thickness.

Three grain configurations have been tested using the pulsed DB/AB T-burner: end discs, cylinders, and cups. Of these, the end disc grain is preferred for qualitative testing. For this grain configuration, products from the igniter can be spread uniformly across the propellant surface and the web thickness is constant; thus, simultaneous and uniform ignition of the grains can be achieved reproducibly.

For quantitative testing in which a distinction is made between the response functions associated with end- and side-burning surfaces, tests can be conducted with both cylindrical and end-disc grains. The cylinder geometry does not present any new problems associated with ignition; however, difficulties associated with uneven burnout can be encountered if the grain is long (see §3.4.2.1). Methods of testing to determine if uneven burnout occurs in the pulsed DB/AB method are given in §3.3.3.

The cup grain is not suggested for pulsed DB/AB testing. Although uniform ignition of the propellant is possible, uniform burnout is precluded due to the fillet of propellant that remains at the outer periphery of the cup base; see Fig. 3.4-4. Removal of this 'fillet' material by machining could eliminate this problem. However, the cup grain would be expensive to fabricate. In addition, to use the cup grain in quantitative testing would require tests with cups of two different lengths to separate  $B_e$  and  $B_g$ .

Recommendation: For qualitative testing, end disc grains should be used in the pulsed DB/AB method. The amount of propellant and the cost for machining are minimized for this grain configuration. For quan-

titative testing, end disc and cylindrical grains are recommended. Cup grains are not recommended for use in the pulsed DB/AB method.

### 3.3.2.2 Methods of mounting the propellant grains.

Methods for mounting end disc grains are described on pp. 25-30 of ref. 3-1. A schematic of a typical mounting is shown in Figure 3.3-6, and a detailed assembly procedure is given in refs. 3-11 and 3-13.

Two methods for mounting cylinder grains in the pulsed DB/AB T-burner are shown in Figure 3.3-7. One method gives a time during burning when constant cross-sectional area prevails in the chamber (hereafter referred to as flush conditions). The second method gives flush conditions when the cylinder grain "burns out." Both of these mounting configurations are used in a series of pulsed DB/AB tests with cylinders (see §3.3.3).

To provide a flush condition during burning, shown in Figure 3.3-7(a), the cylinder is recessed into the chamber wall and the bore diameter of the grain is slightly smaller than the inside diameter of the chamber. The small protruding web of propellant provides a short burn time before flush conditions so that the chamber is filled with combustion products when flush conditions occur. Burning of the outer and end surfaces of the cylinder is undesirable; thus, these surfaces are inhibited. Inhibitors that create char material should not be used on the edge of the cylinder facing the T-burner vent. Such residue can cause acoustic disturbances. A light coating of silicone grease (e. g. Dow Corning No. 11) has been found to restrict burning on this surface without char material forming.

For the flush condition at burnout, shown in Figure 3.3-7(b), the propellant grain protrudes into the chamber and the outer diameter of the cylinder is approximately the same as the inside diameter of the T-burner chamber (allowance must be made for inhibitor). As in the flush-at-burning configuration, only the bore of the cylinder is allowed to burn and the end of the grain facing the T-burner vent is coated with a non-charring inhibitor.

3.3.3 Test Procedures. The testing procedure for the pulsed DB/AB T-burner is described in terms of (1) the number of tests recommended to determine  $\alpha_c$  and  $\alpha_d$  for a given pressure and frequency, and

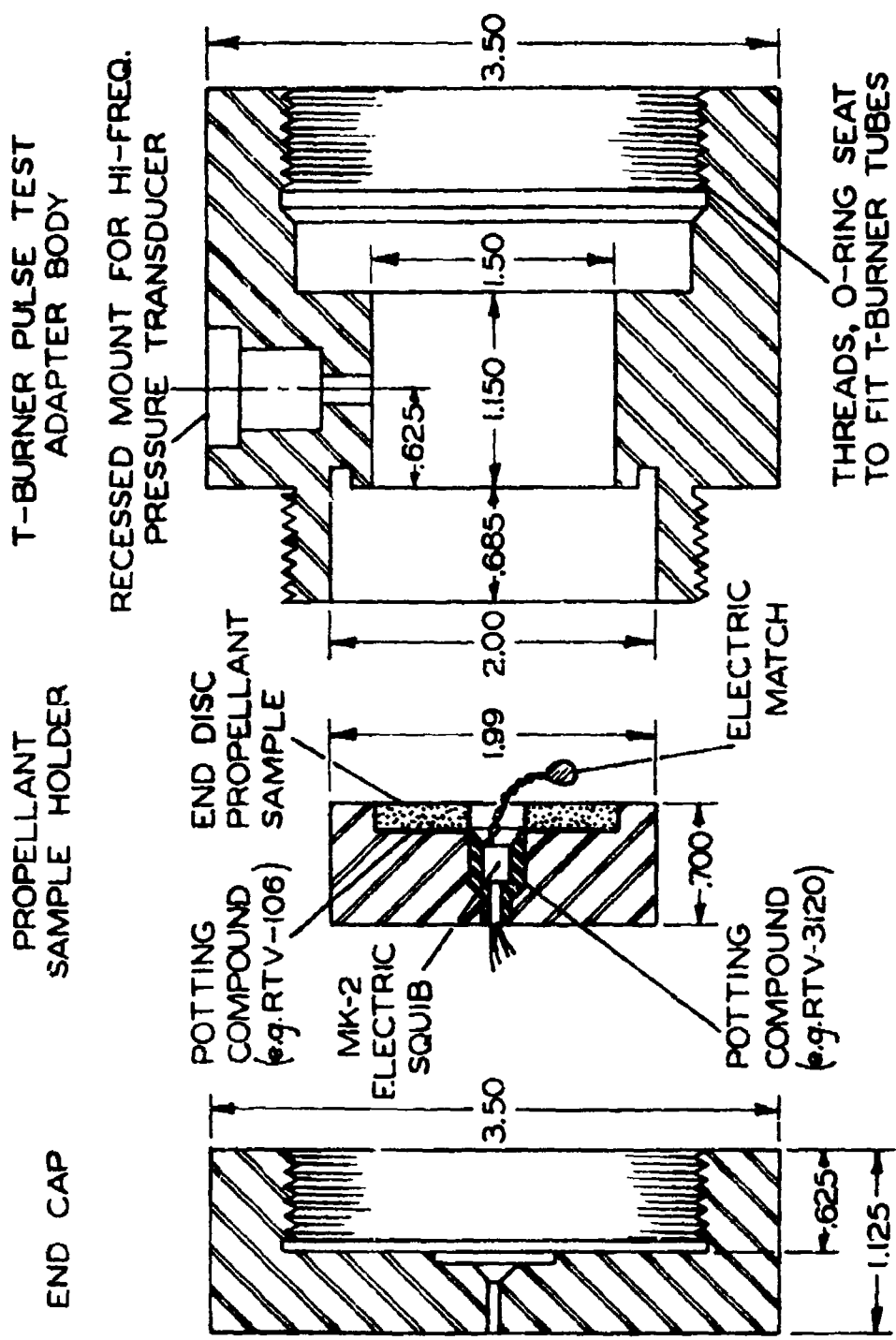


Figure 3.3-6 End Disc Mounting for Pulsed DB/AB Testing (ref. 3-11)

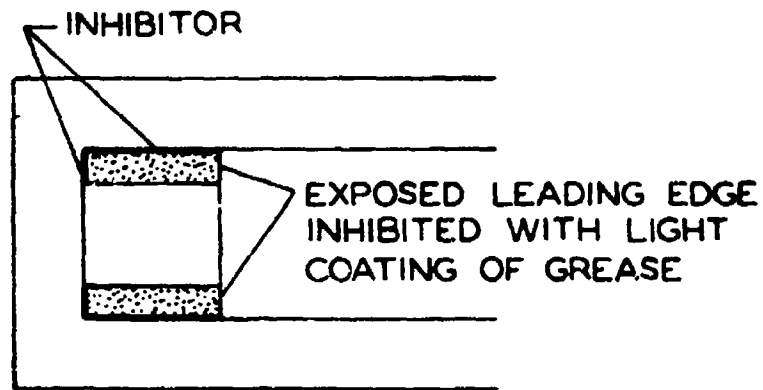
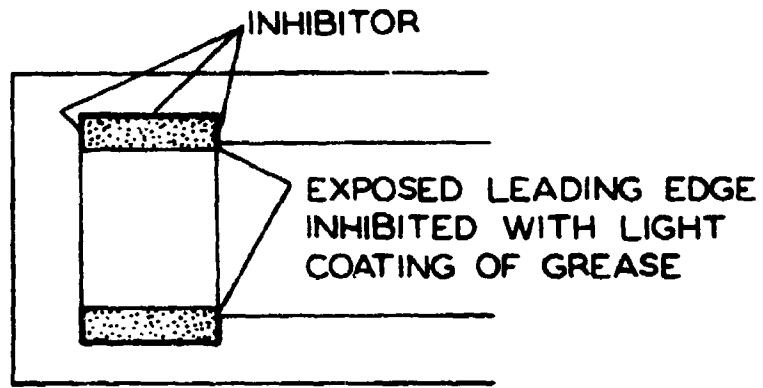


Figure 3.3-7 Mounting Cylindrical Grains for Flush Conditions During and After Burning

(2) the details of hardware and instrumentation preparation for a test series.

### 3.3.3.1 Recommended test series.

This section describes what pulsed DB/AB tests should be conducted for a given frequency and pressure level. A typical test record for ANB-3066 propellant is shown in Figure 3.3-8.

For flat samples, the timing of the DB pulse is chosen such that

- (a) the burner has had time to be flushed of igniter products, filled with propellant products, and approach equilibrium gas temperature (typically the equivalent of 90 cycles after ignition at 800 Hz);
- (b) the burner pressure has leveled off after the ignition transient and all oscillations stimulated by ignition have decayed;
- (c) sufficient time is allowed after the pulse for the system to recover to steady conditions before burnout (time depends on decay rate of pulse, which can be estimated or determined in the first firing of a test set).

In the case of ANB-3066 propellant, the use of 0.125-in. thick propellant samples and a DB pulser firing at approximately three quarters of the time to burnout easily met these requirements, as can be seen in Figure 3.3-8.

In the case of the DB pulse with cylindrical propellant charges, it is recommended that the above requirements be met and the pulser fired at the time when the burning propellant is flush with the burner walls. With flush conditions, an analytical correction (Appendix C) is not required, and undesirable flow effects associated with a step or lip are minimized. It is recommended that data for determining a mean  $\alpha_1$  from DB pulses be derived from a minimum of five tests.

The AB pulses are fired to determine the damping alpha. If the appropriate TABO for  $\alpha_d$  for a propellant is known from previous testing (as in the case of lot-to-lot propellant quality control testing), a series of five tests with the AB pulser fired at that TABO is recommended.

If there is no a priori knowledge of the appropriate TABO, a series of ten tests should be conducted in which an AB pulse is fired at different times following burnout. A recommended time interval is 0.010 seconds over a 0.100 second period. This procedure is necessary in

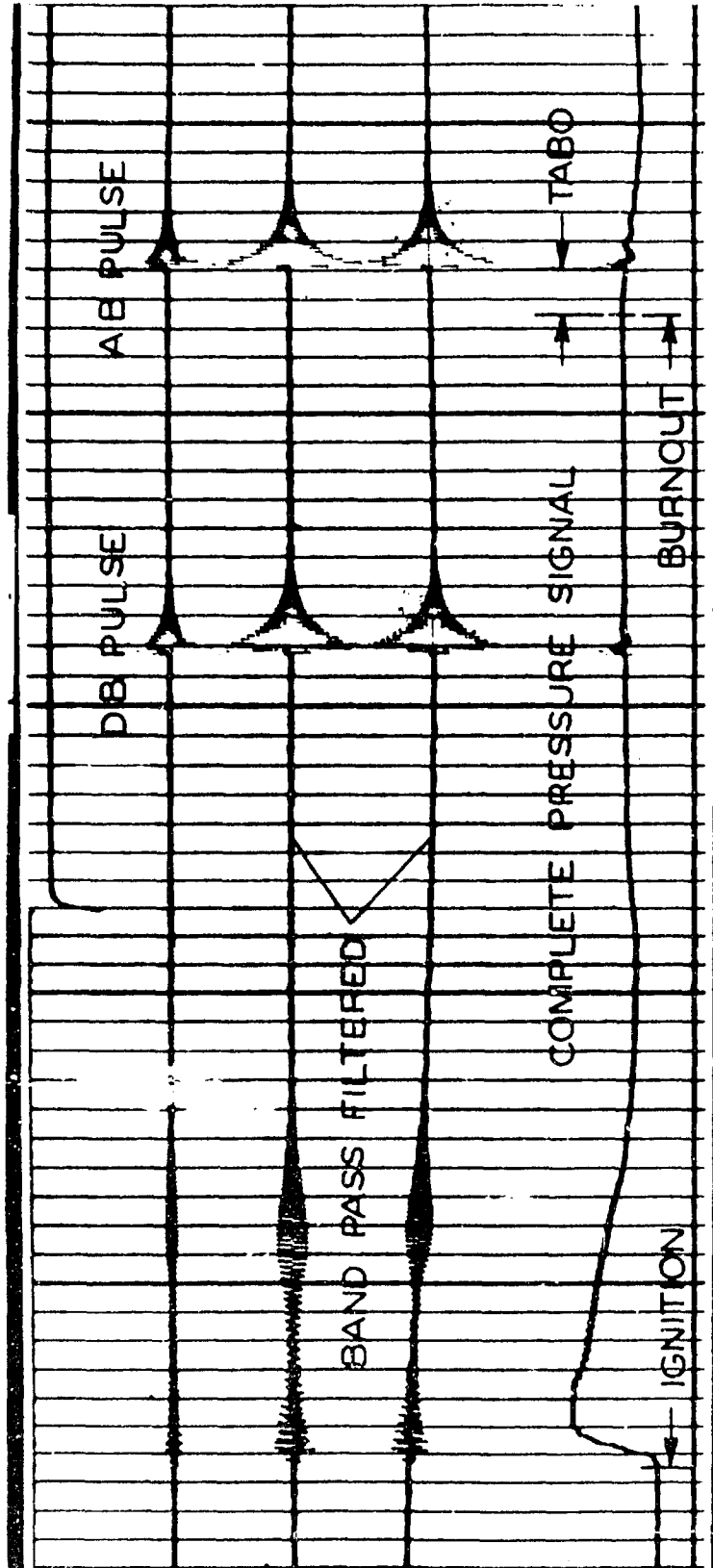


Figure 3.3-8 A Typical Test Record Obtained from a DB/AB Test.

The apparent spontaneous growth and decay of oscillations shortly after ignition is due to an interaction of chamber filling and electronic filters. As the temperature rises, the frequency increases into the band pass of the filters, and oscillations appear to grow. Subsequently, the oscillations decay as the burner fills with combustion products, which produce damping ( $Al_2O_3$  particles). (ref. 3-13)

order to determine the  $\alpha_d$  from the series of AB alphas ( $\alpha_2$ ). An examination of the  $\alpha_2$  versus TABO relationship (see §5. 1. 1. 2) obtained would indicate whether, and at what TABO's, additional firings are needed.

The reasoning behind this procedure for determining  $\alpha_d$  is that if a pulse is fired while the propellant is still burning, a value of  $\alpha_2$  comparable to that obtained from a pulse during  $\alpha_1$  will be obtained; at a later time, as the propellant is burning out, a somewhat higher decay alpha will be measured because the contribution from the propellant\* will be less and the decay will be more nearly indicative of only damping. At a time when propellant burning has ceased completely,  $\alpha_2$  will be at its largest value; thereafter, it will be smaller due to cooling of the gases (decrease in frequency) and due to a reduction in particle damping because of particle agglomeration and condensation and due to back flow from the surge tank. Thus, there will be a time after burnout (TABO) when  $\alpha_2$  will have the largest value. The largest value of  $\alpha_2$  (which occurs at a particular TABO) is taken to be the damping that would be present during burning and is designated as  $\alpha_d$ . It should be pointed out that the damping measured in this manner is somewhat less than the actual damping, since it is determined by taking the largest value that can be measured during the disappearance of one perturbing effect (gradual burnout), and the appearance of others which reduce the decay rate. How much these perturbing processes overlap has not been determined, and hence how much this "maximum" value of the damping deviates from the damping which actually occurs during burning is not known. From tests of several propellants it appears that the relationship between  $\alpha_d$  and TABO is a function of propellant composition, pressure, and frequency.

The approximate TABO's for  $\alpha_d$  for a few propellants that have been extensively tested are: ANB-3066, 0 - 0.030 seconds at 500 psi and 820 Hz; medium-energy CMDB, 0.060 - 0.080 at 350 psi and 820 Hz; and a high-energy CMDB, 0.080 - 0.140 seconds at 1000 psi and 880 Hz.

In the case of AB pulses with cylindrical grains, the above procedure is recommended, with the additional condition that the "burned out"

---

\*The trend described here is for the case of a propellant with positive combustion response. The idea is the same, but TABO trends are correspondingly changed, when  $\alpha_c$  is negative.

propellant sample be flush with the burner wall. Since flush conditions are desired for both the DB and AB pulses, separate tests are conducted to obtain DB and AB pulse data using the grain configurations shown in Figure 3.3-7.

To summarize, the minimum number of tests recommended for any one test condition depends upon the a priori knowledge the investigator has on the propellant and on the propellant grain configuration to be tested. The following matrix based on tests at 800 Hz can be used as a guide:

TABO for $\alpha_d$ (msec)	Flats			Cylinders		
	$\alpha_1$	$\alpha_2$	total*	$\alpha_1$	$\alpha_2$	total**
known	5	5	5	5	5	10
unknown	5	10	10	5	10	15

\* DB and AB pulse data are obtained from a single test.

\*\* DB and AB pulse data are obtained from separate tests designed to give flush conditions.

Ordinarily, one is interested in test results over a range of frequencies and possibly a range of pressures. Thus, the above matrix should be considered for each frequency and pressure desired.

### 3.3.3.2 Preparation of instrumentation and hardware.

In preparation for a test series, a transducer calibration is first made. Checkout of instruments prior to each test consists of verifying filter, oscilloscope, oscillograph, amplifier, and pressure transducer settings. Once the instruments are set, a group of tests (as many as 10 to 15) may be fired with no major changes. Instrumentation channels that record pulse data are calibrated by introducing an oscillating voltage of known frequency and amplitude into the system in place of the pressure transducer output (AC calibration). An oscillograph recording is made for the appropriate frequency and filter setting for a given test series sequence; the deflections are measured as a part of the data reduction procedure.

The following sequential steps are followed in assembling the center-block type T-burner:

(a) The suitable burner parts are chosen from stock, inspected, and wiped clean -- especially joining surfaces.

(b) A light film of grease (e. g. Dow Corning No. 11 silicone grease) is wiped over male threads and ends of tubes.

(c) Burner parts are assembled by hand, and all joints are "made up" by applying a pipe wrench to each end of the assembly and torquing tight.

(d) The interior of the assembly is visually inspected to assure that sections line up properly and that there are no gaps at any of the joints.

(e) The burner assembly is then placed on the neck assembly and turned up tight.

(f) Previously prepared sample holders are placed in the counter-bores provided in the end adaptors and the end caps screwed on with final tightening by a pipe wrench.

(g) The appropriate electrical connections are made to the squib and igniter wires.

Following the assembly of the T-burner, (1) the surge tank pressure is adjusted to the desired pressure with high-pressure air; (2) the T-burner and heat exchanger tank are pressurized with nitrogen to the desired pressure and the ball valve connecting the two tanks is opened; and (3) the firing sequencer is activated, which starts the oscillograph, activates the oscilloscope camber, fires the igniters and pulsers, and stops the oscillograph.

After firing, the valve that isolates the heat exchanger tank and surge tank is closed, and the T-burner is depressurized. Then the end cap and sample holders are removed from the T-burner, the residue exhaust products are drawn off through an exhaust system, and the T-burner is cleaned.

3.3.4 Operational Limitations. The pulsed DB/AB T-burner has been operated successfully over a frequency range of 220 to 2000 Hz and a pressure range of 200 to 2000 psi.

It appears that the upper frequency limit might be extended to 3500 Hz: the limiting factor is that the pulse decay rate becomes quite

high as the frequency increases, and a sufficient number of decay cycles may not occur to permit usefully accurate measurements to be made. At the low frequency end, there are the problems of filling the T-burner chamber with representative combustion products and obtaining sufficient temperature before the pulses are fired due to the small amount of propellant that is burned. The use of thicker propellant samples (longer burning time) might improve this situation somewhat.

It appears that the pressure range over which the T-burner can be operated could be extended. Operation at lower pressures probably would depend only on the combustion characteristics of various propellants. The upper pressure limit, as far as the hardware capability and practical gas (nitrogen and air) supply is concerned, is approximately 2500 psi.

3.3.5 An Example of Raw Data. Figure 3.3-8 shows an oscillograph record of a pulsed DB/AB T-burner firing. Details on data reduction are given in §5.5.1.

### 3.4 Variable Area T-Burner (VATB) Method

In this subsection, the variable-area T-burner (VATB) method of testing aluminized propellants is discussed in detail. Included are both the VATB and pulsed-VATB methods. An attempt has been made to organize this section so that it contains all of the information necessary to use the VATB method. However, there are unavoidable areas of overlap between the pulsed DB/AB and the VATB method. Where such overlap occurs, appropriate reference is made to the pulsed DB/AB method sections.

3.4.1 Hardware Configuration. The VATB method is described in the T-burner report for unaluminized propellants (ref. 3-1); however, at the time of writing that report, only limited VATB data were available to guide writing that would describe VATB hardware. Accordingly, it is recommended that the user of this report follow recommendations contained herein when a conflict of ideas exists between the two reports.

#### 3.4.1.1 T-burner chambers.

T-burner chambers for the VATB and pulsed-VATB methods have been designed for cups or cylinders with a propellant bore diameter smaller than, equal to, and larger than the inside diameter of the T-

burner: these are referred to as protruding, flush, and recessed grains, respectively. Typical T-burner hardware for different types of grain configurations are shown in Figures 3.4-1 and 3.4-2. Additional comments on the selection of grain configuration are given in §3.4.2.

The test frequency for a T-burner having end discs is determined by the length of the T-burner,  $L$ , and the speed of sound of the gas/particle mixture in the T-burner,  $\bar{a}$ :

$$f_0 = \frac{\bar{a}}{2L} \quad (\text{Hz}) .$$

For the VATB, propellant grains can cause shifts in the acoustic mode shape due to changes in cross-sectional area of the T-burner chamber. In addition, the speed of sound is higher due to the larger propellant grains. For selecting a T-burner chamber length to conduct VATB tests at a desired frequency, the plot of observed frequency versus T-burner length shown in Figure 3.3-2 can be used. However, this plot is valid only for propellant grains that are flush to the inside wall of the chamber. For grains which protrude or recede, a modest shift in frequency will occur. The shift due to geometry effects can be determined from Figure C-2 of Appendix C and similar results.

#### Recommendation for selecting T-burner length

Based on existing VATB data, it appears reasonable to use Figure 3.3-2 for selecting the chamber length when recessed propellants are used. For protruding grains, the chamber lengths determined from Figure 3.3-2 should be increased by approximately 25 per cent.

The inside diameter of the T-burner chamber has not been standardized. T-burner chamber sizes for different laboratories are summarized in Table 3.4-1.

Table 3.4-1 T-Burner Chamber Diameters

inside Diameter (inches)	Laboratory	Method
1.8, 2.5	Lockheed Propulsion Co. (ref. 3-4)	VATB
2.0	Thiokol Chemical Corp. (ref. 3-5)	VATB
1.5	Aerojet Solid Propulsion Co. (ref. 3-11)	pulsed VATB
1.5, 2.9	Hercules, Inc. (ref. 3-6)	pulsed VATB

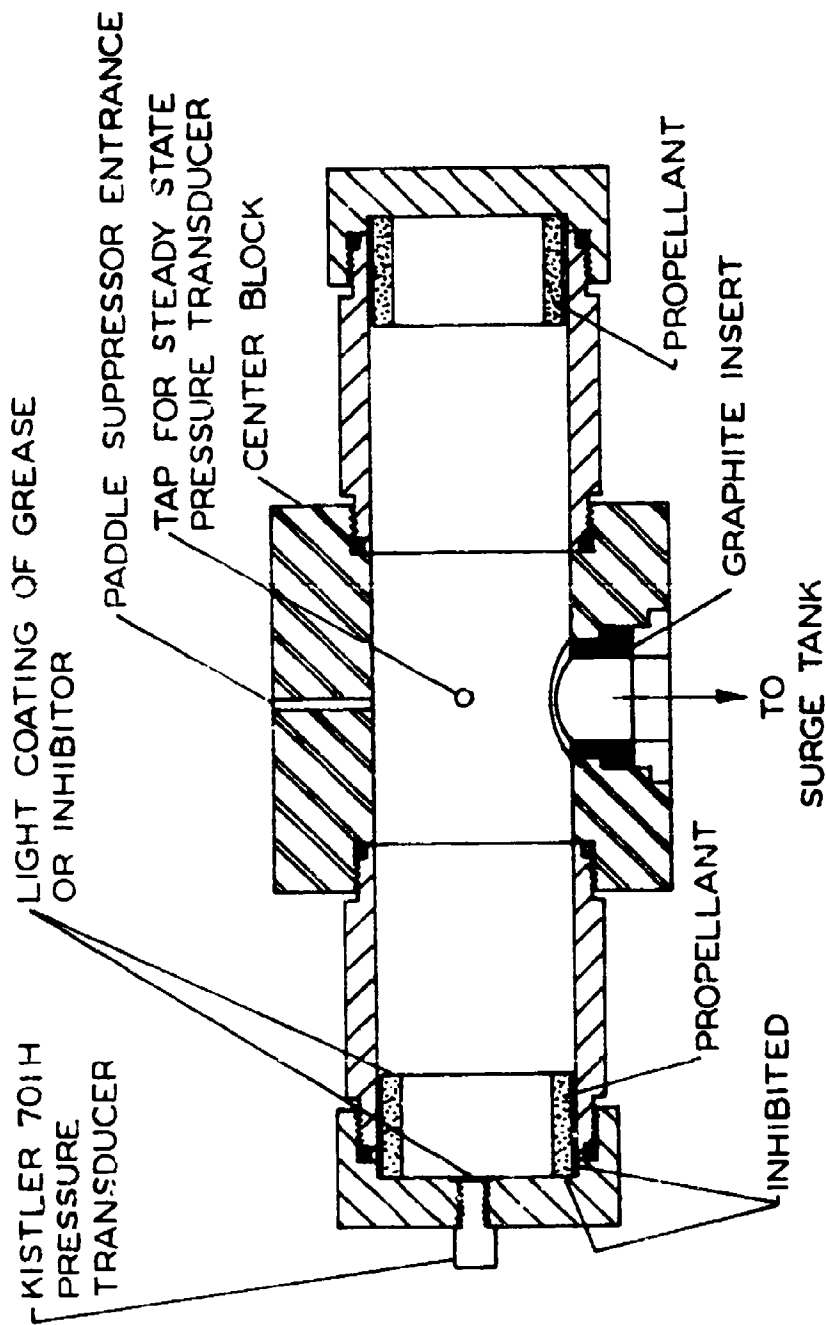


Figure 3.4-1 Hardware for VATB Tests Using Protruding Grains  
(ref. 3-4)

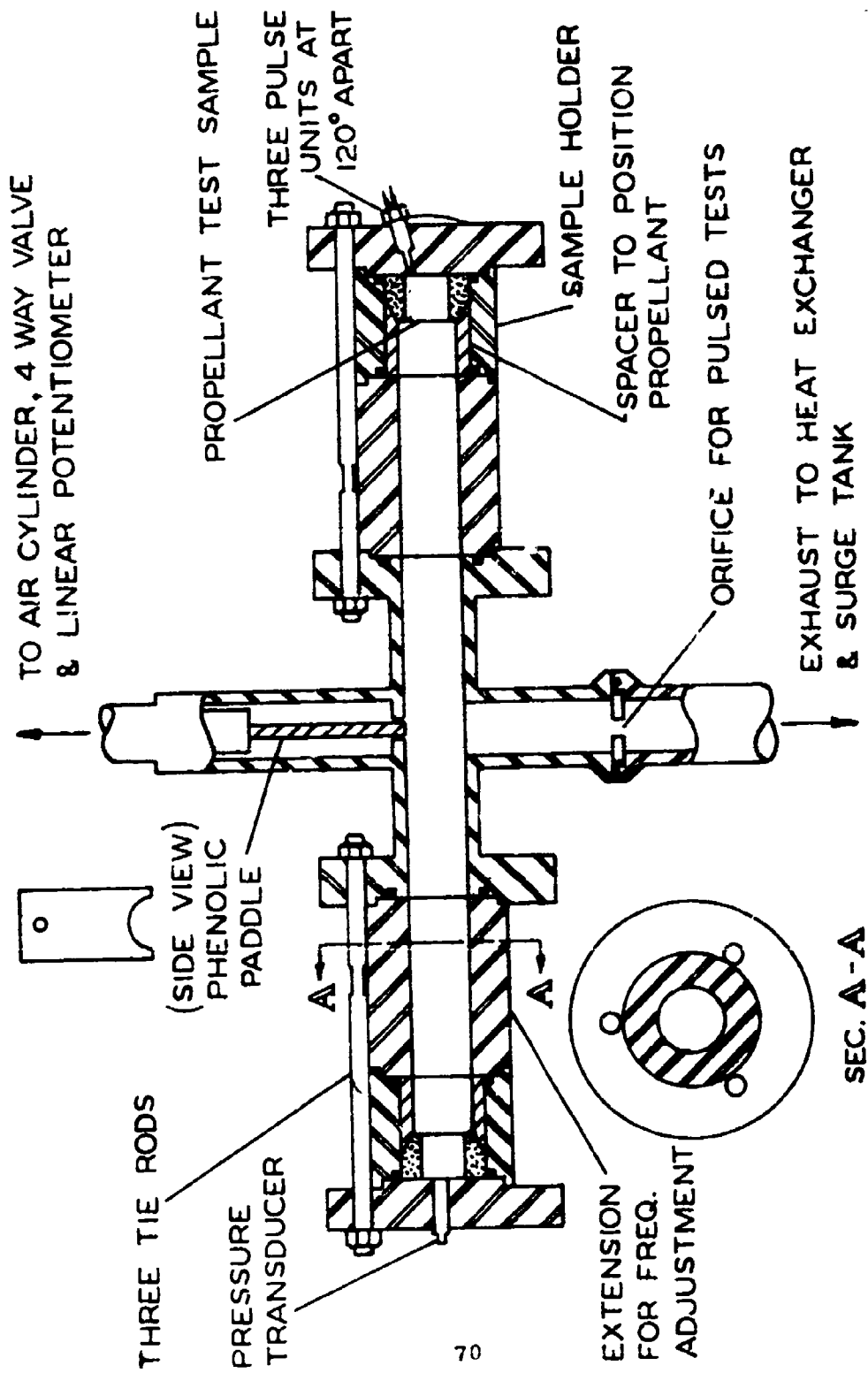


Figure 3.4-2 Hardware for Pulsed VATB Tests Using Recessed Tapered Grains (ref. 3-6)

Factors that should be considered in the selection of T-burner diameter are as follows:

Cost: smaller diameter T-burner chambers reduce the quantity of propellant required for a test series. In addition, the cost of the chambers and associated hardware (e. g. the surge tank) is reduced with smaller T-burner diameter. The T-burner chamber size also has an impact on the turn-around time between tests. Smaller chambers are easier to handle.

Geometry: in VATB testing, smaller diameter T-burner chambers allow the use of shorter grain lengths ( $\beta$ ) for a given area ratio ( $S_{bs}/S_{co}$ ). Thus, smaller diameter produces smaller shifts in frequency during a single VATB test, reduces the potential for velocity coupling, and reduces the mean flow/acoustic interactions (see §2 and Appendices E and F for more discussion on these aspects).

Wall Losses: in theory, dissipation of acoustic energy in a tube shows wall losses inversely proportional to chamber diameter (ref. 3-15). The dependence on frequency has been verified experimentally. However, available data show that the effect of  $D_{co}$  on wall losses is negligible compared to particle damping. Thus, this aspect is deemed unimportant in T-burner tests using metallized propellants.

Combustion Efficiency: some propellants show a reduced burning rate in the smaller test hardware listed in Table 3.4-1 (ref. 3-16). It has been suggested that this reduced burning rate is a result of poor combustion efficiency. Tests in the larger hardware apparently improved the combustion efficiency and increased the burning rate. In addition, it was noted that data scatter was reduced for these propellants when a larger T-burner chamber was employed.

#### Recommendation for T-burner chamber diameter

Based on the foregoing, it is recommended that a chamber diameter of 1.5 in. can be employed in T-burner testing.

#### 3.4.1.2 Surge tank versus sonic orifice.

The VATB can be operated in two exhaust modes. First, a sonic orifice can be installed at the exhaust port. The orifice is designed for a

choked flow that results in the desired test pressure. A second approach is to couple the T-burner exhaust port to a large volume surge tank that is pressurized to the desired test pressure. In this mode of operation, the exhaust flow is not choked at any time.

Sonic Flow Orifice: the advantage of the choked nozzle approach is simplicity in construction and lower cost because the additional tankage and plumbing necessary for a surge tank system are not required. However, there are several disadvantages to the choked nozzle that offset these attractions. First, the design of the choked nozzle to provide a desired pressure has the usual complications of nozzle design (viz., accuracy of burn rate characteristics for the propellant, variations in propellant burn area and delivered  $C^*$ , as well as the problem of deposition in the nozzle throat where metallized propellants are considered). Because pressure is an independent variable in T-burner tests, large pressure variations resulting from these uncertainties cannot be tolerated, and considerable test data will have to be rejected if the delivered pressure differs markedly from the desired level. A second disadvantage of the choked nozzle results from the possibility that oscillations could grow during the pressure transient leading to the desired equilibrium pressure. This could occur in cases of large  $L^*$  where filling times are large. The use of a suppressor (discussed in §3.4.1.3) to delay oscillations during this transient period eliminates this problem.

Surge Tank: the advantage of the surge tank approach is that pressure in the T-burner can be controlled accurately.

The mean test pressure is dictated by the pressure in the surge tank. Pressure transients are eliminated as long as the flow area from the T-burner to the surge tank is sufficiently large to minimize pressure drops and the surge tank has adequate volume and heat loss characteristics to preclude pressure buildups in the overall system during a test. Small volume surge tanks can be used with success if chain is placed in the tank so that the hot gases are cooled as they enter the tank or a regulated hot valve is incorporated in a surge tank vent.

There are several disadvantages associated with the use of a surge tank. First, the tankage and plumbing are expensive and must be

fabricated from material that can withstand a corrosive environment. Second, the surge tank must be acoustically isolated from the T-burner to prevent communication of the low frequency associated with the surge tank to the T-burner. This can result in low frequency modulation of the oscillations developed in the T-burner. Third, heating of the propellant and contamination of the propellant surface by hot combustor products stored in the surge tank can introduce an unknown variable in the T-burner tests (i. e., the surface of the propellant sample could be heated or altered so that the burning rate changes during a T-burner test). This disadvantage can be overcome by pressurizing the T-burner with clean nitrogen before opening the valve connecting the T-burner to the surge tank. Fourth, the surge tank is subjected to corrosive gases that can attack and weaken the tank walls. As a result, particular care must be given to material selection and operating procedures to minimize the risk of a tank rupture. It is recommended that periodic hydrostatic tests be made of all tanks and tubing exposed to exhaust products to ensure that corrosion has not exceeded critical limits.

One method of eliminating acoustic coupling between the T-burner and surge tank is to minimize the natural frequency of the surge tank. This can be accomplished by packing chains in the surge tank to reduce the gas temperature and therefore the speed of sound of the exhaust gases. Another method is to employ a long tank or pipe leading to the surge tank. In these precautions still result in acoustic coupling, an orifice or a series of baffles can be incorporated in the surge tank vent, as shown in Figure 3.3-3.

Sizing of the surge tank can be accomplished through a simple energy balance such as the following (ref. 3-15):

$$V = \frac{m R_g}{P_f - P_i} \left( T_i + \frac{\gamma_i + 1}{\gamma_i - 1} T_c \right)$$

This simple calculation yields a conservative value for the surge tank volume because it does not include heat losses due to the presence of chains in the surge tank. Typical surge tanks for VATB testing have a free volume on the order of 20 to 35 ft<sup>3</sup> (refs. 3-4, 3-5, and 3-6) with heat exchangers containing ~ 75 to 100 lbs. of chain.

For the surge tank approach, the diameter of the VATB must be greater than the critical diameter for choked conditions. The precise value for the vent diameter depends upon the surge tank configuration, the mass flow rate expected, and the maximum acceptable pressure rise. If acoustic coupling between the surge tank and T-burner occurs at an unacceptable level, isolation can be achieved by minimizing the vent diameter. It should be recognized, however, that pressure rise during the test increases with decreasing vent diameter. Another observation is that a large vent tends to reduce the even harmonics significantly (ref. 3-6), resulting in a more linear waveform. Typical surge tank - VATB installations are shown in Figures 3.4-3 and 3.4-4. Additional comments pertaining to surge tanks are given in §3.3.1.2.

#### Recommendation

The surge tank approach is recommended for VATB testing. However, the sonic flow orifice approach is acceptable if the aforementioned disadvantages are addressed properly.

#### 3.4.1.3 Suppressors.

Following ignition of a metallized propellant in a VATB, conditions in the chamber are nonuniform and changing until ignition products are exhausted and equilibrium conditions are achieved. To avoid growth of oscillations during periods of nonequilibrium, a means is required for suppressing oscillations for a time following ignition. For metallized propellant testing, two approaches have been employed. In one approach, a paddle is introduced at the center of the T-burner to divide the T-burner into two chambers and acoustically isolate the propellant grains (ref. 3-17). Similarly, a butterfly valve can be used as described in ref. 3-18. Typical paddle suppressors are shown in Figures 3.4-3 and 3.4-5. Growth of oscillation occurs when the paddle is rapidly removed from the T-burner chamber. In the second approach, a Helmholtz resonator (HR) is incorporated into one end of the T-burner (ref. 3-19). A typical Helmholtz resonator is shown in Figure 3.4-6. The resonator is tuned to the fundamental frequency of the T-burner. Growth of oscillations occurs when the resonator volume is closed to the T-burner chamber.

The time between ignition and first growth should be based on the length of the T-burner and the mass rate of flow of gases in the T-burner.

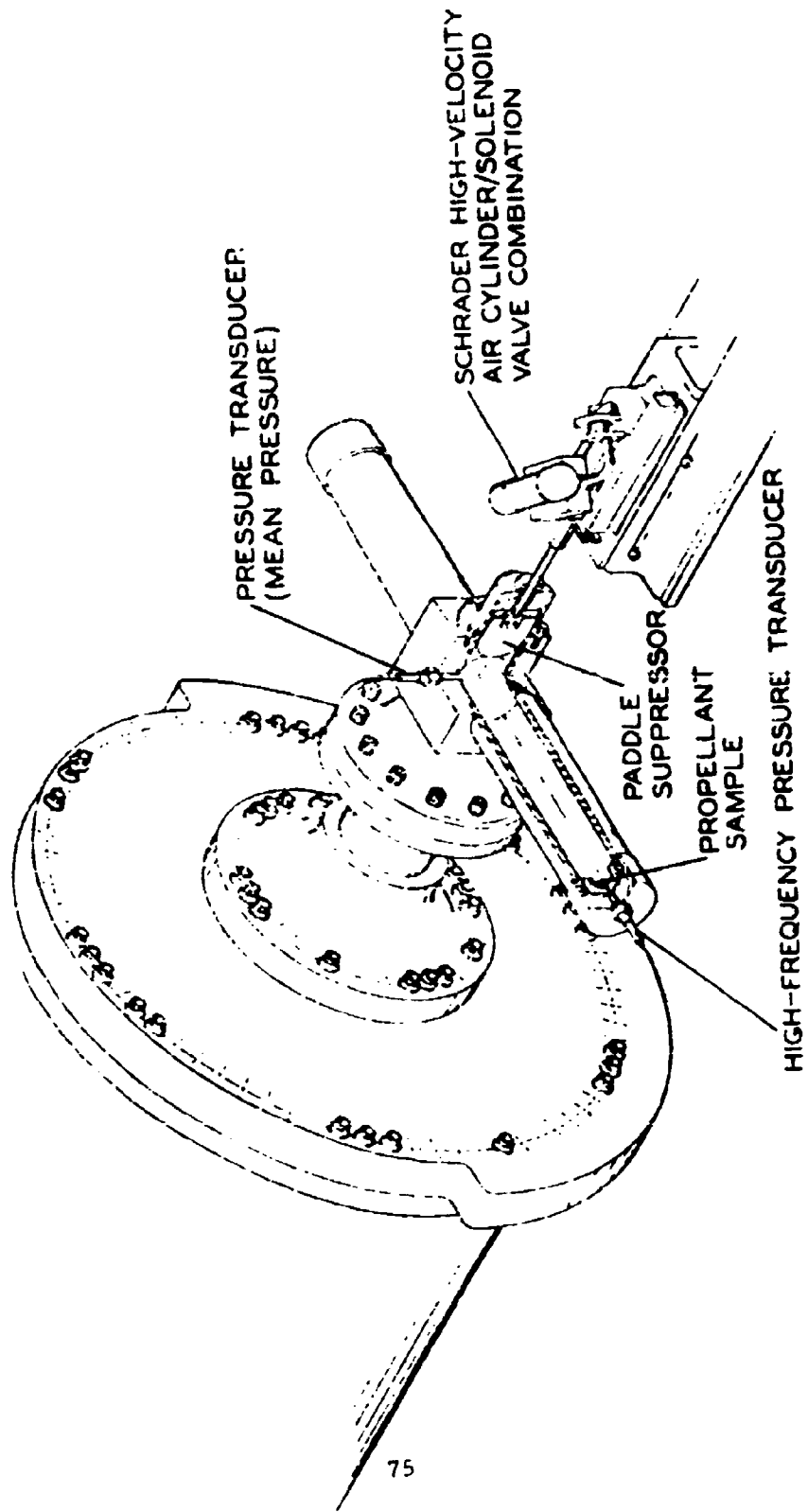
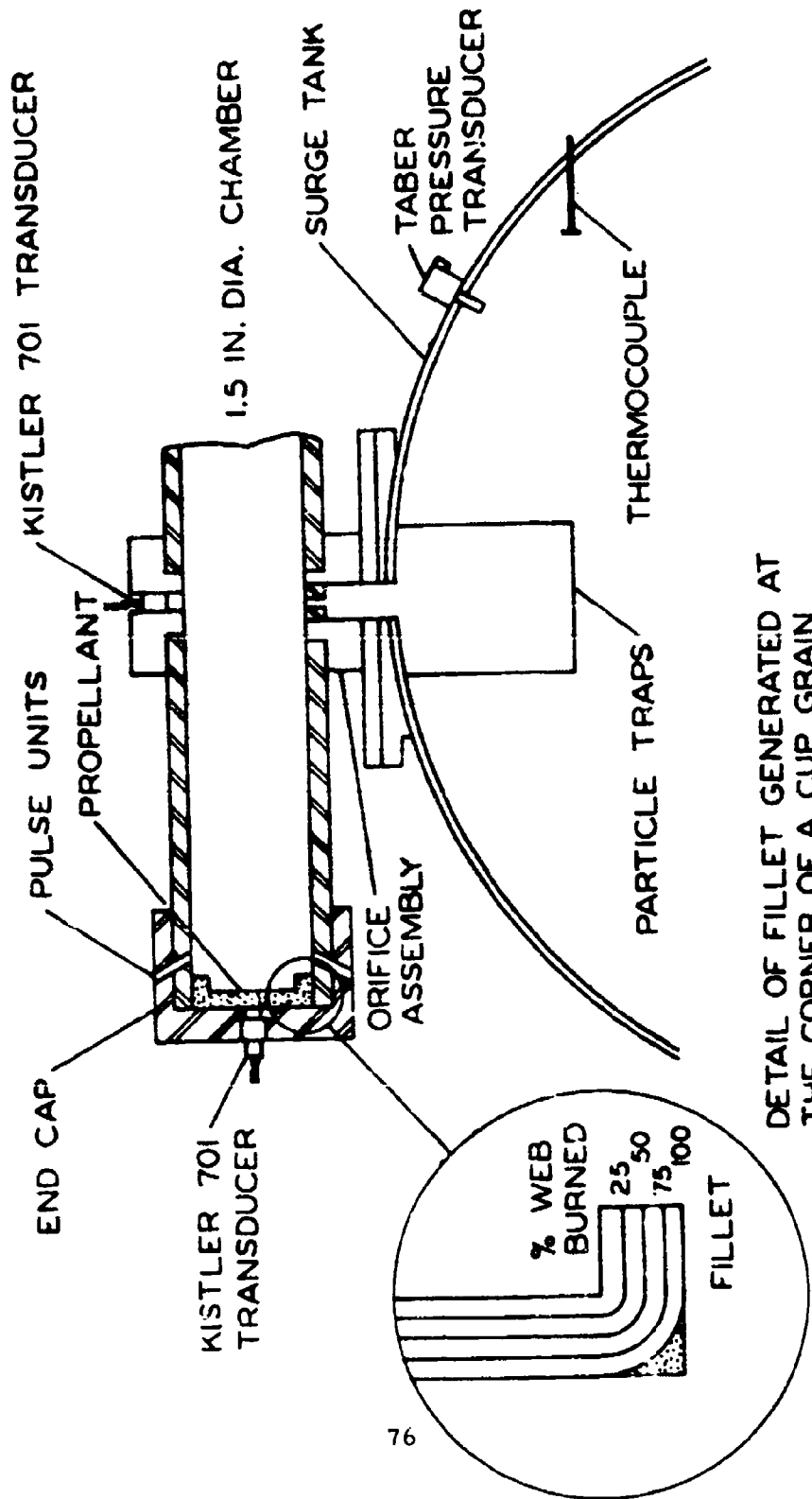
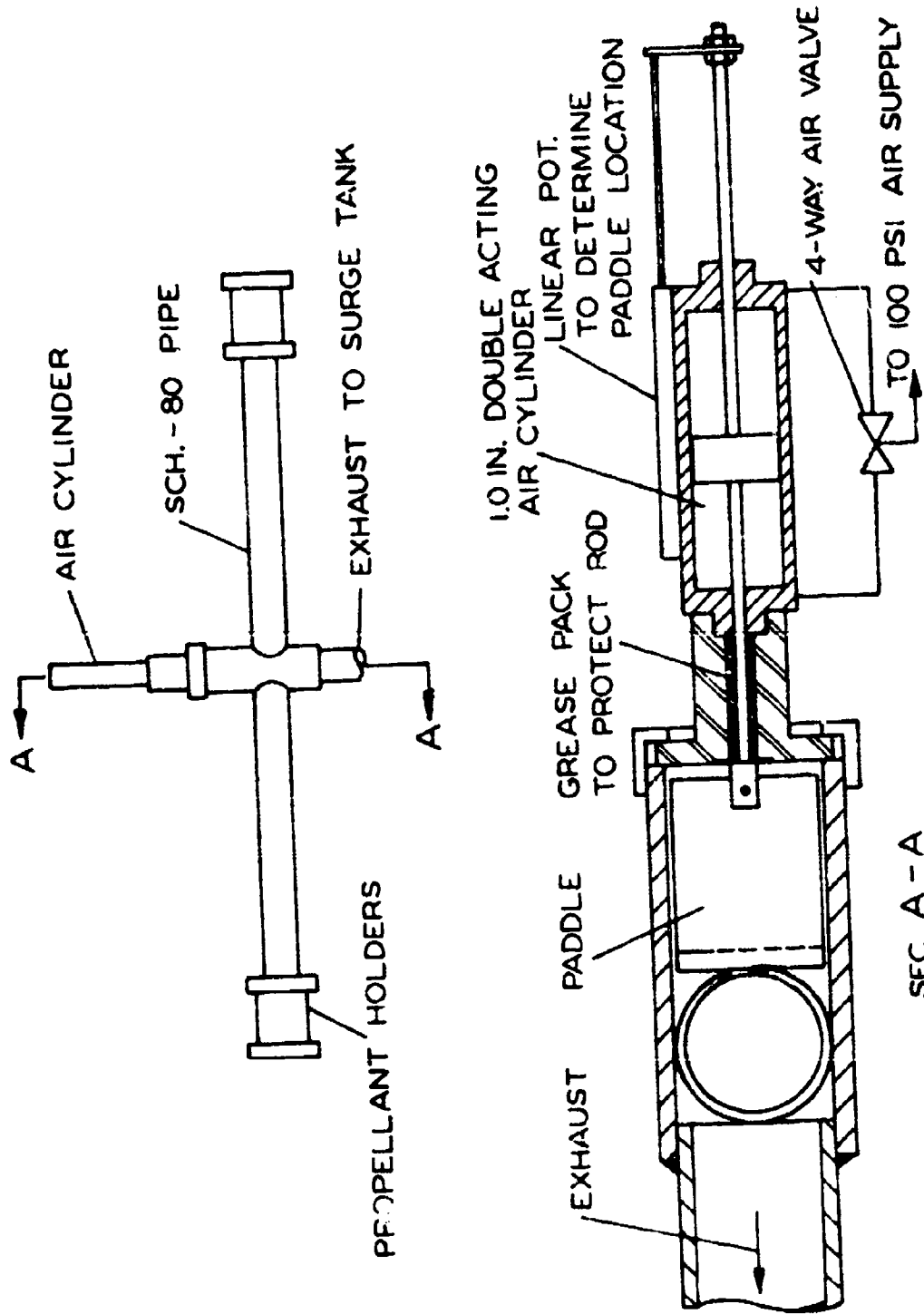


Figure 3.4-3 Surge Tank for VATB Apparatus with a Paddle Suppressor  
(ref. 3-4)



DETAIL OF FILLET GENERATED AT THE CORNER OF A CUP GRAIN

Figure 3.4-4 Details of a Surge Tank for VATB Apparatus (ref. 3-14)



SEC. A - A

Figure 3.4-5 A Typical Paddle Suppressor (ref. 3-6)

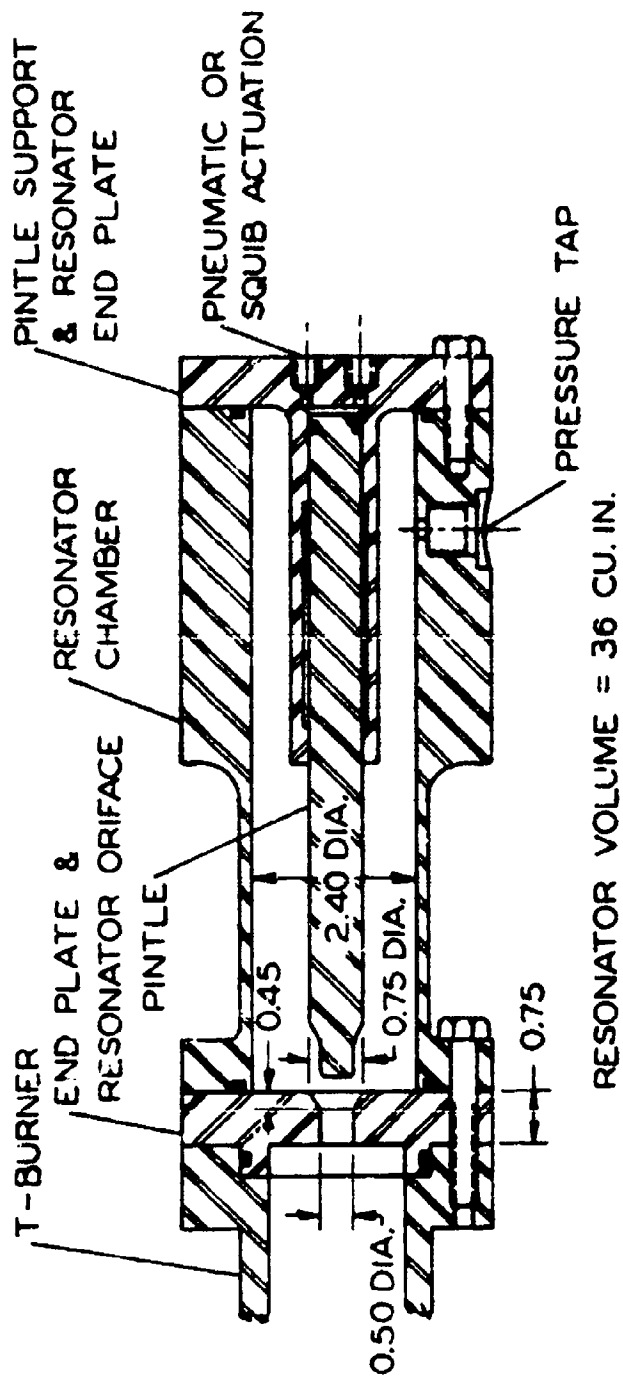


Figure 3.4-6 A Typical Helmholtz Resonator Used as a Suppressor  
(ref. 3-5)

A lower limit for suppression time can be determined by dividing one half of the T-burner length by the average gas velocity in the T-burner chamber.

Both the paddle and Helmholtz resonator have proved effective in damping oscillations in a T-burner. Characteristics of these suppressors have been studied in detail (ref. 3-17). These are outlined in Table 3.4-2.

Table 3.4-2. Characteristics of Suppressors

Paddle Suppressor

The paddle does not require tuning.

Under severe conditions (short T-burner length, high flow rates, and high metal loading and with extended use, the paddle erodes.

The paddle is mounted at the center of the T-burner. Thus, the ends of the T-burner are not affected by its presence.

The travel time of the paddle is long compared to the HR. For high growth conditions, the paddle can still be in the chamber during the first cycles of the growth period.

A mechanical shock can be transmitted to the T-burner when the paddle retracts.

Helmholtz Resonator

The HR must be tuned for each frequency tested. This is critical and can lead to problems where large frequency shifts occur in a test. When tuned properly, the damping is less than that found with the paddle.

There is a small acoustic loss associated with the decoupled HR. This could be a problem at high frequencies.

The HR couples at one end of the T-burner. Thus, a hole must be bored in propellant grains if a cup is used.

The travel time of the HR is less than the paddle.

A mechanical shock can be transmitted to the T-burner when the HR pintle seats.

Recommendations

The most significant factor in selecting a suppressor is the problem of tuning the Helmholtz resonator. This constitutes such a disadvantage that the paddle is recommended for suppressing oscillation in the VATB.

3.4.1.4 Ignition system.

Two igniter approaches have been used in VATB studies. One

uses a bag igniter containing BKNO<sub>3</sub> pellets. The second uses a hot wire/pellet igniter with pyrotechnic paste on the propellant surface.

Bag Igniter: a typical bag igniter design used in VATB tests is shown in Figure 3.4-7. One bag is placed at each end of the T-burner. Although the bag igniter introduces considerable combustion products and residue from the bag, the suppressor holds off oscillations until igniter products have been swept out of the T-burner. The bag igniter is normally designed to provide a large pressure spike that can denote the time of ignition.

Hot Wire/Pellet Igniter: this igniter approach is similar to that described in the CPIA T-Burner Manual (ref. 3-1) for nonmetallized propellants. The initiator may be made from a short length (3/8" - 1") of nichrome wire soldered to copper leads. The leads are 32-gauge enameled copper wire. A small tablet of pyrotechnic paste is molded around the nichrome bridge wire. The hot wire/pellet is then mounted so that the pellet is centered in the VATB propellant grain. To ensure rapid and uniform ignition of the grain, the surface to be ignited is coated with a thin layer of pyrotechnic paste. A typical pyrotechnic paste formulation is given in Table 3.4-3

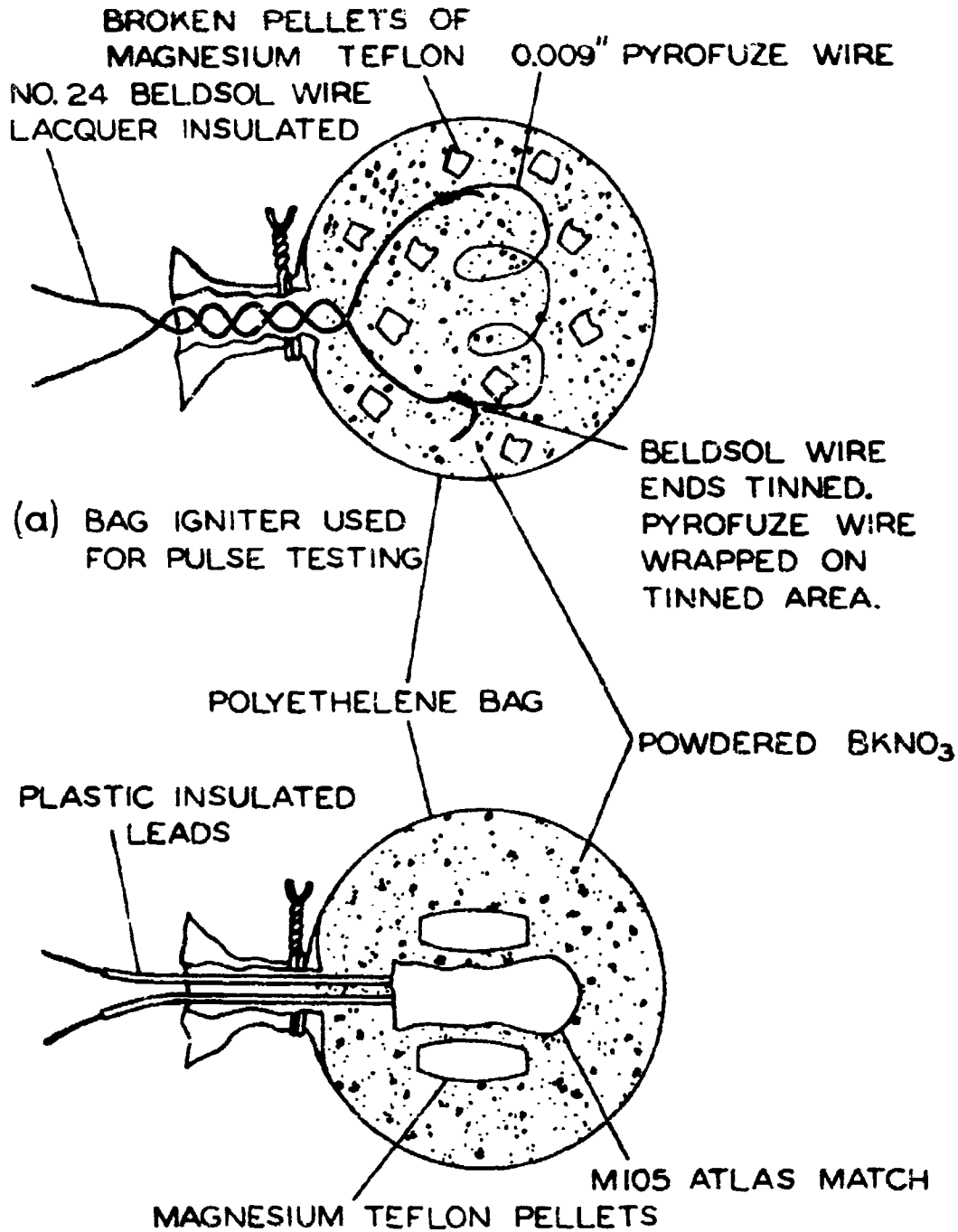
Table 3.4-3 Typical Formulation of Pyrotechnic Paste (ref. 3-4)

<u>Ingredient</u>	<u>Wt. %</u>	<u>Representative Sources</u>
Magnesium	57.16	Reade Manufacturing Co.
Potassium perchlorate (15 micron)	23.80	Kerr - McGee
Barium nitrate (15 micron)	14.28	Harshaw Chemical Co.
Vistanex-MM, L-120	4.76	Enjay Chemical Co.
Hexane*	---	---

\* Vistanex is pre-dissolved (50 parts hexane per 10 parts Vistanex) to serve as binder/vehicle for paint-on application.

Both of the aforementioned igniters have been found to give rapid and uniform ignition of propellant grains in VATB tests.

Wire fragments that remain in the T-burner can produce unknown



(b) STANDARD BAG IGNITER

Figure 3. 4-7 Bag Igniters Used in VATB Testing (ref. 3-6)

and nonreproducible effects on the acoustic losses in the T-burner. For various VATB approaches, igniter wires have been introduced through the center block, through the side of the T-burner chambers downstream from the propellant grain, and through the end cap. The approach of introducing the wires through the end cap minimizes problems associated with wires remaining in the T-burner during testing. However, holes through which the wires are introduced or any other surface irregularities must be considered as possible nonreproducible sources of damping and should be minimized to the extent possible. It has been found that wires in all three approaches are expelled from the T-burner or vaporized prior to the oscillation growths if sufficiently fine wire (e. g. 32-gauge) is used. The use of heavier wire should be avoided.

#### 3.4.1.5 Pulsers.

The pulse units used in variable-area testing provide the same function as those used in pulsed T-burner testing. Both the Bermite Mk 2 and ARC special squib have been used with satisfactory results in a 1.5" variable area T-burner (see § 3.3.1.4 for a discussion of these pulse units). However, for pulsing in larger diameter hardware, a stronger pulse is needed. For use in a 2.9" T-burner, pulses have been provided by use of a Mk 2 0 squib, 1 gram of black powder and a 0.008" brass rupture disc, as shown in Figure 3.4-8 (see ref. 3-6). This combination results in oscillations with an initial amplitude of approximately 20 psi in the 2.9" burner.

#### Recommendation

For 1.5" or 2" hardware, either the Mk 2 or ARC special squibs may be used with satisfactory results. For larger hardware, a stronger pulse unit must be used, tailored to give the desired pulse amplitude depending on the volume of the burner.

#### 3.4.1.6 Transducer location.

When cylinder grains are used in the VATB, the high frequency transducer can be mounted in the end cap without interference from the propellant. When cup grains are used, however, the transducer can be mounted behind the end disc of the propellant (as described in ref. 3-1, pp. 25-30) or a hole can be bored in the end disc so that the sensing sur-

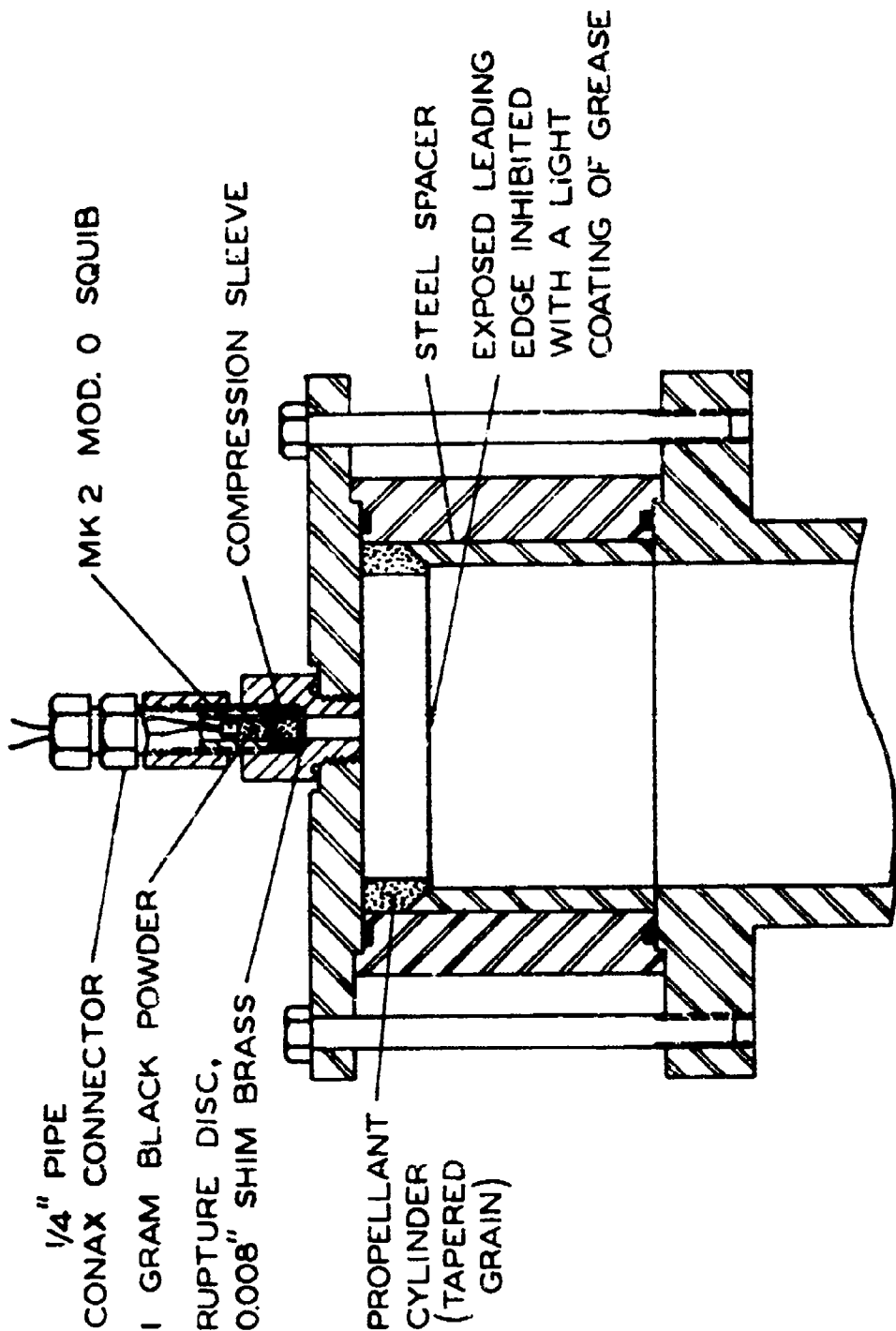


Figure 3.4-8 Hardware Used in Pulsing a 2.9" T-Burner (ref. 3-6)

face of the transducer is exposed to the acoustic field. Either approach should give valid data. The mean pressure in the VATB should be measured at the center of the T-burner (vent location). See additional comments in §3.3.1.6.

### 3.4.2 Propellant Grain Configurations

#### 3.4.2.1 Cups versus cylindrical grains.

VATB testing of metallized propellants requires  $S_b/S_{co} > 1.0$  if spontaneous instability is desired. Both cylinders and cups have been used in the VATB. See also refs. 3-21 to 3-23 for a modified form.

The relative merits of using cylinders or cups are as follows.

For cup grains, burnout is not uniform because a fillet is generated between the lateral and end-burning surface (see detail in Figure 3.4-4). Also, nonuniform burnout can result from the end of the cylindrical section of the cup burning out before the end adjacent to the fillet. This burnout phenomenon has been observed with cylinder grains. Tests have shown (ref. 3-20) that cylindrical grains of length greater than two inches, in a chamber of 1.5-inch diameter, burn out at the end closest to the T-burner vent 15 - 20 msec before the other end. Since delay after burning data are not required for the VATB test technique, this is not a crucial problem. However, nonuniform burnout could be a source of error in the determination of the propellant burning rate during the T-burner test.

If pulsers are located at the ends of the T-burner (pulsed-VATB method), a small hole must be drilled in the end disc of the cup. This hole could create an acoustic loss. No modification is necessary for a cylindrical grain.

For cup grains, both lateral and end-burning surfaces drive oscillations. Thus, based on the T-burner theory, correlation of cup data should yield both the end and side response functions ( $B_e$  and  $B_g$ ). However, attempts at correlating cup data from a VATB test series have not been satisfactory (see §§ 3.2.1 and 3.2.3.2). For inhibited or recessed cylinders, only lateral surfaces are present, and the side response function can be obtained.

#### Recommendation

It is recommended that cylindrical grains be used in VATB testing.

### 3.4.2.2 Recessed versus protruding grains.

Two methods for mounting propellant grains have been utilized in VATB testing: (1) the propellant grain protrudes into the T-burner chamber as shown in Figure 3.4-1; and (2) the propellant grain is recessed into the chamber wall as shown in Figure 3.4-2.

For protruding grains, the outer surface and the surface facing the end cap are inhibited. If the end surface closest to the vent burns, its contribution to acoustic driving must be included in Eq. (3.2.1), viz., the area ratio  $S_{be2}/S_{co}$  is non-zero. On the other hand, if this end surface is inhibited, the inhibiting material must not produce char that would protrude into the acoustic and mean flow field.

For recessed grains, the bore diameter is slightly larger than the inside diameter of the T-burner, as shown in Figure 3.4-2. The small web of propellant that protrudes from the chamber wall serves to fill the T-burner with combustion products before the burning surface is flush with the chamber wall. Only the bore of the grain is allowed to burn. All other surfaces are inhibited. The end surface that protrudes above the chamber wall before flush and recessed conditions occur should be coated with a non-charring material that is removed as the grain surface burns.

The change in T-burner cross-sectional area due to a recessed or protruding propellant grain could lead to complications in VATB data interpretation. More specifically, three-dimensional flow phenomena (e. g. flow separation and vortices) could occur at this area discontinuity. Since such phenomena are not represented by the T-burner analysis [Eq. (3.2.1)], correlations of VATB could yield inaccurate results. This problem can be minimized by obtaining VATB data when the propellant grain is close to flush conditions. Because of this, the recessed grain configuration is preferred over the protruding grain configuration. The recessed grain configuration is flush to the chamber wall shortly after ignition and provides burn time when multiple growth (or decay) measurements can be made (see §3.4.3) with the propellant near flush conditions.

In one laboratory (ref. 3-6), the recessed propellant grain has a taper in the end of the propellant as shown in Figure 3.4-2. This taper

reduces the effect of changes in cross-sectional area and is specifically designed to maintain the area ratio  $S_{bs}/S_{co}$  constant throughout a test. The latter feature is important when the rate of oscillation growth is slow compared to the burn rate of the propellant. However, the advantages of the taper are offset somewhat by increased costs in grain fabrication and complexities in test hardware.

#### Recommendations

The recessed grain configuration is recommended, and data should be obtained when the grain is close to flush conditions with the chamber wall. The use of a tapered grain is optional.

#### 3.4.2.3 Case bonded versus cartridge loaded grains.

One method of fabricating propellant grains is to cast the propellant into a phenolic sleeve. The cured sample is then mounted in a lathe and the center perforation is bored in the sample. An alternative is to machine the grains from large blocks of propellant.

The approach of casting propellants in phenolic sleeves allows cartridge loading of the grains. If the grain is machined from a large block of propellant, the grain must be secured in the T-burner by a potting compound, or it must be of such a dimension as to allow a pressure fit. The latter approach requires that an inhibitor (e. g. grease) be applied between the grain and the T-burner case.

#### Recommendations

Both approaches are satisfactory. The selection of case bonded or cartridge loaded grains should be based on the availability of casting equipment.

#### 3.4.3 Test Procedures.

##### 3.4.3.1 Recommended test series.

The scope of test programs required to characterize the acoustic response of a propellant is usually determined by factors such as motor geometry, ballistics, budget limitations, etc. Assuming all these things are accounted for, the present subsection addressed how the testing should be performed to obtain the desired data at a given pressure and frequency.

Generally, 10 to 15 datum points distributed over a range of area

ratios, are desired to give statistically significant response functions. The range of area ratios tested can be increased by using the pulsed/VATB approach, which will increase the confidence level of the data. To minimize the actual number of tests performed, multiple cycling of a suppressor (or multiple pulsing) can provide more than one datum point per firing.

Typical test conditions often lead to a burning duration of  $\sim 1$  sec. Approximately 200 msec are usually needed to recycle a suppressor and allow for a growth period (longer times are required for low growth rate conditions). Allowing for the ignition transient, three growth rates are typically obtained for such conditions. Thus, the desired quantity of data can be obtained with as few as 4 or 5 tests using this approach. When using this small number of tests, data should be obtained at a minimum of 3 different area ratios. Actually, when testing a new propellant with unknown characteristics, more tests are usually needed, as it is rarely possible to obtain multiple growths consistently unless the propellant characteristics are somewhat understood. For example, there are area ratios for every propellant that will not produce oscillations of sufficient strength to permit a growth measurement. To circumvent this situation, it is usually best to test at the largest available area ratio first and then at smaller area ratios. In this manner, the area ratios that don't produce oscillations can be determined by plotting growth rate versus area ratio. Using the pulsed/VATB technique, testing should begin with the lowest area ratio (pulse testing), followed by the largest area ratio (spontaneous oscillations). Interpolation will then allow optimum conditions to be selected for the remaining tests.

#### 3.4.4 Operational Limitations

##### 3.4.4.1 Pressure, frequency, and temperature.

The upper pressure limit for VATB testing is dependent upon the strength of the T-burner and associated plumbing and surge tank. In addition, since the burn time decreases with increasing pressure, another upper limit can be defined at the pressure where burn time is so short that growth or oscillations is precluded. The true upper limit for mean pressure is the smaller of these two limits.

General rules for frequency limitations cannot be defined for

VATB tests. At low frequencies, long T-burner chambers must be employed. These long chambers have larger exposed area that can lead to heat loss, and therefore a longer equilibration period over which oscillation suppression is necessary. Thus, the lower frequency limit for VATB testing is dependent upon burn time and the time necessary for the T-burner to establish equilibrium conditions. Factors affecting these are pressure, propellant burn rate characteristics, vent size, and propellant web thickness. Another problem that is encountered at low frequencies is the undesired presence of higher modes of oscillations. This problem is discussed in more detail in § 5.2.3. Based on available VATB data, the low frequency limit is approximately 200 - 300 Hz.

Because metallized propellants are usually much more stable at increasing frequencies, spontaneous oscillation growth requires higher burn area ratio  $S_b/S_{co}$ , and therefore longer grains. Since there is an upper limit to the grain length (see § 3.4.4.2), the upper frequency limit is different for the pulsed VATB and VATB methods. For frequencies where spontaneous growth requires grain lengths longer than the specified upper limit, the pulsed VATB method must be relied upon for data. An approximate upper limit for the VATB method is 1100 Hz (for a 1.5" T-burner) and 2000 Hz for the pulsed VATB method (for a 1.5" T-burner).

With regard to temperature limitations, it is recommended that the propellant temperature be maintained at  $\pm 5^\circ\text{F}$  about the desired test temperature.

#### 3.4.4.2 Propellant grain.

Propellant grains that are flush to the inside diameter of the T-burner ( $S_{co}/S_c \approx 1.0$ ) are preferred for VATB testing. However, based on available VATB data using metallized propellants, consistent trends are realized in the range  $0.6 < S_{co}/S_c < 2.0$ .

For conditions where the propellant is relatively stable, large values of  $S_b/S_{co}$  are necessary to achieve inherent instability. Thus,  $S_b/S_{co}$  can be achieved by increasing the grain length, or the propellant bore diameter (decreasing  $S_{co}/S_c$ ). If the lower limit on  $S_{co}/S_c$  is

reached, the length of the grain must be increased. In doing this, attention must be given to the possibility that acoustic driving due to velocity coupling is being introduced in the T-burner. The important parameter that should be considered is not the length of the propellant grain,  $L_b$ , but the non-dimensional length of the propellant grain,  $\beta = 2L_b/L$ . If velocity coupling is to be avoided,  $\beta$  must be maintained as small as possible. For low frequency tests (long T-burner chambers) this is not a problem. However, for high frequency tests (short T-burner chambers) when the losses are large, large values of  $\beta$  may be necessary to achieve self-excited oscillations. To minimize errors introduced by neglecting velocity coupling,  $\beta \leq 0.1$  is desirable. For larger values of  $\beta$ , some accounting of velocity coupling may be required (see §5.4.4).

3.4.5 An Example of Experimental Results. Figure 3.4-9 shows an oscillograph trace of pressure oscillation growth periods for a VATB test. Included are the suppressor activation signal and the fire pulse for the test. Details on data reduction are given in §5.1.2.

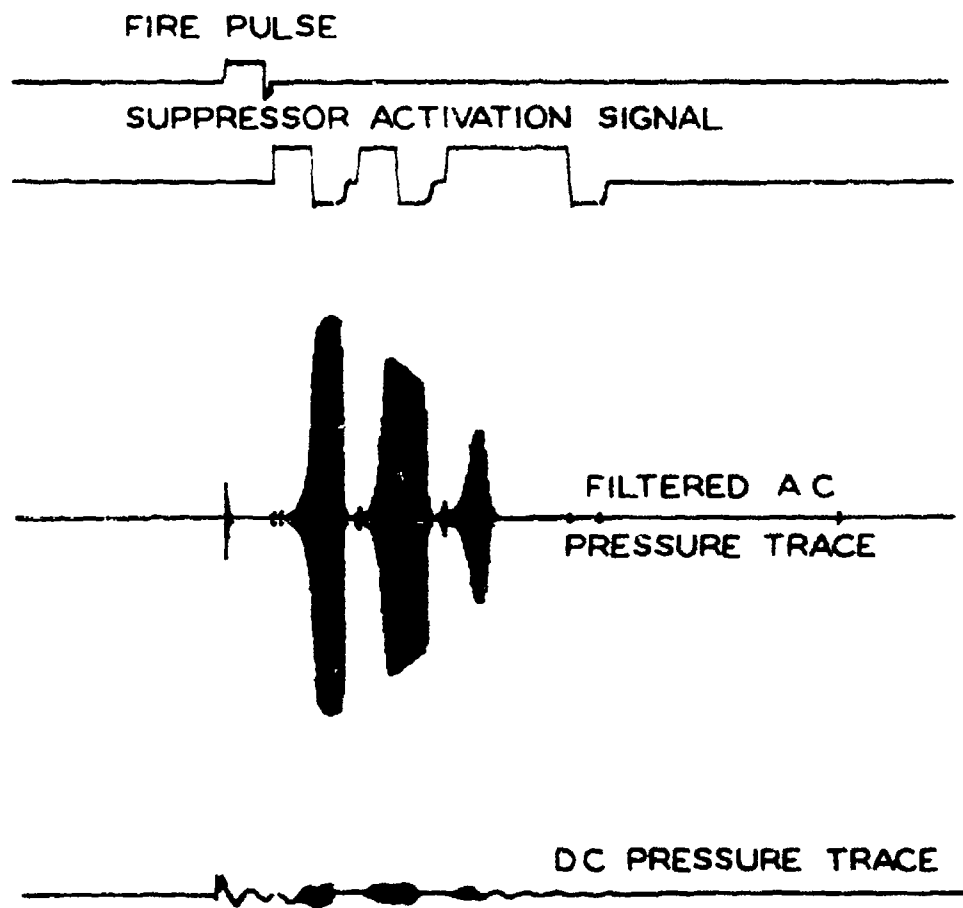


Figure 3.4-9 Reproduction of a VATB Test Record (ref. 3-5)

## REFERENCES

- 3-1 "T-Burner Manual," CPIA Publication No. 191 (November 1969), Chemical Propulsion Information Agency, Silver Spring, Md.
- 3-2 Price, E. W., Mathes, H. B., Madden, O. N., and Brown, B. G. "Pulsed T-Burner Testing of Combustion Dynamics of Aluminized Solid Propellants," Astronautics and Aeronautics, V. 10, no. 4 (April 1972), pp. 65-67. (Pulsed T-burner, U. S. Patent No. 3788126, 29 January 1974)
- 3-3 Coates, R. L. "Double-end Burner Experiments," Proceedings, Third Meeting -- Technical Panel on Solid Propellant Combustion Instability, Applied Physics Laboratory, TG 371-5 (May 1963).
- 3-4 Derr, R. L. "Development and Evaluation of the Variable Area T-burner for Metallized Propellants," AFRPL-TR-72-97 (November 1972), Lockheed Propulsion Co., Redlands, Calif.
- 3-5 Peterson, J. A., Muhlfeith, C. M., and Sayer, L. H. "Final Report -- Pressure Oscillation Investigation for Minuteman III," AFRPL-TR-72-98 (November 1972), Thiokol Chemical Corp., Wasatch Division.
- 3-6 Beckstead, M. W., Bennion, D. U., Butcher, A. G., and Peterson, N. L. "Variable Area T-Burner Investigation," AFRPL-TR-72-85 (December 1972), Hercules, Inc., Bacchus Works, Magna, Utah.
- 3-7 Andrepont, W. C. and Schoner, R. J. "The T-Burner Test Method for Determining the Combustion Response of Solid Propellants," AIAA/SAE 8th Joint Propulsion Specialist Conference, New Orleans, La. (Nov. 26-Dec. 1, 1972).
- 3-8 Letter reports from H. B. Mathes (Naval Weapons Center) to R. D. Kinert (Naval Material Command, PM-1) concerning Quality Control of FKM Propellant over the period March 1970 through May 1974 (copies available from Aerothermochemistry Division, Code 608, Naval Weapons Center, China Lake, Calif.); see also, Bennion, D. U., Beckstead, M. W., West, L. R., and Jessen, E. C. "The Variable Area T-Burner as a Quality Assurance Tool," 8th JANNAF Combustion Meeting (November 1971).
- 3-9 Price, E. W. and Mathes, H. B. "Effect of Ingredient Variables on Combustion of FKM Propellant," NWC TN 608-110, Revision 1 (May 1972), Naval Weapons Center, China Lake, Calif.
- 3-10 Wendelken, C. O., Weiss, R. R., and Chew, T. J. C. "Combustion Instability Characteristics of Several Solid Rocket Propellants for Booster and Tactical Rocket Applications," 9th JANNAF Combustion Meeting (December 1972), CPIA Publication 231.

- 3-11 Micheli, P. L. "Evaluation of Pulse T-Burner for Metallized Propellants: Vol. I. Experimental Procedures for the T-burner," AFRPL-TR-72-54 (January 1973), Aerojet Solid Propulsion Co., Sacramento, Calif.
- 3-12 Wendelken, C. P. "Combustion Stability Characteristics of Solid Propellants, AFRPL-TR-73-63 (October 1973), Air Force Rocket Propulsion Laboratory, Edwards, California.
- 3-13 Crump, J. E., Price, E. W., Mathes, H. B., and Dehority, G. L. "Oscillatory Combustion Experimentation and Analysis Work in Support of an Air Force Program, 1971-1972," NWC TP 5630 or AFRPL-TR-73-108 (June 1974), Naval Weapons Center, China Lake, California.
- 3-14 Lovine, R. L. "Evaluation of Pulse T-burner for Metallized Propellants: Vol. III. Piston Pulser Development," AFRPL-TR-72-54 (January 1973), Aerojet Solid Propulsion Co., Sacramento, Calif.
- 3-15 Perry, E. H. "Investigations of the T-Burner and Its Role in Combustion Instability Studies," Ph. D. Thesis, California Institute of Technology, Pasadena, California (May 1970).
- 3-16 Bennion, D. U., Hopkins, B. D., Beckstead, M. W., and West, L. R. "Final Report for Subtask 2, T-Burner, of Task 5, Pressure Oscillation Study," Report No. MTO-1124-50 (Aug. 1971), Hercules, Inc.
- 3-17 Bennion, D. U., Beckstead, M. W., West, L. R., and Jessen, E. C. "The Variable Area T-Burner as a Quality Assurance Tool," 8th JANNAF Combustion Meeting (November 1971), CPIA Pub. 220.
- 3-18 Mathes, H. B. and Price, E. W. "Measurements of Combustion Dynamics of Solid Propellants on the Low Frequency Range," AIAA Paper No. 67-70; 5th Aerospace Sciences Meeting, New York (Jan. 23-26, 1967).
- 3-19 Coates, R. L. and Sayer, L. "On Improved Burner Design for Testing Dynamic Burning Properties of Solid Propellants," Rev. Sci. Instr., V. 42, no. 11 (November 1971), pp. 1718-1719.
- 3-20 Beckstead, M. W. Data presented at 3rd Workshop on T-Burners for Metallized Propellants, AFRPL (October 1972).
- 3-21 Gould, R. D. and Penny, P. D. "An Experimental Investigation of the Burning Rate of Propellant ANB 3066 under Oscillatory Pressure and Oscillatory Velocity Conditions," AFRPL-TR-73-95, Rocket Propulsion Establishment, Westcott, Aylesbury, Bucks., UK (Nov. 1973).
- 3-22 Gould, R. D., Penny, P. D., and Gittins, J. "T-Motor Programs," Notes Prepared for the Third AFRPL T-Burner Workshop, AFRPL 14-15 Oct. 1971, Rocket Propulsion Establishment, Westcott.
- 3-23 Gould, R. D., Penny, P. D., Gittins, J., and Channon, N. D. "T-Motor Programme," Notes prepared for the 6th T-Burner Workshop, AFRPL, 19-20 July 1972, Rocket Propulsion Establishment, Westcott, Aylesbury, Buckinghamshire, United Kingdom.

## 4. INSTRUMENTATION AND DATA ACQUISITION

Similar instrumentation is required for using the pulsed, pulsed-variable area, and the spontaneous growth variable-area T-burners (refs. 4-1 through 4-6). The instrumentation consists basically of high quality pressure transducers, signal conditioning devices such as amplifiers, an electronic filter, and a recording system such as an FM tape deck and/or oscillographs. An event sequencer is also needed to control the ignition, actuation of the suppression device or the pulser, time delay between spontaneous growths or pulses, and the termination of tests.

### 4.1 General Description of Instrumentation

Figure 4.1-1, taken from ref. 4-4, shows the simplest form of the instrumentation required. A more elaborate system is shown in Figure 4.1-2. The specific instrumentation and detailed arrangements vary with each facility, depending on the available equipment. The most important considerations in designing and operating T-burner instrumentation are to ensure durability, adequate frequency response capability and resolution; to reduce intrinsic noise to very low levels; and to generate both immediate and permanent records which can be examined manually and later processed electronically.

The capability of processing the data electronically, either simultaneously with the test or at a later time, is often not essential. Direct display of the band pass filter's signals on the oscillograph can be a more economical option. The pulsed DB/AB method (refs. 4-6 and 4-10) has been developed successfully without expensive recording equipment. Tests based on the variable area, and pulsed variable-area methods can also be conducted without incurring the large expense of an FM tape deck. However, for work at high frequencies, the use of a tape deck may be required to obtain detailed information.

An option to get a quick-look at the data can be advantageous for monitoring the tests as they are performed. An oscilloscope fitted with a Polaroid camera or an oscillograph can be used for this purpose (refs. 4-1, 4-2, and 4-8).

Detailed specifications for each unit of the instrumentation are not

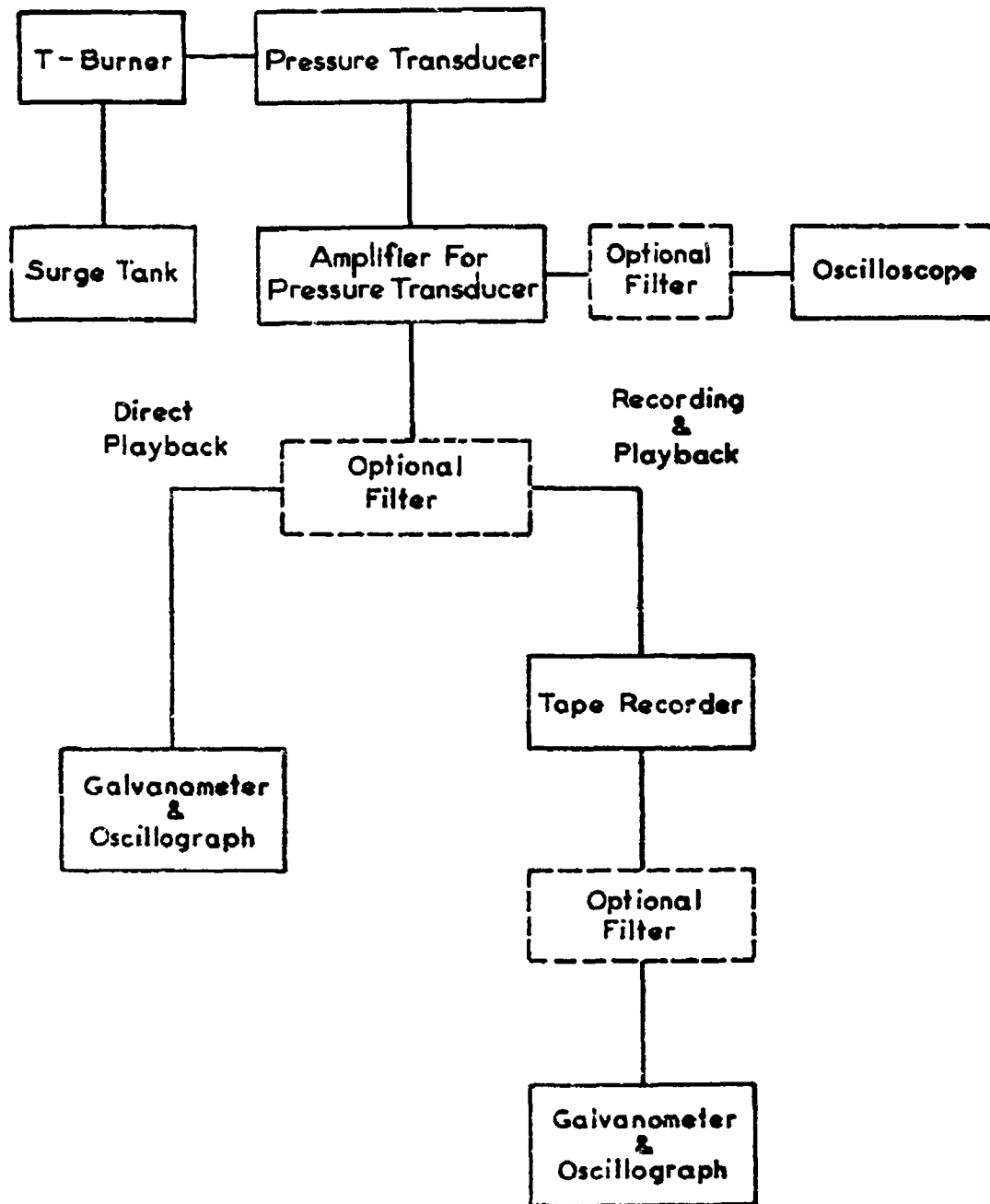


Figure 4. 1-1 Block Diagram of Basic Instrumentation



presented here because of the highly specialized nature of such information. Typical instrumentation is listed in Table 4.1. Optional instruments are enclosed by the dashed lines in Figure 4.1-2.

TABLE 4.1 Typical Instruments Used in  
Existing T-Burner Facilities\*

Pressure Transducers:

Oscillatory Pressure: Kistler Model 701A, 603A, and 701H;

Photocon Type 403; Dynagage Model 403

Mean Pressure: Norwood 111, Tabor 206, Dynisco PT 79T

Amplifiers:

Kistler Model 568 and 504

Bay Laboratories, Inc. Model 3512

Filters:

Krohnite Models 310-AB, 3700 R, and 330 MR

Spencer Kennedy Laboratories Model 302

Burr-Brown Model HP2B-10R0

Oscillograph:

Honeywell Model 1508 Visicorder; CEC Models 5-114, 6-124, and 5-133

Tape Recorders:

Ampex Models AR-200, FR-1300, and ES-100; Sangamo 47B

Precision Instruments Model 400A

Oscilloscopes:

Tektronix Model 555 and Model 535

Beattie-Coleman Periscope for Polaroid Camera

---

\* From references 4-1, 4-3, 4-5, 4-6, 4-8, and 4-9. The identification of specific manufacturers models is not an endorsement of the product. Components of quality comparable to those listed could be substituted.

Detailed instrumentation diagrams are given on page 99 of ref. 4-2, page 9 of ref. 4-5 for the variable area method; and page 16 of ref. 4-9, Figure 8 of ref. 4-3, and reference 4-6 for the pulsed methods.

#### 4.2 Pressure Transducers

Two basic types of transducers have been utilized in T-burner testing. Most commonly, a piezoelectric transducer is used to measure the incipient oscillations and a strain gauge type to measure the mean pressure. Kistler Instrument Corp.'s model 603 and 701 transducers and the Dynagage model 403 have been used extensively at several facilities. Kistler model 504 and 568 charge amplifiers and the Kistler model 562 calibrator are used in conjunction with the piezoelectric gauge. Mean pressures have been measured with Norwood III, Taber 206, and Dynisco PT 79T gauges.

Transducers should be checked for the effect of acceleration of the T-burner on the data. This can be accomplished by blind mounting an identical pressure transducer next to the regular transducer and pressurizing the burner. Actuation of the suppression device provides the impulse needed to accelerate the transducer (4-5).

The high temperature gases will not affect the flush mounted Kistler unit for durations of several seconds, with only a thin film of silicone grease as protection. The coating of grease also protects the transducer from chemical attack by the corrosive products of combustion.

Periodic calibration of the pressure transducers is recommended. Calibration after 100 routine tests should be adequate (refs. 4-4 to 4-6). Recalibration sooner may be required if a major pressure excursion is noted, or if the transducer is exposed directly to the combustion products. Maintenance and care of the transducers, cables, and associated equipment can be found in the manufacturers' literature.

#### 4.3 Oscillograph Records

Recording oscillographs not requiring chemical processing of the film or paper are most convenient for recording the data. The oscillographs are also used to provide a visible record of data played back from FM recorders and for the quick-look examination of the data. Recorders which have been used are CEC models 5-114, 5-124, 5-133, and Honeywell model 1508. The oscillograph should be capable of relatively high speed recording (recommended  $\geq 60$  ips).

Among the galvanometers used are the CEC 7-362 and 7-361 which have flat responses within 5 per cent to 2500 and 5000 Hz, respectively. Galvanometers capable of flat response to approximately 25,000 Hz are available but generally not required in T-burner operations.

#### 4.4 Filtering

Oscillatory pressure data can be directly recorded on FM and played back through appropriate filters, or recorded directly on an oscillograph for the permanent record or for quick-look examination. One procedure is to pass the signal through a high band pass filter and then through a set of band pass filters set at  $\pm 10$  per cent of the T-burner natural frequency.

The Spencer Kennedy Laboratories (SKL) model 302 and Krohnite models 3700R, 330 MR, and 310AB have been used successfully.

Care must be exercised in setting the filters; experience has indicated that amplification or reduction of the signal may occur if the settings are respectively too wide or too narrow (ref. 4-5). A signal generator can be used to determine whether distortion occurs in the amplifiers, or filters. The appropriate setting of the band pass filters can be determined by examining an oscillograph record of the reference signal from the generator.

#### 4.5 Magnetic Recording and Spectral Analysis

FM magnetic recording systems are used to provide a wide frequency band of recording capability. The FM tape also provides a permanent record of the data which can be retrieved, manipulated, and examined at any time. Saturation of the tape could become a problem for some test conditions because of the high amplitude pressure signal. Thus, the input signal amplifiers must be adjusted for various test conditions. FM tape decks which have been used for T-burner data recording are: Ampex FR-1300, Ampex ES-100, Ampex AR-200, and Sangamo 47B.

The capability of reprocessing the data on the tapes is particularly helpful for analysis of harmonic content. A Spectral Dynamics Model 101A (ref. 4-5) and Quan-Tech equipment (ref. 4-1) have been used for spectral analysis.

The Quan-Tech equipment incorporates an electrically-controlled

variable band pass filter system having a frequency analysis capability from 10 Hz to 50,000 Hz. The data display output of this equipment is in visicorder format, and several options for data display are available. The initial display identified all frequencies present in the data over any given time interval. Specific frequencies can be selectively tracked to provide a plot of frequency versus time and amplitude versus time of the tracked frequency. Frequency data are accurate to within  $\pm 5$  per cent. This equipment has the additional capability of performing phase analysis by reading directly the phase difference between the filtered signals from two channels of data (ref. 4-1).

#### 4.6 Instrumentation for Suppression Devices

Control of the time of onset of oscillation growth is discussed in §§ 3.2 and 3.3. A Helmholtz resonator coupled to one end of the T-burner (refs. 4-5 and 4-2), a retractable paddle at the vent section (refs. 4-1 and 4-2), and a rotating valve (ref. 4-3) have been used to control the growth period onset. Details of the operation can be found in the literature (refs. 4-1 to 4-3, and 4-5).

Monitoring the action of the suppression device is recommended to ascertain its location in relationship to the onset or suppression of the oscillatory pressure. A linear potentiometer (e. g. Collins, LVDT model 55-08) attached to the actuation mechanism is satisfactory (ref. 4-2).

The T-burner pressure, frequency, and propellant influence the force required to actuate the suppression device. The operation conditions required to achieve rapid actuation of the suppression device must be determined experimentally.

#### 4.7 Peak Follower Circuit (PFC)

An electronic PFC has been developed (ref. 4-11) which can be used effectively in simplifying the reduction of T-burner data.

Many advantages are present in the application of the PFC concept to the acquisition and reduction of T-burner data, including:

- (a) simplicity of data reduction,
- (b) higher accuracy,
- (c) consistent results,
- (d) time savings.

As an indication of the time which can be saved in the reduction of T-burner data by using the PFC, the growth or decay constant can be obtained from the oscillograph record in approximately 3 minutes. This data reduction technique enables an investigator to immediately determine which are the linear portions of the growth or decay curves. The PFC reduction method provides "quick-look" data, for the growth and decay constants, which are as accurate as the time consuming hand-reduced data or the expensive computer-reduced data.

#### REFERENCES

- 4-1 Beckstead, M. W., Bennion, D. U., Butcher, A. G., and Peterson, N. L. "Variable Area T-Burner Investigation," Technical Report AFRPL-TR-72-85 (December 1972), Hercules Inc., Bacchus Works, Magna, Utah.
- 4-2 Derr, R. L. "Evaluation of a Variable Area T-Burner for Metallized Propellants," Technical Report AFRPL-TR-72-97, Lockheed Propulsion Co., Redlands, Calif. (February 1973).
- 4-3 Micheli, P. L. "Evaluation of Pulsed T-burner for Metallized Propellants," Vol. I. Experimental Procedure for the T-Burner, Technical Report AFRPL-TR-72-54 (September 1973), Aerojet Solid Propulsion Co.
- 4-4 "T-Burner Manual" CPIA Publication No. 191, CPIA, Silver Spring, Md. (November 1969).
- 4-5 Peterson, J. A., Muhlfeith, C. M., and Sayer, L. H. "Pressure Oscillation Investigation for Minuteman III," Technical Report AFRPL-TR-72-98 (January 1973), Thiokol Chemical Corp., Brigham City, Utah.
- 4-6 Crump, J. E. "Oscillatory Combustion Experimentation and Analysis," Technical Report AFRPL-TR-72-99, Naval Weapons Center, China Lake, Calif. (Dec. 1972).
- 4-7 Price, E. W. "Experimental Measurements in Solid Propellant Rocket Combustion Instability," Section 3.4, Experimental Methods (pp. 53-74), Combustion Research, edited by J. Surugue, Pergamon Press, New York (1961).
- 4-8 Gould, R. D. and Penny, P. D. "An Experimental Investigation of the Burning Rate of Propellant ANB-3066 Under Oscillatory Pressure and Oscillatory Velocity Conditions," AFRPL-TR-73-95 (November 1973), Rocket Propulsion Establishment, Westcott, United Kingdom.

- 4-9 Wendelkin, C. P. "Combustion Stability Characteristics of Solid Propellants," Technical Report AFRPL-TR-73-63, Edwards Air Force Base, California
- 4-10 Crump, J. E., Price, E. W., Mathes, H. B., and Dehority, C. L. "Oscillatory Combustion Experimentation and Analysis Work in Support of an Air Force Program, 1971-1972," NWC TP 5630, AFRPL-TR-73-108, Naval Weapons Center, China Lake, Calif.
- 4-11 "Peak Follower Circuit Program," Technical Report AFRPL-TR-74-14 (April 1974), Hercules, Inc., Bacchus Works, Magna, Utah.

## 5. ANALYSIS AND REDUCTION OF DATA

The purpose of this section is to cover in some detail the general problem of obtaining quantitative results from T-burner tests. Not all questions have been settled; further discussion and results may be found in refs. 5-1 to 5-6. Most of the material in this section rests on the subjects already covered in § 2-4. Appreciation of many of the courses of action suggested here, and the difficulties encountered, will require a good understanding of the preceding material. Some of the problems discussed here are also encountered in testing with propellants not containing metal. Consequently, the earlier T-Burner Manual (ref. 5-7) contains useful background information.

### 5.1 Methods for Reducing Data

In this section, methods are described for reducing data taken with the pulsed DB/AB and VATB test methods. For this discussion, it is assumed that the T-burner data are contained on an oscillograph record. The methods for data reduction, therefore, are described in terms of "hand reduction" approaches. If computerized methods are to be employed, the same basic information is applicable in the development of the computer programming. A few brief remarks and references on work making more elaborate use of computers are given in § 5.1.3.

#### 5.1.1 Pulsed DB/AB Method

##### 5.1.1.1 Measurements from the pulsed DB/AB test records.

A typical oscillograph record from a pulsed DB/AB test is shown in Figure 3.3-8. Data that should be extracted from such a test record are as follows:

- |          |   |
|----------|---|
| $t_i$    | <u>the time of ignition.</u> This time is defined as the time when the mean pressure starts to rise, as shown in Figure 5.1-1.  |
| $t_{bo}$ | <u>the burnout time.</u> This time is defined as the time corresponding to the intersection of lines drawn through the pressure (during burning) and pressure decay (after burning) as indicated in Figure 5.1-1. |
| TABO     | <u>the time after burnout.</u> The time after burnout is the time interval between $t_{bo}$ and the first "usable" cycle  |

of the AB pulse as shown in Figure 5.1-1. The first "usable" cycle is the first cycle that is sinusoidal in shape and is followed by oscillations of decreasing amplitude.

$\bar{f}$  frequency. The average frequency for the DB and AB pulse decays is determined from the number of cycles measured in the decay period and the corresponding time interval for the total number of cycles counted (Figure 5.1-2).

$$\bar{f} = \frac{\text{number of cycles counted}}{\text{time period of cycles counted}}$$

$\hat{p}$  amplitude of pressure oscillations during a decay period. The peak-to-peak amplitude of pressure oscillation during the decay period is measured as shown in Figure 5.1-2. Lines are constructed between the minimum peaks of adjacent oscillations (shown as dashed lines in Figure 5.1-2); the vertical distance between that line and the encompassed maximum peak is measured to give the amplitude of a cycle. This measured amplitude can be utilized in subsequent calculations or converted to pressure based on the calibration data for the high frequency pressure transducer.

$\bar{p}$  mean pressure for the test. This pressure is defined as the initial pressure in the surge tank. Because of the small amount of propellant used in the DB/AB method, the mean pressure rise during burning is only 2 - 4 per cent.

#### 5.1.1.2 A Method of reducing pulsed DB/AB data

In this section, the method used in ref. 5-1 is described. The final data obtained from a pulsed DB/AB test consist of the following:

- run number
- propellant type and lot number
- grain configuration
- T-burner length, L

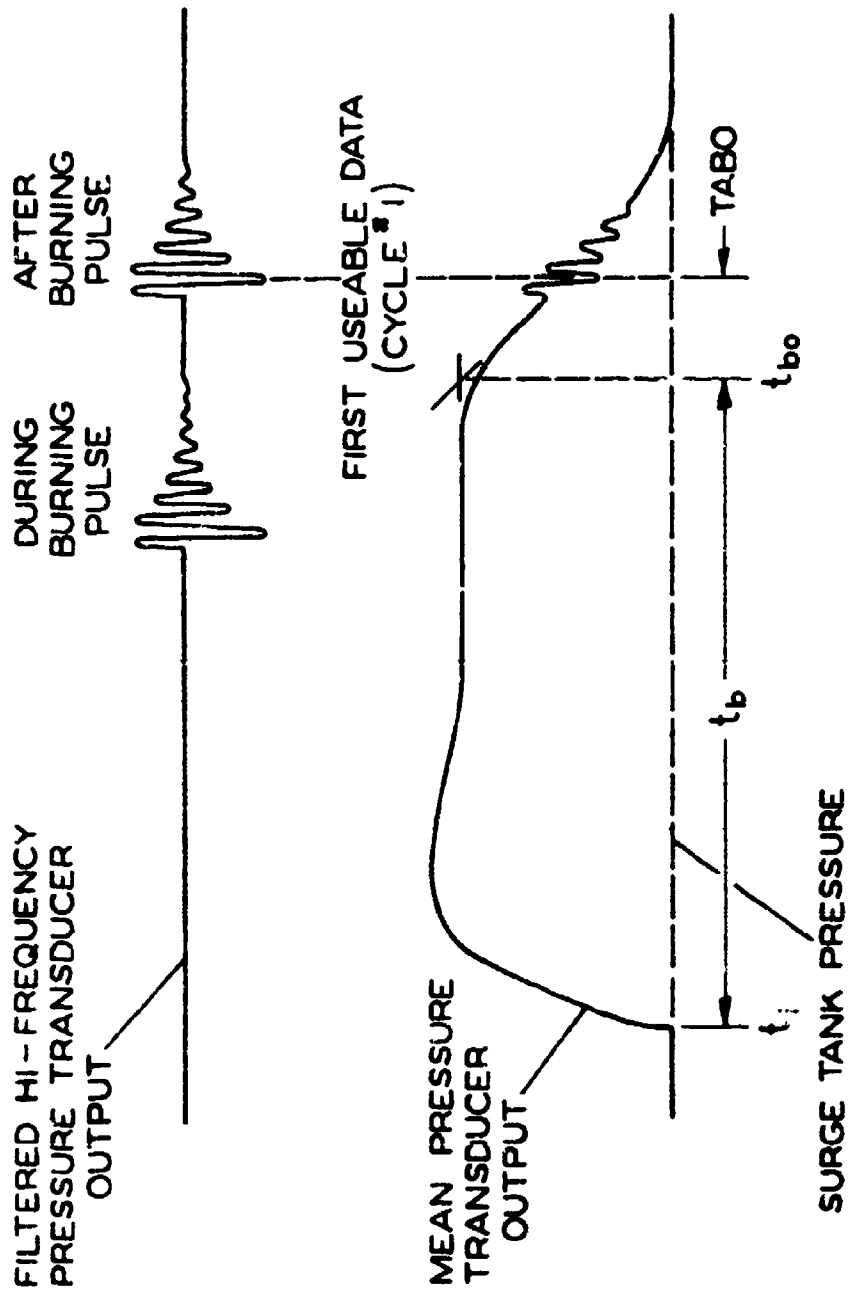


Figure 5.1-1 Sketch of a Pulsed DB/AB Test Record for Defining Measured Quantities

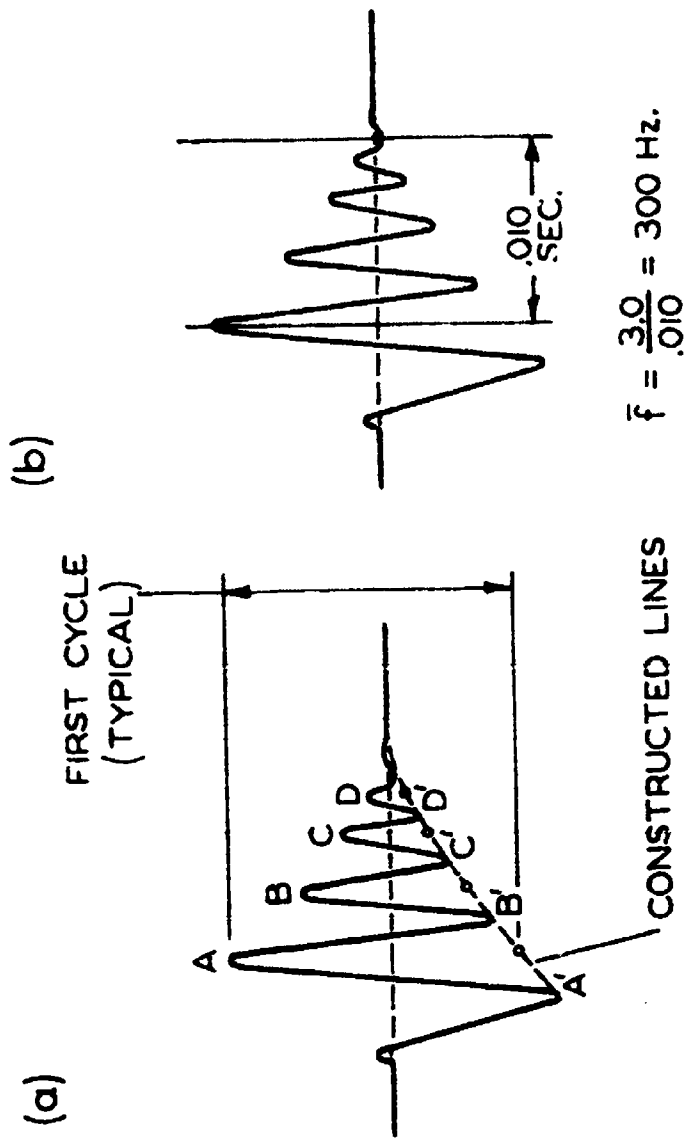


Figure 5.1.1-2 Diagrams Showing Measurement of Pressure Amplitude and Frequency

burn area ratio,  $S_{i ei} / S_{co}$  or  $S_{bs} / S_{co}$

frequency of oscillations,  $\bar{f}$

mean pressure,  $\bar{p}$

average burn rate,  $r = \frac{\text{web thickness}}{t_{bo} - t_i}$

during burning decay constant,  $\alpha_1$

after burning decay constant,  $\alpha_2$

The only parameters that require discussion are the decay constants,  $\alpha_1$  and  $\alpha_2$ . The decay constant can be defined as

$$\hat{p}_n = \hat{p}_0 \exp(-\alpha t_n),$$

where

$\hat{p}_0$  is the amplitude of the first cycle,

$\hat{p}_n$  is the amplitude of the  $n^{\text{th}}$  cycle,

$t_n$  is the time interval between  $\hat{p}_0$  and  $\hat{p}_n$ .

Ideally, the decay constant can be determined from the slope of a straight line drawn through the data plotted on a  $\ln(\hat{p}_n)$  versus cycle number plot.

The decay constant is

$$\alpha = \frac{\ln(\hat{p}_0 / \hat{p}_n)}{t_n} \quad \text{or} \quad \alpha = \frac{\ln(\hat{p}_0 / \hat{p}_n)}{\bar{f}} n$$

where  $n$  is the number of cycles between the  $\hat{p}_0$  and  $\hat{p}_n$  measurements.

However, it has been found (ref. 5-8) that the data do not fall along a straight line on such a plot. More specifically, the slope of the line is dependent upon the amplitude of oscillations. Thus, this simple approach to determining the decay constant is not employed. Instead, the data are fitted by an equation representing a nonlinear oscillator (ref. 5-9). With the assumption that  $d\alpha/d\Delta p = 0$  and  $\Delta p = 0$ , the form of the equation used to fit the experimental pulse decay data is

$$\Delta p^2 = \frac{C_0 \Delta p^2 \exp^{2C_0 t}}{C_0 + C_2 \Delta p^2 (1 - e^{2C_0 t})} \quad (5.1.1)$$

where  $C_0$  and  $C_2$  are "curve fitting" parameters.

A computer program can be used to minimize the least squares deviation of the fitted curve and the data points. The function form of

Eq. (5.1.1) gives a quite satisfactory fit to the data over the range of experimental data (Figure 5.1-3) and also gives a reasonable value of  $\alpha$  when extrapolated to zero pressure amplitude (ref. 5-1). The explicit expression for  $\alpha$  is:

$$\alpha = C_0 + C_2 \left[ \frac{C_0 \Delta p^2 e^{2C_0 t}}{C_0 + C_2 \Delta p^2 (1 - e^{C_0 t})} \right]. \quad (5.1.2)$$

A computer data reduction procedure for a set of tests involves the following steps. The data for the DB pulses are first individually fitted by Eq. (5.1.1); then the mean value of DB pulse data is obtained from a least squares fit of the data from individual pulses using Eq. (5.1.1). The mean value of  $\alpha_1$  for the set of data is determined from Eq. (5.1.2) as a function of the pressure amplitude. The sample deviation of  $\alpha_1$  about the mean curve is also calculated.

The data for the AB pulses are also individually fitted by Eq. (5.1.1) and  $\alpha$  versus  $\Delta p$  is determined for each pulse. The "raw" time after burnout (TABO') measured from the time of burnout to the first "usable" pulse cycle is corrected by the amount of time for the pressure to decay from the first usable cycle to a given amplitude; that time is designated TABO for that particular amplitude. The values of  $\alpha$  from different tests are plotted as a function of time after burnout as indicated in Figure 5.1-4. In order to approximate the reasoning of § 3.3.3.1 regarding the variation of  $\alpha$  with time for a pulse after burnout, the following is done. The plotted points  $\alpha_2$  versus TABO are fitted (by a least squares method) with a third order polynomial. The polynomial is constrained so that it passes through the mean value of  $\alpha_1$  for the DB pulses, at an arbitrary time after burnout (TABO)<sub>0</sub> less than zero, with slope of zero. Following this fitting procedure,  $\alpha_d$ , representing all losses, is taken as the value of  $\alpha_2$  at the maximum magnitude as indicated in Figure 5.1-4. The sample deviation about the fitted curve is taken as the sample deviation about  $\alpha_d$ .

The reasoning behind this procedure is depicted in Figure 5.1-4. In the case of a destabilizing contribution from the burning propellant (positive  $\alpha_c$ ), the relationship between  $\alpha_2$  and TABO is reasoned to be

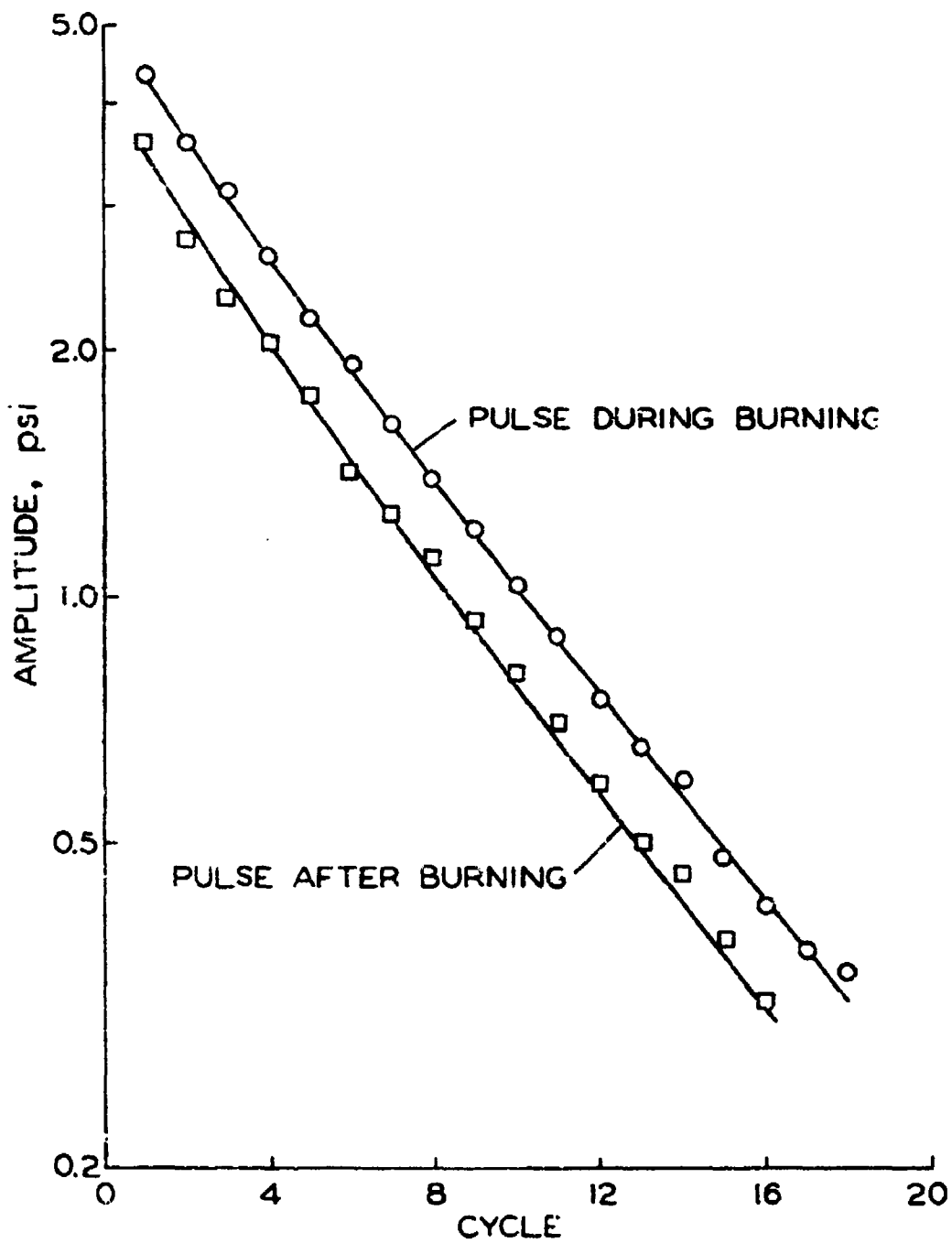
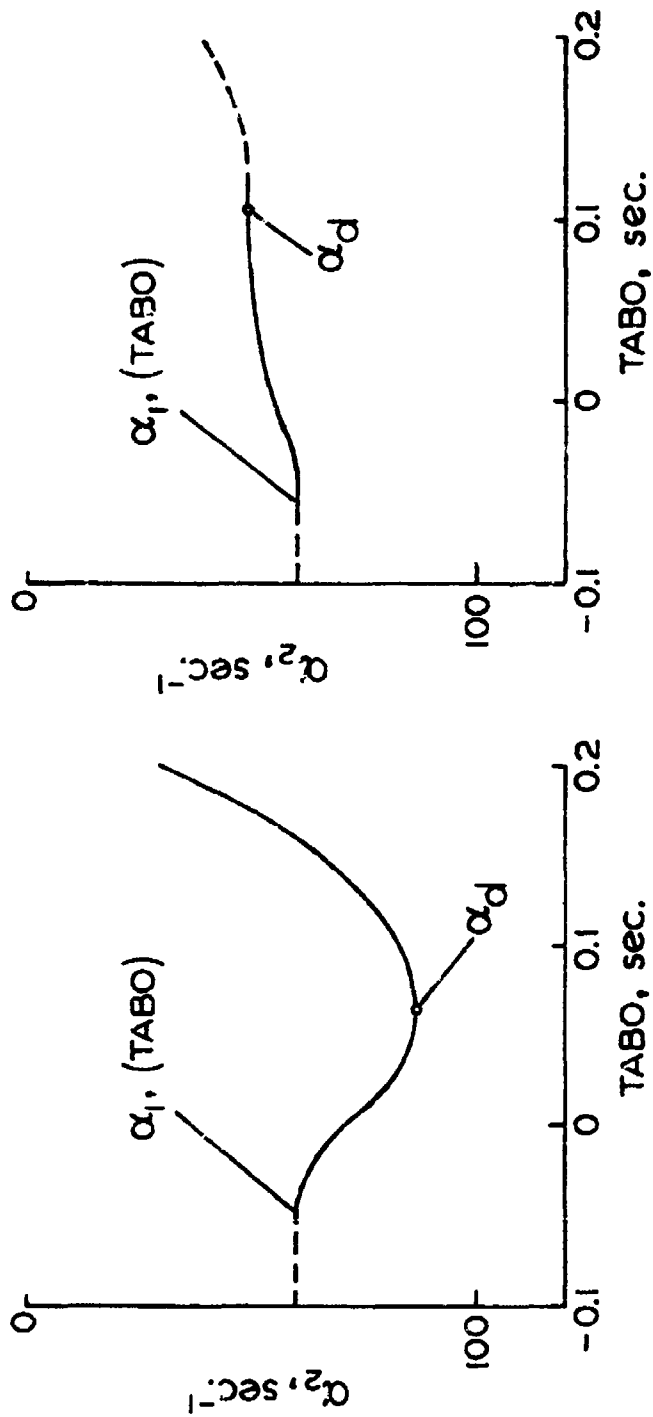


Figure 5. 1-3 Least Squares Fit (Eq. 5. 1. 1) to Experimental Data



(a) POSITIVE  $\alpha_c$  (b) NEGATIVE  $\alpha_c$

Figure 5.1-4 Illustration of Third Order Polynomial Fit to Data for  $\alpha_2$  Versus TABO (ref. 5-1)

similar to that shown in Figure 5.1-4(a). At TABO's less than zero,  $\alpha_2$  should have the value of the mean DB decay alpha, i. e.,  $\bar{\alpha}_1$  equal to  $\alpha_2$ ; the imposition of zero slope at  $(\text{TABO})_0$  accounts for a gradual transition from  $\bar{\alpha}_1$  to  $\alpha_d$ . The effect of the "arbitrary" choice of  $(\text{TABO})_0$  was evaluated in ref. 5-1; it was concluded that a reasonable choice of  $(\text{TABO})_0$  did not critically affect the value of  $\alpha_d$ , i. e., the variation of  $\alpha_d$  with  $(\text{TABO})_0$  was small compared to the sample deviation about  $\alpha_d$ .

In the case of a stabilizing contribution from the propellant (negative  $\alpha_c$ ), the relationship between  $\alpha_2$  and TABO is also fit by a third order polynomial as shown in Figure 5.1-4(b). The same reasoning as above is applied in this case, except that  $\alpha_d$  is taken as the "plateau" or inflection point of the fitted curve. The situation of a negative  $\alpha_c$  has been observed on occasion. If it were a more common occurrence, one would probably find that a fifth order curve fit (as indicated by the dashed line in Figure 5.1-4(b)) would be a much better approximation.

With many propellants tested using the DB/AB method, the frequency of the AB decay is sufficiently lower than that of the DB decay so that a correction in frequency is felt necessary in order to calculate  $\alpha_c$  from the  $\alpha_1$  and  $\alpha_d$  data. The procedure used in the DB/AB method is to conduct tests at various frequencies to develop an empirical relationship between  $\alpha_d$  and frequency. From the relationship  $\alpha_d$  is "corrected" to the frequency of  $\alpha_1$  before the calculation of  $\alpha_c$  is made.

#### 5.1.1.3 Some examples of experimental results.

An example of pressure amplitude decay data from a pulsed DB/AB T-burner test was shown in Figure 5.1-3. The correlating line for each pulse decay was the least squares fit to the measured data using Eq. (5.1.1). The values of  $\alpha$  for pulses during burning were obtained as a function of oscillatory pressure amplitude by using Eq. (5.1.2); the coefficients  $C_0$  and  $C_2$  were determined by the least squares fit to the amplitude-time data. An example of these reduced data,  $\alpha_1$  versus  $\Delta p$ , for a particular test is shown in Figure 5.1-5.

The values of  $\alpha$  for pulses after burnout are calculated in the same manner as above. For the general case where those values, obtained as a function of TABO, are used to determine  $\alpha_d$ , plots are constructed for  $\alpha$  as a function of TABO for a series of pressure amplitudes (usually 1, 2,

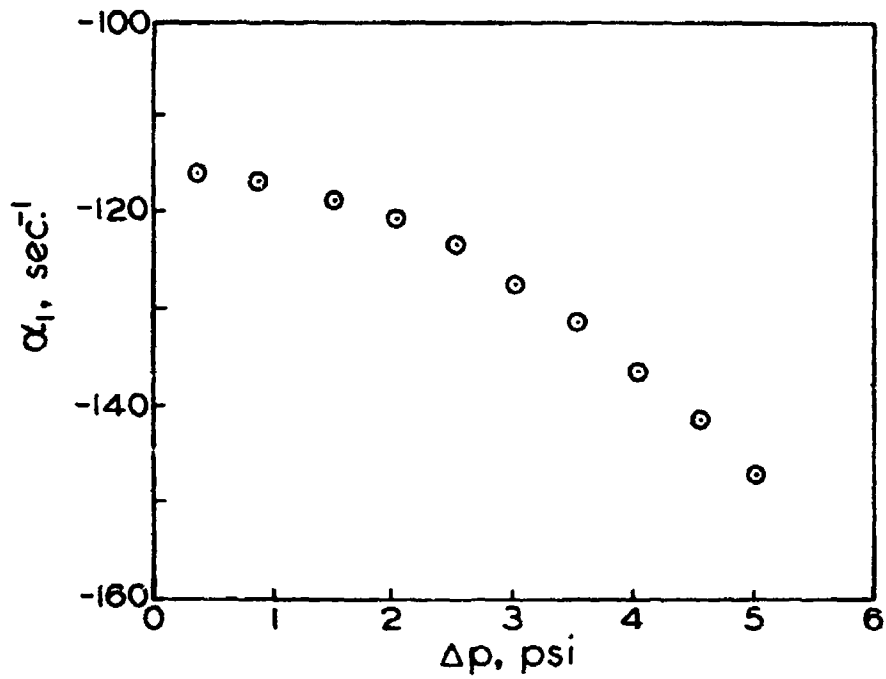


Figure 5.1-5 Values of  $\alpha_1$  for Pulses During Burning as a Function of Pressure Amplitude for a Typical Test Series (ref. 5-1)

3, 4 psi); the data are then fitted by a least squares method to a third order polynomial for each pressure amplitude. A typical plot is shown in Figure 5.1-6 for a pressure amplitude of 4 psi; the value of  $\alpha_d$  obtained from these data is  $-170 \text{ sec}^{-1}$ .

The variation of  $\alpha_2$  with pressure amplitude for ANB 3066 propellant is shown in Figure 5.1-7(a) to indicate the degree of  $\alpha_d$  dependence on pressure amplitude. The data bars indicate one standard deviation.

The variation of  $\alpha_c$  with pressure amplitude for ANB 3066 propellant is shown in Figure 5.1-7(b). This was determined by combining  $\alpha_1$  and  $\alpha_d$  at the appropriate pressure amplitudes and frequency. The data bars indicate one standard deviation.

### 5.1.2 Variable Area T-Burner Method

#### 5.1.2.1 Measurements from the VATB test records.

A typical oscillograph record from a VATB test is shown in Figure 3.4-9. An enlargement of one growth cycle is presented in Figure 5.1-8 for the purpose of describing methods of data reduction. Data that should be extracted from such a test record are as follows:

$t_{ig}$      the time of ignition

This time is measured at the igniter peak pressure as indicated by the output of the mean pressure transducer shown in Figure 5.1-8.

$t_{bo}$      the time of burnout

This time is measured at the onset of pressure oscillation decay as indicated by the output of the high frequency transducer. A line should be drawn through the limiting amplitude of oscillation preceding decay onset as shown in Figure 5.1-8. The intersection of these lines is the time of burnout.

$\bar{p}_i$      the initial mean pressure

This pressure is measured from the output of the mean pressure transducer after an equilibrium pressure is established following the ignition transient. An example is shown in Figure 5.1-8.

$\bar{p}_f$      the final mean pressure

This pressure is measured from the mean pressure transducer at time  $t_{bo}$ . For pulsed VATB tests (where there is no limiting amplitude oscillation at burnout), an orifice is normally placed in the T-burner exhaust vent to cause a DC pressure rise. Burnout is then determined as in the pulse technique, as shown in Figure 5.1-1.

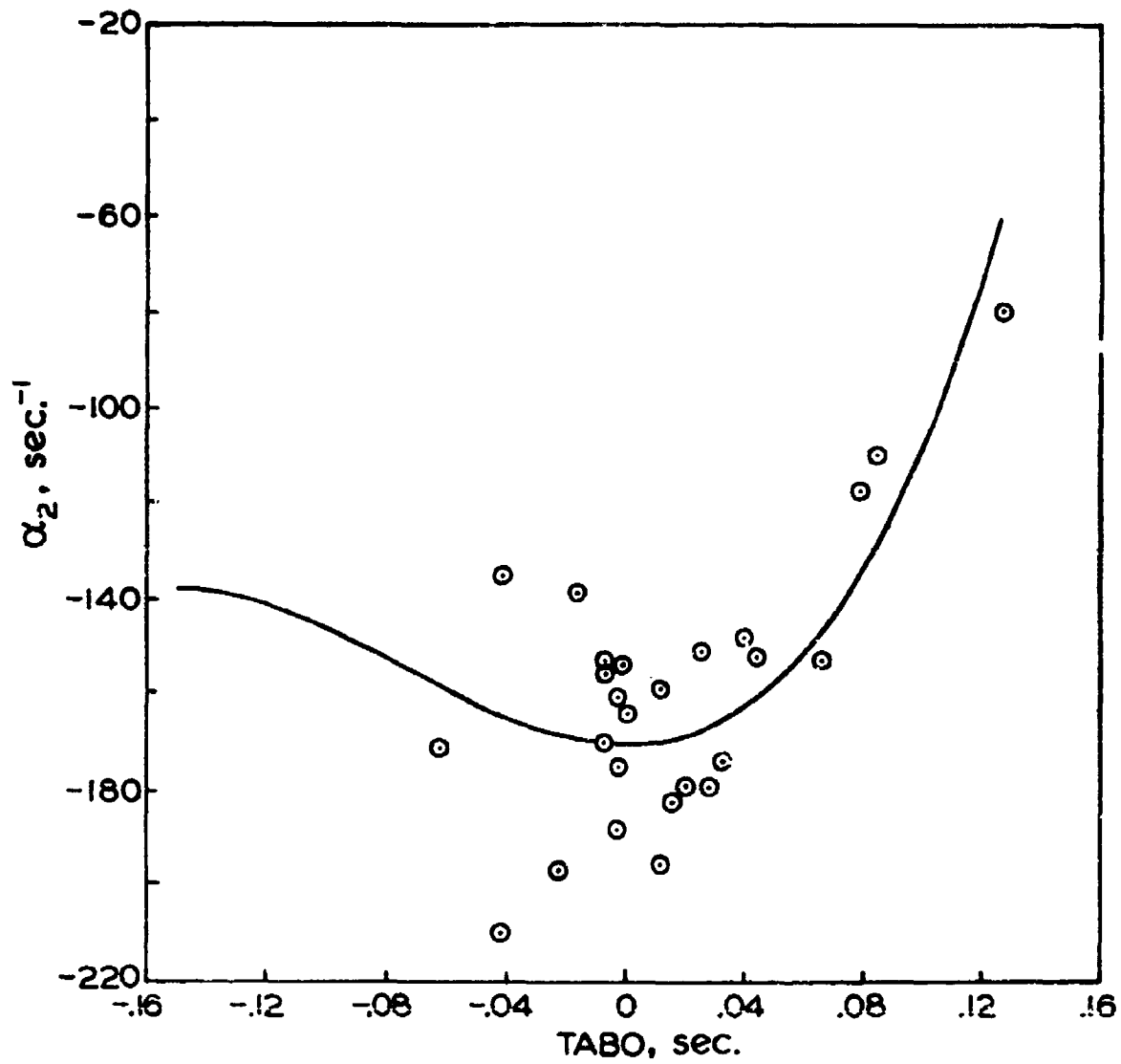


Figure 5.1-6 Values of  $\alpha_2$  for Pulses After Burnout As a Function of TABO for  $\Delta p = 4$  (ref. 5-1)

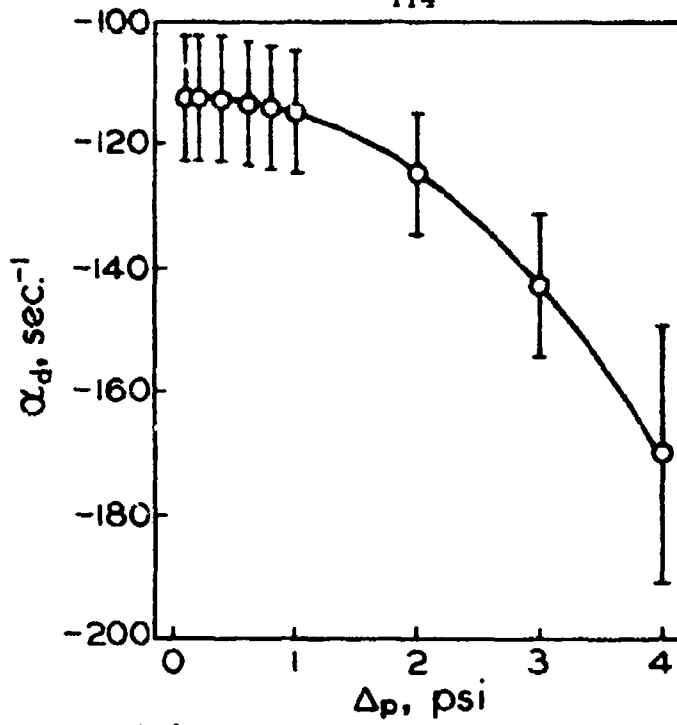
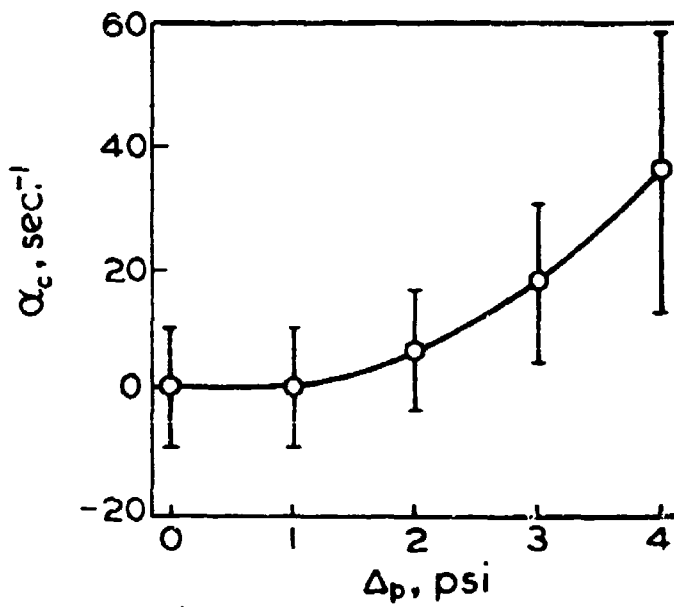
(a)  $\alpha_d$ (b)  $\alpha_c$ 

Figure 5.1-7 Variation of  $\alpha_d$  and  $\alpha_c$  with Pressure Amplitude for ANB 3066 Propellant:  $f \approx 820$  Hz,  $\bar{p} \approx 500$  psia (ref. 5-1)

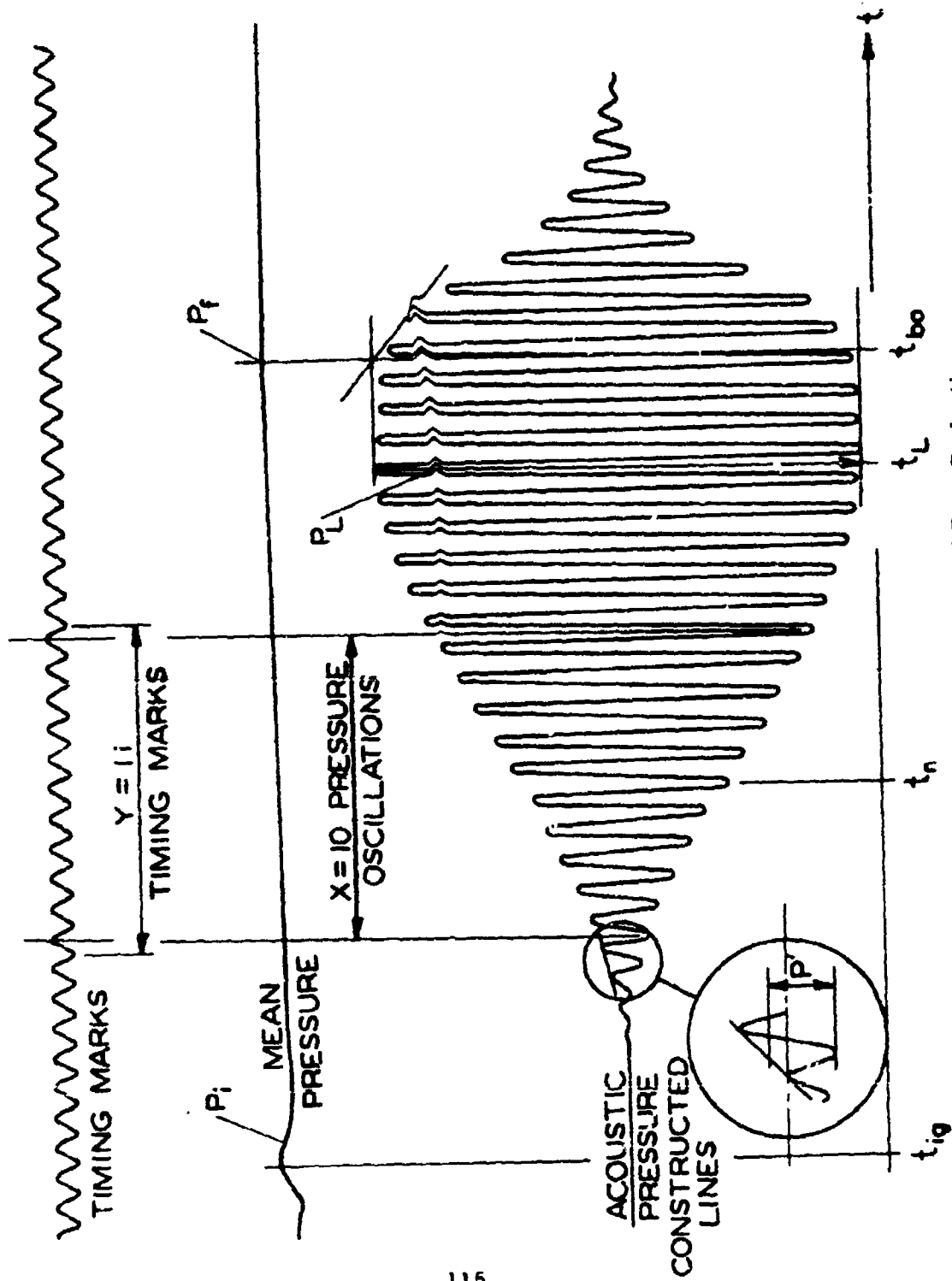


Figure 5.1-8 Example of Data Reduction

$\bar{p}_n$       the amplitude of pressure oscillations during the growth  
(or decay) period

This pressure is measured from the output of the high frequency transducer during the growth period(s). The peak-to-peak amplitude is measured as shown in Figure 5. 1-8. A series of straight lines is constructed along lines parallel to the timing lines. The measurement of amplitude should be initiated at a time where peak-to-peak amplitude of sinusoidal waves first exceeds 0. 10 inches and should be terminated at a time where a limiting amplitude is achieved. The number of measurements depends upon the frequency of the oscillations and/or the number of cycles occurring during the growth period. The amplitude of at least 10 cycles should be measured during a linear growth period. If fewer cycles are found to occur during the growth period, then each cycle should be measured. If more than 10 cycles occur, then 10 cycles (with approximately equal spacing) should be measured. If no linear regime is found from a  $\ln p'$  versus cycles plot, additional cycles should be examined in regimes where linearity is suggested. Of course, the best approach is to measure the amplitude of each cycle; however, this is very time consuming for cases of high frequency and/or slow growth.

$t_n$       the time of  $n^{\text{th}}$  growth during a VATB test

This time is measured at the middle of the linear region associated with the  $n^{\text{th}}$  growth as shown in Figure 5. 1-8.

$f_n$       the frequency of the  $n^{\text{th}}$  growth during a VATB test

This frequency is determined by first measuring the distance between  $x$  cycles in the growth period. The distance measured is then converted to time by measuring the distance between  $y$  timing marks or cycles. These initial and final timing marks or cycles should be located to encompass the space interval dictated by the  $x$  cycles considered in the growth period as shown in Figure 5. 1-8. The frequency of the pressure oscillations is calculated from the expression

$$f = f_0 \frac{y \text{ timing marks}}{\text{distance between } y \text{ timing marks}} \times \frac{x \text{ cycles}}{\text{distance between } x \text{ cycles}}$$

where  $f_0$  is the timing mark frequency.

The number of pressure oscillations to be included in this approach and the oscillograph paper speed dictate the error in this computation.

The following "rule of thumb" is recommended for paper speed:

$$\text{paper speed} = \frac{.05 \text{ to } .1}{\text{period of oscillations}}$$

and the number of oscillations should be at least ten, or all that occur during the linear region of a  $\ln p'$  versus cycles plot.

$\hat{p}_l$       the limiting pressure amplitude

This pressure is measured at a point in time where the acoustic pressure achieves a limiting value immediately following the growth period.

$t_l$       the time of limiting pressure amplitude

This time is measured at the point where  $\hat{p}_l$  is measured (e. g. see Figure 5.1-8).

#### 5.1.2.2 Methods of reducing VATB data.

The final data obtained from VATB testing should consist of the following parameters (additional nomenclature is shown in Figure 5.1-9): run number; propellant type and lot; grain configuration and length; T-burner length, L; suppressor cycle, n; time of growth,  $t_n$ ; inert area associated with the leading edge of the grain,  $IA_2$ ; end area ratio at the end cap,  $S_{be1}/S_{co}$ ; end area ratio at the leading edge of the grain,  $S_{be2}/S_{co}$ ; side area ratio,  $S_{bs}/S_{co}$ ; cross-sectional area change,  $S_{co}/S_c$ ; dimensionless grain length; frequency of oscillations, f; mean pressure,  $\bar{p}$ ; average burning rate  $\bar{r}$ ; limiting pressure,  $\hat{p}_l$ ; time of limiting pressure,  $t_l$ ; growth constant,  $\alpha$ .

Methods of calculating the geometric parameters are presented in Table 5.1-1.

#### 5.1.2.3 Some examples of experimental results.

Figure 5.1-10 shows three portions of a typical pressure record from a VATB test. Parts (a) and (b) show the behavior during the time periods when the paddle suppressor is inserted and withdrawn. Part (c) shows the growth period subsequent to the time when the paddle was withdrawn. The oscillations in this case grew with no apparent distortion (but see also Figures 2.4-1 and 2.4-2). Figure 5.1-11 is a plot of the peak-to-peak amplitude for the oscillations. The data are plotted as measured amplitude versus cycle number. It can be seen that

TABLE 5.1-1 Computations for VATB Data.

Grain Configuration	Web Burned $W$	$\beta$	$S_{be1}/S_{co}$	$S_{be2}/S_{co}$	$S_{bs}/S_{co}$
inhibited cylinder	$r(t-t_i)$	$2 \frac{L_b}{L}$	0	0	$\frac{4(D_c + 2w)L_b}{D_{co}^2}$
tapered cylinder (recessed)	$r(t-t_i)$	$2 \frac{L_b(1-w \cos \theta)}{L}$	0	0	$\frac{4(D_c + 2w)(L_b)(1-w \cos \theta)}{L}$
inhibited cylinder (protruding)	$r(t-t_i)$	$2 \left( \frac{L_b - w}{L} \right)$	0	$1 - \frac{S_c}{S_{co}} - \frac{IA_2}{S_{co}}$	$\frac{4(D_c + 2w)(L_b - w)}{D_{co}^2}$
inhibited cup	$r(t-t_i)$	$2 \left( \frac{L_b + w}{L + 2w} \right)$	$\frac{S_c}{S_{co}} - \left( \frac{D_{IA1}}{D_{co}} \right)^2$	0	$\frac{4(D_c + 2w)(L_b + w)}{D_{co}^2}$
uninhibited cup	$r(t-t_i)$	$2 \frac{L_b}{L + 2w}$	$\frac{S_c}{S_{co}} - \left( \frac{D_{IA1}}{D_{co}} \right)^2$	$\left( \frac{D_{IA2}}{D_{co}} \right)^2 \frac{S_c}{S_{co}}$	$\frac{4(D_c + 2w)(L_b)}{D_{co}^2}$

1-1

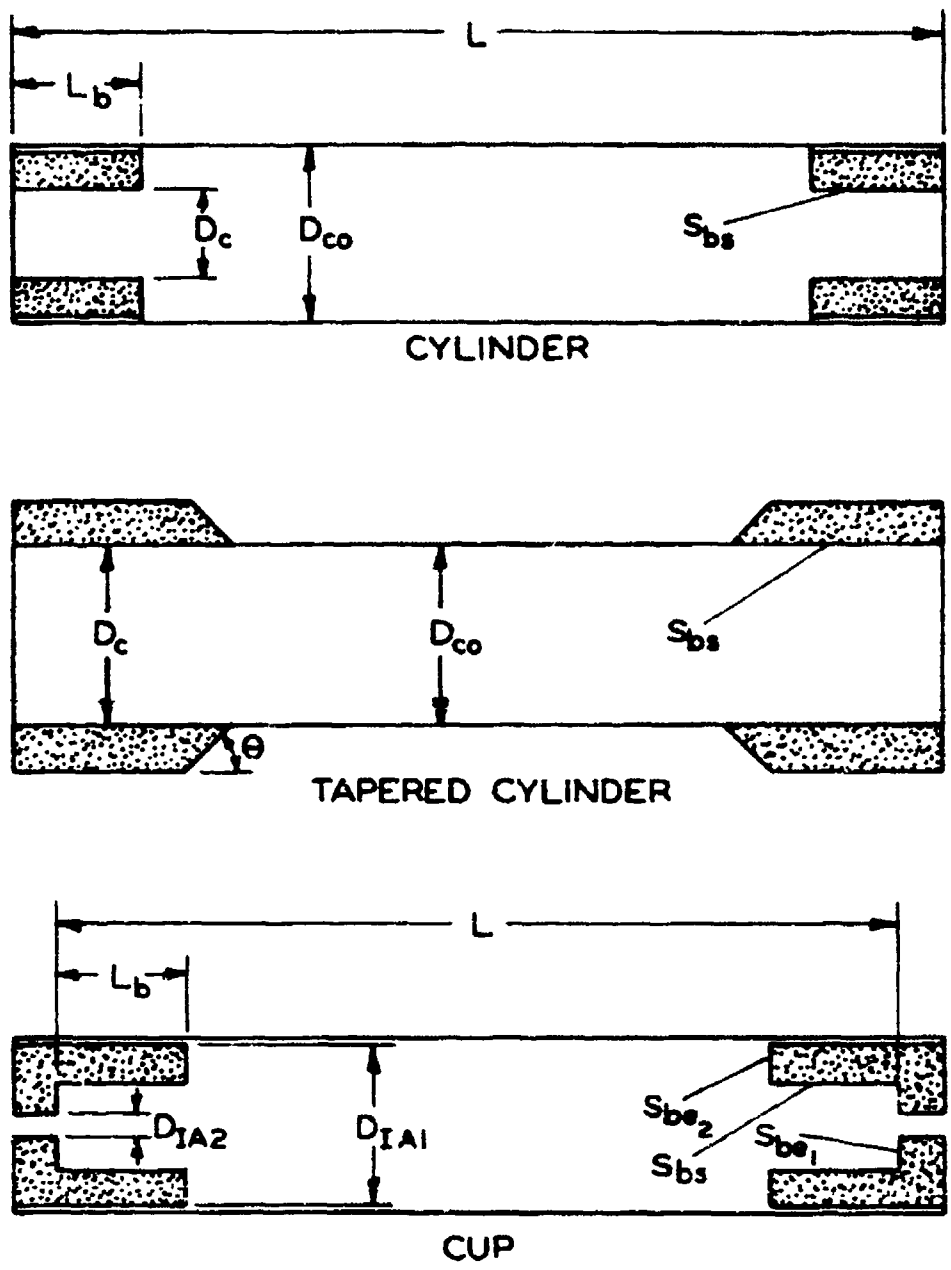
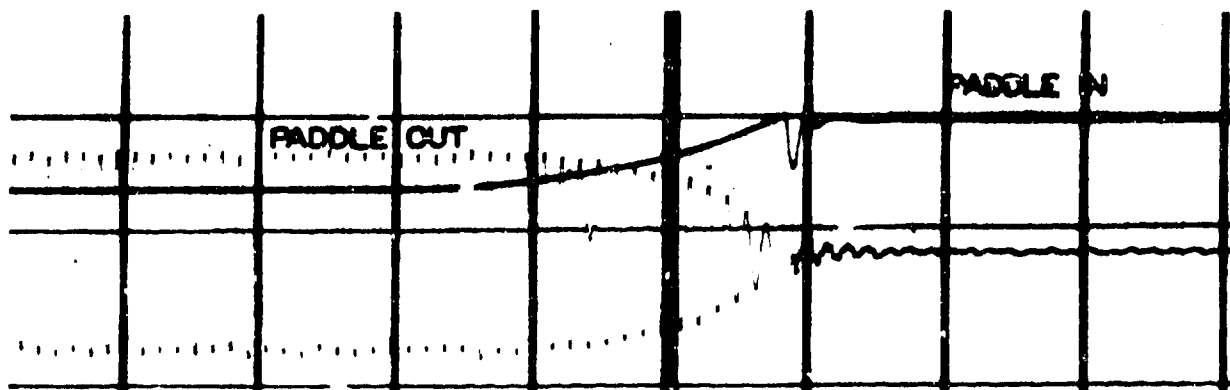
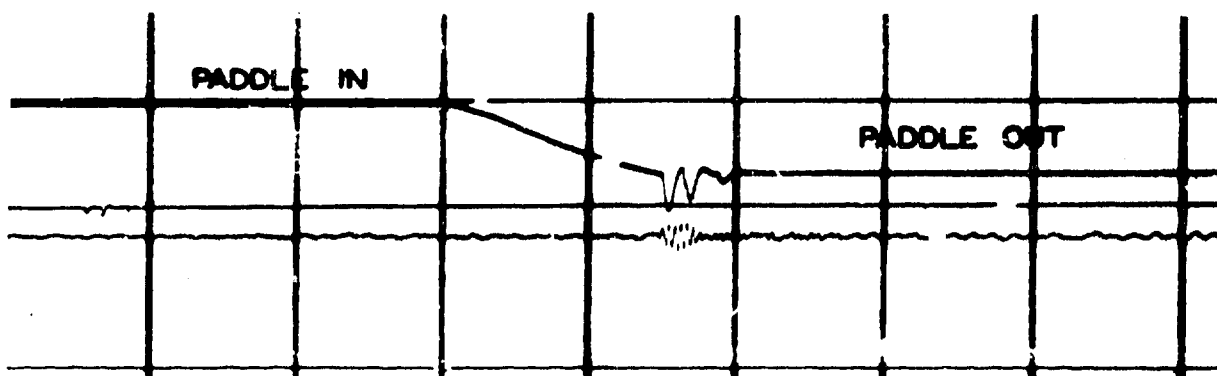


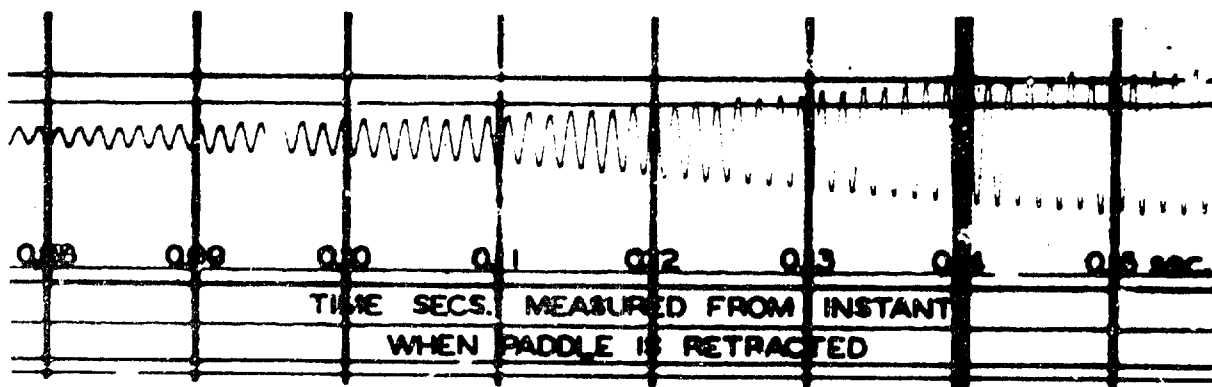
Figure 5.1-9 Nomenclature for Different Grain Configurations



(a) Paddle Inserted



(b) Paddle Removed



(c) Growth period subsequent to (b)

Figure 5.1-10 Reproduction of Portions of a Typical Pressure Record from a VATB Test (ref. 5-2)

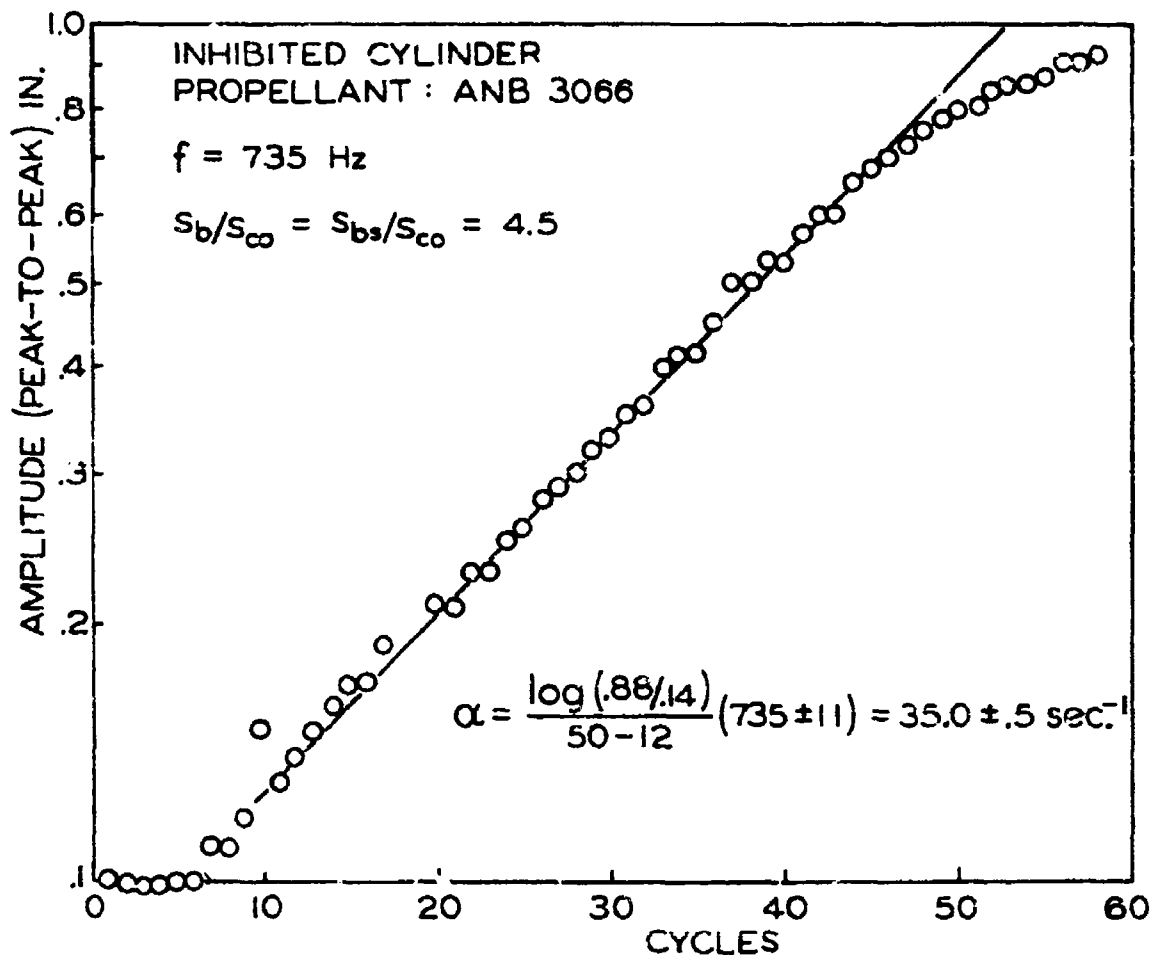


Figure 5.1-11 Plot of the Growth Period Shown in Figure 5.1-10 (ref. 5-2)

the growth period is linear on this semi-logarithmic plot and that the growth constant is constant over a growth period exceeding thirty cycles.

Figure 5.1-12 shows a plot of VATB data correlated in the manner suggested by the one-dimensional analysis, Eq. (3.2.1). The coordinates of the plot are described in §3.2.1 and Figure 3.2-1. As noted in the key, the data were obtained in various laboratories.

In Figure 5.1-13, some of the data from ref. 5-3 are shown plotted directly as growth constant for three area ratios. The data are for the propellant ANB 3066 tested at 800 Hz and 500 psi in a 1.5-inch burner. The oscillations are spontaneously unstable at the two higher area ratios, but must be pulsed at the lowest. The data were analysed for the propellant response function and damping constant, with and without the pulse data included. The results are summarized in Table 5.1-2; the response to velocity coupling, introduced in §5.4.4, is assigned the fixed value 5. Including the pulse tests reduces the error bands by a factor of 5, showing the advantage of the pulsed/variable area technique. The reduced error bars are a result of testing over a wider range of area ratios.

Table 5.1-2 Pulsed/Variable Area Data

Case	$B_s$	$\alpha_d$ ( $\text{sec}^{-1}$ )	VF	$R_v^{(i)}$	Correlation Coefficient
no pulsed data	$2.2 \pm 0.5$	$-66 \pm 47$	-1	5	0.853
pulse data included	$2.3 \pm 0.1$	$-74 \pm 9$	-1	5	0.985

5.1.3 Digital Data Reduction. In ref. 5-5, a method for converting recorded analog data to digital data has been described. Values of the growth or decay constant for each period of an oscillation were produced as part of the output. A similar approach was examined as part of the program reported in ref. 5-2, but discarded because of the expense. The potential advantages of data reduction by machine are the subjective bias might be removed, and spectral content of the data can be carried out. The disadvantages are the expense involved; and, particularly in research

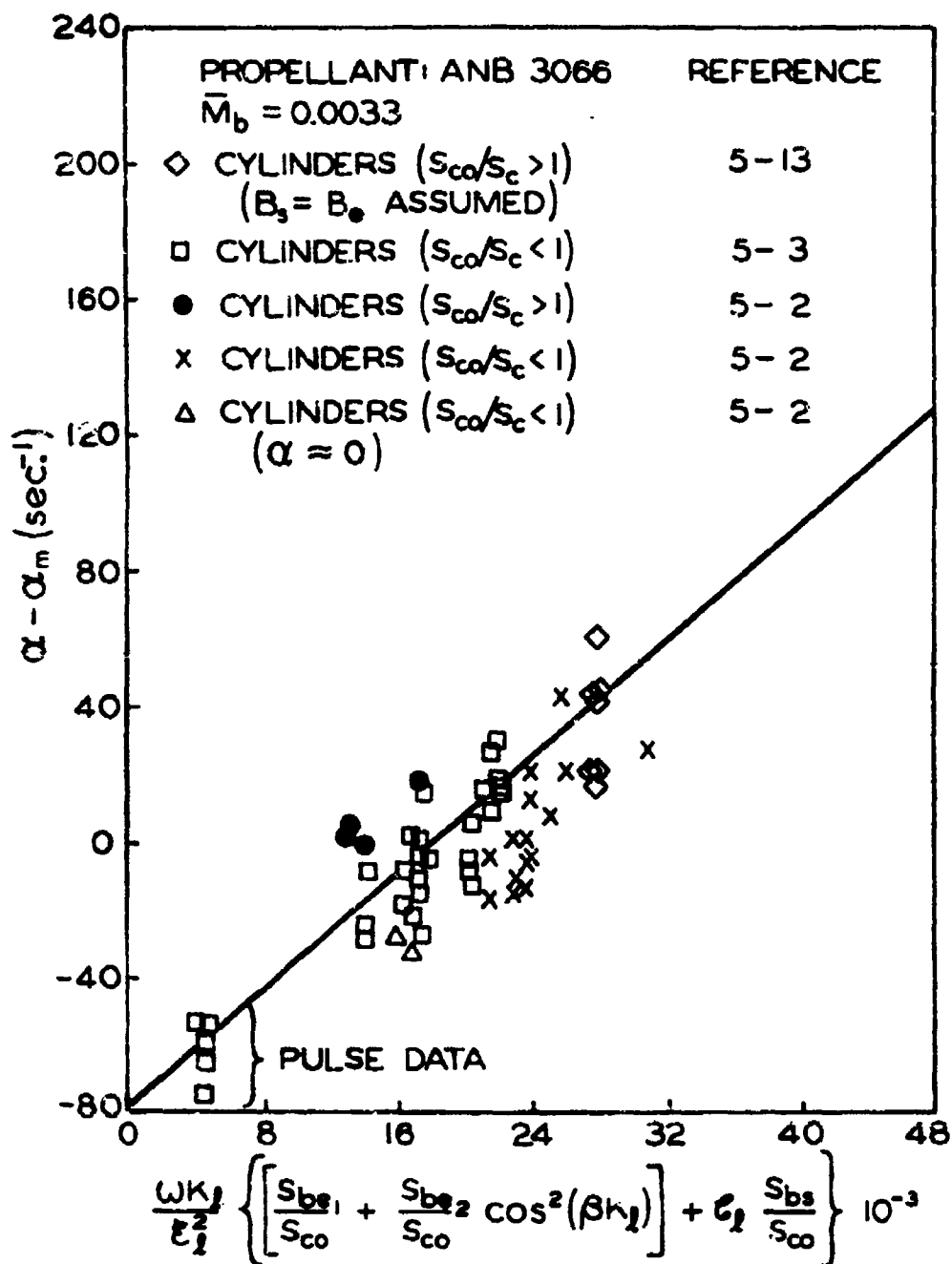


Figure 5.1-12 Typical VATB Data for ANB 3066:  $f \approx 800$  Hz,  
 $\bar{p} \approx 500$  psia (ref. 5-2)

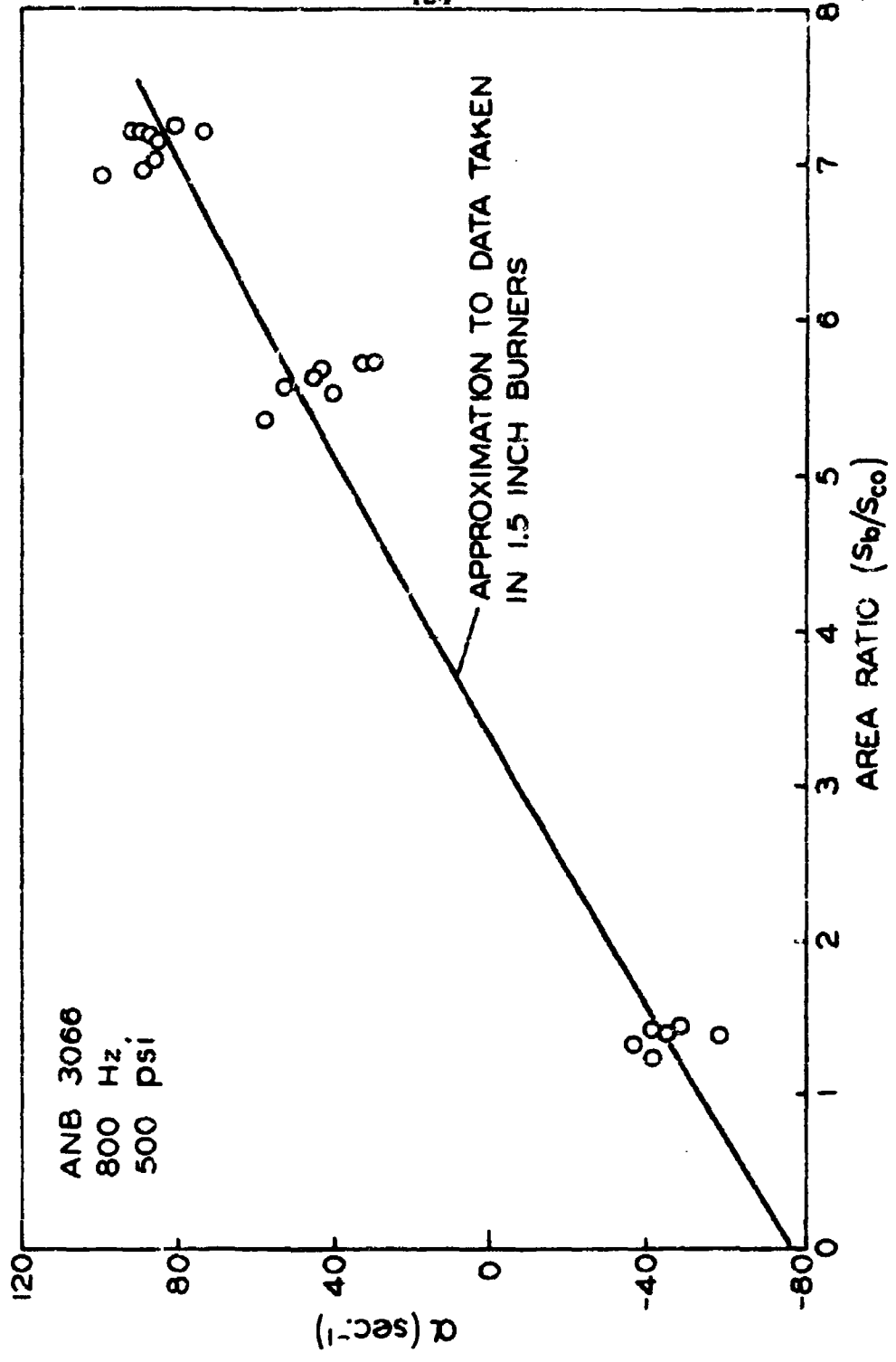


Figure 5.1-13 Typical Data Taken with Pulsed VATB Bests for ANB 3066:  $f \approx 800$  Hz,  $\bar{p} \approx 500$  psia (ref. 5-3)

programs, the fact that records for new propellants, and those showing unusual behavior, must in any case be examined visually. Automated data reduction has not been widely used. It may eventually prove more attractive for application to routine testing when large amounts of data must be reduced. No positive recommendation can be made on the basis of experience to date.

## 5.2 Preliminary and Qualitative Evaluation of Data

Considerable expense and effort can be saved if raw data are carefully reviewed before detailed reduction is carried out. Early display of the pressure record on an oscilloscope is very useful for detecting failures of equipment or of experimental procedure. With experience, more can be learned from records, short of quantitative analysis. It is the purpose of this section to summarize briefly some of the characteristics more commonly encountered, and their interpretation. The central question is whether or not a record is to be accepted as valid data.

5.2.1 Acceptance Criteria for VATB Data. Ideally, data taken with a variable-area T-burner should satisfy the following requirements:

- (a) ignition of the grains should be simultaneous and uniform, thereby assuring as nearly as possible identical histories during burning, and simultaneous burnout;
- (b) the growth of the amplitude of oscillations occurs when the suppression device is totally inactive: the paddle must be fully retracted, or the resonator disconnected;
- (c) the amplitude increases linearly on a semi-log plot versus time;
- (d) the oscillation shown on an unfiltered trace is a clean sinusoid at the fundamental frequency, containing little or no content of higher modes.

The first two items are matters of experimental procedure. Non-simultaneous ignition may be exhibited as two humps in the early portion of the pressure record, or as an unusually gradual decay of pressure at the end. If a transducer is installed at each end of the burner, a more precise indication is possible. Because the condition of the suppression device, e. g. the position of the paddle, should be indicated on the oscillograph

record, it is a simple matter to determine whether oscillations occur during an acceptable time interval.

The second two items above may not in fact be satisfied, but do not necessarily constitute a basis for rejecting the data. It is not possible to generalize, because different propellants may produce quite different behavior. If doubt exists, the obvious recourse is repeated tests. Further comments on the presence of frequencies other than the fundamental are given below in §5.2.3.

If the growth of oscillations is relatively slow, significant changes in the grain geometry (especially the area ratio  $S_b/S_{co}$ ) may occur. This may produce an uncertainty in establishing the geometry corresponding to the measured growth constant. Roughly, if the growth constant is less than  $20 \text{ sec}^{-1}$ , the change of geometry should be examined and appropriately taken into account.

5.2.2 Acceptance Criteria for Pulsed DB/AB and Pulsed VATB Data. In addition to items (a), (c), and (d) listed above, the following should be noted:

- (a) in pulsed DB/AB tests, if the burning time of a test deviates by more than  $\pm 5$  per cent of the average of a set, the data from the pulse after burnout should be rejected;
- (b) if the slope of the decay constant versus pressure amplitude for a pulse is positive (i. e., the magnitude of damping increases with decreasing pressure amplitude as the pulse decays), then the pulse data should be rejected.

The first should be enforced to eliminate tests in which simultaneous burnout does not occur. If the behavior noted in item (b) is observed, it may reflect abnormal burning, such as the presence of a sliver, or non-simultaneous burnout if the pulse is "after-burnout." The behavior is rarely seen consistently, but examples of repeated records of this sort have been found.

5.2.3 Presence of Higher Modes in T-Burners. It is an essential assumption for the test methods described in §3 and most commonly used that only a single mode -- almost always the fundamental -- is unstable during a test. However, due to nonlinear effects or broad-band excitation

(as with a pulse), other modes may be observed. Unfortunately, as remarked in §2.5, relatively large amounts of higher modes may not cause obvious distortion in oscillograph records.

For simplicity, the presence of higher modes will often be referred to here as "harmonic content." The importance of harmonic content, both for the reduction of data and in respect to the fundamental processes involved in the combustion/flow field coupling, is not understood. It is necessary nonetheless to examine records at least qualitatively for the presence of higher modes. No guidelines can be offered, although it is clear that if too much harmonic content is present, the data cannot be interpreted by techniques currently available. How much is "too much" is not known.

#### 5.2.3.1 Harmonic excitation due to pulsing.

It seems inevitable that a certain amount of harmonic content must accompany excitation of oscillations with a pulse. However, proper selection of pulser location and orientation tends to minimize harmonic content (ref. 5-5). The pulser may be located one quarter of the burner length from one end and, as nearly as possible, aimed down the axis of the T-burner toward the nozzle. This orientation seems to generate oscillations that have the cleanest waveforms over the longest length of time.

In general, the harmonic content produced will also be a function of propellant area, pulse amplitude, and vent areas. Consistent trends are not always observed; but in general, larger pulse amplitudes, larger propellant areas, and smaller vent areas produce a higher harmonic content.

#### 5.2.3.2 Harmonic content in the VATB.

Certain conditions in the VATB tend to produce a higher harmonic content. Long grain lengths ( $\beta > 0.25$ ) which are used with high area ratios increase the amount of harmonic content caused by velocity coupling. Also, in general, decreasing area ratios decrease harmonic content. Large negative lips which occur late in a firing with recessed grains are conducive to higher harmonic content (ref. 5-3).

Attempts to test at very low frequencies are often frustrated by an excess amount of harmonic content. This seems to result when the first

mode frequency is significantly lower than that at the peak of the curve for the combustion response as a function of frequency. In that case, the value for the response at the second mode frequency is much larger than at the frequency of the fundamental, and the second mode may be more unstable than the first. As a rough guide, frequencies of 300 Hz and below may be in the troublesome regime.

#### 5.2.3.3 Other sources.

Another source of harmonics that can occur even with low amplitude oscillations is the very poorly understood phenomena of mode coupling. Also, coupling between the surge tank and burner can produce unexpected frequencies, although these are usually lower than the fundamental. Finally, vibration of the burner may produce spurious signals that can be erroneously interpreted as harmonic content or surge tank coupling.

### 5.3 Reproducibility and Data Scatter

The problem of obtaining good reproducible data with T-burners is a difficult one. It has not been satisfactorily solved so far as obtaining quantitative data is concerned. Sufficient experience has been gained that qualitative testing can usually be done successfully with acceptable reproducibility. The discussion in this section is principally directed to questions associated with tests intended to produce quantitative results.

Small variations in propellant composition may cause apparent scatter in data. This problem is not addressed here. Generally, those directly concerned with a particular program must determine the extent to which compositional variables affect the data, and whether it is a matter for practical concern. For example, unstable oscillations in a T-burner may exhibit obviously different behavior with different samples of ostensibly the same propellant tested under the same conditions. If this is a genuine result, not, for example, due to poorly cast samples, then one must consider the possible implications for behavior in a motor.

It is the intent here to treat briefly somewhat more general questions related to test techniques. A fundamental problem is the large number of parameters and variables. These cannot be controlled with arbitrary precision and indeed, some cannot be measured precisely. The average pressure and temperature can usually be set quite accurately and

measured. On the other hand, ignition processes are crucial, but can be assessed only indirectly. The many geometrical variables can be fixed for a series of tests, but the effects of small changes are not necessarily known. Viscous effects, for example, change with geometry, but almost no analyses are available for the problems arising in T-burners.

The analyses described in §§2 and 3 are by no means complete, particularly in respect to viscous processes. When they are used to interpret and reduce data, it is therefore difficult, if not sometimes impossible, to identify disagreement between analysis and experiment as data scatter, lack of reproducibility, or simply the consequence of an incomplete analysis.

For these reasons, statistical analysis of the data, guided by the available formal analytical results, has become increasingly useful. That subject is covered in §5.4.3 and in Appendix B. The remarks here are descriptive only.

5.3.1 Data Scatter Due to Geometric Effects. A principal contribution to data scatter is the size of discontinuity in cross-sectional area which occurs at the end of the cup or cylindrical grain. The dependence predicted by the one-dimensional analysis (§2.2) of this lip effect is shown on Figure 5.3-1. The influence of both the area ratios,  $S_b/S_{co}$  and  $S_{co}/S_c$ , as well as the grain length for the modified one-dimensional model are also shown on the figure. Experimental data as discussed in §3 have been shown to scatter widely, depending on the condition at the end of the grain. The dependence of the normalized growth constant due to combustion only,  $\alpha_c/B_s$ , shown on Figure 5.3-1, does not account for any viscous effects. Unexpected behavior was observed with the pulse-decay technique when "vortex generator" rings were placed in the T-burner (ref. 5-1).

Cylindrical or cup-shaped grains can be tapered to provide a near-constant area ratio during the burn time and to reduce possible flow effects due to an abrupt step. This minimizes variations in  $S_b/S_{co}$  during the measurements of the growth  $\alpha$ , thus improving accuracy and eliminating the need to calculate a changing area ratio during the time the growth constant is measured. Data reduction is simplified, and both data

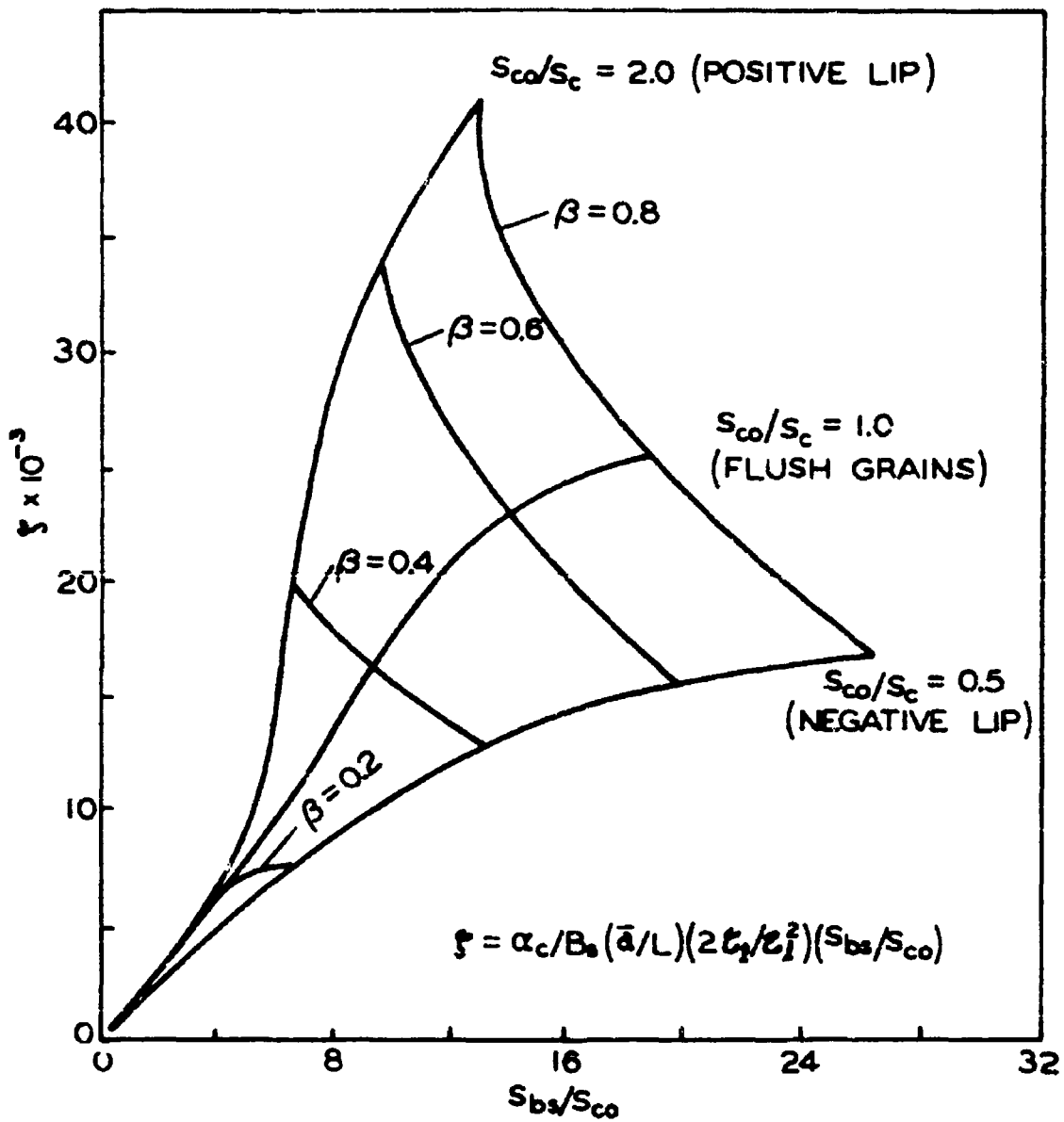


Figure 5.3-1 The Influence of Geometry According to the One-Dimensional Analysis (ref. 5-3)

scatter and uncertainty are reduced. The per cent error in a measured growth constant can be estimated from the rate of change of area ratio per unit time, which can be readily calculated for a cylindrical test sample. The per cent error in the measured growth constant for a cylindrical (non-tapered) grain is:

$$\frac{\Delta \alpha}{\alpha} = \frac{\Delta t}{\alpha} \frac{\Delta \alpha}{\Delta t} = \frac{\Delta t}{\alpha} \frac{\Delta \alpha}{\Delta(S_b/S_{co})} \frac{\Delta(S_b/S_{co})}{\Delta w} \frac{\Delta w}{\Delta t}$$

The time over which a growth constant is measured may be estimated as  $2.3/\alpha$  sec. The term  $\Delta \alpha / \Delta(S_b/S_{co})$  is approximately the growth constant  $\alpha_c$  due to combustion only. The rate of change of area ratio with propellant web is  $D_{co}$  for a cylinder, and  $\Delta w / \Delta t$  is the propellant burn rate. The per cent error is then

$$\frac{\Delta \alpha}{\alpha} = \frac{4.6 \alpha_c}{\alpha^2} \frac{(S_b/S_{co})^2}{D_{co}} \bar{r} = \frac{4.6 \alpha_c}{\alpha^2} \frac{(S_b/S_{co})^0}{D_{co}} \bar{r}$$

For ANB 3066, the magnitude of the error that can be introduced by the change in area ratio is shown in Figure 5.3-2. The error is most significant in a smaller burner and at lower area ratios. The resultant effect on response function data would be roughly 5 per cent in a 1.5-inch burner, and roughly 3 per cent in a 2.9-inch burner. This demonstrates the potential advantage of using the tapered grains, if other uncertainties are relatively less than that treated here.

**5.3.2 Measurement Uncertainties.** As with any experiment, the T-burner test method should be examined for sources of error and the uncertainty of numerical measurements should be estimated. In this subsection, attention is focussed on measurement uncertainties.

Because measurement uncertainties are governed by the T-burner diameter, grain size, and the method of data acquisition, a unique set of uncertainties associated with T-burner measurements cannot be stated. However, general guidelines for determining the uncertainties can be stated along with some typical values for an assumed T-burner.

**5.3.2.1 Guidelines for determining measurement uncertainties.**

Table 5.3-1 presents a summary of important quantities that are measured from the T-burner configuration and calculated from the T-burner data. These quantities are necessary for determining the response

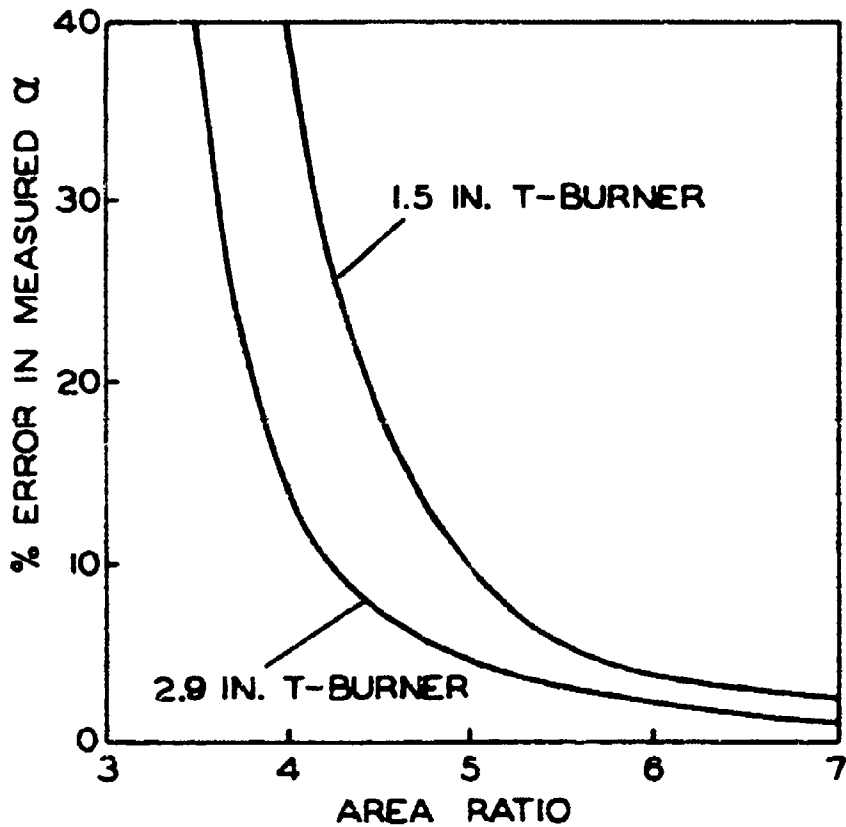


Figure 5.3-2 Calculated Estimate of the Change in the Growth Constant Due to Changing Area Ratio for a Cylindrical Test Sample, ANB 3066 propellant:  $f \approx 800$  Hz,  $p \approx 500$  psia

TABLE 5.3-1 Measurement Uncertainties for T-Burner Data  
Uncertainty Calculation

Measured or Calculated Value	Definition	Method of Calculations	Typical Values
$D_c$	inside bore of cylinder or cup grain	measured	$1.400 \pm 0.005$ in.
$D_{co}$	inside diameter of T-burner	measured	$1.500 \pm 0.005$ in.
$L$	length of T-burner	measured	$28.0 \pm 0.1$ in.
$L_b$	length of cylinder or cup grain	measured	$2.000 \pm 0.005$ in.
$t_{ig}$	time of ignition	measured	$0 \pm 0.01$ sec.
$t_{bo}$	time of burnout	measured	$0.76 \pm 0.01$ sec.
$t_n$	time at oscillation growth (or decay)	measured	$0.390 \pm 0.002$ sec.
web	thickness of cylinder or cup grain wall	measured	$0.250 \pm 0.005$ in.
$r$	cup grain wall burning rate	$\frac{web}{t_b - t_{ig}}$	$0.32 \pm 0.01$ in./sec.
$web _n$	distance burned at $n$	$r t_n$	$0.125 \pm 0.005$ in.
$S_{be}/S_{co} _n$	end area ratio at $t_n$	$\frac{(D_c + 2web _n)L_b}{D_{co}^2}$	$1.21 \pm 0.01$
$S_{bs}/S_{co} _n$	side area ratio at $t_n$	$\frac{4(D_c + 2web _n)L_b}{D_{co}^2}$	$6.57 \pm 0.09$
$S_{co}/S_c _n$	area ratio at $t_n$	$\frac{D_{co}^2}{(D_c + 2web _n)^2}$	$0.83 \pm 0.01$
$f$	frequency	$\frac{\text{no. of cycles}}{t_2 - t_1}$	$1000 \pm 20$ Hz*

\* Assume 10 cycles over a time period of 0.010 sec. ( $t_2 = t_1 \pm 0.001$  sec.)

function of the propellant. The uncertainty expression for each measured or calculated quantity is included in the table.

#### 5.3.2.2 Some examples.

A knowledge of measurement uncertainty is useful for identifying the number of significant figures that should be carried in data recorded from the T-burner test. In Table 5.3-1, a set of assumed measured quantities are listed along with assumed uncertainties associated with the measurements. Based on the assumed values, the uncertainties for calculated quantities are listed.

### 5.4 Methods for Obtaining the Response Functions and Particle Damping from Experimental Data

An essential problem arising in the use of T-burners to obtain quantitative results is that the items eventually desired cannot be measured directly. In principle, pressure records contain the information, but numerical values for the response functions and particle damping can be determined only by making use of a stability analysis. Consequently, the results inevitably rest on some approximations and assumptions. After a brief discussion of the assumptions generally used, the direct application of stability analyses and statistical analysis are treated in this section. Some of the material has already been discussed in §§2 and 3; further details of specific applications may be found in the references.

5.4.1 Assumptions and Approximations. The major assumptions and approximations used in the one- and three-dimensional analyses have been summarized in §2. For the stability analyses commonly used, the most important requirements, built into the formalism, are that the Mach number of both the acoustic and average flow fields be small, and, in fact, the acoustic Mach number should be smaller than the average Mach number. There is no experimental information which will place more definite limits. It seems to be true that linear behavior (the amplitude grows exponentially in time) is observed not only for larger amplitudes than one has reason to expect, but also under conditions when the acoustic Mach number, in at least part of the chamber, is much larger than the average value. The nonlinear analyses discussed in §2 suggest possible reasons for this result, but the question is not yet sat-

isfactorily answered.

In any event, the analyses described earlier are used as presented, or in simplified form for special cases. Beyond the formal assumptions, a number of approximations are usually made in respect to physical processes in the burner; these include the following:

- (1) The response functions are independent of position on the burning surface. Although a distinction has been made between the values for lateral and end surfaces, the quantities  $B_s$  and  $B_e$  are almost always assumed to be constant on the side (lateral) and end surfaces respectively.
- (2) Possible influences of the mean flow on the response functions and damping processes are ignored.
- (3) The various contributions to both the growth and decay constant are assumed to be independent of time.
- (4) The influence of the products introduced by hot pulse units is ignored.
- (5) The influence of flow from the surge tank into the burner due to cooling after burnout is ignored when the decay constant or a pulse after burnout is analyzed.
- (6) The combustion of the last layers of propellant is assumed to be unaffected by cool adjacent wall, so that the combustion products in the chamber after burnout are the same as those present during burning.
- (7) The influences of residual burning within the volume are usually ignored, so particle sizes are assumed to be independent of position and length of burner.
- (8) The combustion products, in particular the size of particles, is assumed to be independent of mean flow.

This is not intended to be a complete list. Additional assumptions and approximations may be usefully introduced in special situations. Further discussion of these and related questions may be found in §7.

5.4.2 Direct Methods for Obtaining the Response Functions and Particle Damping. The analyses carried out to obtain the response functions and particle damping, or particle size, range from quite crude

(which can be very useful) forms to application of the complete results discussed in §2.

#### 5.4.2.1 Values obtained from DB/AB data.

Testing by the pulse method has proved most useful for obtaining qualitative information and for quantitative comparisons based on the decay constants observed during and after burning. In principle, values for the response function can be obtained, but those who have used the technique most extensively (ref. 5-1) have done so only in an approximate way. The formula (3.2.10) is used,

$$\alpha = 4f \frac{S_{be}}{S_{co}} B + \alpha_d \quad (5.4.1)$$

with the following assumptions:

- (1) The value of  $\alpha_d$  during burning is the same as  $\alpha_d$  after burnout. A frequency correction is made (see ref. 5-1) so the value of  $\alpha_d$  used is that for the frequency observed during the growth period.
- (2) The vent is assumed to have no influence.
- (3) The average burning rate is computed from T-burner tests as the ratio of web thickness to burn time.
- (4) The velocity of sound is computed from the length of burner and observed frequency with the formula  $\bar{a} = 2Lf$ .

Equation (5.4.1) may then be solved for  $B_e$ . Because only end discs have been used in DB/AB testing, the response function for end grains is obtained. If one assumes that  $\alpha_d$  is entirely due to particle damping, then the values of the decay constant for the pulse after burnout can be used, with formulas such as that given in Appendix D.1, to obtain an estimate for the average particle size. Values obtained in this way have been reported, for example, in ref. 5-2.

#### 5.4.2.2 Values obtained from VATB and pulsed VATB data.

Equation (2.2.3), or a modified form, has been most commonly used to interpret data taken with variable-area T-burners. The simplest forms arise in the cases of end grains, or short lateral grains flush with the walls:

$$\alpha = \left[ \frac{\bar{a}}{L} \frac{S_{be}}{S_{co}} \right] B_e + \alpha_d \quad (\text{end grains only}) \quad (5.4.2)$$

$$\alpha = \left[ \frac{\bar{a}}{L} \frac{S_{bs}}{S_{co}} \left( \frac{\hat{p}}{\bar{p}} \right)^2 \right] B_s + \alpha_d \quad (\text{lateral grains}) \quad (5.4.3)$$

where  $(\hat{p}/\bar{p})_s$  is the pressure fluctuation at the location of the sample. For (5.4.3) to be valid, the grain must be sufficiently short that the pressure is essentially uniform, but fluctuating in time. Otherwise, the brackets multiplying  $B_s$  contain the function  $g_s$ , and depend on the length of the grain as well as its position in the burner. All of the assumptions listed in §5.4.1 are used to obtain (5.4.2) and (5.4.3). It should be recalled (see §2.6.1 and Appendix E) that the quantity  $B$  is related to the real part of the response function by

$$B = A_b(r) + \frac{\bar{u}_b}{\bar{a}} = \frac{\bar{u}_b}{\bar{a}} R_b(r) \quad (5.4.4)$$

The original suggestion for testing with variable area (see ref. 5-1) was based on Eq. (5.4.2). As suggested above, the ratio  $\bar{a}/L$  can be replaced by twice the observed frequency. A plot of the measured values of  $\alpha$  versus  $\bar{a} S_{be} / LS_{co}$  has slope  $B_e$  and intercept  $\alpha_d$  if the losses are constant for the series of tests. A similar plot using (5.4.3), subject to the many approximations used, will give  $B_s$ . For metallized propellants, small disturbances will generally not be unstable if only end grains are used; to obtain  $B_e$ , one must then either use a pulse technique, or use cylindrical and end grains together. The appropriate simplified equation is

$$\alpha = \left[ \frac{\bar{a}}{L} \frac{S_{be}}{S_{co}} \right] B_e + \left[ \frac{\bar{a}}{L} \frac{S_{bs}}{S_{co}} \left( \frac{\hat{p}}{\bar{p}} \right)^2 \right] B_s + \alpha_d \quad (5.4.5)$$

It has already been noted in §3.2 that accurate values for  $B_e$  are difficult to obtain in this way because the first term in (5.4.5) is a relatively small contribution to the right hand side when heavily metallized propellants are tested.

Perhaps the most obvious indication that one or more of the assumptions may be violated is that the plot of the growth constant versus the variable brackets in (5.4.3) - (5.4.5) is not a straight line.\* Significant causes include the finite length of grains, variable combustion response

\* Another possible explanation is that velocity coupling (§5.4.4) may be significant.

over the burning surface, and dependence of the losses, i. e.,  $\alpha_d$ , on geometry. Nevertheless, this simple approach has often been used successfully to obtain estimates of  $B_e$  and  $B_g$ .

Pulsing with variable area serves most importantly to provide data in the range of lower area ratios. The curve of  $\alpha$  versus area ratio is thereby better defined, and yields better values of both  $B$  and  $\alpha_d$ . Figure 5.1-3 clearly shows this feature.

To obtain  $R_b^{(r)}$ , the real part of the response function, from values of  $B$ , the average speed  $\bar{u}_b$  of the gases leaving the burning surface must be known. This is generally computed in the following way. Conservation of mass applied to the flow across the solid/gas region at a burning surface requires

$$\rho_s \bar{r} = \bar{\rho}_g \bar{u}_b + \bar{\rho}_p \bar{u}_p \quad (5.4.6)$$

Assume that the average speeds of the particles and gases are the same, and that the local value of  $\bar{\rho}_p / \bar{\rho}_g = C_m$  at the edge of the combustion zone is the equilibrium value for the propellant. Hence, (5.4.6) gives

$$\bar{u}_b = \frac{\rho_s \bar{r}}{\bar{\gamma} \bar{p}} \left[ \frac{\bar{\gamma} R \bar{T}}{1 + C_m} \right] = \frac{\rho_s \bar{r} \bar{a}^2}{\bar{\gamma} \bar{p}} \quad (5.4.7)$$

where  $\bar{a}$  is the speed of sound for the product mixture in the chamber, and  $\bar{\gamma}$  is the ratio of the specific heats for the mixture (see Appendix E). All quantities on the right hand side of (5.4.8) are therefore known.

The procedures become increasingly complicated as the geometry differs more from a uniform tube, and if the losses ( $\alpha_d$ ) depend on geometry. In particular,  $\alpha_d$  contains particle damping, wall losses, and the influence of the vent. All three may vary with geometry. The crudest assumption is that only the particle damping is significant, and is independent of geometry. The formula (D.24) may then be used as an approximation to obtain an effective particle size.

The more complicated result, Eq. (2.2.3) or (3.2.1), is used in essentially the same way as the simpler formulas just described. Mainly, the differences arise from the attempt to take account of geometrical perturbations, and some of the dependence of the losses on the mean flow field and geometry. One way of presenting these corrections is shown in Figure 5.1-12.

Uncertainties associated with the losses, geometrical complications, and difficulties with reproducibility of data have led to quite extensive use of statistical techniques, discussed in the following section.

5.4.3 Statistical Analysis of T-Burner Data. Ultimately, the purpose of conducting quantitative T-burner tests is to provide input data for predictions of motor stability. To accomplish this, the quantities  $B_s$ ,  $B_e$ , and  $\alpha_d$  must be extracted from the T-burner data. Regardless of the T-burner test method used to obtain the data, it is apparent from the earlier discussions that unknown processes and uncertainties in data measurement occur frequently. Consequently, several tests will be required to determine the combustion response and particle damping for any given frequency and pressure, and a statistical analysis of the data must play an important role in the interpretation of the data.

When applied properly, a statistical analysis can yield a quantitative assessment of the combustion parameters and an estimation of their accuracy. In addition, outlying data points can be identified, and one can acquire guidance for the conduct of future tests.

As presented previously, the basic equation for the T-burner is Eq. (2.2.3):

$$\alpha = \left\{ \left( \frac{\omega}{K_l \varepsilon_l^2} \right) \left[ \frac{S_{be1}}{S_{co}} + \cos^2(\beta K_l) \frac{S_{be2}}{S_{co}} \right] \right\} B_e + \left\{ \left( \frac{\omega}{K_l \varepsilon_l^2} \right) (C_l) \left( \frac{S_{bs}}{S_{co}} \right) \right\} \beta_s + \alpha_m + \alpha_d$$

acoustic driving from end-burning surfaces
acoustic burning from side-burning surfaces

$$+ \left( \frac{\omega}{K_l \varepsilon_l^2} \right) (P_l) \left( \frac{S_{bs}}{S_{co}} \right) \quad \text{acoustic driving due to velocity coupling} \quad (5.4.8)$$

Both  $\alpha$  and  $\beta$  are quantities measured during the experiment.  $B_e$ ,  $B_s$ ,  $C_d$ , and  $R_v^{(i)}$  are to be extracted from the data. The term containing  $R_v^{(i)}$  represents the influence of velocity coupling, and has been included here according to the treatment described in ref. 5-6. All other parameters are functions of the test geometry and observed burning rate and can be calculated by the procedures presented elsewhere in this report. Because the value of  $\alpha_m$  cannot be set unequivocally, it is important that whatever value is used be clearly explained.

The T-burner data should be fit to the model through some form of

statistical optimization; the method of least squares is commonly used. A stepwise regression analysis is probably the most informative, but is not required. Once the data fit has been accomplished and  $B_e$ ,  $B_s$ , and  $\alpha_d$  determined, one must evaluate the results and make judgements concerning the quality of the fit. To accomplish this evaluation the optimization technique should be capable of computing certain parameters, namely, the confidence interval and/or partial F-ratios for  $V_s$ ,  $B_e$ , and  $\alpha_d$ , the "per cent variation explained" by the correlation, and a table of residuals showing the differences between what is actually observed and what would be "predicted" by the regression equation. The standard error of estimate ( $\sigma$ ) is also useful. Definitions of the various quantities are given in Table 5.4-1.

The first step in evaluating the quality of the fit is the identification of outlying or "bad" data points. If the data bank contained a "normal" distribution of points one would expect that the residual table would show approximately 30%, 5% and 1% of the predicted points to be  $1\sigma$ ,  $2\sigma$ , and  $3\sigma$  away from the observed data. Significant deviation from this normal distribution is generally indicative of a poor quality fit. For example, a large quantity of  $1\sigma$  points could indicate a high degree of scatter associated with the entire data bank. Conversely, a large amount of  $3\sigma$  points could be indicative of outlying or "bad" data points. If one finds a large percentage of  $3\sigma$  he should re-examine each of these data traces carefully to ascertain their validity. Should a basis be found for discarding some of the data, the data which are retained should also be re-examined by the same procedure, to avoid a possible bias.

The confidence intervals and partial F-ratios for the calculated combustion parameters should then be examined to establish the accuracy to which these quantities have been determined. Generally speaking, the F-ratio should be on the order of 25.0 and the confidence interval should be within  $\pm 20\%$  of the calculated parameter. Unfortunately, this degree of precision is not always obtainable. Problems generally arise because one cannot test over a wide range of one or more of the independent variables. For example, in the variable area T-burner, the quantity  $S_{be}/S_{co}$  cannot be varied significantly from 1.0; on the other hand,  $S_{bs}/S_{co}$  can range from 2.0 to 8.0. Consequently,  $B_s$  can be determined to a much greater precision than  $B_e$ .

The "per cent variation explained" and "standard error of estimate" are good indicators of the overall correlation of the data by the regression equation. If one had many data points, a value of 0.9 for the per cent variation explained would be a reasonable goal. For treatment of twenty to thirty points, 0.95 is not unreasonable. Certainly one tries to minimize the standard error or estimate; however, it is difficult to place levels of acceptability on this parameter since its absolute value will depend heavily on the mean of the measured data.

As an example of the data interpretation procedure, a sample problem was constructed from the data reported in ref. 5-3. A summary of these data is presented in Table 5.4-1. Note that these data were acquired with cylindrically-shaped grains; consequently, only  $B_s$  and  $\alpha_d$  could be extracted. For the purposes of the sample problem, the vent factor, VF, was set equal to zero. Since the vent effect and the combustion driving by the side wall are both directly dependent on  $S_{bs}/S_{co}$ , the quantity one assigns to the vent effect should have little consequence on the quality of the data correlation, however, the value of  $B_s$  is affected.

The data present in Table 5.4-2 comprise 39 points and reflect the results of a well-planned test program. The area ratio was varied over a wide range (1.5-7.2); this should allow for a precise determination of  $B_s$ . Note that several tests were acquired at low area ratios and required pulsing to obtain data. The inclusion of these points will increase the precision to which  $\alpha_d$  will be determined. A least squares regression analysis yielded the following information:

$$B_s = 0.00752 \pm 0.00022 ,$$
$$\alpha_d = -79.9 \pm 3.7 .$$

The relative smallness of the standard error of coefficient for  $B_s$  and  $\alpha_d$  indicates a high degree of confidence in the data fit. This is further substantiated by the F-ratios, which were 475 and 1140, respectively. The "per cent variation explained" by this fit to the data was 0.968. Therefore, one can conclude that the theory, with these values for  $B_s$  and  $\alpha_d$ , describes the data bank; only 3 per cent of the data variation is attributable to "scatter" or to some process not considered by the theory. Finally, a review of the residual error table (Table 5.4-3) shows that the data follow a normal distribution.

Table 5, 4-1

## Definitions of Quantities used in Statistical Analysis

- $\alpha - \alpha_m$   $\begin{cases} \alpha & = \text{measured value of growth constant} \\ \alpha_m & = \text{value given by Eq. (3.22)} \end{cases}$
- $\varphi_{\text{pred}}$  value of  $\varphi$  which is predicted by the theory using the coefficients extracted from the data by "Least Squares"
- $\bar{\varphi}$  mean value of  $\varphi$
- $\bar{\varphi}_{\text{pred}}$  mean value of  $\varphi_{\text{pred}}$
- $N$  number of data points
- $P$  number of parameters used in the correlation equation; usually,  $p = 3$ , the parameters being  $B_e$ ,  $B_s$  and  $\alpha_d$ .

VE Percent Variation Explained

$$\frac{\sum_{i=1}^N (\varphi_i - \varphi_{\text{pred}})^2 - \sum_{i=1}^N (\varphi_i - \bar{\varphi}_{\text{pred}})^2}{\sum_{i=1}^N (\varphi_i - \bar{\varphi}_i)^2}$$

$\sigma$  Standard Error of Estimate

$$\sigma = \sqrt{\frac{\sum_{i=1}^N (\varphi_i - \varphi_{\text{pred}})^2}{N - P}}$$

For the expression  $y = b_0 + b_1 x$

$$\text{Standard Error of } b_0 = \sigma \left[ \frac{\sum_{i=1}^N x_i^2}{N \sum_{i=1}^N (x_i - \bar{x})^2} \right]^{\frac{1}{2}}$$

$$\text{Standard Error of } b_1 = \frac{\sigma}{\sqrt{\sum_{i=1}^N (x_i - \bar{x})^2}} = \frac{\sigma}{\left[ \sum_{i=1}^N (x_i - \bar{x})^2 \right]^{\frac{1}{2}}}$$

$$\text{Partial F Ratio} = \frac{Z^2}{(\text{Standard Error of } Z)^2}$$

where  $Z$  stands for  $B_s$ ,  $B_e$  or  $\alpha_d$

Run	$S_b/S_{co}$	$S_{be}/S_{co}$	$\delta_{b2}/S_{co}$	$S_{be}/S_{co}$	$S_{co}/S_c$	$\beta$	$a$	$f(Hz)$
491	1.540	-0.000	-0.000	1.540	.973	.090	-36.000	820.000
488 A	6.030	-0.000	-0.000	6.030	.842	.327	52.000	795.000
488 B	6.030	-0.000	-0.000	6.030	.783	.316	40.000	800.000
489 A	6.020	-0.000	-0.000	6.020	.883	.335	50.000	820.000
489 B	6.030	-0.000	-0.000	6.030	.800	.319	41.000	790.000
482 A	7.170	-0.000	-0.000	7.170	.831	.200	81.000	795.000
482 B	7.200	-0.000	-0.000	7.200	.693	.184	63.000	780.000
483 A	7.200	-0.000	-0.000	7.200	.840	.202	83.000	800.000
484	7.060	-0.000	-0.000	7.060	1.011	.217	88.000	820.000
484 A	7.210	-0.000	-0.000	7.210	.814	.199	80.000	790.000
485	5.580	-0.000	-0.000	5.580	1.030	.173	53.000	816.000
485 A	5.720	-0.000	-0.000	5.720	.808	.157	38.000	780.000
475	5.100	-0.000	-0.000	5.100	1.200	.171	44.000	812.000
475 A	5.630	-0.000	-0.000	5.630	.953	.168	45.000	793.000
476 A	5.700	-0.000	-0.000	5.700	.851	.161	43.000	795.000
476	5.370	-0.000	-0.000	5.370	1.090	.171	59.000	829.000
493	4.520	-0.000	-0.000	4.520	.930	.259	23.000	833.000
483	6.950	-0.000	-0.000	6.950	1.030	.216	90.000	823.000
482	6.900	-0.000	-0.000	6.900	1.040	.216	101.000	825.000
489	6.020	-0.000	-0.000	6.020	.985	.353	75.000	825.000
488	6.150	-0.000	-0.000	6.150	.944	.353	61.000	833.000
492	1.540	-0.000	-0.000	1.540	.970	.090	-41.000	835.000
475 B	5.720	-0.000	-0.000	5.720	.803	.157	31.000	775.000
476 B	5.740	-0.000	-0.000	5.740	.717	.149	27.000	775.000
484 B	7.240	-0.000	-0.000	7.240	.697	.185	61.000	775.000
478	1.480	-0.000	-0.000	1.480	1.060	.046	-50.000	774.000
479	1.460	-0.000	-0.000	1.460	1.080	.046	-46.000	763.000
480	1.430	-0.000	-0.000	1.430	1.130	.046	-60.000	778.000
481	1.420	-0.000	-0.000	1.420	1.110	.046	-47.000	770.000
481	1.420	-0.000	-0.000	1.420	1.110	.046	-47.000	770.000
477	1.280	-0.000	-0.000	1.280	1.350	.046	-43.000	775.000
477 A	1.370	-0.000	-0.000	1.370	1.180	.046	-38.000	775.000
481	1.420	-0.000	-0.000	1.420	1.110	.046	-47.000	770.000
533	7.150	-0.000	-0.000	7.150	.963	.215	76.000	804.000
533 B	7.070	-0.000	-0.000	7.070	.677	.170	56.000	750.000
534	6.610	-0.000	-0.000	6.610	1.130	.216	88.000	834.000
534 A	7.200	-0.000	-0.000	7.200	.731	.189	79.000	800.000
534 B	7.080	-0.000	-0.000	7.080	.563	.163	51.000	753.000
487	4.500	-0.000	-0.000	4.500	.949	.259	19.000	833.000

Table 5.4-2 Experimental Data Taken in a Pulsed Variable Area  
T-Burner with Cylindrical Grain (Ref. 5-3).

DATA POINT      OBSERVED      PREDICTED      RESIDUAL (OBS. - PRED.)      UNIT NORMAL DEVIATE      95.00 PERCENT CONFIDENCE LIMITS FOR PREDICTED VALUE

1	-3.59046127E+01	-4.22600928E+01	6.35532900E+00	.6942	-4.76932596E+01	-3.68269259E+01
2	5.5950670E+01	4.46235062E+01	1.0971561E+01	1.1985	4.15798960E+01	4.76671164E+01
3	4.32090396E+01	4.33639973E+01	-1.5495768E-01	-.0169	4.03359948E+01	4.63919998E+01
4	5.43643537E+01	4.97302692E+01	4.6340845E+00	.5062	4.66053887E+01	5.28551497E+01
5	4.44136058E+01	4.24239588E+01	1.9896470E+00	.2173	3.94064237E+01	4.54414940E+01
6	8.29180111E+01	8.08617879E+01	2.0562232E+00	.2246	7.67527726E+01	8.49708032E+01
7	6.54771859E+01	7.49672053E+01	-9.4900194E+00	-1.0367	7.10941864E+01	7.88402241E+01
8	8.60082915E+01	8.26859573E+01	3.3223441E+00	.3629	7.85005270E+01	8.68713476E+01
9	9.05590470E+01	8.78459263E+01	2.7131208E+00	.2964	8.34368594E+01	9.22549931E+01
10	8.18889487E+01	8.02284434E+01	1.6605053E+00	.1814	7.61456003E+01	8.43112865E+01
11	5.52933007E+01	5.40987159E+01	1.1945848E+00	.1305	5.08826954E+01	5.73147365E+01
12	3.89345337E+01	4.83645572E+01	-9.4300235E+00	-1.0301	4.52641685E+01	5.14649458E+01
13	4.52416933E+01	4.39884393E+01	1.2532540E+00	.1369	4.09529240E+01	4.70239546E+01
14	4.61874733E+01	5.04848200E+01	-4.2973467E+00	-.4694	4.73455720E+01	5.36240680E+01
15	4.40343997E+01	5.09780339E+01	-6.9436342E+00	-.7585	4.78290779E+01	5.41269898E+01
16	6.02785860E+01	5.19929556E+01	8.2856304E+00	.9051	4.88232469E+01	5.51626643E+01
17	2.53059519E+01	2.55075740E+01	-2.0162206E-00	-.0220	2.24984797E+01	2.85166683E+01
18	9.25614297E+01	8.76360835E+01	4.9253462E+00	.5380	8.32383155E+01	9.20358515E+01
19	1.03511719E+02	8.58995096E+01	1.7612209E+01	1.9239	8.15760550E+01	9.02229642E+01
20	8.01575530E+01	5.42341856E+01	2.5923367E+01	2.8318	5.10150387E+01	5.74533326E+01
21	6.61038621E+01	5.62886846E+01	9.8151774E+00	1.0722	5.30200106E+01	5.95573589E+01
22	-4.09046640E+01	-4.15776134E+01	6.7294945E-01	.0735	-4.69766312E+01	-3.61786957E+01
23	3.19609898E+01	4.74375532E+01	-1.5476563E+01	-1.6906	4.43526588E+01	5.05224475E+01
24	2.78106835E+01	4.65993918E+01	-1.8788708E+01	-2.0524	4.35277067E+01	4.96710770E+01
25	6.24984782E+01	7.48810121E+01	-1.2382534E+01	-1.3526	7.10113110E+01	7.87507132E+01
26	-4.99770163E+01	-4.56269035E+01	-4.3501127E+00	-.4752	-5.12303459E+01	-4.00234611E+01
27	-4.5977651E+01	-4.64795244E+01	5.0175928E-01	.0548	-5.21264204E+01	-4.08326285E+01
28	-5.99769031E+01	-4.65103025E+01	-1.3466601E+01	-1.4711	-5.21587695E+01	-4.08618356E+01
29	-4.69789891E+01	-4.70899283E+01	1.1093921E-01	.0121	-5.27680123E+01	-4.14118444E+01
30	-4.89789891E+01	-4.70899283E+01	1.1093921E-01	.0121	-5.27680123E+01	-4.14118444E+01
31	-4.39810051E+01	-5.00953634E+01	6.1143582E+00	.6679	-5.59279303E+01	-4.42627965E+01
32	-3.79797880E+01	-4.80254760E+01	1.0045688E+01	1.0974	-5.37514860E+01	-4.22994660E+01
33	-4.69789891E+01	-4.70899283E+01	1.1093921E-01	.0121	-5.27680123E+01	-4.14118444E+01
34	7.82815942E+01	8.53611234E+01	-7.0795292E+00	-.7734	8.10610901E+01	8.96611566E+01
35	5.71034995E+01	6.73305659E+01	-1.0227066E+01	-1.1172	6.37344585E+01	7.09266732E+01
36	9.05971307E+01	8.28511604E+01	7.7459702E+00	.8462	7.86587582E+01	8.70435627E+01
37	8.0709232E+01	7.99191952E+01	7.9072799E-01	.0864	7.58590636E+01	8.39893268E+01
38	5.20254372E+01	6.42191240E+01	-1.2193687E+01	-1.3320	6.07248809E+01	6.77133672E+01
39	2.09900514E+01	2.54242526E+01	-4.4342012E+00	-.4844	2.24143525E+01	2.84341528E+01

13 Data Points ( 33.33 Percent) are more than from Predicted Values  
 2 Data Points ( 5.13 Percent) are more than from Predicted Values

Table 5.4-3 Table of Residuals for the Data Shown in Table 5.4-1. The Dependent Variable is  $\alpha - \alpha_m$ .

A few words of caution concerning the use of statistics to interpret the data should be mentioned at this point. Since the statistical analysis will attempt to explain the data in terms of the theoretical expression, one should attempt to acquire data over a wide variation of the dependent variables, usually  $S_{bs}/S_{co}$ . For example, consider a bank of 12 data points taken at three area ratios with cup-shaped grains. The statistical analyses essentially will fit a three-parameter expression ( $B_e, B_s, \alpha_d$ ) through the mean of the data at each area ratio. This is comparable to fitting an expression with three unknowns through three points. Although the statistical parameters could indicate a high quality fit, a so-called "false correlation" probably has been obtained. If the experimenter were limited to obtaining only 12 points, a bank which contained six values of area ratio would be much more preferable.

Even the most carefully planned test series will frequently result in data points that were influenced by processes not accountable by theory. Frequently, the data will have to be screened to extract "bad" data points, or the basic theory will require modification to encompass all the test variances and thus ensure a precise determination of the combustion parameters. Several methods have been tried by various investigators, and the reader is referred to Appendix B for further discussion.

5.4.4 Velocity Coupling. In the variable area T-burner, the propellant extending along the burner wall is exposed to the acoustic velocity parallel to the surface while a disc of propellant in the end of the burner is acted upon by the acoustic pressure only. The potential effects of velocity coupling associated with the lateral grains must be considered. It has been found that, in some cases, the influence of velocity coupling is such that the response functions for pressure coupling, deduced from the data, may be significantly affected. The question remains open and is a subject of current work.

A derivation of the contribution of velocity coupling in a VATB can be found in ref. 5-3 and will not be repeated here. The growth constant due to velocity coupling can be written as

$$\alpha_{vc} = - \left( \frac{W}{K_l \epsilon_l z} \right) \left( \frac{S_{bs}}{S_{co}} \right) \left( \frac{\bar{u}_b}{a} \right) (P_l) R_v \quad (5.4.9)$$

where

$$P_t \equiv \frac{1}{\beta} [(C_t^0)^2 \sin^2 K_t (1 - \beta - \beta_0) - \cos^2(K_t \beta)] . \quad (5.4.10)$$

A response function for velocity coupling has been introduced, having imaginary part  $R_v^{(i)}$ . This is defined analogously to the response function for pressure coupling; the fluctuation of mass flux normal to the burner surface is proportional to the local value of acoustic velocity parallel to the surface:

$$\hat{m}_b = R_v \frac{\hat{u}}{a} . \quad (5.4.11)$$

The value of  $\alpha_{vc}$  is of course simply another additive contribution to the growth constant. Figure 5.4-1 shows the variation of a normalized form of  $\alpha_{vc}^0$  with  $\beta$ , for a flush cylindrical sample in a VATB. Note  $\alpha_{vc}^0$  increases proportionally with frequency, burner diameter, and the imaginary part of the velocity coupled response.

By using the general result shown in Figure 5.4-1, one finds, for the specific case of ANB 3066 propellant at 500 psi and 800 Hz, the behavior shown in Figure 5.4-2. The result shows that for the given conditions, the contribution  $\alpha_{vc}$  by velocity coupling can be as large as 10 to 20 times the velocity coupled response  $R_v^{(i)}$ . For a response of order unity, this represents a significant effect; for larger values of the response, velocity coupling cannot be ignored.

In ref. 5-3, calculations were performed, using actual data, to determine the effect of velocity coupling on data interpretation. Typical results are summarized in Table 5.4-4. Data from velocity-coupled T-burners discussed in ref. 5-6 have been included in cases 1 and 6 to account for the effect of velocity coupling. In the other cases, variable area T-burner data are treated with the velocity coupled response assumed to be zero, some fixed value, or left to float. As can be expected from the preceding figures, very significant errors are introduced if velocity coupling is not accounted for.

The conclusion is reached here that in the VATB for  $\beta \gtrsim 0.1$ , the effects of velocity coupling must be accounted for, or significant errors will be introduced. The velocity-coupled T-burner appears to be a way of evaluating velocity coupling, but it is still in the development stage. Se-

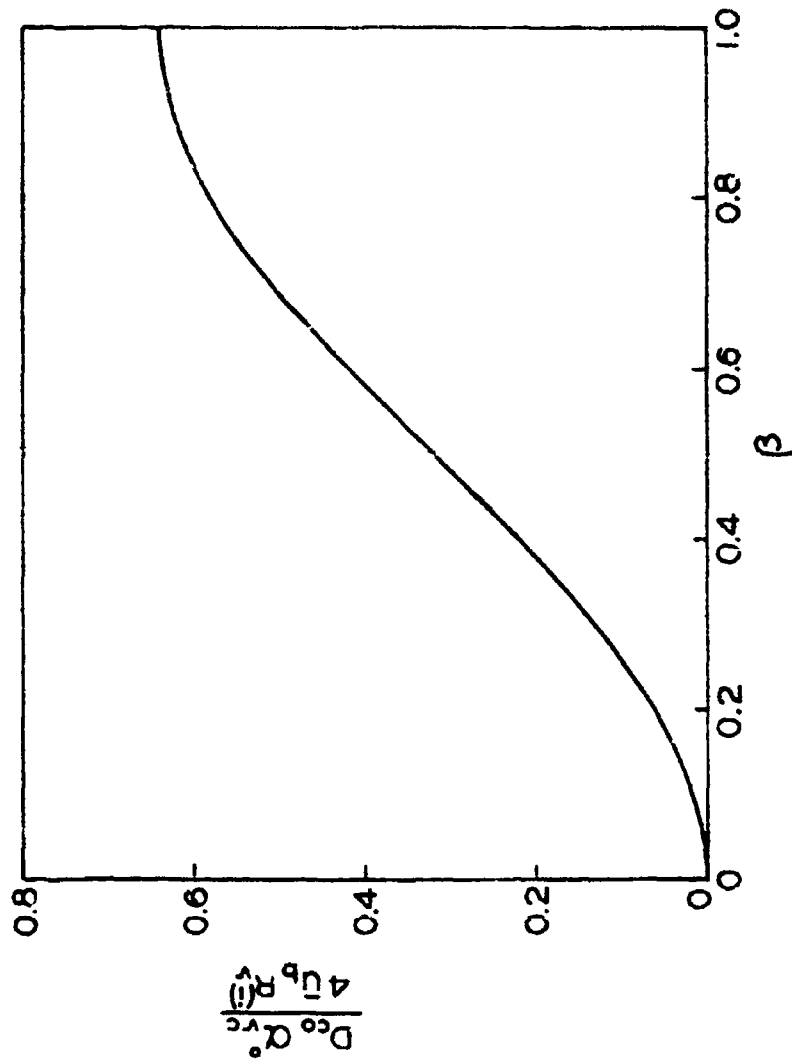


Figure 5.4-1 Contribution of Velocity Coupling in a VATB  
 ( $\alpha^0$  denotes flush conditions)

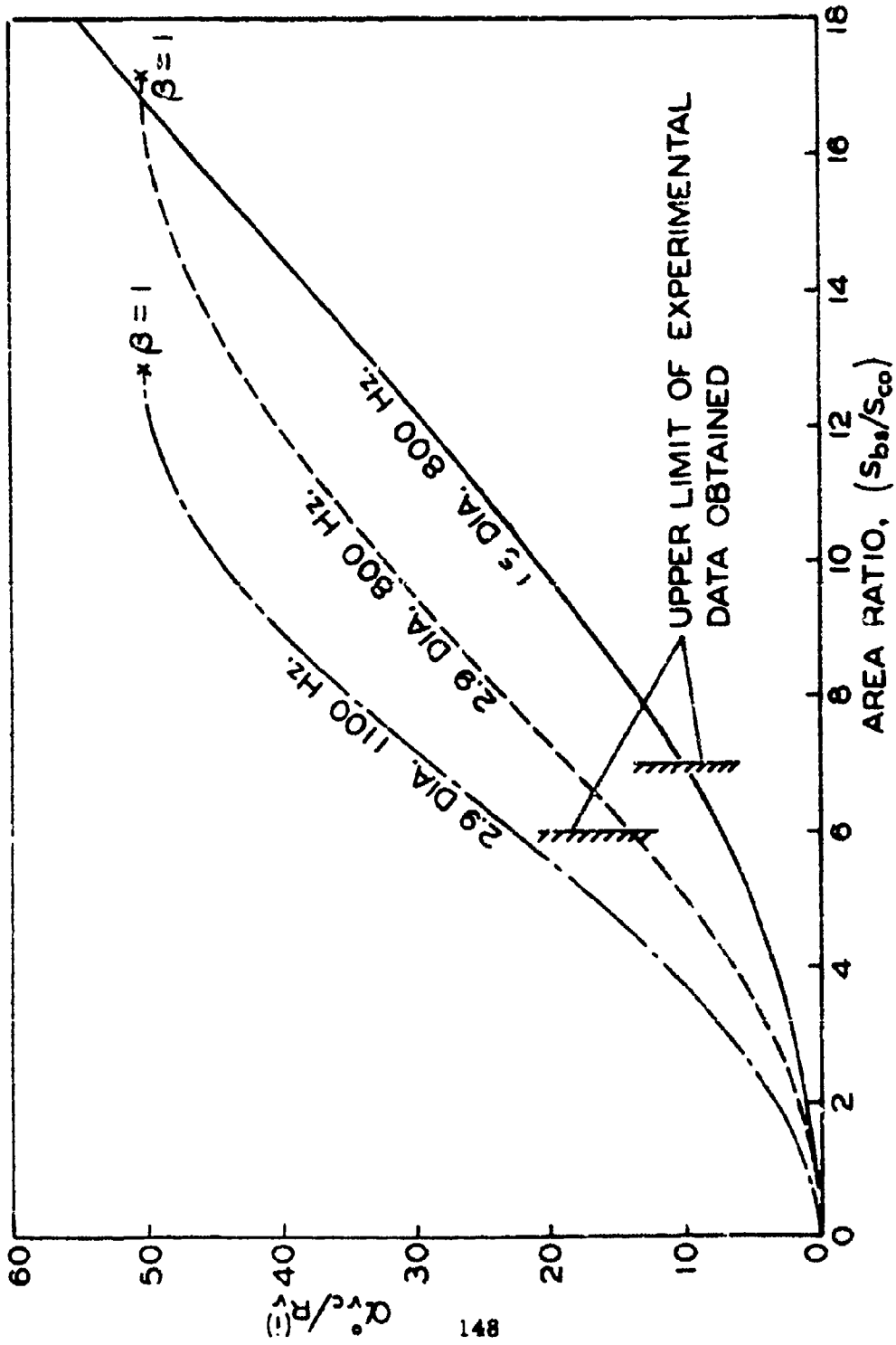


Figure 5.4-2 Contribution of Velocity Coupling for ANB-3066 Propellant as a Function of Frequency and Diameter at 500 psia

Table 5.4-4

## Effect of Velocity Coupling on Data Analysis

Case	Source of Data	$B_s$	$\alpha_d$	$R_v$	Correlation Coefficient	Percent Error in $B_s$
1	Ref. 5-3 (1.5" ID Burner and Ref. 5-6 (VCTB))	$2.2 \pm 0.1$	$-73 \pm 7$	$5.6 \pm 0.3$	0.982	---
2	Ref. 5-3 (1.5" ID Burner)	$3.2 \pm 0.2$	$-85 \pm 12$	0	0.971	45
3	Same	$2.6 \pm 0.1$	$-78 \pm 10$	3.4	0.981	18
4	Same	$2.3 \pm 0.1$	$-75 \pm 9$	5.0	0.985	4.5
5	Same	$1.7 \pm 0.6$	$-65 \pm 11$	$8.7 \pm 2.5$	0.988	25
6	Ref. 5-3 (1.5", 2.9" ID Burners) Ref. 5-2, Ref. 5-6	$2.0 \pm 0.1$	$-60 \pm 10$	$5.1 \pm 0.4$	0.960	---
7	Ref. 5-3 (1.5", 2.9" ID Burners) Ref. 5-6	$3.5 \pm 0.2$	$-97 \pm 19$	$0^x$	0.921	75
8	Same	$2.1 \pm 0.2$	$-67 \pm 14$	$5^x$	0.962	5
9	Same	$2.3 \pm 0.3$	$-73 \pm 15$	$4.1 \pm 0.9$	0.962	15

Cylindrical Grains;  $\bar{p} = 500$  psia,  $f = 100$  Hz; VCTB data obtained from Reference 5-6;

VF/FT = -1/+1.

cause of the magnitude of the errors that are otherwise introduced, it appears that data obtained with a velocity-coupled T-burner, or equivalent information, must be used in conjunction with analyzing VATB data to account for velocity coupling. This will complicate use of the T-burner, but it may be a necessary refinement. If velocity coupling is significant for a propellant used in a T-burner, then it is likely to be significant for the same propellant used in a motor. Consequently, one should take into account this potentially important factor, both in the interpretation of data taken with T-burners and in considering the stability of motions in a motor.

### 5.5 Nonlinear Analysis of Data

Nonlinear analysis has been introduced briefly in §2.4. It has not been used extensively to analyze data, and therefore no standard technique for data analysis has been adopted. The basic approach used by one organization will be referred to here, the interested reader should consult the references for further details on this subject.

Based on the idea that the unsteady motions in a T-burner might be approximated as a single acoustic mode, Culick (ref. 5-9) has shown this behavior can be described as a nonlinear oscillator. The envelope of the pressure oscillation is described by the first order equation

$$\dot{R}/R = \alpha + GR + PR^2 \quad (5.5.1)$$

where  $R$  is the amplitude of the oscillation and  $\alpha$  is the usual linear growth constant.  $G$  and  $P$  are nonlinear 2nd and 3rd order coefficients.

In attempting to evaluate the coefficients in Eq. (5.5.1) by fitting to T-burner data, it was found that equally good fits to a given T-burner record can be obtained with wide ranges of all three parameters ( $\alpha, G, P$ ) (ref. 5-6). The three degrees of freedom are too many to fit a simple curve meaningfully. Approaches have been developed to reduce the degrees of freedom, but even so, the results have not produced quantitative interpretations (refs. 5-6, 5-10). In these attempts at data analysis, the data have been fitted to Eq. (5.5.1) in the form of amplitude versus time. Another approach is based on the limiting amplitude that is ultimately reached. In Eq. (5.5.1) for large times,

$$\begin{aligned} \dot{R}/R &\rightarrow 0, \\ R &\rightarrow R_{\infty} \text{ (i. e., limiting amplitude).} \end{aligned}$$

Solving for  $\alpha/R_{\infty}$  yields

$$\frac{\alpha}{R_{\infty}} = G + PR_{\infty} \quad (5.5.2)$$

In other words, the quantity  $\alpha/R_{\infty}$  (which is based on two experimentally measurable quantities) is a measure of the nonlinearities of the system. Normalizing  $\alpha$  with frequency and the limiting amplitude with mean pressure yields a nonlinear parameter that has been somewhat successful in correlating data. This nonlinear correlating parameter has been defined as

$$\pi = \frac{\alpha/f}{R_{\infty}/\bar{p}} \quad (5.5.3)$$

Details of the work and results may be found in refs. 5-10, 5-11, and 5-12.

#### REFERENCES

- 5-1 Crump, J. E., Price, E. W., Mathes, H. B., and Dehority, G. L. "Oscillatory Combustion Experimentation and Analysis Work in Support of an Air Force program, 1971-1972," NWC-TR-5630 or AFRPL-TR-73-108 (June 1974), Naval Weapons Center, China Lake, Calif.
- 5-2 Derr, R. L. "Development and Evaluation of the Variable Area T-Burner," AFRPL-TR-72-97 (February 1973), Lockheed Propulsion Co., Redlands, Calif.
- 5-3 Beckstead, M. W., Bennion, D. U., Butcher, A. G., and Peterson, N. L. "Variable Area T-Burner Investigation," AFRPL-TR-72-85 (December 1972), Hercules, Inc., Magna, Utah.
- 5-4 Peterson, J. A., Muhlfeith, C. M., and Sayer, L. H. "Final Report: Pressure Oscillation Investigation for Minuteman III," AFRPL-TR-72-98 (January 1973), Thiokol Chemical Corp., Wasatch Division, Utah.
- 5-5 Micheli, P. L. "Experimental Procedures for the T-Burner," in Evaluation of Pulse T-Burner for Metallized Propellants, AFRPL-TR-72-54, Vol. I (January 1973), Aerojet Solid Propulsion Co., Sacramento, Calif.
- 5-6 Beckstead, M. W., Horton, M. D., Krashin, K., and Butcher, A. G. "Velocity Coupling, Combustion Instability," AFRPL-TR-73-73 (September 1973), Hercules, Inc., Bacchus Works, Magna, Utah.
- 5-7 "T-Burner Manual," CPIA Publication No. 191, CPIA, Silver Spring, Md. (November 1969).

- 5-8 Price, E. W., Mathes, H. B., Zurn, D. E., and Brown, B. G. "Combustion Instability of Aluminized Propellants. Part I. Progress on Support of Air Force Program," NWC-TP-5060, Part 1 (April 1971), Naval Weapons Center, China Lake, Calif.
- 5-9 Culick, F. E. C. "Nonlinear Growth and Limiting Amplitude of Acoustic Oscillations in Combustion Chambers," Combustion Science and Technology, V. 3, no. 1 (April 1971), pp. 1-16.
- 5-10 Jensen, R. C. and Beckstead, M. W. "Limiting Amplitude Analysis," AFRPL-TR-73-61 (July 1973), Hercules, Inc., Magna, Utah.
- 5-11 Beckstead, M. W. and Jensen, R. C. "Nonlinear Interpretation of Linear T-Burner Data," 9th JANNAF Combustion Meeting, CPIA Publication 231, Vol. I (Dec. 1972), pp. 239-247.
- 5-12 Jensen, R. C. and Beckstead, M. W. "Nonlinear Analysis of Combustion Instability Data," 10th JANNAF Combustion Meeting, CPIA Publication 243, Vol. II (Aug. 1973), pp. 163-178.
- 5-13 Peterson, J. A., Muhlfeith, C. M., and Sayer, L. H. "Final Report: Pressure Oscillation Investigation for Minuteman III," AFRPL-TR-72-98, Thiokol Chemical Corp., Wasatch Division, Brigham City, Utah (Jan. 1973).

## 6. TEST PROGRAMS AND APPLICATION TO STABILITY OF MOTORS

In this section the experiences of some of those who have been engaged in the use of T-burners are briefly summarized. It is not possible to provide a thoroughly detailed account. Proprietary considerations prevent inclusion of some material, and questions and decisions related to management problems, such as budgets, are not discussed. Only the technical aspects are treated, and largely in an abbreviated fashion.

Test programs may be divided into three classes according to their primary purposes: tests for comparison of propellants; tests to characterize thoroughly a single propellant; and tests directed towards solving a specific problem of instability in a motor. In §6.1 these kinds of programs are described, and in §6.2 the use of T-burner data to study the stability of motors is discussed.

### 6.1 Test Programs

6.1.1 Comparison of Propellants. A test program designed to compare propellants is principally a matter of qualitative testing. There is no question of comparing experimental results with a theory, and the absolute numerical values of the results are not usually important. There are three situations in which this kind of testing has been especially useful: development of a stable (or less unstable) propellant; during production, to monitor the behavior of each lot or batch of propellant, i. e., a surveillance program; and tests performed to study the consequences of relatively large variations in the ingredients. Specific examples are cited below.

Both DB/AB and VATB test methods have been successfully used for establishing the relative behavior of propellants (refs. 6-1, 6-2). The test program is usually not so elaborate as one designed to characterize thoroughly a propellant, but the individual tests must be performed with the same care. Sloppy procedures can easily destroy the validity of the experimental results even if they are intended only for comparison.

It is likely that this kind of program will be associated with a particular propulsion system. The characteristics of the motor serve to fix the temperature, mean pressure, and frequencies at which the T-

burner tests are performed. It is particularly important that the appropriate frequencies be used. If the motor in question has exhibited instabilities, then the frequencies and modes can be determined from observations. Note that a single frequency may not suffice, for two reasons. First, during a firing as the port opens up, the natural frequencies all decrease with time. Second, as conditions in the chamber change, a mode which is unstable early in a firing may subsequently become stable, and a different mode may become unstable. Should the motor be in the design stages, then it is necessary to perform an analysis of the cavity to find the classical modes and frequencies (see §2.5). At the very minimum, tests should be performed at the frequencies likely to be found in the motor. If time and funds permit, it is highly desirable to test over ranges of frequency, to gain some idea of the behavior as a function of frequency. Often, for example, it is helpful to know whether the response of the propellant is increasing or decreasing with frequency. The information may help clarify changes of behavior which may accompany small shifts of frequency in a motor.

The number of tests required for a DB/AB program has been discussed in §3.3.3.1. In that case, the configuration is fixed. If the VATB method is used, some exploratory firings will probably be required to establish the best area ratio to use. A good starting point is  $S_{bs}/S_{co} = 6$ , for a single grain; cylindrical grains mounted at the ends are probably simplest to use. Whatever configuration is finally chosen, it is absolutely essential that the same configuration be used in all comparison tests. Even small changes in geometry and ignition procedures, which might appear to be inconsequential, may in fact have very large effects destroying the validity of the observations.

Attention should be paid to the possibility that velocity coupling is a significant influence. This depends very much on the propellant used, and is more likely important in the case of longitudinal modes in the motor. Should velocity coupling be suspected, the type of burner described in §5.4.4 may be used. \* Driver grains are placed at the ends, and test

---

\* It should be recalled that DB/AB testing with end grains only will give no information about velocity coupling.

grains ( $S_{bs}/S_{co} = 3 - 5$  is a reasonable first choice) are placed at the quarter length positions. The behavior with and without test grains is compared for the propellants being considered. An alternative is to conduct tests with cylindrical test grains displaced various distances from the end. The phase relations between velocity, pressure, and burning rate are particularly crucial to the net effect of velocity coupling in a motor (refs. 6-3, 6-4, 6-5). Those relations vary substantially with frequency. The phase relations cannot be determined, with a T-burner, from tests at a single frequency. Consequently, tests must be conducted over a range of frequencies, even if one is concerned only with a single frequency in a motor.

When VATB testing is used, it is difficult to obtain a good value for the losses by determining the intercept of the curve of growth constant versus area ratio (see § 5.4). Pulsing at low area ratios, for which the fundamental mode is stable, improves the values obtained, but also complicates the test program. For qualitative purposes it may prove useful to compare values of the decay constant following burnout. However, care must be used because large uncertainties may result from poor ignition, continued burning of small slivers of propellant, and possibly residual combustion within the volume.

At least two attempts (ref. 6-6) have been made to check the losses determined from the intercept with those found by measurement of the decay following burnout. Good quantitative agreement has been found only under limited conditions. The simplicity of making the decay measurement is an attractive feature; use of these data for comparative purposes, at least, might profitably be examined further.

The most elaborate program of qualitative testing to date has been reported in ref. 6-1, using the DB/AB technique for a single propellant, in production.\* There are two purposes of the program: to monitor the combustion and particle damping for production lots of propellant; and to study the consequences of ingredient variations greater than those permitted by the normal manufacturing specifications. Photographic tests

---

\*Mr. B. T. Mathes (Naval Weapons Center, China Lake) provided the material for the examples discussed here.

in a window bomb, and T-burner tests are conducted in all cases.

For each sample, T-burner tests are conducted at a single pressure and five frequencies; five tests are made at each frequency. Thus, sufficient data are obtained to determine meaningful standard deviations. Figures 6.1-1 and 6.1-2 show results for the quantity  $\alpha_1 - \tau_2$ , proportional to the combustion response (see §3.2.2.1) and the decay constant  $\alpha_2$  for the pulse after burnout. In Figure 6.1-3, the results for  $\alpha_2 - \alpha_1$  are shown for a number of samples, covering tests at 800 Hz. The mean, and  $2\sigma$ ,  $3\sigma$  deviations shown are for all tests conducted on all samples at this frequency. Samples giving results lying between  $2\sigma$  and  $3\sigma$  from the mean should cause concern: the combustion response is then measurably different from the average of all lots.

For this propellant, lots of propellant showing somewhat higher response in the T-burner have, in some cases, produced greater than normal instability in a motor. The T-burner tests have not been used to reject lots of propellant which have passed the usual tests for burning rate, impulse and physical properties. On the whole, the specifications for this propellant appear to provide a uniform product, and variations of instability in the motors have been within acceptable limits.

Figures 6.1-4 and 6.1-5 show data for the decay following burnout, and for  $\alpha_2 - \alpha_1$ , for four different compositions, including that specified for production (labeled "reference propellant"). In each of the three other cases, the only change from the reference propellant was a change of particle size of one of the ingredients.

No attempt will be made here to interpret the results. The main point is that the tests evidently do provide a means of detecting changes of behavior due to changes of composition. A similar conclusion has been supported by the results of VATB test programs. It must be emphasized that the data shown here serve to characterize qualitatively some features of the behavior, but are insufficient for determining quantitatively the stability characteristics of a motor.

6.1.2 Characterizing a Single Propellant. Complete Characterization of a propellant involves essentially all the material included in this report. The test program necessarily becomes very extensive, because tests should be carried out over a range of temperature, mean

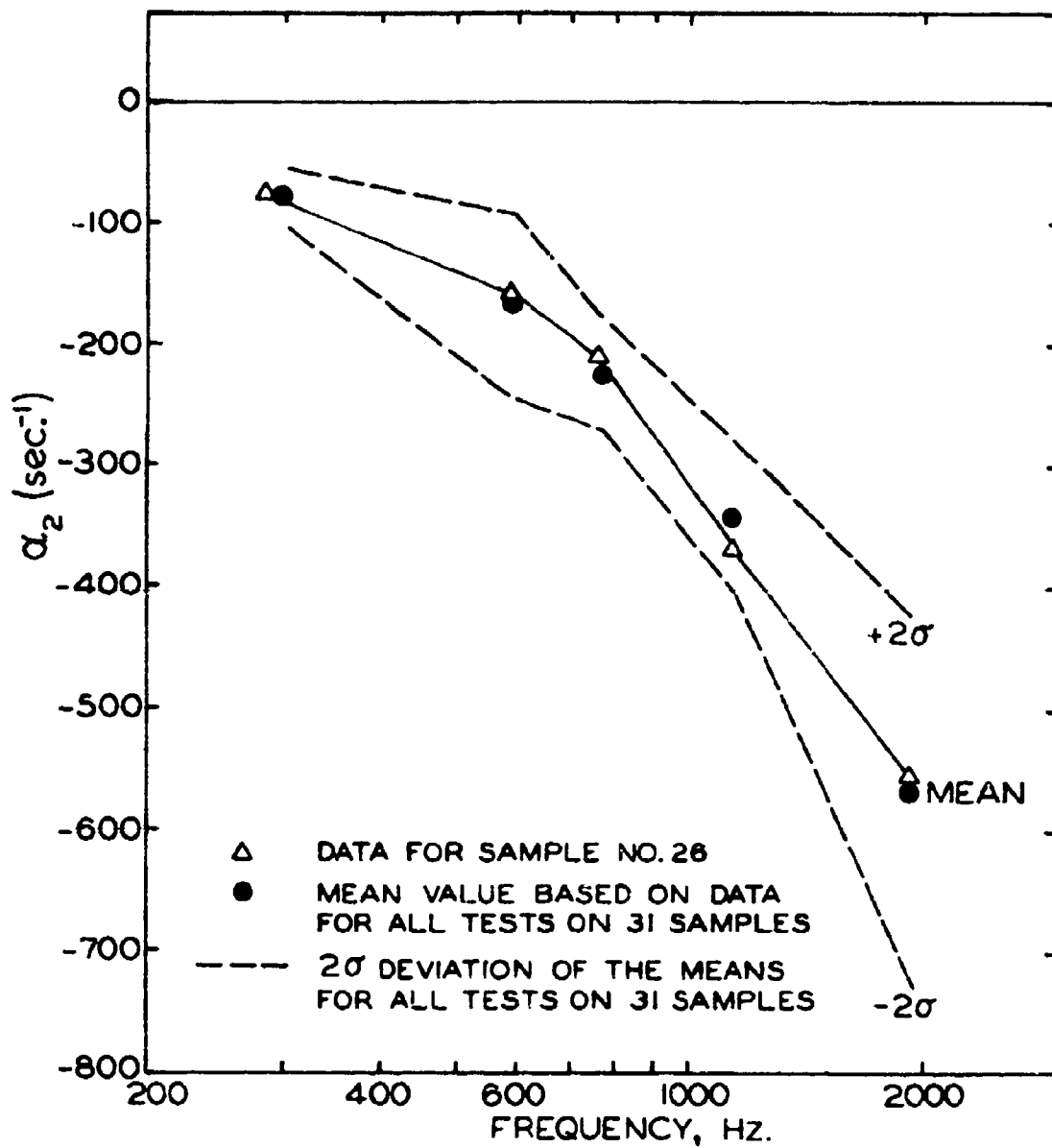


Figure 6.1-1 Particle Damping Data for Propellant Sample No. 26

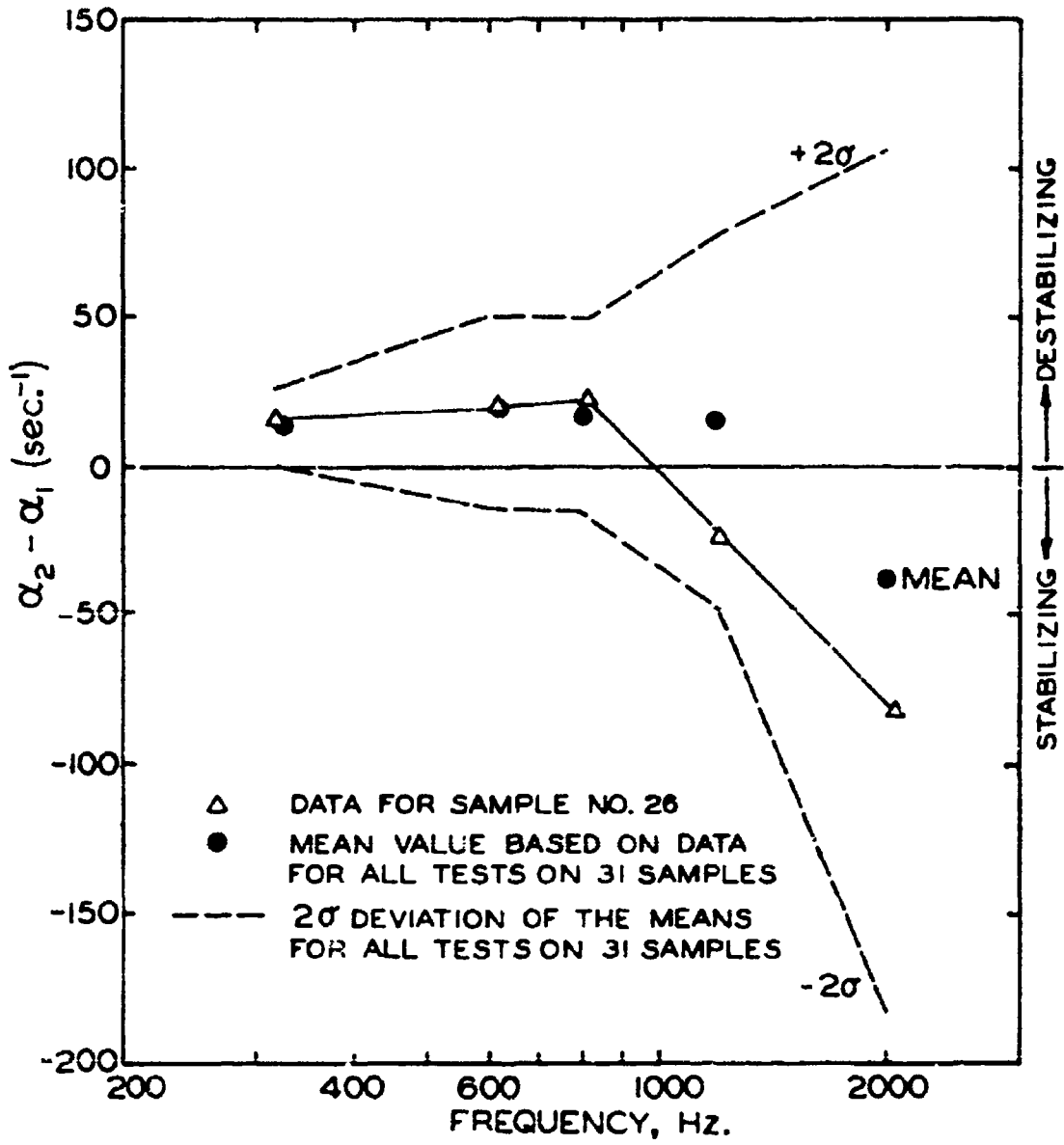


Figure 6.1-2 Combustion Characteristics for Propellant Sample No. 26

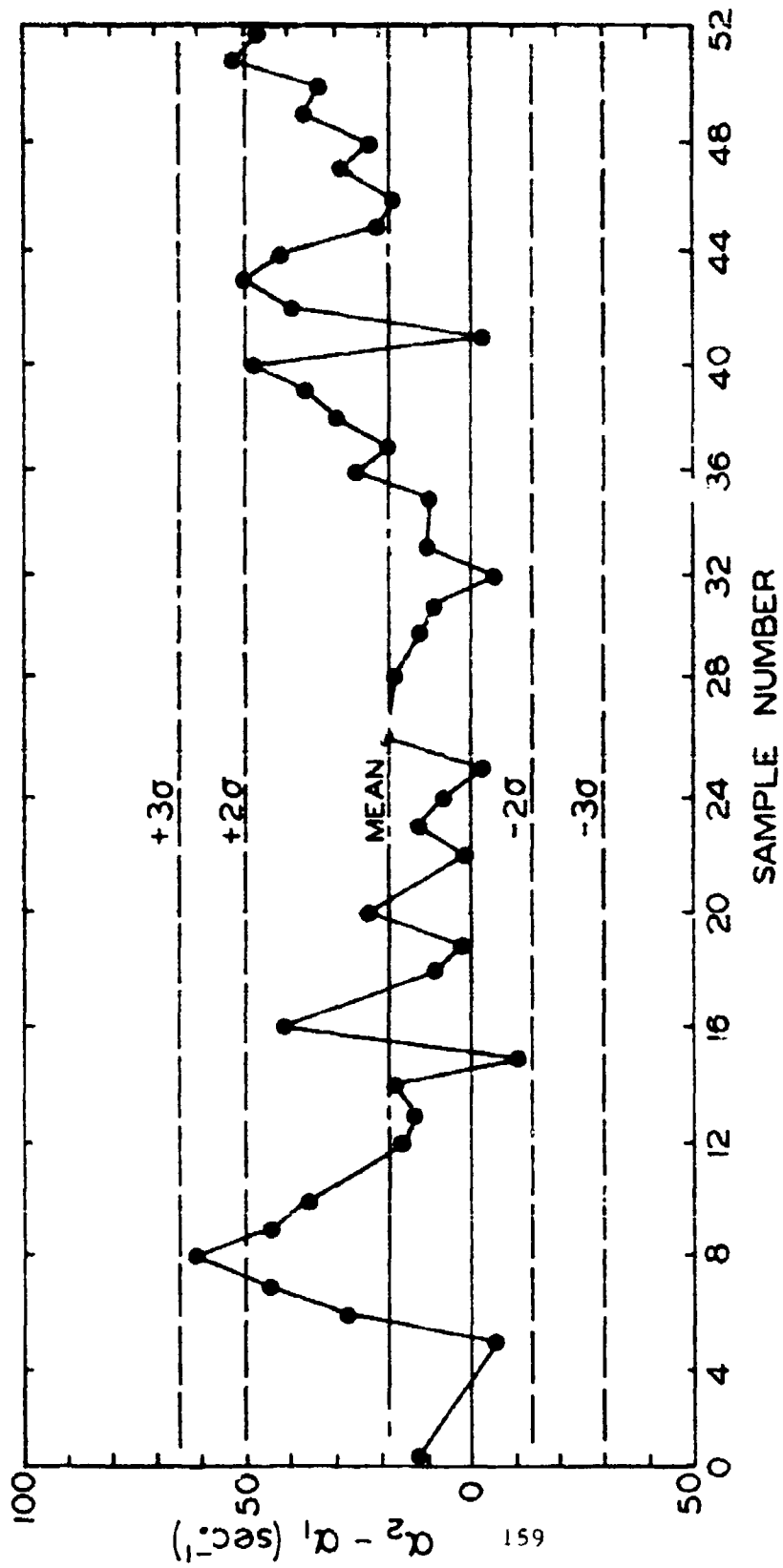


Figure 6.1.1-3 Combustion Characteristics at 800 Hz as a Function of Propellant Sample

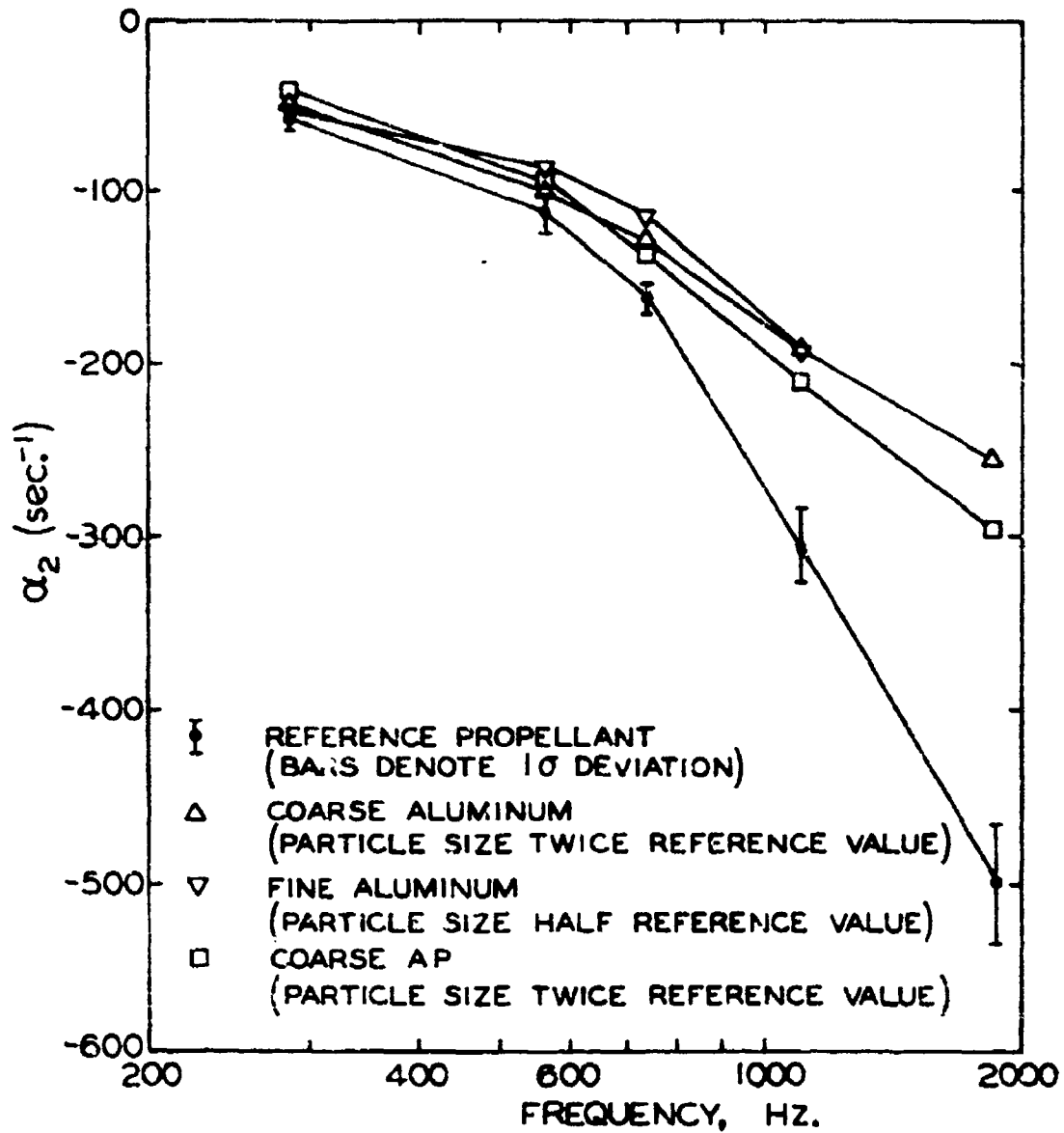


Figure 6.1-4 Effect of Propellant Ingredient Variations on Damping Rate of Acoustic Waves

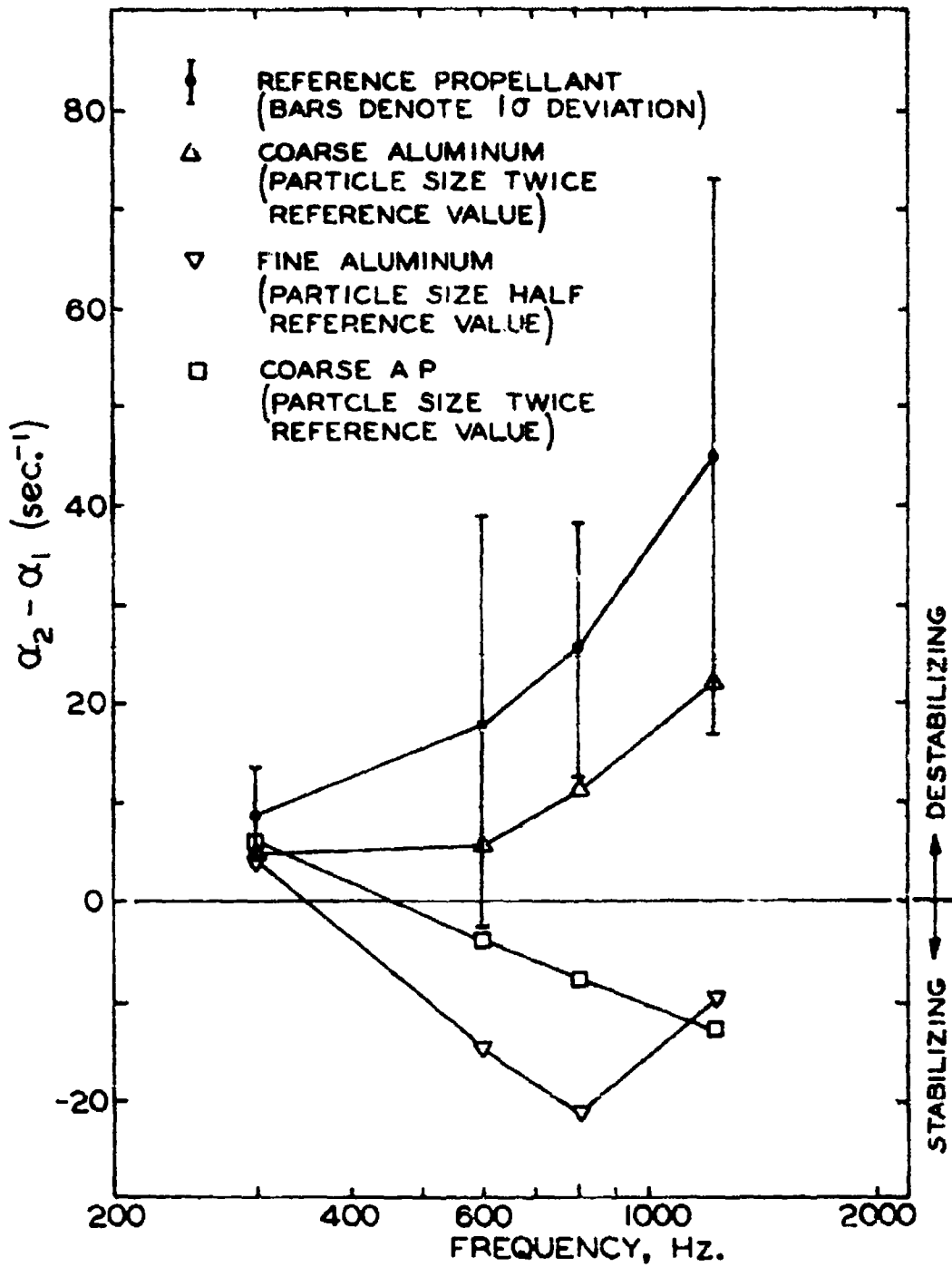


Figure 6.1-5 Effect of Propellant Ingredient Variations on Combustion Characteristics

pressure, and frequency. Moreover, to obtain good values with VATB testing, for the response functions, tests must be done over a broad range of area ratios, the smaller values requiring pulsed tests. Both DB/AB and VATB tests have been used for detailed characterizations. By far most of the work to date has been done for pressure coupling, but for a thorough assessment, tests for velocity coupling should be carried out.

To gain a rough idea of how many tests are involved, consider first VATB testing, for a single propellant at one value of mean pressure. As noted in 3.4.3.1, the minimum number of tests to define a curve of growth constant versus area ratio is about five at each frequency. To obtain even an approximation to the shape of the response curve, results for at least five frequencies are required, yielding a minimum number of twenty-five tests for each value of mean pressure. On the other hand, if each DB/AB test gives usable data (i. e., there is no difficulty with the timing and behavior of the pulse after burnout), the corresponding number of tests is fifteen -- one at each frequency and pressure.

In practice, more tests will be required, with each technique, to determine reproducibility and hence the reliability of the numerical values obtained from the measurements.

6.1.3 Tests for Application to Motor Stability. A test program designed to give the information required in a stability analysis is essentially like that required to characterize a propellant. The main difference is that the ranges of pressure, temperature and frequency need not be so large.

What range of frequency should be studied can be determined only from observations of the motor itself, or by a preliminary stability analysis. Principally, it is necessary to gain some idea of what modes might be unstable. Generally, the lowest two or three modes are most likely to be troublesome. Obviously, this cannot be done accurately without knowing the response of the propellant, but at least estimates can be made. Some effort spent on this task is worthwhile to reduce the possibly unnecessary expense of testing over too broad a frequency range.

As a practical matter, more tests are likely to be required at low frequencies and high pressures. In general, the response of a pro-

pellant is low at low frequencies (it may also be low at high frequencies), and if the T-burner is only weakly unstable it may be difficult to obtain with VATB testing a good definition of the curve for the growth constant versus area ratio. The corresponding difficulty in the DB/AB technique is that, for small combustion response,  $\alpha_2 \approx \alpha_1$  and it is then difficult to extract reliable values for the response, or  $\alpha_2 - \alpha_1$ . At high pressures, the increased burning rate produces shorter firing times, thereby reducing the opportunities for obtaining multiple growth periods in a VATB test.

## 6.2 Application of T-Burner Data to Problems of Stability in Motors

A brief introduction to the general problem of stability in motors was given in §2; see particularly Figure 2.1-1 for a simplified representation. Analysis of linear stability produces the very important result that the growth or decay constant  $\alpha$  is simply equal to the sum of contributions from the various physical processes taking place in the chamber. At the present time, T-burner testing is the only practical means of determining the contribution to  $\alpha$  from interactions between an unsteady flow field and surface combustion. In addition, the experimental techniques described in this report provide important clues to the attenuation of energy associated with particulate matter in the combustion products.

Testing with T-burners therefore is virtually an indispensable aid to assessing both the principal gain of acoustic energy and a major contribution to the losses. Less obviously, effort which has been expended on reconciling experimental results with analyses of the T-burner is important as well to the treatment of full-scale motors.

Because the T-burner is really just a special kind of rocket motor, the same analyses apply to both. The major formal difference is that in the T-burner, measured values of the growth constant are used to determine the combustion response and particle damping; but for a motor, everything else must be known, and the value of the growth constant is calculated. The analyses discussed in §2, and Appendices E and F, are applicable. Surveys of the general problem may be found in refs. 6-7 to 6-12; examples of calculations for specific motors have been published in refs. 6-13 to 6-16.

It is important to appreciate that values of growth or decay constants measured in T-burners are not directly applicable to motors. One must extract quantities which are normalized to a unit area or a unit volume. The response functions are in this sense valid representations of the surface combustion processes. Values of  $R_p^{(r)}$  for pressure coupling and the corresponding quantity  $R_v^{(i)}$  for velocity coupling can be used directly in a calculation of motor stability. It is fortunate that, in principle, these quantities can be determined from data taken in T-burner tests without calling upon a detailed analysis of the combustion processes.

The last statement is really only approximately true. The approximation is one that must be made, and cannot presently be satisfactorily improved upon, namely, that the response functions are independent of position on the burning surface. It has been emphasized elsewhere in this report that, on phenomenological grounds at least, the assumption can not be strictly true (for example, because of the influence of the local mean flow), but there is no available analysis or data to serve as the basis for rational improvements.

The situation is similar for particle damping. One can compute an expression (see Appendix D.1) for the dissipation of energy per unit volume associated with a given number density of particles having a given size. This can be extended in a straightforward manner to accommodate a distribution of particle sizes. Thus, if the damping due to particulate matter in a T-burner could be determined accurately, one could extract a value for the dissipation of energy per unit volume, which could then be used in the stability analysis of a motor. The crucial assumption must be made, however, that the average particle size produced in a T-burner is the same as that produced in a motor. This is not likely to be exactly true because of residual burning or agglomeration of particles, or both.

At the present time, estimates of particles sizes, and hence particle damping, rest on intelligent guesses. These are justified by the results of T-burner tests, and direct measurements of particle sizes from experiments with combustion of single particles, or from collections of combustion products produced in motors and T-burners (e. g. see refs. 6-17 to 6-19 for recent work). It is really the weight of various evi-

dences rather than the unquestioned accuracy of any single measurement which has justified the particular choices of particle sizes.

In the work reported in ref. 6-15, several motors, both sub-scale and full size, have been studied using the techniques described above. Tests with T-burners provided data for both the combustion response and attenuation by the condensed phase. Numerical analysis gave the natural frequencies and mode shapes. Calculations of the linear growth constant ( $\alpha$ ) were carried out prior to the motor firings. Generally, the predictions showed roughly the trends which were found in the tests although, as one should expect, the comparison was not particularly good quantitatively. This work is the most extensive yet published, and with the work reported in ref. 6-1, illustrates very well the practical values of T-burner testing.

Figure 6.2-1, taken from ref. 6-15, shows one example, for a demonstration motor thirty inches long, having fins in the aft end. Three propellants, referred to as VMV, VMO, and VMH, were tested in T-burners and fired in the motors. The motors were all stable initially, and later in the firing oscillations were observed, a trend predicted by the analyses. Measured values of the growth constant were substantially larger than those predicted. The discussion in ref. 6-15 contains several other examples and includes a detailed description of the results.

The use of data taken in T-burners for the study of behavior in motors raises the question of scaling: generally, T-burners are smaller than motors. One might hope that the values of the response functions and particle sizes determined from tests with T-burners would be applicable to motors. The hope, however, will probably not be fulfilled to perfection.

In ref. 6-20 an attempt was made to examine quantitatively the influence of diameter. Six sets of data obtained in the 1.5- and 2.9-inch T-burners, at pressures of 200, 500, and 700 psia, were examined. Experience with motors has shown that the burning rate decreases as the size of motor is increased, tending (roughly) asymptotically to the value measured in strand burners. If one assumes that the same behavior is exhibited by T-burners, this suggests plotting the data as shown in Fig-

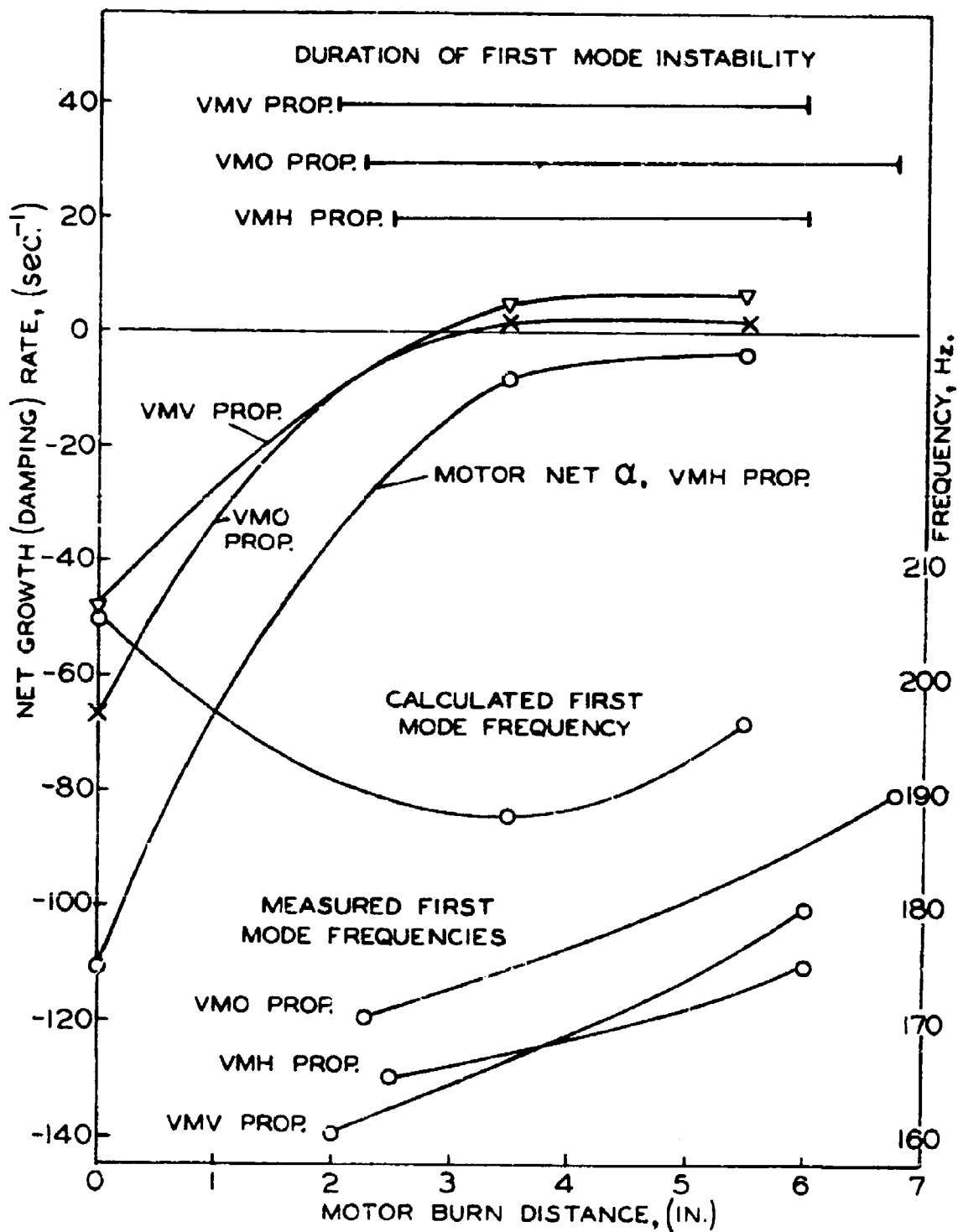


Figure 6.2-1 Comparison of Predictions and Observations for the Stability Characteristics of a 30-Inch Demonstration Motor

ure 6.2-2 for the response function. The data are shown correlated for two different combinations of the factors VF and FT.

The value of  $B_s$  appears to be within  $\approx 98$  per cent of "full scale" for the 2.9-inch T-burner and within  $\approx 90$  per cent for the 1.5-inch T-burner. Thus, typical T-burner data are roughly  $\approx 5$  to 10 per cent in error relative to the values one might use in full-scale motors, if this reasoning is correct. A greater degree of confidence is expressed in the 500 psi data because more data were available. The scaling factors that appear most reasonable for the 500 psi data are 1.06 for the 1.5-inch T-burner and 1.015 for the 2.9-inch T-burner. The data at 200 and 700 psi indicate larger scaling factors. However, fewer data were obtained at these pressures and less confidence is placed in the data.

Based on the data taken at 500 psia, it appears that a scaling factor of the form

$$\text{scaling factor} = 1 + A/D_{co}^2$$

is required to scale T-burner data. For the ANB-3066 propellant at 800 Hz and 500 psia, the value of A is  $\approx 0.13$  inches<sup>2</sup>. For the 200 and 700 psia data, the value of A appears to vary with  $B_s$ ; the results are less conclusive. The postulated scaling relationship indicates that for a scaling effect of around 1 per cent or less, a T-burner diameter of about  $3\frac{1}{2}$  to 4 inches would be required.

Similar results were found for the values of the decay constant associated with particle damping. The conclusion is that to scale T-burner data to motors larger than 10 inches in diameter, both  $B_s$  and the decay constant measured in T-burners should be increased by 1.06 (data from the 1.5-inch burner) or 1.02 (data from the 2.9-inch burner). This conclusion cannot be represented as a general result; indeed, it rests on very little evidence. Moreover, the diameter is of course only one of several variables. But the intent is certainly valid and must be recognized. There is, in all probability, an influence of scale; it appears to be at most a few per cent, which can nevertheless be significant in calculations of stability. The general question of scaling remains unanswered.

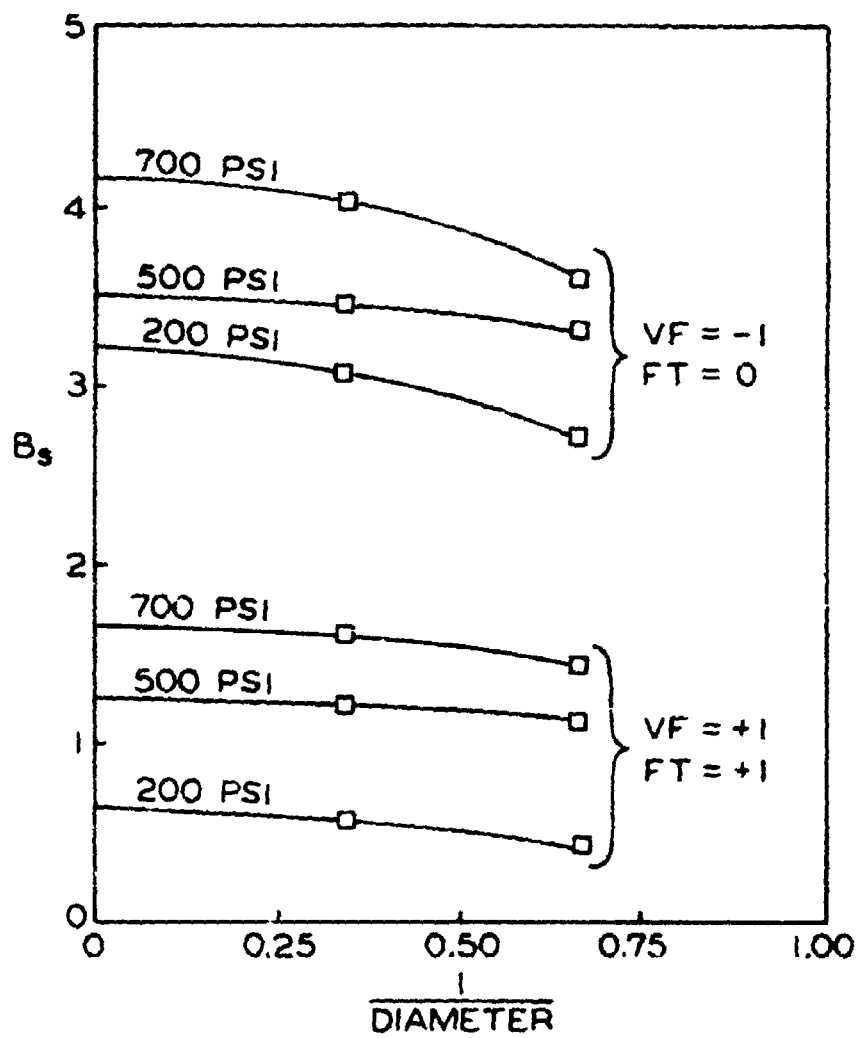


Figure 6.2-2 Effect of Scaling on the Combustion Response

In summary, the general problem of treating the stability of small motions in a motor is a bootstrap operation. It is impossible to produce quantitative results from first principles. Many independent pieces of information are required, and the T-burner is currently an indispensable source of values for two crucial items: the driving of unstable oscillations by surface combustion, and the loss of energy associated with the particles produced by the combustion of a metallized propellant.

#### REFERENCES

- 6-1 Letter reports from H. B. Mathes (Naval Weapons Center) to R. D. Kinert (Naval Materiel Command, PM-1) concerning Quality Control of FKM Propellant over the period March 1970 through May 1974 (copies available from Aerothermochemistry Division, Code 608, Naval Weapons Center, China Lake, Calif.).
- 6-2 Bennion, D. U., Beckstead, M. W., West, L. R., and Jessen, E. C. "The Variable Area T-Burner as a Quality Assurance Tool," 8th JANNAF Combustion Meeting (November 1971).
- 6-3 McClure, F. T., Bird, J. F., and Hart, R. W. "Erosion Mechanism for Nonlinear Instability in the Axial Modes of Solid Propellant Rocket Motors," ARS Journal, V. 32, no. 3 (March 1962), pp. 374-378.
- 6-4 Price, E. W. and Dehority, G. L. "Velocity Coupled Axial Mode Combustion Instability in Solid Propellant Rocket Motors," 2nd ICRPG/AIAA Solid Propulsion Meeting (June 1967).
- 6-5 Culick, F. E. C. "Stability of Longitudinal Oscillations with Pressure and Velocity Coupling in a Solid Propellant Rocket," Combustion Science and Technology, V. 2 (1970), pp. 179-201.
- 6-6 Beckstead, M. W., Hercules, Inc., Magna, Utah; Cohen, N., Lockheed Propulsion Company, Redlands, Calif. (unpublished private communications).
- 6-7 Hart, R. W. and McClure, F. T. "Theory of Acoustic Instability in Solid-Propellant Rocket Combustion," Tenth Symposium (International) on Combustion, The Combustion Institute, Pittsburgh, Pa. (1965), pp. 1047-1065.
- 6-8 Price, E. W. "Experimental Solid Propellant Combustion Instability," Tenth Symposium (International) on Combustion, The Combustion Institute, Pittsburgh, Pa. (1965), pp. 1060-1082.

- 6-9 Price, E. W. "Recent Advances in Solid Propellant Combustion Instability," Twelfth Symposium (International) on Combustion, The Combustion Institute, Pittsburgh, Pa. (1969), pp. 101-113.
- 6-10 Coates, R. L. and Horton, M. D. "Design Considerations for Combustion Stability," J. Spacecraft and Rockets, V. 6, no. 3 (1969), pp. 296-302.
- 6-11 Culick, F. E. C. "Research on Combustion Instability and Application to Solid Propellant Rocket Motors," AIAA/SAE 7th Propulsion Joint Specialist Conference (June 1971), AIAA Paper No. 71-753.
- 6-12 Culick, F. E. C. "Research on Combustion Instability and Application to Solid Propellant Rocket Motors, II," AIAA/SAE 8th Propulsion Joint Specialist Conference (November 1972), AIAA Paper No. 72-1049.
- 6-13 Browning, S. C., Kraskin, M., and Thacher, J. H. "Application of Combustion Instability Technology to Solid-Propellant Rocket Motor Problems," J. Spacecraft and Rockets, V. 9, no. 5 (May 1972), pp. 293-294.
- 6-14 Culick, F. E. C. and Kumar, R. N. "Combustion Instability in Large Solid Rocket Motors," 10th JANNAF Combustion Meeting (August 1973).
- 6-15 Beckstead, M. W. "Acoustic Stability Characterization of the Trident I C4 Motors," 11th JANNAF Combustion Meeting (September 1974).
- 6-16 Lovine, R. L. and Micheli, P. L. "Verification of the T-Burner for Stability Measurement," 11th JANNAF Combustion Meeting (September 1974).
- 6-17 Eisel, J. L., Price, E. W., Stine, C. E., and Brown, B. G. "Pressure and Velocity Dependence of  $Al_2O_3$  Particles Produced During Solid Propellant Combustion," 10th JANNAF Combustion Meeting (August 1973).
- 6-18 Derr, R. L., Churchill, H. L., and Fleming, R. W. "Aluminum Behavior Near the Burning Surface of a Composite Propellant," 10th JANNAF Combustion Meeting (August 1973).
- 6-19 Kraeutle, K. J. "The Analysis of Combustion Residues of Aluminum Propellants and Its Significance for the Study of Acoustic Damping," 10th JANNAF Combustion Meeting (August 1973).
- 6-20 Beckstead, M. W., Bennion, D. U., Butcher, A. C., and Peterson, N. L. "Variable Area T-Burner Investigation," AFRPL-TR-72-85, Hercules, Inc., Magna, Utah (December 1972).

## 7. CONCLUDING REMARKS

Despite its apparent simplicity, the T-burner has been the subject of continued development during the period of almost twenty years since it was introduced (ref. 7-1). Initially, the purpose was to produce oscillatory combustion in a laboratory device so that the phenomenon of combustion instability could be studied systematically under controlled conditions. As studies progressed, the burner was adapted to more sharply defined objectives, and the observed behavior was subjected to increasingly detailed measurement and interpretation. Principally as a result of the trend to widespread use and quantitative interpretation of results, the experimental and analytical techniques were standardized as far as possible and summarized in ref. 7-2.

It has only been since the publication of that report that the T-burner has been widely applied to testing metallized propellants. The techniques have been summarized in the preceding sections of this report. Particular emphasis has been placed on procedures, both experimental and for interpretation of data, which are currently used. Significant success has been achieved, both for research and for direct application to the design and development of motors.

There remain, however, a number of problems and unresolved issues, some of which have already been alluded to or discussed briefly. Because the T-burner continues to be the most important laboratory device for studying combustion instability, it is appropriate here to take notice of those problems which might profitably be examined more thoroughly in subsequent work. Even though the user of the T-burner may not be concerned with fine details, it is essential that he be aware of possible difficulties that he may encounter.

The following discussion covers a wide range of subjects, none of which are explored thoroughly. No attempt is made to assess the relative importance of the items covered. Indeed, it is impossible to do so, because the significance of a particular problem will vary with test conditions and the intended application of the T-burner. It is quite possible that some of the difficulties noted may in the future be either shown unimportant or they may be trivially resolved.

## 7.1 Analysis of the T-Burner and the Assumption of One-Dimensional Flow.

Analytical modeling of the T-burner serves two major purposes. It provides a rational basis for design of experiments and interpretation of results; and it provides a sufficiently rigorous look at the conservation arguments to avoid any gross omissions. On the other hand, the physical processes are very complicated, and a tractable analysis is necessarily a simplified representation. Available analysis of the burner involves the assumption at some stage that the flow is one-dimensional and/or isentropic. Modifications are then made to "correct" for the more gross deviations from the assumptions, modifications based on theoretical or experimental examinations of the three-dimensional nonisentropic processes. Since neither the original analysis nor the corrections provide a rigorous treatment of these aspects of the T-burner behavior, they merit specific discussion.

7.1.1 Nonisentropic Oscillations of the Combustion Zone (Pressure-Coupled). In representing the dynamic response of the combustion zone to incident pressure disturbances, the admittance function has been introduced, Eq. (E.34):

$$A_b = \frac{\hat{u}_b / \bar{a}}{\hat{p} / \bar{\gamma} p_o}$$

This has been related, Eqs. (E.38) and (2.6.4), to the response function  $R_b$  and nonisentropic temperature fluctuations  $\Delta \hat{T} / T_o$  by

$$A_b + \frac{\bar{u}_b}{\bar{a}} = \bar{\gamma} \frac{\bar{u}_b}{\bar{a}} \left( R_b + \frac{\Delta \hat{T} / T_o}{\hat{p} / p_o} \right)$$

where

$$R_b = \frac{\hat{m}_b / \bar{m}}{\hat{p} / p_o}$$

and

$$\frac{\Delta \hat{T}}{T_o} = \frac{\hat{T}_f}{T_o} - \frac{\bar{\gamma} - 1}{\bar{\gamma}} \frac{\hat{p}}{p_o}$$

The actual fluctuation of temperature at the edge of the (presumably thin) combustion zone is  $\hat{T}_f$ , and the second term is the isentropic fluctuation associated with a pressure fluctuation in the chamber. It may be noted

that by use of the perfect gas law, one can also relate  $A_b$  and  $R_b$  by

$$A_b = \bar{\gamma} \frac{\bar{u}_b}{\bar{a}} \left( R_b - \frac{\hat{\rho}_f / \rho_o}{\hat{p} / p_o} \right)$$

where  $\hat{\rho}_f$  is the actual density fluctuation at the edge of the combustion zone.

The pressure-coupled response function,  $R_b$ , has been the subject of both analytical and experimental studies (e. g. refs. 7-3 through 7-7). For high frequency oscillations, when a small element of gas in the combustion zone does not move appreciably during a cycle of oscillation, it has often been assumed that the actual temperature and density fluctuations are isentropic,

$$\frac{\hat{T}_f}{T_o} = \frac{\bar{\gamma}-1}{\bar{\gamma}} \frac{\hat{p}}{p_o}, \quad \frac{\hat{\rho}_f}{\rho_o} = \frac{1}{\bar{\gamma}} \frac{\hat{p}}{p_o}$$

In this case,  $A_b = \bar{\gamma} \bar{u}_b R_b / \bar{a}$ . Most experimental determinations of the response function have used this assumption, but its validity is highly suspect at frequencies of interest. In fact, the assumption appears to be incompatible with the assumption of quasi-steady behavior of the gas phase, commonly used in analyses of  $R_b$  for the combustion zone.

While most analyses will produce formulas for  $\hat{T}_f / T_o$  and  $\hat{\rho}_f / \rho_o$ , within the context of special models of the combustion zone, it appears that we are not in a position to separate  $R_b$  from  $\Delta \hat{T} / T_o$  (or  $\hat{\rho}_f / \rho_o$ ) in present experiments. This is especially true for aluminized propellants with their slow-reacting aluminum droplets and distributed combustion.

7.1.2 Boundary Layer - Combustion Zone Interactions. The principal combustion reactions occur (in side wall burners) in a region substantially coincident with the boundary layers of the mean flow and acoustic flow. The flow in this region is neither one-dimensional nor isentropic -- but its interaction with the combustion can apparently be critical to both combustion response (ref. 7-8) and the droplet size of the product  $Al_2O_3$ , and the associated energy dissipation (refs. 7-11, 7-12.) These effects are discussed in greater detail in §§ 7.3.2 and 7.6. They appear to be important to interpretation of T-burner test results, and may be even more important in motors. One reflection of concern for these effects is

the use of different response functions ( $B_e, B_s$ ) for end and side grains.

A recent calculation, ref. 7-10, is the first to treat the acoustic boundary layer with average mass flow normal to the surface. Combustion was not accounted for and the results have not yet been incorporated in the interpretation of T-burner data.

7.1.3 Flow-Turning of the Mass Addition at the Sidewalls. The one-dimensional analysis produced a "damping" term previously unsuspected, a contribution related to the fact that in some burner designs, the propellant products are introduced at the side walls of the channel, without the axial acoustic momentum of the main stream. In the one-dimensional model, mass addition is accommodated by assuming the mass "materializes" uniformly over the plane of addition, and shares the state and motion variables of the main gas column at that axial location; the flow variables are modified incrementally by the addition of the new mass, in accordance with the conservation equations. In the one-dimensional model, this set of assumptions and calculations gives rise to an acoustic loss term [see Eqs. (E. 33) and (F. 18)] which, in motor stability analyses, is often large, particularly in the early part of a firing when mean flow velocities are high. Because some motors have exhibited first axial mode instability particularly at this time during burning, one might suspect that the mass addition flow-turning losses may not be as large as calculated. One can judge from the description of the way in which side wall mass addition is accommodated in the one-dimensional analysis that it does not represent a mechanistic description of the actual three-dimensional non-isentropic mixing - flow turning of a two-phase oscillating flow from the side wall. Thus, it seems reasonable that the indicated loss process is real, but the magnitude of the loss remains uncertain, and is probably less than that given by Eqs. (E. 33) and (F. 18).

7.1.4 Flow Adjoining Channel Wall Discontinuities. The one-dimensional analysis is adapted to accommodate steps in channel area such as occur at the ends of side wall charges. However, this does not cover the effects of three-dimensional viscous flow, such as vortex formation or boundary layer detachment and reattachment. These effects in themselves may not be important, but they may exert perturbation effects on the combustion zone that are not encompassed as such in interpretation

of test results. Because of uncertainties involved in this area, many investigators restrict their data-taking to configurations and times during burning when the test sample is nearly flush with the burner wall (§§ 3.3.2.2 and 3.4.2.2).

7.1.5 Vent Out-Flow. The reaction products flowing toward the mid-point of the T-burner must execute a right angle turn to flow out the vent. Within the one-dimensional model, one is confronted with the question, what becomes of the acoustic (kinetic) energy of this exiting material? One might assume that the acoustic waves with their high velocity propagate through the turning flow without distortion; or at the other extreme, that all exiting flow carries with it its full complement of acoustic energy (see Appendix G). In effect, both of these assumptions have had advocates, although the resulting debates have led to an intermediate view, which is currently being quantified by experiment and by computations of three-dimensional viscous flow. This vent contribution, first identified in one-dimensional analysis, may yet turn out to be near zero, but the correct value or its quantitative dependence on test conditions remains to be determined.

7.1.6 Flow Immediately Following Pulses. In the pulsed DB/AB method, the oscillations often decay rapidly, leaving only ten or so measurable cycles. The first one or two cycles are ordinarily excluded from data reduction because of concern (and evidence) that normal oscillations are not established (§5.1.1). One probable (but unevaluated) cause of this anomalous character of the first oscillations is no doubt the three-dimensional nonisentropic injection and mixing of the pulser jet, with its foreign and possibly reacting materials. At present, this effect, which differs with the method of pulsing used, has received relatively little study. Instead, it has been customary to exclude as many as five cycles at the start of oscillation when enough cycles are available. Even then, there may be residual effects related to the presence of the pulser gases -- an uncertainty that dictates care in pulser design and use of minimum usable pulse size.

7.1.7 Distributed Combustion. The concept of a combustion response function that is characteristic of the propellant is closely linked to the assumption of a thin combustion zone (localized near the propellant

surface), and our handling of combustion instability problems rests heavily on these concepts. The one-dimensional modeling of the T-burner behavior makes a provision for a portion of the combustion occurring in the bulk gas field, but the process has not yet been treated in detail.

In the case of aluminized propellants, the aluminum droplets often burn so slowly that their combustion can no longer be regarded as localized near the burning surface. Combustion of the aluminum droplets as a "cloud" raises questions such as (a) how should the dynamic combustion response of the cloud be determined and included in the interpretation of burner tests? (b) how should the droplet size distribution and damping be handled? and (c) how should the spatial distribution of the properties of the medium (density, temperature, velocity of sound, etc.) be handled in the flow and mode calculations? The magnitude of this problem is unknown at present, although it is presumably less serious for situations where the aluminum agglomeration - droplet size is small and/or mean flow velocities are low so that aluminum combustion is concentrated near the burning surface.

## 7.2 Nonreproducibility

Aside from any questions of absolute accuracy of the test measurements or quantities derived therefrom, the utility of any repetitive experiment is dependent on the ability to duplicate the test. The alternative is to run enough repeat tests to have confidence in the average of the results. From the sample results discussed in 5.4.3 and Appendix B, it is evident that considerable economy in testing could be realized if more reproducible results could be achieved. While efforts have been made in this report to minimize sources of nonreproducibility, unrelenting efforts to find and control sources of variability appear to be in order. These sources presumably include the propellant, the burner and component "fit," the instrumentation and calibration, test record measurement, and data reduction.

## 7.3 Some Problems Associated with the Reduction of Data

To the present time, "reduction of data" means in the first instance measurement of the slope of the envelope of oscillations. That this should

be an important quantity is based on the results of an idealized representation of linear behavior. Consequently, quite apart from the usual difficulties with accuracy of measurement, more fundamental problems arise because the real behavior in the T-burner is imperfectly accounted for by the model. Considerable effort must be spent interpreting the numbers obtained from the data.

7.3.1 Nonlinear Growth and Decay. It is a basic result of linear behavior that an unstable motion grows exponentially with time,  $p' \sim \exp(\alpha t)$ , and a stable motion decays exponentially,  $p' \sim \exp(-\alpha t)$ . The growth or decay constant,  $\alpha$ , is ideally constant in time. Fortunately -- and in a sense remarkably -- much of the data obtained with T-burners does produce values of  $\alpha$  which are constant over fairly broad ranges of amplitude well above the noise level. Substantial deviations are, however, seen occasionally during growth but usually during decay. Especially for the decay following a pulse, the apparent nonlinear behavior cannot be ignored. The scheme for reducing data, discussed in §5.1.1, at best provides a method for accommodating this difficulty. It can produce essentially no explanation for the physical basis.

In a general sense, there are at least two important reasons why the quantity  $\alpha$  may vary with time. One or more nonlinear processes are necessarily acting when an unstable motion approaches a limiting value. It is an assumption in the linear analysis that such processes are negligible during some portion of the growth and decay at relatively low amplitudes. If the quantity  $\alpha$  is not constant, then an obvious possibility is that in fact not all nonlinear processes are negligible. Another assumption in the linear analysis is that the oscillatory motions take place about constant average values. If the average values change with time, then one or more parameters may change, causing apparent nonlinear behavior. One possibility, for example, is a shift of the average temperature which, among other things, affects the velocity of sound.

7.3.2 Extrapolation of the Variable Area T-burner Results to Zero Area Ratio. The original concept of a variable-area burner was based on the idea that the combustion response should be a property of the propellant, independent of location in the burner or mean flow conditions.

Likewise, the damping was viewed as a property of the combustion products and burner, independent of changes related to variation of area. Under these conditions, the variation of the growth constant with area ratio (Figure 5.3-3) was viewed as a straight line having  $\alpha_c$  and intercept (area ratio = 0) equal to  $\alpha_d$  (ref. 7-13). For the end burner configurations envisioned in ref. 7-2 this was probably an adequate interpretation. However, the use of large area ratio side-burning charges, required for testing aluminized propellants, brings in effects producing a curvilinear variation of  $\alpha_g$  with area ratio (§§7.1.3, 7.6). Further, because no spontaneous oscillations occur at low area ratios, the method requires a long extrapolation of the  $\alpha_g$  - area ratio curve to obtain the intercept representing the value of  $\alpha$  associated with the losses. As a result, large uncertainties may be introduced. To solve this problem, efforts are being made to fit the experimental results for the growth constant versus area ratio in such a way as to include such effects as velocity coupling, position on the acoustic mode, effect of acoustics/mean flow interactions and vent effects. In addition, data points are sought at lower area ratios by pulse-testing, thus reducing the range of extrapolation. If these corrective measures are all used, the value of the decay constant  $\alpha_d$  obtained by extrapolation should have more consistent meaning in successive experiments. However, the proper value of some of the corrections (e. g. vent effect) are still uncertain; and the use of data from pulsed tests brings the uncertainties associated with that experimental method. For best results, according to accepted practice, the procedures treated in §5.1 should be followed.

7.3.3 Reconciliation of Results of Different Test Methods. Ideally, the combustion and damping effects of interest should be measured by two or more independent methods, and found to be consistent among methods. In the work conducted in support of the present report, a concerted effort was made to achieve consistent results with different forms of the T-burner experiment, particularly with ANB 3066 propellant. The trend of results is suggested by Figure 5-3.3 for a given test frequency and pressure. It will be noted that the results from the pulsed end burner tests are not a natural extension of the data from tests on cylindrical test samples. This difference has been demonstrated to be a consistent effect for aluminized propel-

lants. While the difference may be related to systematic errors in one or both experimental methods (pulsed DB/AB and VATB), the same contrast in results did not occur in tests on an un-aluminized propellant (ref. 7-11). Thus, it seems likely that the combustion-flow coupling is different for end burners and side burners with aluminized propellants.

The difference must be accommodated in the interpretation of data; accordingly, the two response functions  $B_s$  and  $B_e$  have been introduced. To date, the data available are insufficient to merit any quantitative conclusions. Work devoted to this aspect of the problem must continue, particularly because of the relevance to understanding behavior of motors.

7.3.4 Correlation of Particle Damping. In view of the importance of  $Al_2O_3$  particle damping, it is notable that the T-burner measurements of particle damping are subject to some uncertainties, and information of the particle size distribution (critical to the damping) is minimal. Ultimately, one would hope that systematic measurements of damping and of particle size distribution will be made and successfully correlated. In the event that the droplet size distribution is dependent on flow conditions (§7.6.2), burning surface orientation, or any unsuspected variable, this will presumably have to be reconciled before successful correlation of T-burner results will be achieved (§§7.3.2, 7.3.3). Once again, the information involved will probably be crucial to accurate calculation of motor stability as well.

#### 7.4 Nonlinear Behavior

Modeling of the T-burner and interpretation of the data are based primarily on the one-dimensional small perturbation theory summarized and used in this report. The extent to which nonlinear processes are important in detail is as yet undetermined; but, for example, the observations of limiting amplitudes, non-sinusoidal oscillations, and non-exponential decays after pulsing are evidences of nonlinear behavior. There are specific processes that are believed to exert nonlinear influences; among these are nonlinear gasdynamics, velocity coupling, particulate damping, and droplet combustion.

As far as interpretation of linear behavior is concerned, the nonlinear processes are unimportant if they do not cause inaccurate measurement of the behavior of the first axial mode of the burner, and do not af-

fect the behavior in the first axial mode (e. g. transfer of first mode energy to higher modes). The report directs considerably attention to the questions of signal conditioning (filtering) and data processing to deal with the presence of higher modes and non-exponential pulse decays (§§3.3.1.5, 5.1.1, 5.2.3) so as to obtain accurate measurements.

Our knowledge of the nonlinear processes is too limited to assure that they are not affecting the behavior of the first mode during the periods of growth or decay when linear behavior is normally assumed. The nonlinear analysis of data described in §5.5 is a crude attempt to study the observed limiting amplitudes. Linear behavior at very low amplitudes is built into the representation, and whatever nonlinear processes are acting are all contained in coefficients evaluated from the data. A few specific processes should be noted.

7.4.1 Gasdynamic Nonlinearities; Mode Coupling. The development of a small-amplitude compressive wave into a sharp-fronted wave, or shock, is of course a well-known and basic phenomenon in gasdynamics. One of the remarkable aspects of the unsteady motions in both motors and T-burners is that quite large amplitude sinusoidal waves are observed to have unexpectedly little content of harmonics. The tendency for a low amplitude wave (usually the first mode) to develop sharp fronts, or other forms of distortion, seems to be mitigated by other processes in the system. Because any sort of distortion of the fundamental mode can be interpreted as a generation of higher modes, mode coupling associated with the gasdynamics has become an interesting and potentially important phenomenon to study.

A complete treatment of non-linear behavior necessarily must be done numerically (e. g. refs. 7-16 to 7-19). It is difficult to extract detailed information about the generation of higher modes, but some features -- e. g. the behavior of the sum of all even modes -- can be displayed quite easily. The approximate analysis constructed in ref. 7-19 is based on an expansion in the normal modes and therefore provides more direct information about mode coupling.

7.4.2 Nonlinearities Associated with Combustion Processes. With a relatively simple model as the basis, treatment of nonlinear pressure

coupling has been studied in numerical analysis, refs. 7-16 to 7-19. The results suggest that there are conditions under which the driving of waves by the combustion processes will depend on the amplitude of the motions, even at modest amplitudes. Because of the many approximations involved, and because the results are limited, it is not possible to state how important this influence may be in practical situations. It has never been accounted for in reducing data.

There is an intrinsic nonlinearity associated with velocity coupling, namely rectification, which tends to couple modes. This will cause the response of a burning surface to depend on the amplitude of the disturbance, and both the growth and decay of oscillations will depart from the ideal exponential behavior. Although an increasing amount of work has been devoted to velocity coupling (see §5.4.4), most aspects remain poorly understood. What has been done relates mainly to the kinematics of the problem.

Very little is known about the crucial physical processes involved in the nonlinear combustion of either surfaces or droplets. It is amply clear from combustion photography that, particularly for aluminized propellants, the processes occurring at and near the gas/solid interface must be very sensitive to the amplitudes of oscillation.

#### 7.5 Assumptions Concerning the Mode Shapes

All calculations of stability, for both motors and T-burners, involve integrals containing the mode shape. For example, the total acoustic energy itself is the integral of the square of the mode shape. One would anticipate that both combustion and mean flow should affect the mode shape; it is certainly not a priori obvious how precisely one must know the actual mode shape. What is required for most practical applications is surprisingly simple. According to the formal analysis outlined in Appendices E and F, a proper and good first approximation is that the mode shapes to use are those appropriate to the real geometry, with a closed boundary, and with no mean flow. In T-burners, it is important that changes of area long the duct be accounted for. Additional corrections might be necessary under some conditions, but no detailed results are available. It is worth remarking upon the sources of possible refinements.

7. 5. 1 Heat Transfer. The analysis in §2 and Appendices E and F involves the assumption that the mean local density and velocity of sound in the combustor cavity are uniform (i. e., independent of position). In tests where propellant surface area (and therefore the total mass flow) is small and burner wall area is large (low frequency burner), the effect of heat loss is large and the assumption of uniform conditions in the burner may need attention. For example, Figure 3. 3-2 shows the reduction of frequency with increasing length due to heat losses. This is accompanied by internal temperature gradients which influence the speed of sound, mode structure, and natural frequency. Apart from a correction noted in ref. 7-2, this problem has not been treated.

7. 5. 2 Strong Acoustic Sources and Sinks. For all calculations of stability which have been carried out to date, the classical mode shapes, undistorted by combustion, mean flow, or any other sources or sinks of acoustic energy, have been used. There are broad conditions under which that approximation will be entirely adequate for computing the growth or decay constant,  $\alpha$ . Of course, the actual mode shapes in a combustion chamber are in fact slightly distorted, and the formal analysis can be used to produce corrections to first and higher orders in the average Mach number of the mean flow. The formulas for  $\alpha$  and  $\omega$  given in Appendices E and F are really the first terms for an iterative solution.

For high burning rates, and in motors early in a firing when the Mach number may be high over large regions of the chamber, the distortion of the acoustic field by the average flow may be so large that the approximation calculation should be carried out to higher order. There is no fundamental difficulty in doing so, but no numerical results are available; there are no experiments relevant to this problem.

7. 5. 3 Rate of Change of Oscillation Amplitude. A further assumption that is built into the analysis is that the amplitude of oscillation does not change rapidly; specifically,  $\alpha/\omega \ll 1$ . This is a consequence of the fact that the correction to the unperturbed frequency is proportional to the average Mach number,  $M_b$ , but  $\alpha$  itself is proportional to  $M_b$ . Thus,  $\alpha/\omega \sim M_b$ , which is required to be much less than unity. If observed values of  $\alpha/\omega$  are large, then the analysis used must be changed to accommodate this. Formally, and on physical grounds, one might expect that

this situation and the problem discussed in 7.5.2 are intimately connected.

## 7.6 Influences of the Mean Flow

The basic analysis includes the presence of mean flow in the burner insofar as the conservation laws for the gas motion are concerned. However, the mean flow is apparently responsible for some effects that are not encompassed in the data reduction, effects that have yet to be evaluated quantitatively.

7.6.1 Assumption of Spacewise Uniformity of Combustion Response. It has been noted (§7.3.2) that interpretation of test results has included the assumption that the combustion response is not affected by the surrounding mean flow field. However, it is observed that with high area ratio (long) propellant charges, the mean burning rate is higher toward the downstream end of the charge, indicating that the mean flow encroaches on the combustion zone. It is reasonable to assume that such encroachment will modify the dynamic behavior of the combustion zone as well, although there is no information regarding the magnitude of this effect. In the case of charges with high area ratio,  $S_b/S_{CO}$ , it may be necessary to relax the assumption of uniform response function -- just as present results indicate that a different value of the response is needed for end burners and side burners (§7.1.2 and ref. 7-11). This is a matter of greater concern with rocket motors, where very high mean flow velocities prevail. It is the acoustic counterpart of the classical erosive burning problem. As an alternative to assuming that the response function may vary with position on the burning surface, which would greatly complicate interpretation of data, it might be better to limit the length of grains used. Experimental measurements bear only indirectly on this problem; the influence of mean flow may be partly responsible for the observations leading to the restriction on  $S_b/S_{CO}$  (or  $\beta$ ) noted in §3.4.4.2.

7.6.2 Aluminum Oxide Droplet Size. The size distribution of the  $Al_2O_3$  droplets in the combustion products is critical to the damping in T-burner tests (and motors). The factors governing this droplet size distribution are qualitatively understood; of the steps involved, the key process of formation of aluminum accumulations on the burning surface appears to be particularly responsive to mean flow in the burner (ref.

7-9) and hence of charge area rates. Modification of the aluminum accumulation could thus change  $Al_2O_3$  droplet size distribution in a manner dependent on area ratio of the charge, and hence on location in the burner and time during burning (these effects could be misinterpreted as "lip effects," "stay-time effects," etc.). The data available to date suggest that this is a significant effect, which is probably dependent on pressure, frequency, and type of aluminized propellant. It has obvious implications for §§7.3.2 and 7.3.4, and for quantitative applicability of Eqs. (2.2.2) and (2.2.4). It is also of concern in motor applications.

#### 7.6.3 Comparison of During Burning and After Burnout Pulses.

The accuracy of the assumption that decay rate of a pulse (properly timed) after burnout is a measure of damping during burning (§3.1.1) is suspect on several grounds. One is the presence of mean flow to the vent during burning, and possible flow into the burner from the surge tank during the pulse after burnout. Until the importance of the mean flow - associated vent effect is established, the test technique using pulses during and after burning involves a potentially serious uncertainty. Because of the low mean flow Mach number in pulse tests, the uncertainty is not a large percentage error in damping determinations (the two pulse decay rates are nearly the same). But the combustion response is calculated by forming the difference between two large and nearly equal numbers; the error may then be quite substantial.

#### 7.7 Closure

The preceding paragraphs encompass a broad spectrum of problems which remain unresolved. Neither are they all of comparable significance nor should the recognition of them be allowed to obscure the demonstrated value of the T-burner as a test device for both research and applications as discussed in §6. It is important to emphasize that many of the questions which have been raised during work with the T-burner arise also in connection with motors. Most of what is learned from experience with the simpler and much less costly laboratory device is directly applicable to full-scale motors.

## REFERENCES

- 7-1 Price, E. W., Mathes, H. B., and Crump, J. E. "Evolution of Laboratory T-burners for Study of Solid Propellant Combustion Instability," Technical Note 608-109, Revision 1 (26 August 1972), Naval Weapons Center, China Lake, Calif.
- 7-2 "T-Burner Manual," CPIA Publication No. 191 (November 1969), CPIA, Silver Spring, Md.
- 7-3 Culick, F. E. C. "A Review of Calculations for Unsteady Burning of a Solid Propellant," AIAA J., V. 6, no. 12 (Dec. 1968), pp. 2241-2255.
- 7-4 "Experimental Studies on the Oscillatory Combustion of Solid Propellants," NWC TP 4393, Naval Weapons Center, Aerothermochemistry Division, China Lake, Calif.
- 7-5 Brown, R. S., Muzzy, R. J., and Steinle, M. E. "Surface Reaction Effects on the Acoustic Response of Composite Solid Propellants," AIAA J., V. 6, no. 3 (March 1968), pp. 479-
- 7-6 Beckstead, M. W. and Culick, F. E. C. "A Comparison of Analysis and Experiment for Solid-Propellant Combustion Instability," AIAA J., V. 9, no. 1 (January 1971), pp. 147-154.
- 7-7 Perry, E. H. "Investigations of the T-Burner and Its Role in Combustion Instability Studies," Ph. D. Thesis, California Institute of Technology, Pasadena, Calif. (May 1970).
- 7-8 Krier, H., Tien, J. S., Sirignano, W. A., and Summerfield, M. "Nonsteady Burning Phenomenon of Solid Propellants: Theory and Experiment," AIAA J., V. 6, no. 2 (1968), pp. 278-285.
- 7-9 Tien, J. S. "Oscillatory Burning of Solid Propellants Including Gas Phase Time Lag," Combustion Science and Technology, V. 5, (1972), pp. 47-54.
- 7-10 Flandro, G. "Interaction of Acoustic Waves with a Solid Propellant Burning Surface," 11th JANNAF Combustion Meeting, Pasadena, Calif. (Sept. 1974).
- 7-11 Price, E. W., Mathes, H. B., and Crump, J. E. "Adaptation of T-Burners to Measurements on Metallized Propellants," NWC TN 608-111 (23 May 1972), Naval Weapons Center, China Lake, Calif.

- 7-12 Price, E. W. "NWC Experimental Work Related to Acoustic/Mean Flow Interactions (and Other Effects Related to Interaction Measurement)," NWC Technical Note 608-122, Naval Weapons Center; presented at the California Institute of Technology, 13-14 March 1973.
- 7-13 Eisel, J. L., Price, E. W., and Brown, B. G. " $Al_2O_3$  Particles Produced During Solid Propellant Combustion," AIAA Paper No. 74-197, AIAA 12th Aerospace Sciences Meeting, Washington, D. C. (Jan. 30-Feb. 1, 1974).
- 7-14 Culick, F. E. C. "The Stability of One-Dimensional Motions in a Rocket Motor," Combustion Science and Technology, V. 7 (1973), pp. 165-175.
- 7-15 Coates, R. L. "Double-End Burner Experiments," Proceedings, 3rd Meeting Technical Panel on Solid Propellant Combustion Instability, Applied Physics Laboratory, Johns Hopkins University, TC 371.5 (May 1963).
- 7-16 Levine, J. N. and Culick, F. E. C. "Nonlinear Longitudinal Combustion Instability in Solid Rocket Motors," 10th JANNAF Combustion Meeting (August 1973); CPIA Publication 243, Vol. 1 (Dec. 1973).
- 7-17 Kooker, D. E. and Zinn, B. T. "Numerical Solution of Axial Instabilities in Solid Propellant Rocket Motors," 10th JANNAF Combustion Meeting (August 1973); CPIA Publication 243 (Dec. 1973).
- 7-18 Levine, J. N. and Culick, F. E. C. "Nonlinear Analysis of Solid Rocket Combustion Instability," Ultrasystems, Inc., Technical Report AFRPL-TR-74-45 (July 1974).
- 7-19 Culick, F. E. C. and Levine, J. N. "Comparison of Approximate and Numerical Analyses of Nonlinear Combustion Instability," AIAA 12th Aerospace Sciences Meeting, Washington, D. C. (Jan. 1974), AIAA Paper No. 74-201.
- 7-20 Culick, F. E. C. "Nonlinear Behavior of Acoustic Waves in Combustion Chambers," 10th JANNAF Combustion Meeting, August, 1973; CPIA Publication 243 (December 1973).
- 7-21 Price, E. W., Mathes, H. B., Madden, O. H., and Brown, B. G. "Pulsed T-Burner Testing of Combustion Dynamics of Aluminized Solid Propellants," AIAA/SAE 7th Propulsion Joint Specialist Conference (June 14-18, 1971); see also Patent No. 3,788,126 issued 29 January 1974.

APPENDIX A  
NOMENCLATURE

A few symbols defined in the text and used but briefly are not included in this list.

$\bar{a}$	speed of sound for a two-phase mixture, Eq. (E. 19)
A	parameter in the response function, Eq. (2.6.6)
$A_b$	admittance function for a burning surface, Eqs. (2.6.3) and (E. 34)
B	parameter in the response function, Eq. (2.6.6)
$B_e$	admittance function with mean flow, end surface, Eq. (2.6.5)
$B_s$	admittance function with mean flow, lateral or side surface, Eq. (2.6.5)
C	specific heat for the particulate material
$C_m$	mass fraction of particulate material, $C_m = \rho_p / \rho_g$
$C_p$	specific heat for the gas only
$\bar{C}_p$	specific heat for the two-phase mixture, $\bar{C}_p = \frac{(C_p + C_m C)}{(1 + C_m)}$
$C_v$	specific heat for the gas
$\bar{C}_v$	specific heat for the two-phase mixture, $\bar{C}_v = \frac{(C_v + C_m C)}{(1 + C_m)}$
$C_l^o$	coefficient defined in Eq. (C. 7) and given by Eq. (C. 11)
$C_l$	function defined in Eq. (C. 16)
D	diameter of the chamber
$D_c$	port diameter for a cylindrical grain
DB/AB	abbreviation for "during burning/after burnout" pulsed test
$e_o$	stagnation internal energy for the gas
$e_{po}$	stagnation internal energy for the particles
$e_{os}, e_{pos}$	$e_o$ and $e_{po}$ evaluated at the surface
E	time-averaged total acoustic energy in a chamber, $E = E_l^2 / 2\bar{\rho} \bar{a}^2$

$E_l^2$	integral defined by Eq. (E. 39) for the $l^{\text{th}}$ longitudinal mode
$E_N^2$	integral defined by Eq. (F. 16) for the $N^{\text{th}}$ three-dimensional mode
$\mathcal{E}$	energy source, introduced in Eq. (F. 2)
$\varepsilon_l^2$	normalized acoustic energy, $\varepsilon_l^2 = 2E_l^2/S_{co}L$
$f$	function defined by Eq. (F. 14)
$f_l$	function defined by Eq. (E. 17)
(FT)	flow-turning factor, introduced in Eq. (E. 51)
$F_p$	force of interaction between particles and gas, Eq. (D. 6)
$\delta F_p$	differential force of interaction, Eq. (E. 11)
$g_l$	function defined by Eq. (C. 15)
$h$	function defined by Eq. (F. 13)
$h_l$	function defined by Eq. (E. 16)
$h_{os}$	stagnation enthalpy of the gas, evaluated at the surface
$k_l$	wavenumber for the $l^{\text{th}}$ longitudinal mode, $k_l = \omega_l/\bar{a}$
$k_N$	wavenumber for the $N^{\text{th}}$ three-dimensional mode, $k_N = \omega_N/\bar{a}$
$K_l$	dimensionless wavenumber, $K_l = Lk_l/2 = L\omega_l/2\bar{a}$
$L$	length of the burner, Figure C-1
$L_o$	displacement of a cylindrical grain, Figure C-1
$L_b$	length of grain along the lateral boundary, Figure C-1
$m$	mass flux (mass/area-sec.)
$m_b$	mass flux of gas at and normal to a burning surface
$m_b^{(p)}$	mass flux of particulate material at and normal to a burning surface
$M_b$	Mach number for the gas leaving a burning surface, $M_b = u_b/\bar{a}$
$\hat{n}$	unit vector outward at a boundary
$p$	pressure

$\hat{p}_l$	spatial mode shape of pressure for the $l^{\text{th}}$ longitudinal mode
$\hat{p}_N$	spatial mode shape of pressure for the $N^{\text{th}}$ three-dimensional mode
$p_o$	stagnation pressure
$P'$	function defined by Eq. (F. 10)
$P_l$	function defined by Eq. (E. 18)
$Pr$	Prandtl number, $Pr = \bar{C}_p \mu / k$
$q$	perimeter of a surface
$Q$	heat source defined in Eq. (F. 20)
$Q_p$	heat transfer between particles and gas, Eq. (D. 7)
$\delta Q_p$	differential heat transfer, Eq. (E. 12)
$R$	gas constant, for the gas only
$\bar{R}$	gas constant for the two-phase mixture, Eq. (E. 4)
$R_b$	response function, defined by Eq. (E. 35)
$Re$	Reynolds number based on the particle diameter and relative speed, Eq. (D. 8)
$S_b$	area of burning surface in one-half of a T-burner
$S_{be1}$	defined in Figure C-1
$S_{be2}$	defined in Figure C-2
$S_{be}$	area of burning surface on one end of a T-burner, Figure C-1
$S_{bs}$	area of burning surface on the lateral boundary in one-half of a T-burner, Figure C-1
$S_c$	port area for a cylindrical grain, Figure C-1
$S_{co}$	cross-sectional area of the burner, Figure C-1
$t$	time
$T$	temperature (usually, of gases in the chamber)
$T_o$	stagnation temperature

$T_p$	temperature of the particulate material
$\delta T_p$	differential temperature defined by Eq. (E. 10)
$\Delta T$	temperature difference between the gas in the chamber and the gas leaving the burning surface, $\Delta T = T - T_s$
$\vec{u}$	velocity
$u_b$	speed of gas leaving a burning surface
$u_p$	velocity of particulate material
$\delta u_p$	differential temperature defined by Eq. (E. 9)
$V$	volume, $V = LS_{co}$ for a uniform tube
VATB	abbreviation for "variable-area T-Burner"
(VF)	vent factor, introduced in Eq. (E. 51)
$w_p$	source of mass, rate of conversion of particulate material to gas (mass/volume-sec.)
$z$	coordinate parallel to the axis of a T-burner, $z = 0$ at the left-hand end
$\alpha$	decay or growth constant, in $\exp(\alpha t)$
$\alpha_1$	decay constant measured for a pulse during burning
$\alpha_2$	decay constant measured for a pulse after burnout
$\alpha_c$	growth constant due to combustion, Eq. (3.2.12)
$\alpha_p$	decay constant due to particle/gas interactions
$\alpha_m^{FT}$	defined by Eq. (E. 48)
$\alpha_m^v$	defined by Eq. (E. 50)
$\beta$	$\beta = 2L_b/L$
$\beta_o$	$\beta_o = 2L_o/L$
$\gamma$	ratio of specific heats for the gases, $\gamma = C_p/C_v$
$\bar{\gamma}$	ratio of specific heats for the two-phase mixture, $\bar{\gamma} = \bar{C}_p/\bar{C}_v$

$\lambda$	complex function of the dimensionless frequency, $\Omega$ , appearing in Eq. (2.6.6): $\lambda(\lambda-1) = i\Omega$
$\mu$	viscosity
$\nu$	kinematic viscosity, $\mu/\rho_g$
$\rho$	density of the two-phase mixture, $\rho = \rho_p + \rho_g$
$\rho_g$	gas density
$\rho_p$	density of particulate matter, mass per unit volume of chamber
$\rho_o$	average density of the two-phase mixture
$\rho_s$	density of the condensed material
$\sigma$	average diameter of the particles
$\tau_d$	relaxation time defined by Eq. (D.11)
$\tau_t$	relaxation time defined by Eq. (D.12)

#### Subscripts and Superscripts

$(\bar{\quad})$	time-averaged value
$(\quad)'$	fluctuation value
$(\hat{\quad})$	amplitude for a harmonic motion, e. g. $p' = \hat{p} \exp(i\omega t)$
$(\quad)_o$	average value for the two-phase mixture
$(\quad)_e$	value for an end surface
$(\quad)_l$	value for the $l^{\text{th}}$ longitudinal mode
$(\quad)_N$	value for the $N^{\text{th}}$ three-dimensional mode
$(\quad)_s$	value for a side (lateral) surface
$(\quad)^{(p)}$	value for particulate material
$(\quad)^{(i)}$	imaginary part
$(\quad)^{(r)}$	real part

## APPENDIX B

### Statistical Analysis of Data

Difficulties with reproducibility of data, and limitations of the theoretical description of the T-burner have been thoroughly discussed in the body of this report. Frequently, data scatter is such that many points are actually "bad" data and should be discarded. This has been mentioned in § 5.4.3 where it was suggested that the points 30 or greater from the "predicted" values be re-examined for possible reasons to exclude them. Often, however, significant differences between theory and experiment may be due to the fact that the data are not acquired under conditions to which the simplified expressions for the T-burner apply. For example, large variations in  $S_{co}/S_c$  can produce significant deviations from the intended fundamental frequency. If the combustion response and the losses are assumed to be constant when the analytical results are used to correlate the data, considerable errors may be introduced.

Additional complications may arise from the influence of velocity coupling. Most applications of the analysis to interpretation of data have accounted only for pressure coupling; this produces an erroneously high value for the pressure coupled response if the test data include tests with long grains (large  $\beta$ ).

Other errors may be introduced simply due to assumptions used in the development of the statistical optimization procedure. As an example, the procedure known as "least squares" inherently assumes that the data scatter (error) is independent of the magnitude of the quantity being measured. Since very high or very low (near zero) values of growth constant are difficult to measure, this assumption frequently fails for data presently available.

Among the problems likely to be encountered are those associated with velocity coupling and large variations in the measured frequency. To illustrate possible techniques for accounting for these effects a sample problem has been compiled from the data for ANB-3066 propellant reported in refs. B-1 and B-2, summarized in Table B-1. In contrast to the sample case discussed in § 5.4.3, these data contain information related to end burning grains. A least squares fit of the data to Equation (3.2.1) without velocity coupling yields the following values:

Run	$S_b/S_{co}$	$S_{be}/S_{co}$	$S_{b2}/S_{co}$	$S_{bu}/S_{co}$	$S_{co}/S_c$	$\beta$	$\alpha$	$f$ (Hz)
491	1.540	-0.000	-0.000	1.540	.973	.090	-36.000	820.030
488 A	6.030	-0.000	-0.000	6.030	.942	.327	52.000	795.000
489 D	6.030	-0.000	-0.000	6.030	.783	.316	40.000	800.000
489 A	6.030	-0.000	-0.000	6.030	.383	.335	50.000	820.000
489 B	6.030	-0.000	-0.000	6.030	.000	.319	41.000	790.000
482 A	7.170	-0.000	-0.000	7.170	.831	.200	81.000	795.000
482 B	7.200	-0.000	-0.000	7.200	.693	.184	64.000	780.000
483 A	7.200	-0.000	-0.000	7.200	.840	.202	84.000	800.000
484	7.060	-0.000	-0.000	7.060	1.011	.217	88.000	820.000
484 A	7.210	-0.000	-0.000	7.210	.814	.199	80.000	790.000
485	5.580	-0.000	-0.000	5.580	1.030	.173	54.000	816.000
485 A	5.100	-0.000	-0.000	5.100	1.200	.171	44.000	812.000
475 A	5.630	-0.000	-0.000	5.630	.953	.168	45.000	793.000
476 A	5.700	-0.000	-0.000	5.700	.851	.161	43.000	795.000
476	5.370	-0.000	-0.000	5.370	1.090	.171	59.000	829.000
493	4.520	-0.000	-0.000	4.520	.935	.259	23.000	833.000
483	6.950	-0.000	-0.000	6.950	1.030	.216	90.000	829.000
482	6.900	-0.000	-0.000	6.900	1.040	.216	101.000	825.000
489	6.020	-0.000	-0.000	6.020	.985	.353	75.000	825.000
488	6.150	-0.000	-0.000	6.150	.944	.353	61.000	833.000
492	1.540	-0.000	-0.000	1.540	.970	.090	-41.000	835.000
475 B	5.720	-0.000	-0.000	5.720	.803	.157	31.000	775.000
476 B	5.740	-0.000	-0.000	5.740	.717	.149	27.000	775.000
484 B	7.240	-0.000	-0.000	7.240	.697	.185	61.000	775.000
483 B	7.240	-0.000	-0.000	7.240	.696	.185	61.000	775.000
478	1.480	-0.000	-0.000	1.480	1.060	.046	-50.000	772.000
479	1.460	-0.000	-0.000	1.460	1.080	.046	-46.000	763.000
480	1.430	-0.000	-0.000	1.430	1.130	.046	-60.000	778.000
5404 2	1.490	.588	.412	.490	1.700	.020	-49.000	827.000
5405 2	1.490	.588	.412	.490	1.700	.020	-56.700	810.000
5405 3	1.520	.769	.231	.520	1.300	.020	-61.300	789.000
5408 3	1.490	.769	.412	.309	1.300	.020	-49.000	800.000
5409 2	2.060	.588	.231	1.060	1.700	.040	-51.800	816.000
5409 3	2.190	.769	.231	1.190	1.300	.040	-59.100	810.000
5410 1	1.900	.444	.556	.900	2.250	.040	-44.300	837.000
5410 2	2.060	.588	.412	1.060	1.700	.040	-38.500	816.000
5410 3	2.190	.769	.231	1.190	1.300	.040	-45.400	810.000
5412 2	1.900	.588	.412	.900	1.700	.040	-51.000	835.000
481	1.420	-0.000	-0.000	1.420	1.110	.046	-47.000	770.000
5412 3	2.060	.769	.231	1.060	1.800	.040	-35.900	816.000
477	1.280	-0.000	-0.000	1.280	1.350	.046	-44.000	775.000
477 A	1.370	-0.000	-0.000	1.370	1.180	.046	-38.000	775.000
533	7.150	-0.000	-0.000	7.150	.963	.215	76.000	804.000
533 B	7.070	-0.000	-0.000	7.070	.677	.170	56.000	750.000
534	6.610	-0.000	-0.000	6.610	1.130	.216	88.000	834.000
534 A	7.200	-0.000	-0.000	7.200	.731	.189	79.000	800.000
534 B	7.080	-0.000	-0.000	7.080	.563	.163	51.000	753.000
487	4.500	-0.000	-0.000	4.500	.949	.259	19.000	833.000

TABLE B-1. Compilation of T-Burner Data (Refs. B-1 and B-2).

$$B_g = 0.00747 \pm 0.00024$$

$$B_e = 0.00290 \pm 0.00132$$

$$\alpha_d = -79.48 \pm 4.11$$

$$VF = 0.974$$

$$\sigma = 9.32$$

The effects of velocity coupling could be analyzed by using the expression used in Ref. B-3 and shown in Eq. (3.2-3). One tests the data for the influence of this phenomenon by adding this term to the T-burner expression and extracting a value for  $R_v$ . When this is accomplished for the data set of Table B-1, the following results are found:

$$B_g = 0.00578 \pm 0.00038$$

$$B_e = 0.00275 \pm 0.00106$$

$$\alpha_d = -75.1 \pm 3.40$$

$$R_v = 3.00 \pm 0.58$$

$$\sigma = 7.46$$

$$VF = 0.984$$

The inclusion of velocity coupling did improve the quality of the fit; the decrease in  $\sigma$  is significant. A substantial improvement in VF could not be expected because the relatively low values of  $\beta$  preclude a significant impact due to velocity coupling. Although  $R_v$  appears to have been determined to a high degree of precision, it is probably safest to follow the recommendations presented earlier, namely, minimize the effects of velocity coupling by testing at relatively low values of  $\beta$  and  $S_{bs}/S_{co}$  and conduct specialized tests to measure  $R_v$ .

The data shown in Table B-1 cover tests conducted over a frequency range of 770 Hz to 835 Hz. Because both the combustion response and particle damping depend on frequency, it is probable that the data are affected. In Ref. B-1, the following expression is used for particle damping:

$$\alpha_d \sim \frac{-Cm}{2} \frac{\omega^2 \tau_d}{1 + (\omega \tau_d)^2 + Cm}$$

The regression analysis then fits to  $\tau_d$  rather than the constant damping

term  $\alpha_d$ . This approach requires a nonlinear regression analysis rather than the simple linear techniques presently under discussion. Another approach is to assume that the frequency variation is narrow enough that particle damping is nearly linear with frequency. The damping could then be represented by

$$\alpha_d \sim K_d f$$

The correlation analysis would extract  $K_d$ .

Another approach to the problem of frequency variation involves the combustion response. One could use, instead of  $B_s$  and  $B_e$ , the formula for the combustion response discussed in ref. B-4. However, this expression is fairly complicated and would require a non-linear regression analysis. As an alternative, the procedure suggested above for particle damping may be used, with the approximation to  $B_s$ :

$$B_s = B_{s0} + B_{sf} f .$$

The regression analysis then extracts  $B_{s0}$  and  $B_{sf}$ . This approach was applied to the data of Table B-1 and yielded the following:

$$B_e = 0.00237 \pm 0.00106$$

$$B_{s0} = 0.00499 \pm .000240$$

$$B_{sf} = 1.550 \times 10^{-5} \pm 2.97 \times 10^{-6}$$

$$\alpha_d = -78.4 \pm 3.29$$

$$VF = 0.984$$

$$\sigma = 7.44$$

This correlation does not appear to offer any significant improvement over the case where velocity coupling was added to the theory. However, this is somewhat to be expected since pressure coupling alone is explaining ~97% of the data. The result that  $B_{sf}$  is positive suggests that  $B_s$  is increasing with frequency at 800 Hz. However, because only data over a narrow frequency range have been used, no firm conclusion can be justified.

The data were tested further by adding both velocity coupling and frequency dependent terms to the correlation analysis. The best fit was obtained with the following values:

$$\begin{aligned}B_{sf} &= 7.84 \times 10^{-6} \pm 4.7 \times 10^{-7} \\B_{sc} &= 0.0 \\B_e &= 0.00256 \pm 0.00096 \\R_v &= 2.08 \pm 0.58 \\\alpha_d &= 76.0 \pm 3.14 \\VF &= 0.986 \\\sigma &= 6.86\end{aligned}$$

The "best" overall correlation of data was obtained with  $B_{sc}$  equal to non-zero value. However, the inclusion of  $F_{sc}$  significantly decreased the precision of the other parameters, and it was decided to eliminate the  $B_{sc}$  term. This problem is most likely due to the limited number of data points available for the correlation.

It should be emphasized that the methods outlined in this appendix are intended as guidelines to be followed in the event that one has difficulty interpreting any given collection of T-burner data. The procedures have not been fully explored to ascertain their validity and have not yet gained universal acceptance. The T-burner experimenter is definitely encouraged to follow the procedures presented earlier to ensure that velocity coupling is minimized and that the frequency is carefully controlled.

#### REFERENCES

- B-1 Beckstead, M. W., et al. "Variable Area T-Burner Investigation," AFRPL-TR-72-85 (December 1972), Hercules, Inc., Magna, Utah.
- B-2 Micheli, P. L. "Evaluation of Pulsed T-Burner for Metallized Propellants," AFRPL-TR-72-54 (Sept. 1973), Aerojet Solid Propulsion Co., Redlands, California.
- B-3 Beckstead, M. W., et al. "Velocity Coupled Combustion Instability, Final Technical Report," AFRPL-TR-72-85 (September 1973), Hercules, Inc., Magna, Utah.
- B-4 Culick, F. E. C. "A Review of Calculations for Unsteady Burning of a Solid Propellant," AIAA Journal, V. 6, no. 12 (Dec. 1968), pp. 2241-2255.

## APPENDIX C

### CALCULATION OF THE ACOUSTIC MODES FOR A T-BURNER

All analyses of linear and nonlinear behavior require complete knowledge of the unperturbed acoustic modes for the geometry of the chamber. In general, for motors it is necessary to carry out numerical calculation; closed-form solutions cannot be found for configurations having slots and fins, re-entrant nozzles, or ports other than simple cylinders. In T-burners, the geometry is relatively simple, but the perturbations due to extended lateral grains are often significant. For these cases, both numerical analysis and a one-dimensional analysis can be used.

#### C.1 One-Dimensional Analysis of the Acoustic Modes

A complete description of this problem may be found in refs C-1 and C-2. The analysis is carried out for configurations of the sort sketched in Figure C-1, in which the various geometrical variables are defined. As shown in Appendix E, Eqs. (E.28) and (E.29), the problem of finding the normal modes for a chamber having variable cross-sectional area  $S_c$  reduces to the problem of solving the wave equation with boundary condition:

$$\frac{1}{S_c} \frac{d}{dz} \left( S_c \frac{d\hat{p}_l}{dz} \right) + k_l^2 \hat{p}_l = 0 \quad (\text{C.1})$$

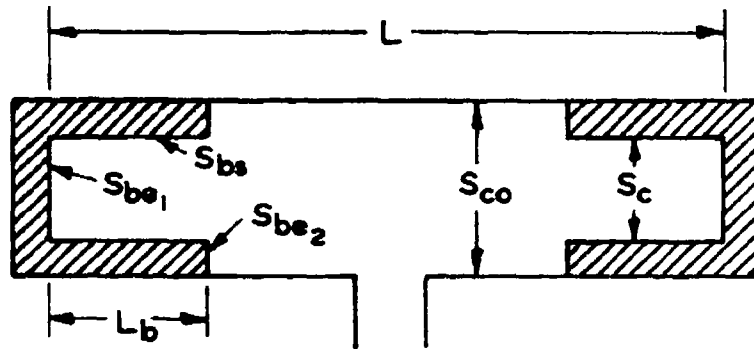
$$\frac{d\hat{p}_l}{dz} = 0 \quad (z = 0, L) \quad (\text{C.2})$$

For general distributions of area,  $S_c(z)$ , the problem cannot be solved in closed form; but for the cases sketched in Figure C-1, the cross-sectional area is uniform (i. e.,  $S_c$  is constant) between abrupt discontinuities, and piecewise solutions can be found without great difficulty. Really, one has to solve the equation

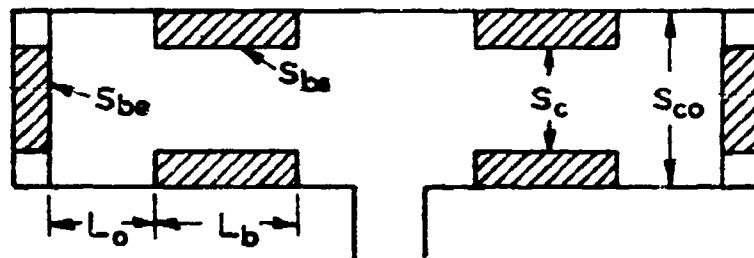
$$\frac{d^2 \hat{p}_l}{dz^2} + k_l^2 \hat{p}_l = - \frac{d\hat{p}_l}{dz} \frac{1}{S_c} \frac{dS_c}{dz} \quad (\text{C.3})$$

The right hand side is either zero or, at the discontinuities, infinite. The problem is solved by using solutions to (C.3) with the right hand side equal to zero, and matching at the discontinuities so that the pressure and mass flow are continuous.

## (a) CUP GRAINS



## (b) CYLINDRICAL &amp; DISC GRAINS



- $S_c$  = CROSS-SECTIONAL AREA OF THIN CYLINDRICAL GRAIN  
 $S_{co}$  = CROSS-SECTIONAL AREA OF THE BURNER  
 $S_{bs}$  = AREA OF BURNING SURFACE ON THE LATERAL BOUNDARY  
 $S_{be}$  = AREA OF BURNING SURFACE ON THE ENDS  
 $L_b$  = LENGTH OF GRAIN ALONG LATERAL BOUNDARY  
 $L_o$  = DISPLACEMENT OF CYLINDRICAL GRAIN FROM THE END  
 $L$  = TOTAL LENGTH OF BURNER BETWEEN THE END GRAINS

## DIMENSIONLESS PARAMETERS

$$\beta = 2L_b/L$$

$$\beta_o = 2L_o/L$$

$$K_l = Lk_l/2 = L\omega_l/2\bar{a}$$

Figure C-1 Configurations and Definitions of Geometrical Variables

That the pressure should be continuous is obvious. To see that continuity of mass flow is the correct second condition to apply, multiply (C. 1) by  $S_c$  and integrate the result from just downstream to just upstream of a discontinuity located at, say,  $z_0$ .

$$\int_{z_0-\epsilon}^{z_0+\epsilon} \frac{d}{dz} \left( S_c \frac{d\hat{p}_l}{dz} \right) dz + k_l^2 \int_{z_0-\epsilon}^{z_0+\epsilon} S_c \hat{p}_l dz = 0 .$$

For  $\epsilon \rightarrow 0$ , the second term vanishes, because in any case both  $\hat{p}_l$  and  $S_c$  are finite. The first term gives

$$\left( S_c \frac{d\hat{p}_l}{dz} \right)_{z=z_0+\epsilon} = \left( S_c \frac{d\hat{p}_l}{dz} \right)_{z=z_0-\epsilon} . \quad (C. 4)$$

But the acoustic velocity is proportional to  $d\hat{p}_l/dz$ , so after multiplication by  $\bar{\rho}$ , (C. 4) obviously represents continuity of mass flow for the acoustic field.

It is simplest to divide the hierarchy of modes into even and odd classes. Since mainly the fundamental mode is excited in T-burner firings, only odd modes will be examined here. Since cup grains (Figure C-1a) are special cases of the cylinder/disc configuration, results will be given here for the latter. For odd modes, in addition to the boundary conditions (C. 2), the pressure fluctuation itself must vanish at the center of the chamber:  $p = 0$  at  $z = L/2$ . Thus, for the geometry shown in Figure C-1b, the pressure field may be represented in three pieces for a half-chamber:

$$0 \leq z \leq L_0 \quad p_l = \cos k_l z \quad (C. 5)$$

$$L_0 \leq z \leq L_0 + L_b \quad p_l = \cos k_l z + B_l^0 \sin k_l (z - L_0) \quad (C. 6)$$

$$L_0 + L_b \leq z \leq L/2 \quad p_l = C_l^0 \sin k_l (L/2 - z) \quad (C. 7)$$

Continuity of pressure and mass flux at  $z = L_0$  and  $z = L_0 + L_b$  lead to the four relations:

$$\underline{z = L_0} \quad \cos(K_l \beta_0) = \cos(K_l \beta) \quad (C. 8a)$$

$$S_{c0} \sin(K_l \beta_0) = S_c [\sin(K_l \beta) - B_l^0] \quad (C. 8b)$$

$$\underline{z = L_0 + L_b} \quad \cos K_l (\beta + \beta_0) + B_l^0 \sin K_l = C_l^0 \sin K_l (1 - \beta - \beta_0) \quad (C. 9a)$$

$$S_c [\sin K_l(\beta + \beta_o) - B_l^o \cos K_l \beta] = S_{co} C_l^o \cos K_l(1 - \beta - \beta_o) \quad (C. 9b)$$

The first of these is an identity because of the way in which the representations (C. 5)-(C. 7) were chosen. Hence, there are three equations for the three unknowns,  $K_l = Lk_l/2$ ,  $B_l^o$ , and  $C_l^o$ . It is a matter of algebra to find the results:

$$B_l^o = - \left( \frac{S_{co}}{S_c} - 1 \right) \sin K_l \beta_o \quad (C. 10)$$

$$C_l^o = \frac{(S_c/S_{co})}{\cos K_l(1 - \beta_o - \beta)} \left[ \sin K_l(\beta + \beta_o) + \left( \frac{S_{co}}{S_c} - 1 \right) \sin K_l \beta_o \cos K_l \beta \right] \quad (C. 11)$$

$$\tan K_l(1 - \beta_o - \beta) \left[ \frac{\tan K_l(\beta + \beta_o) + \left( \frac{S_{co}}{S_c} - 1 \right) \frac{\sin K_l \beta_o \cos K_l \beta}{\cos K_l(\beta + \beta_o)}}{1 - \left( \frac{S_{co}}{S_c} - 1 \right) \frac{\sin K_l \beta_o \sin K_l \beta}{\cos K_l(\beta_o + \beta)}} \right] = \frac{S_{co}}{S_c} \quad (C. 12)$$

Equation (C. 12) is, of course, a transcendental equation for  $K_l$  and must be solved numerically.

Some typical results are shown in Figures C-2 to C-5 for the frequencies and mode shapes. Note that all results are for unit pressure amplitude at the ends of the chamber. The acoustic velocity at the center vent is proportional to  $C_l^o$ . Hence,  $C_l^o$  is an interesting quantity because it enters explicitly in discussions of energy losses due to the vent (see Eq. (2.2.4) and Appendix G). A few values are shown in Figures C-6 and C-7. More extensive results may be found in ref. C-2.

Another important quantity is the acoustic energy in the chamber. The time-averaged total energy is

$$\frac{1}{4\rho a} \int_0^L \left[ \hat{p}_l^2 + \frac{1}{k_l^2} \left( \frac{d\hat{p}_l}{dz} \right)^2 \right] S_c dz \quad (C. 13)$$

The second term can be integrated by parts, and after use of the wave equation (C. 1), one finds that it is equal to the first term. Hence, the time-averaged energy is simply  $E_l^2/2\rho a^2$ , where  $E_l^2$  is defined as

$$E_l^2 = \int_0^L \hat{p}_l^2 S_c dz \quad (C. 14)$$

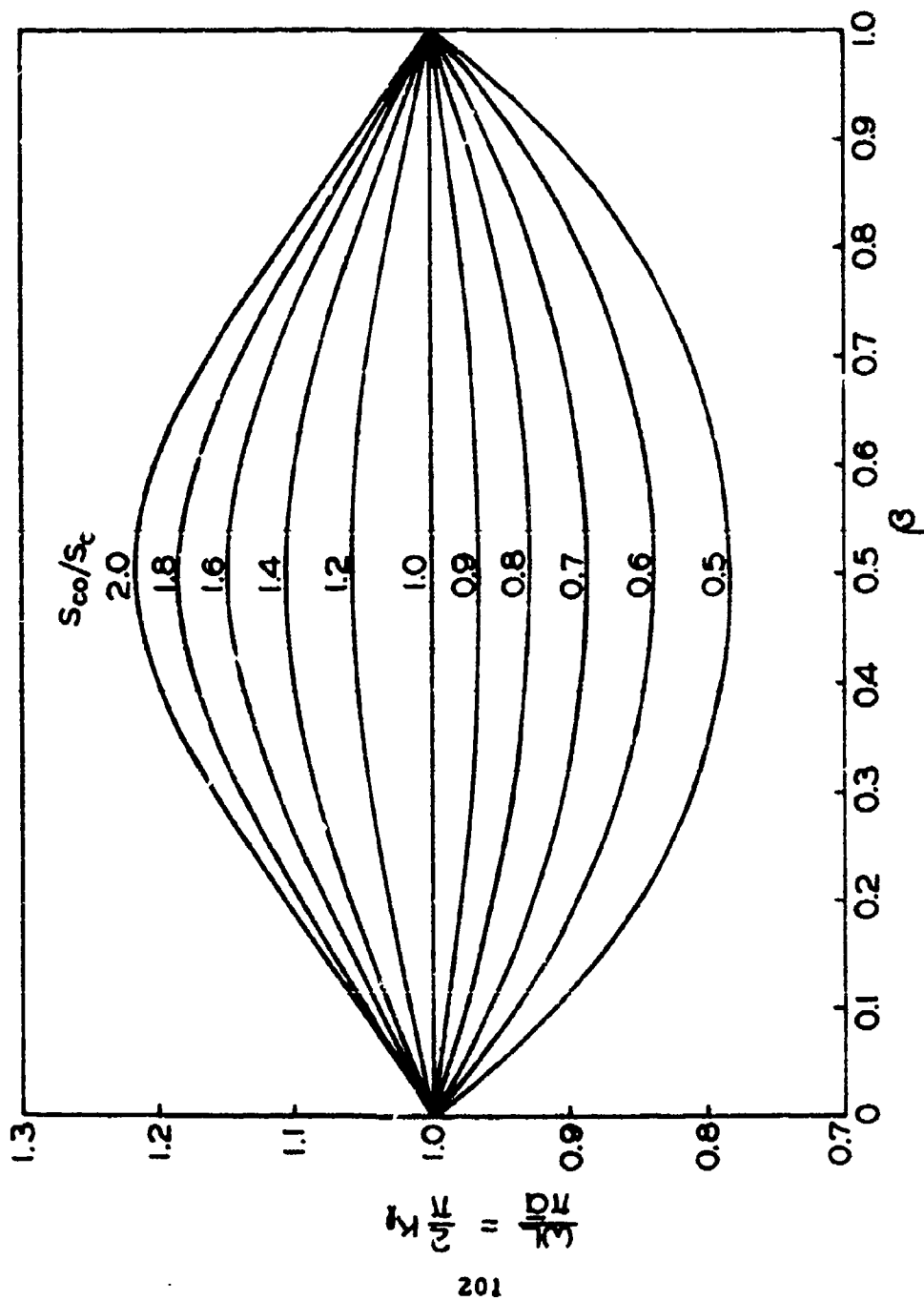


Figure C-2 Natural Frequency of the Fundamental Mode with Pro-pellant Grains at the Ends of a T-Burner ( $\beta_0 = 0$ )

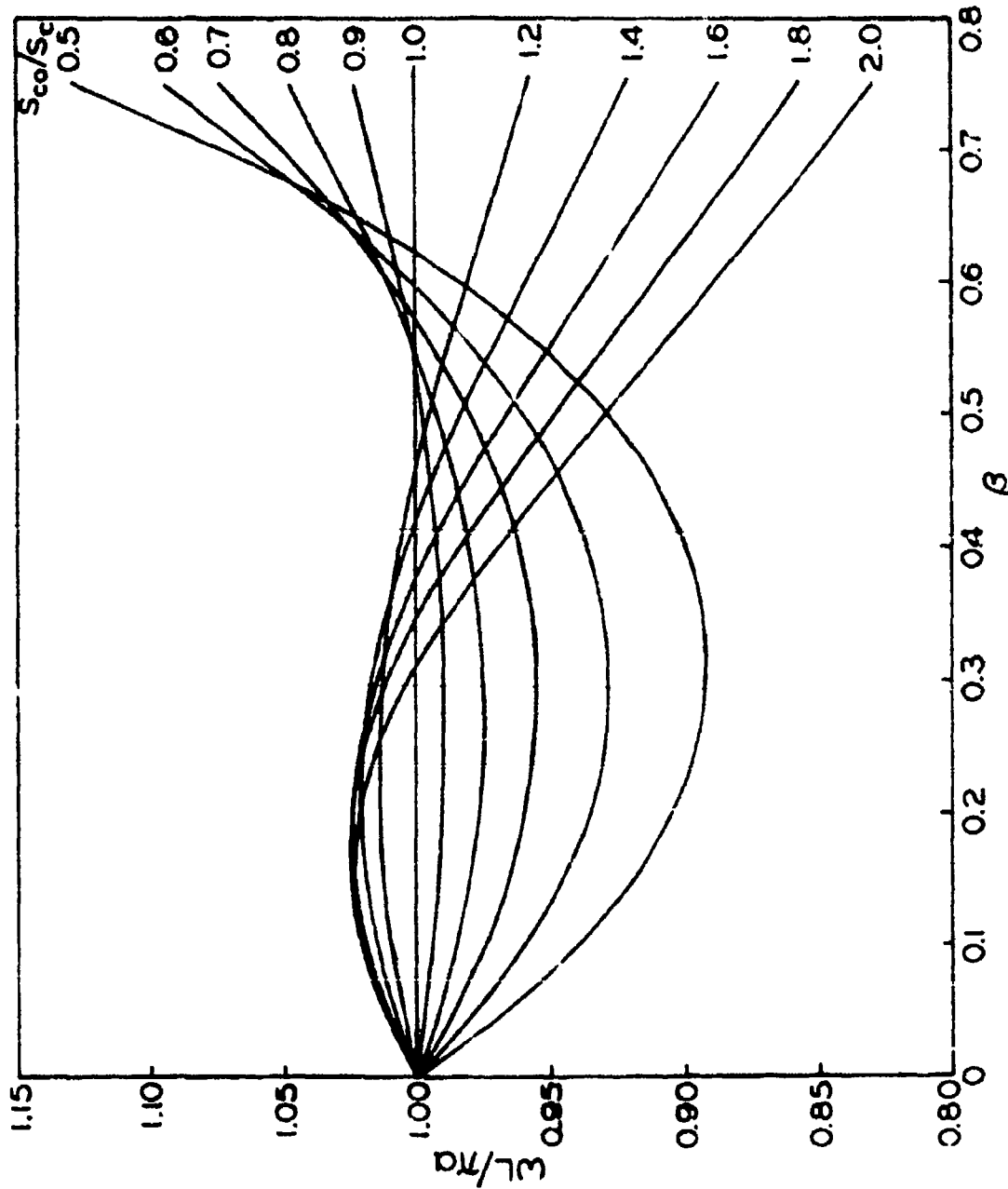


Figure C-3 Natural Frequency of the Fundamental Mode with Propellant Grains Displaced from the Ends of a T-Burner ( $\beta_0 = 0.25$ )

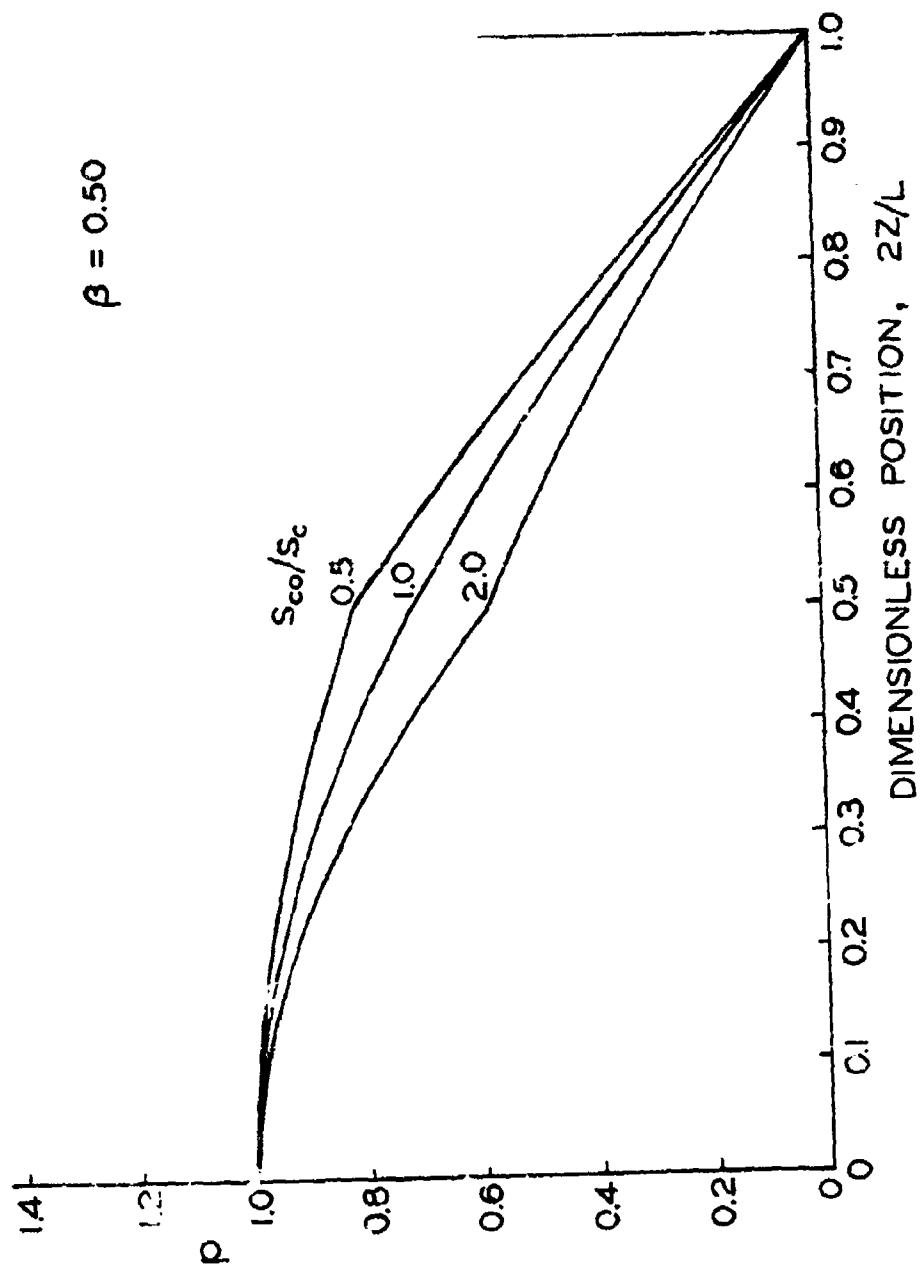


Figure C-4 Fundamental Mode Shape for Recessed and Protruding Grains Located at the Ends of a T-Burner ( $\beta_o = 0$ )

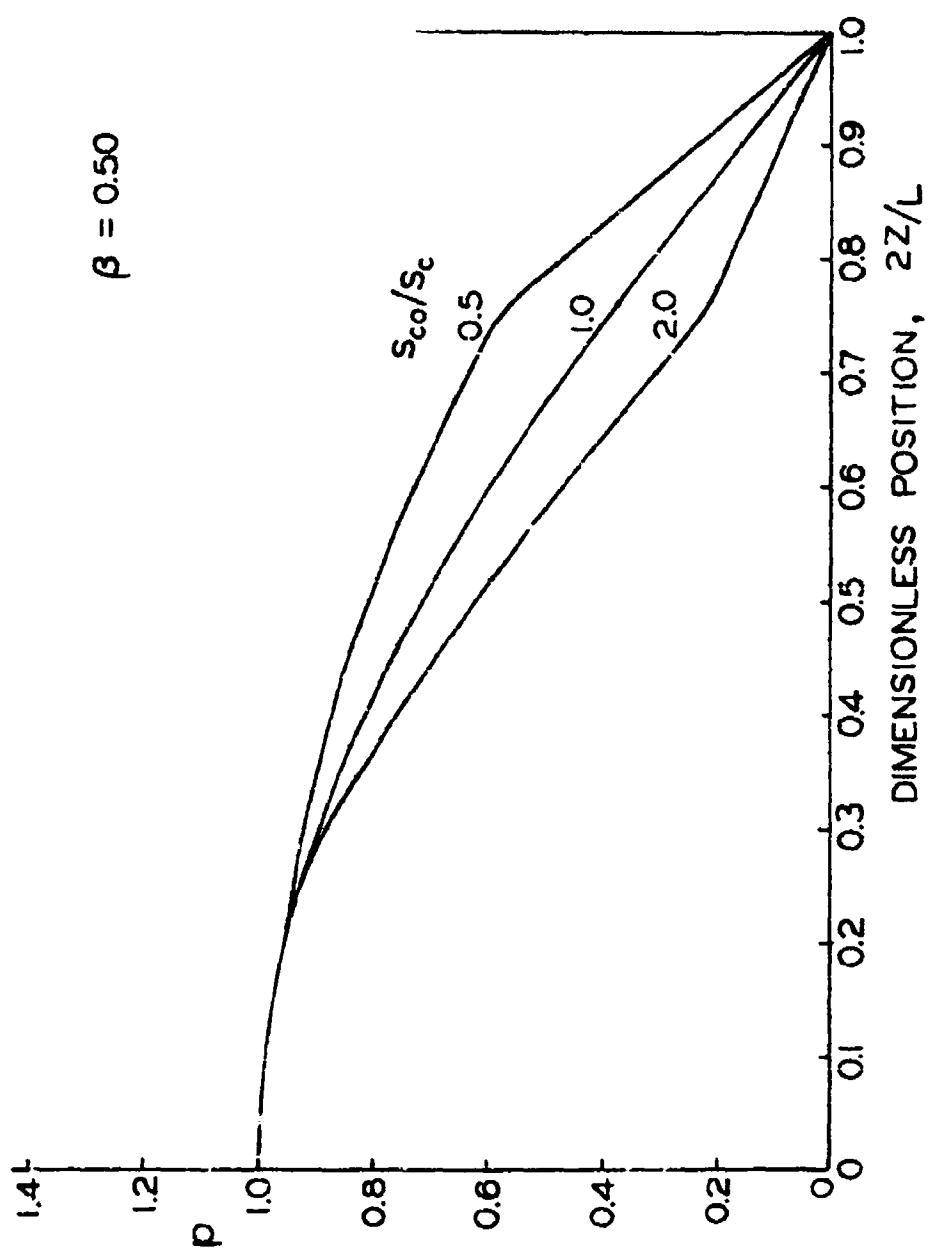


Figure C-5 Fundamental Mode Shapes for Recessed and Surrounding Grains Displaced from the Ends of a T-Burner ( $\beta_0 = 0.25$ )

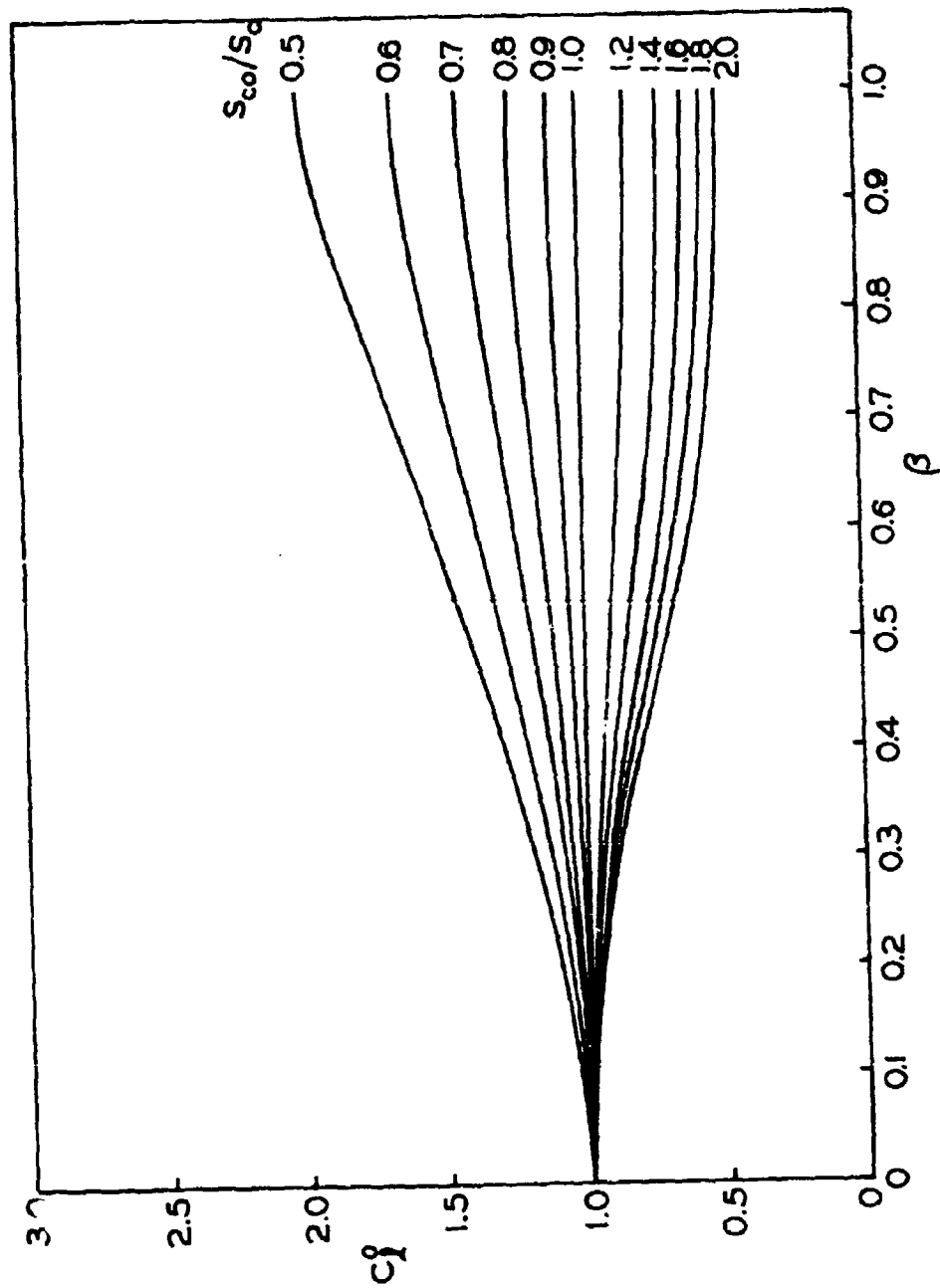


Figure C-6  $C_1^0$  Versus  $\beta$  for Recessed and Protruding Grains: Fundamental Mode ( $\beta_0 = 0$ )

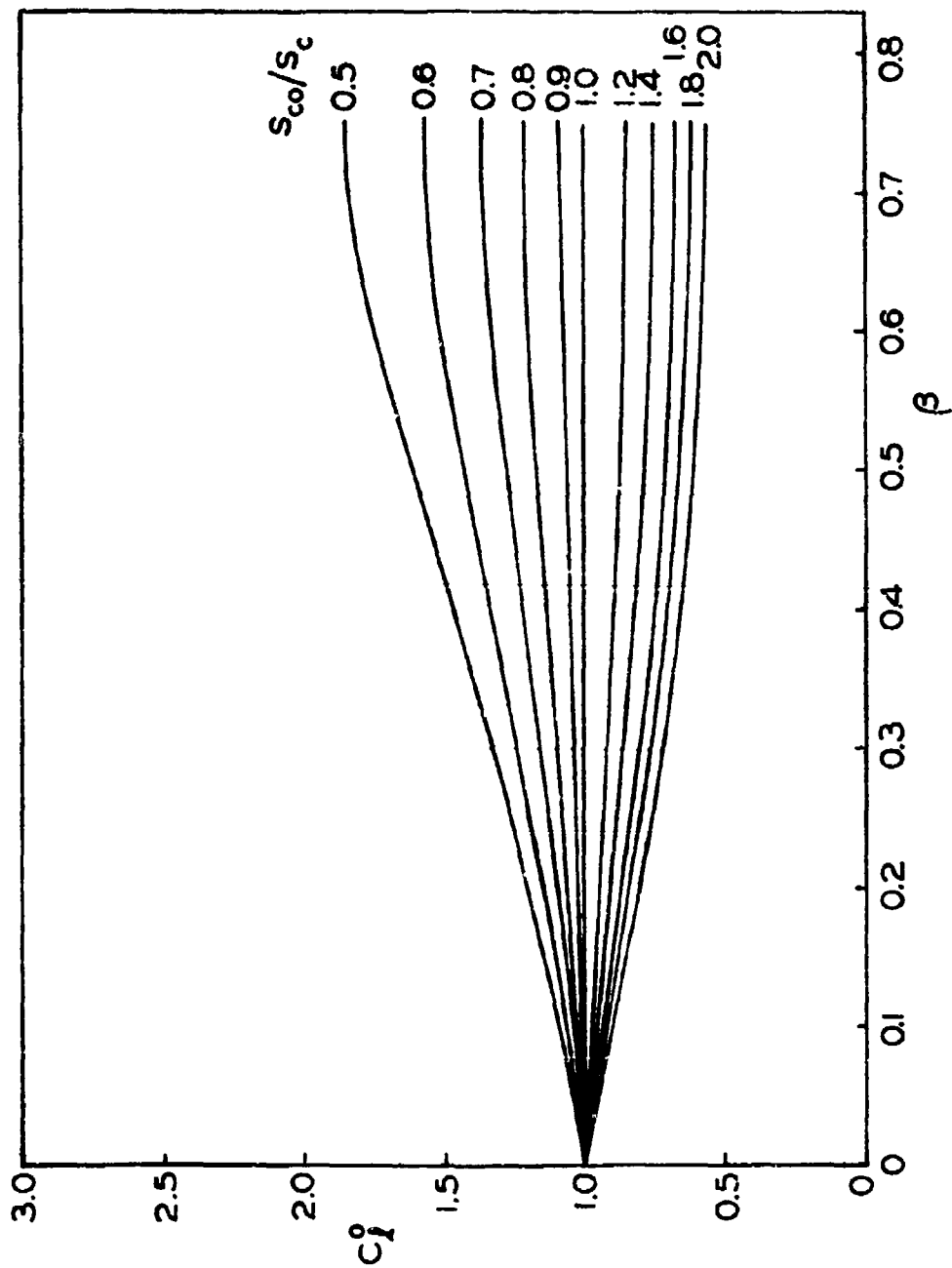


Figure C-7  $C_i^0$  Versus  $\beta$  for Recessed and Protruding Grains: Fundamental Mode ( $\beta_0 = 0.25$ )

The energy in the chamber depends on the geometry; some results for the normalized energy,  $e_t^2 = 2E_t^2/S_{co}L$ , are shown in Figures C-8 and C-9. The expressions (C.5) to (C.7) have been used to evaluate  $\hat{p}_t^2$  in (C.14).

Two other integrals arise in the analysis of the stability of T-burners:

$$g_t = \frac{1}{S_{bs}} \int_0^L \frac{1}{k_t^2} \left( \frac{d\hat{p}_t}{dz} \right)^2 \int dq dz \quad (C.15)$$

$$C_t = \frac{1}{S_{bs}} \int_0^L \hat{p}_t^2 \int dq dz \quad (C.16)$$

The first is a measure of the magnitude of the "flow-turning" loss, Eq. (2.2.4) and the second weights the energy gain due to combustion of lateral surfaces, Eq. (2.2.3). Figures C-10 and C-11 show some numerical results.

### C.2 Numerical Calculation of the Acoustic Modes

For analyzing the stability of small disturbances in practical motors, it is necessary to be able to compute numerically acoustic modes and frequencies. The geometries are usually such that analytical solutions cannot be found. For most work with T-burners, the one-dimensional analysis discussed above is adequate; limited two-dimensional numerical calculations have shown that the one-dimensional approximation is satisfactory for the grain configurations commonly used. More to the point, recent tests (ref. C-4) have been conducted in chambers at room temperature with no flow. The predicted frequencies are really quite close to the measured values over the range of geometrical configurations normally used in T-burners.

If very large discontinuities in cross-sectional area are used (a precise statement of the limits cannot be given), then numerical calculations may be necessary. Difficulties may also arise if the diameter of the vent is comparable to the diameter of the burner; this problem has not been examined. In ref. C-3, a brief description is given of one numerical technique which has been successfully used.

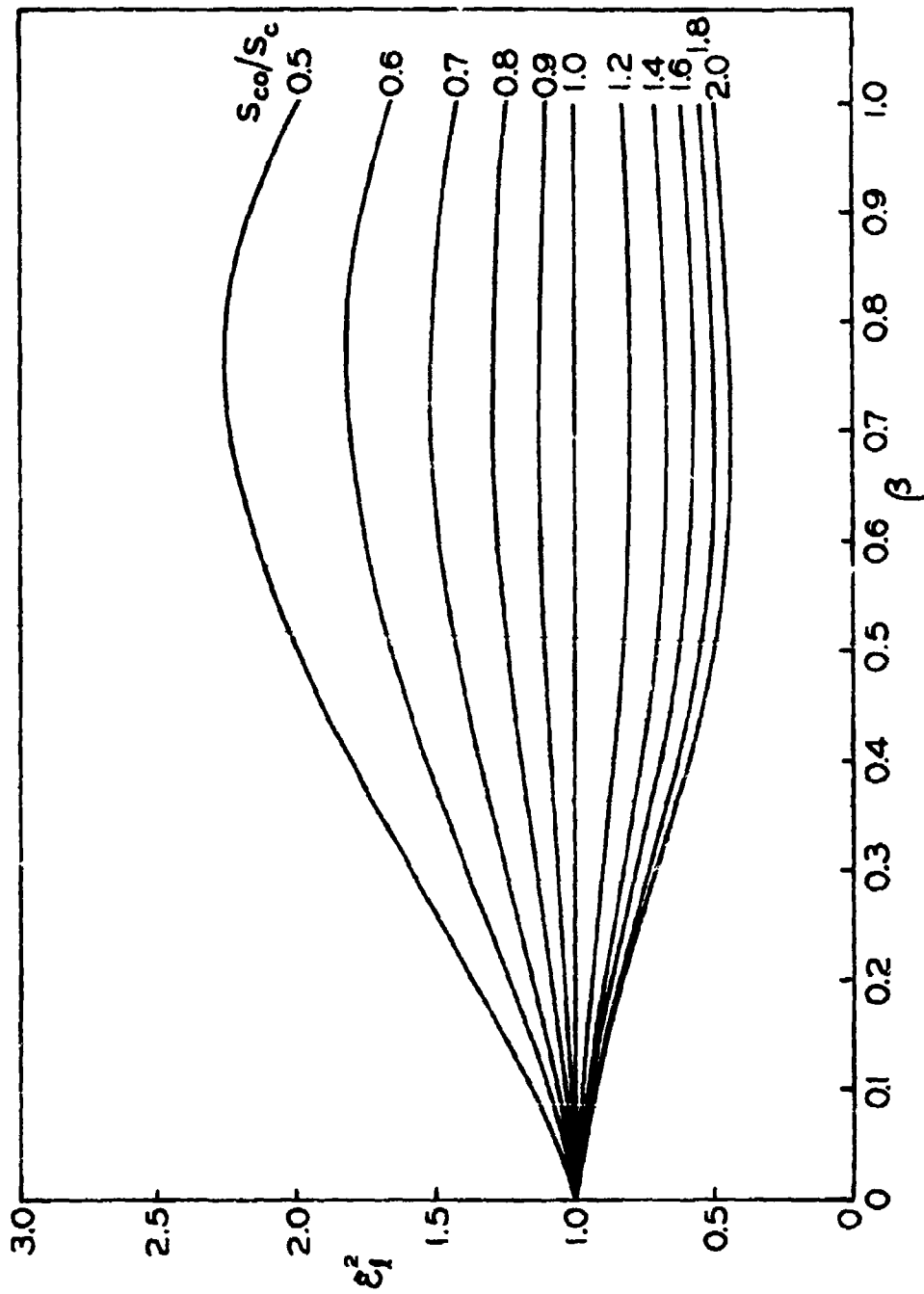


Figure C-8  $\epsilon_1^2$  Versus  $\beta$  for Recessed and Protruding Grains: Fundamental Mode ( $\beta_0 = 0$ )

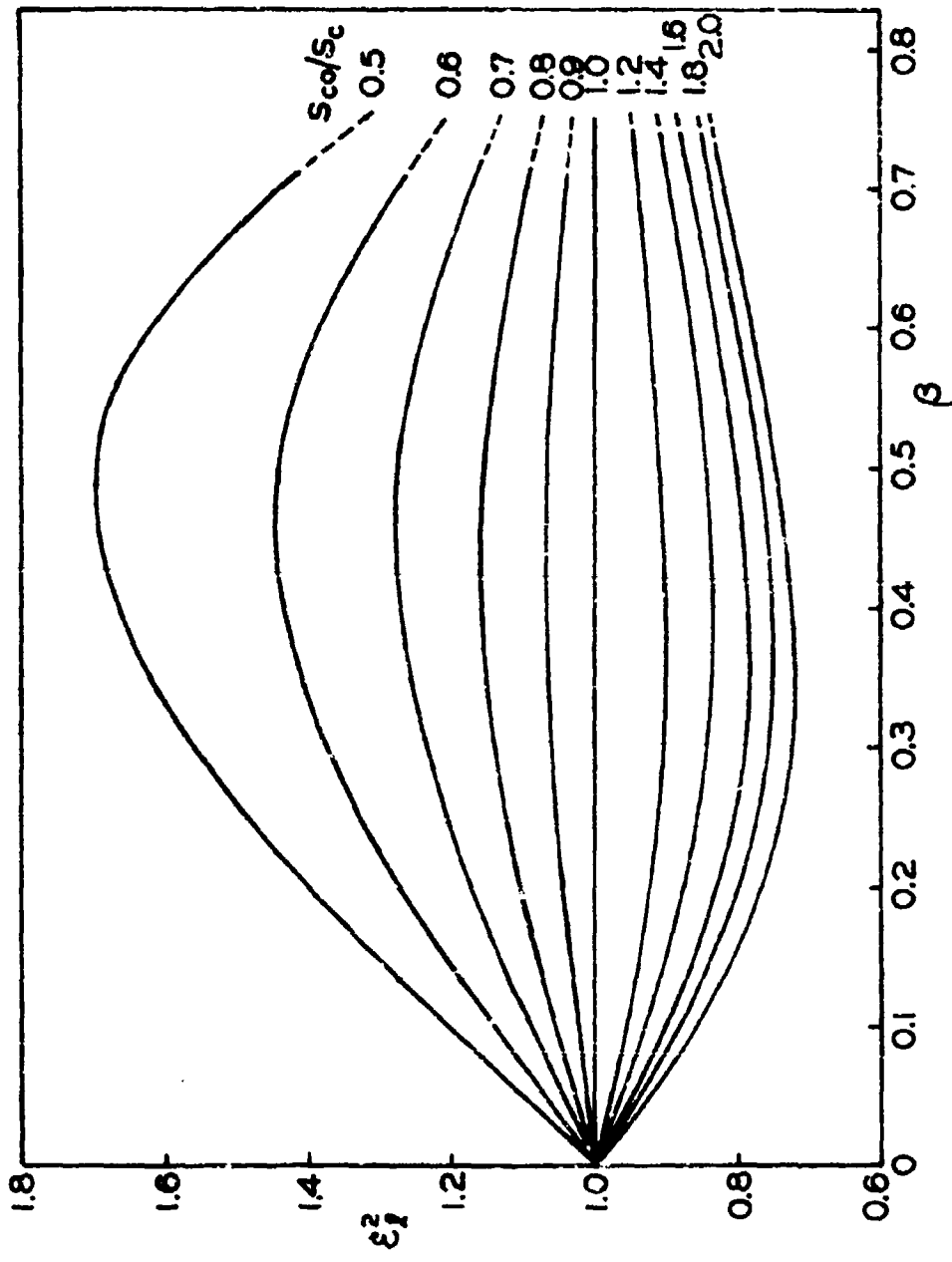


Figure C-9  $\epsilon_1^2$  Versus  $\beta$  for Recessed and Protruding Grains: Fundamental Mode ( $\beta_0 = 0.25$ )

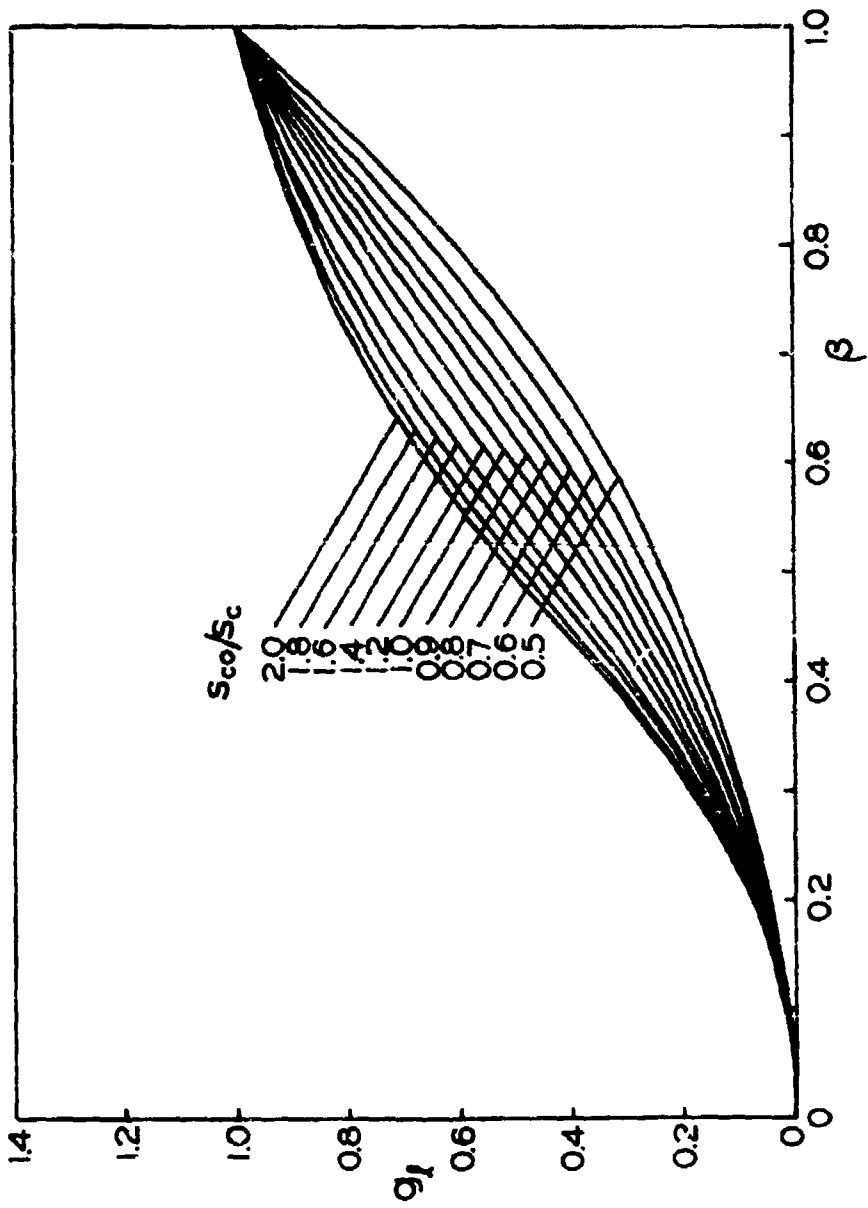


Figure C-10  $g_L$  Versus  $\beta$  for Recessed and Protruding Grains: Fundamental Mode ( $\beta_0 = 0$ )

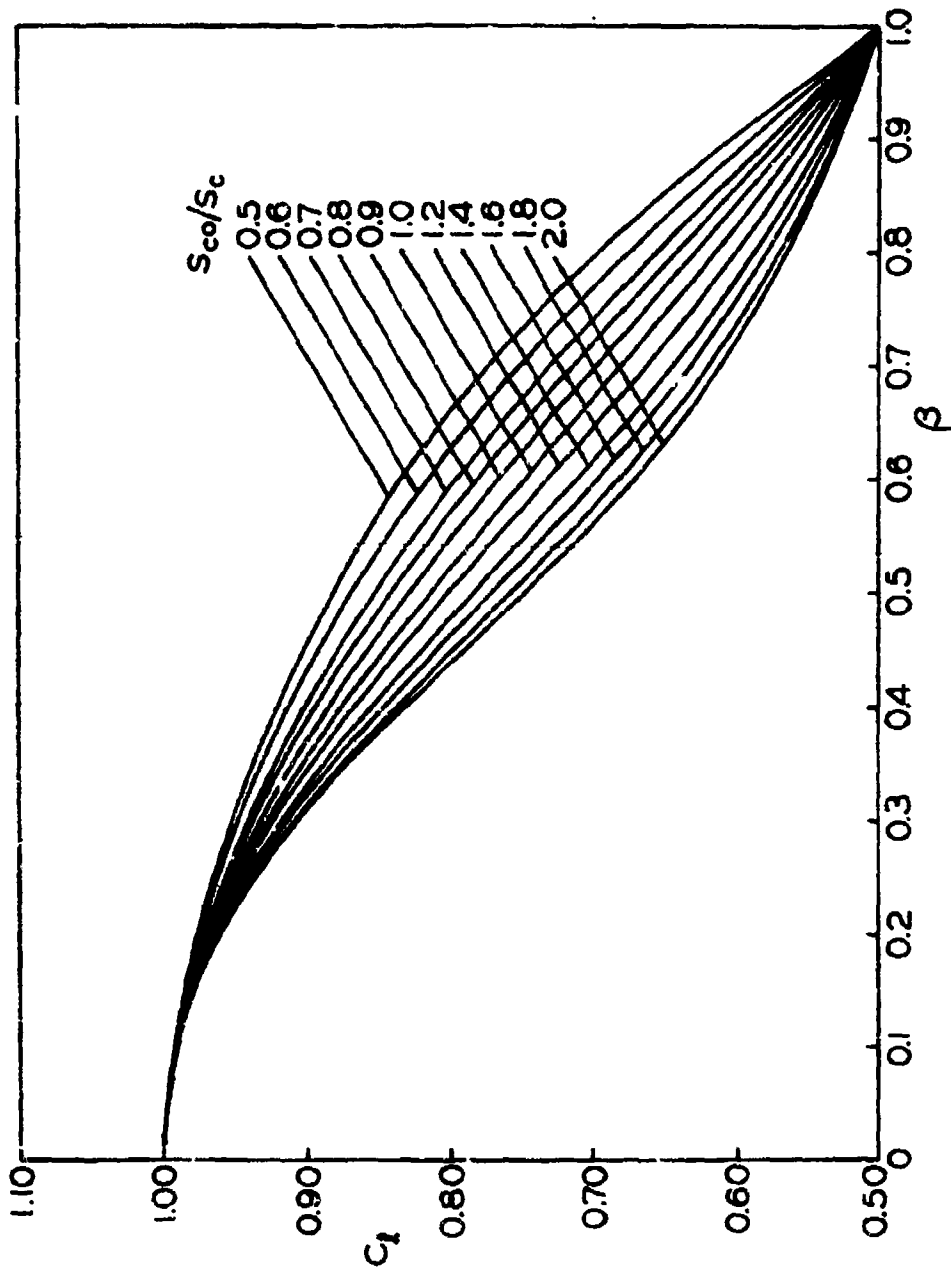


Figure C-11  $C_1$  Versus  $\beta$  for Recessed and Protruding Grains: Fundamental Mode ( $\beta_0 = 0$ )

## REFERENCES

- C-1 Gulick, F. E. C., Derr, R. L., and Price, E. F. "Linear Analysis of One-Dimensional Oscillations in a Variable-Area T-Burner," 9th JANNAF Combustion Meeting (September 1972).
- C-2 Derr, R. L. "Evaluation of a Variable Area T-Burner for Metalized Propellants," Lockheed Propulsion Company, Technical Report AFRPL-TR-72-97 (February 1973).
- C-3 "Minuteman III Third Stage Pressure Oscillation Study," Final Report, Contract 0469-67-C-0004, Aerojet Solid Propulsion Co., Report 387-01F (August 1971), pp. 91-94.
- C-4 Derr, R. L. and Mathes, H. B. "Cold Gas Acoustic Tests for Resolving T-Burner Uncertainties," 11th JANNAF Combustion Meeting (September 1974).

APPENDIX D  
APPROXIMATE FORMULAS FOR PARTICLE DAMPING  
AND SURFACE LOSSES

For ideal conditions it is possible to compute quite accurately the dissipation of energy due to the particles suspended in a gas. The early analysis reported in ref. D-1 gave results from non-interacting inert spherical particles. Measurements (refs. D-2 and D-3) have supported the predictions, and also the validity of later simplified calculations (ref. D-4). The formulas for the decay constant and change of the speed of sound are in the first instance valid for particles having the same size. By simple superposition, however, they can be generalized for distributions of particle sizes.

In a T-burner, and in motors, the particles are neither all spherical nor inert. Moreover, the distribution of sizes is unknown, and agglomeration may occur. It is within the limits of what is presently known to use rather simple formulas, and to assume that the particulate matter can be characterized by a single average size. These approximations have been used in practically all analyses of data obtained in T-burners. It is the purpose of § D. 1 to show how the simplified formulas can be deduced from the linear analyses described in Appendices E and F.

Similarly, the classical formula for the dissipation of energy in a laminar acoustic boundary has been verified (e. g. refs. D-5 and D-6) by measurements within about 8 - 10 per cent. The analysis is valid only for a flow having uniform average temperature, and the measurements have all been taken at room temperature. Especially the influence of non-uniform average temperature through the boundary layer may be important in T-burners (ref. D-6). Present knowledge is such, however, that an improvement on the classical formula cannot be accomplished; some sort of average temperature must be used and the results accepted as estimates. For testing with heavily-loaded metallized propellants, the surface losses are generally much smaller than the losses associated with particle damping. A derivation of the decay constant for surface losses is given in § D. 2, also based on the linear analysis of Appendices E and F.

### D.1 Attenuation of Acoustic Energy by Particle/Gas Interactions

If only the contributions from the particulate matter are retained, and the residual combustion of the particles is ignored, the imaginary part of Eq. (F. 17) becomes a formula for  $\alpha_p$ , the decay constant due to the presence of particulate matter.

$$2 \left( \frac{\omega_N}{a} E_N^2 \right) \alpha_p = \int \delta \hat{F}_p^{(i)} \cdot \nabla \hat{p}_N dV + \frac{\omega_N}{a} \frac{\bar{R}}{C_v} \int \delta \hat{Q}_p^{(r)} \hat{p}_N dV . \quad (D.1)$$

The calculation of  $\delta \hat{F}_p^{(i)}$  and  $\delta \hat{Q}_p^{(r)}$  is done for linearized motions of the particles and with no average flow. Moreover, it is perfectly adequate to assume one-dimensional flow, so that in fact one can use Eq. (E. 33). The problem solved here is therefore that of the attenuation of waves in a closed box having rigid walls.

The differential force and heat transfer are given by the linearized forms of Eqs. (E. 11) and (E. 12):

$$\delta F_p = -\bar{\rho}_p \frac{d\delta u_p}{dt} , \quad (D.2)$$

$$\delta Q_p = -\bar{\rho}_p C \frac{d\delta T_p}{dt} . \quad (D.3)$$

Hence, it is necessary to compute  $\delta u_p$  and  $\delta T_p$ . These are found by solving the linear forms of the equations of motion, (E. 7) and (E. 8), for the particles:

$$\frac{du_p}{dt} = -\frac{1}{\bar{\rho}_p} F_p , \quad (D.4)$$

$$\frac{dT_p}{dt} = -\frac{1}{\bar{\rho}_p C} Q_p . \quad (D.5)$$

Approximations to the force and heat transfer have been quoted in ref.

D-7:

$$F_p = \bar{\rho}_p \frac{16\mu}{\rho_s \sigma^2} (u_p - u) \left[ 1 + \frac{1}{6} Re^{2/3} \right] , \quad (D.6)$$

$$Q_p = \bar{\rho}_p \frac{12C\mu}{Pr \rho_s \sigma^2} (T_p - T) \left[ 1 + .23 Pr^{.23} Re^{.55} \right] \quad (D.7)$$

where

$$Re = \frac{\bar{\rho}_g \sigma}{\mu} |u_p - u| \quad (D. 8)$$

The diameter and material density of the particles are  $\sigma$  and  $\rho_s$ ; the viscosity coefficient and specific heat of the gas are  $\mu$  and  $C_p$ .

The linear motions (Stokes' flow),  $Re \rightarrow 0$ , and (D. 6) and (D. 7) become

$$F_p = \frac{\bar{\rho}_p}{\tau_d} \delta u_p \quad (D. 9)$$

$$Q_p = \frac{\bar{\rho}_p C}{\tau_t} \delta T_p \quad (D. 10)$$

where

$$\tau_d = \frac{\rho_s \sigma^2}{18\mu} \quad (D. 11)$$

$$\tau_t = \frac{3}{2} \frac{C}{C_p} Pr \tau_d \quad (D. 12)$$

are the relaxation times for momentum and heat exchange between the particles and the gas.

With (D. 9) and (D. 10), Eqs. (D. 4) and (D. 5) can be written

$$\frac{d\delta u_p}{dt} = \frac{1}{\tau_d} \delta u_p - \frac{du}{dt} \quad (D. 13)$$

$$\frac{d\delta T_p}{dt} + \frac{1}{\tau_t} \delta T_p = -\frac{dT}{dt} \quad (D. 14)$$

Here,  $u$  and  $T$  represent the local acoustic velocity and temperature.

Short-term transients, behaving as  $\exp(-t/\tau_d)$  and  $\exp(-t/\tau_t)$  are ignored, and the solutions to (D. 13) and (D. 14) are

$$\delta u_p = \frac{1}{\tau_d} e^{-t/\tau_d} \int_0^t e^{t'/\tau_d} u dt' - u \quad (D. 15)$$

$$\delta T_p = \frac{1}{\tau_t} e^{-t/\tau_t} \int_0^t e^{t'/\tau_t} T dt' - T \quad (D. 16)$$

Because the short term transients have been ignored, arbitrary initial conditions,  $\delta u_p(0)$  and  $\delta T_p(0)$  don't appear. Substitution of (D. 15) and (D. 16) into (D. 2) and (D. 3) gives the formulas

$$\delta F_p = \frac{\bar{p}}{\tau_d} \left[ \frac{e^{-t/\tau_d}}{\tau_d} \int_0^t e^{t/\tau_d} u dt - u \right] + \bar{p} \frac{du}{dt}, \quad (D. 17)$$

$$\delta Q_p = \frac{\bar{p} C}{\tau_t} \left[ \frac{e^{-t/\tau_t}}{\tau_t} \int_0^t e^{t/\tau_t} T dt - T \right] + \bar{p} C \frac{dT}{dt}. \quad (D. 18)$$

What is required here are the results for harmonic motions in the  $N^{\text{th}}$  acoustic mode:

$$u = \hat{u}_N e^{i\omega_N t} \quad T = \hat{T}_N e^{i\omega_N t} \quad (D. 19)$$

where

$$\hat{u}_N = \frac{i}{\rho \omega_N} \frac{d\hat{p}_N}{dz}, \quad (D. 20)^*$$

$$\hat{T}_N = \left( \frac{\bar{\gamma}-1}{\bar{\gamma}} \right) T_0 \frac{\hat{p}_N}{p_0}. \quad (D. 21)^*$$

Use of (D. 19)-(D. 21) in (D. 17) and (D. 18), plus a bit of arithmetic, leads to

$$\delta F_p = \delta \hat{F}_p e^{i\omega_N t} \quad \delta Q_p = \delta \hat{Q}_p e^{i\omega_N t}$$

with

$$\delta \hat{F}_p = -\frac{\bar{p}}{\rho} \frac{i\omega_N \tau_d}{1+i\omega_N \tau_d} \frac{d\hat{p}_N}{dz}, \quad (D. 22)$$

$$\delta \hat{Q}_p = -\frac{\bar{p}}{\rho} \frac{i\omega_N \tau_t}{1+i\omega_N \tau_t} (\bar{\gamma}-1) \left( \frac{CT_0}{a} \right) \hat{p}_N. \quad (D. 23)$$

(The fact that  $\bar{a}^2 = \bar{\gamma} \bar{R} T_0 = \bar{\gamma} p_0 / \bar{\rho}$  has been used here; see Appendix E for a summary of the properties of the mixture.)

Finally, substitution of (D. 22) and (D. 23) into the one-dimensional form of (D. 1) leads to

$$\alpha_p = -\frac{1}{2} \left( \frac{C_m}{1+C_m} \right) \left\{ \frac{i\omega_N (\omega_N \tau_d)}{1+(i\omega_N \tau_d)^2} + (\bar{\gamma}-1) \frac{C}{\bar{C}_p} \frac{i\omega_N (\omega_N \tau_t)}{1+(i\omega_N \tau_t)^2} \right\}. \quad (D. 24)$$

Particular note should be taken of the factor  $C_m/(1+C_m)$  multiplying the

---

\* Note that  $\bar{p}$  and  $\bar{\gamma}$  here are the average density and ratio of specific heats for the gas/particle mixture.

brackets and the fact that  $\bar{y}$  and  $\bar{C}_p$  are properties of the mixture. Both are consequences of combining the equations for the two-phase flow (Appendix E) in such a manner that the equilibrium properties of the mixture are correctly used in zeroth order. The accuracy of (D.24) has been demonstrated by comparison with exact numerical results for waves in a box (ref. D-8); agreement within about 1 - 2 per cent has been obtained for some special cases. The factor  $1+C_m$  is crucial for the agreement. It should be noted that the same formula can be obtained by the method of ref. D-4, although the result does not appear as the form (D.24) in that work.

If the real part of (F.17) is treated in the same way as the imaginary part, then a formula for the frequency is found. This shows the influence of particle size on the speed of sound, and again is equivalent to the result given in ref. D-4. Changes in the speed of sound with particle size are much smaller than the reduction already accounted for in the formula (E.19) for the gas/particle mixture. It has not been possible to detect the influence of particle size on the speed of sound in T-burners or motors.

#### D.2 Linear Viscous Losses on an Inert Surface

Consider waves in a uniform tube, closed at the ends, with no mean flow or combustion. In the three-dimensional formulation discussed in Appendix F, let the only non-zero perturbations on the right hand sides of the conservations equations be the force  $\vec{F}$  in the momentum equation and the heat addition  $\mathcal{E}$ . Then the imaginary part of Eq. (F.17) gives the formula for  $\alpha_s$ , the decay constant associated with surface losses:

$$2 \left( \frac{\gamma_N}{a^2} E_N^2 \right) \alpha_s = \int \hat{F}^{(j)} \cdot \nabla \hat{p}_N dV + \frac{\gamma_N}{a^2} \frac{\bar{R}}{\bar{C}_v} \int \hat{\mathcal{E}}^{(r)} \hat{p}_N dV \quad (D.25)$$

Now  $\vec{F}$  and  $\mathcal{E}$  are net force and heat addition per unit volume; they may therefore be taken equal, respectively, to  $\nabla \cdot \vec{\tau}$  and  $-\nabla \cdot \vec{Q}$  where  $\vec{\tau}$  is the viscous stress tensor and  $\vec{Q}$  is the heat flux vector.

In particular, for one-dimensional viscous motion in the acoustic boundary layer near a surface,

$$\vec{F} = \nabla \cdot \vec{\tau} = \frac{\partial}{\partial y} \left( \mu \frac{\partial u}{\partial y} \right) \hat{i}_z \quad (D.26)$$

$$\mathcal{E} = -\nabla \cdot \vec{Q} = \frac{\partial}{\partial y} \left( k \frac{\partial T}{\partial y} \right) \quad (D.27)$$

where  $\hat{i}_z$  is the unit vector parallel to the surface. Once again,  $u$  and  $T$  represent unsteady velocity and temperature, the velocity being parallel to the wall; the coordinate  $y$  is measured normal to the surface. Both  $\vec{F}$  and  $E$  are supposed to be significant only near the surface, and vanish far away. The volume element  $dV$  is  $dSdy$  where  $dS$  is the element of surface area; then the terms on the right hand side of (D.25) can be partially integrated as follows:

$$\int \hat{F}^{(i)} \cdot \nabla p_N dV = \int \frac{d\hat{p}_N}{dz} dS \int_0^\infty \frac{\partial}{\partial y} \left( \mu \frac{\partial \hat{u}^{(i)}}{\partial y} \right) dy = - \int \frac{d\hat{p}_N}{dz} \left( \mu \frac{\partial \hat{u}^{(i)}}{\partial y} \right)_w dS \quad (D.28)$$

$$\int \hat{E}^{(r)} \hat{p}_N dV = \int \hat{p}_N dS \int_0^\infty \frac{\partial}{\partial y} \left( k \frac{\partial \hat{T}^{(r)}}{\partial y} \right) dy = - \int \hat{p}_N \left( k \frac{\partial \hat{T}^{(r)}}{\partial y} \right)_w dS \quad (D.29)$$

Subscript  $( )_w$  denotes values at the wall. Hence, (D.25) is

$$2 \left( \frac{w_N}{a} E_N^2 \right) \alpha_s = -\mu \int \frac{d\hat{p}_N}{dz} \left( \frac{\partial \hat{u}^{(i)}}{\partial y} \right)_w dS - k \frac{w_N}{a} \frac{\bar{R}}{\bar{C}_v} \int \hat{p}_N \left( \frac{\partial \hat{T}^{(r)}}{\partial y} \right)_w dS \quad (D.30)$$

The known solutions for the velocity and temperature in an acoustic boundary layer are (ref. D-9)

$$\hat{u} = \hat{u}_N [1 - e^{-\lambda y}] = \frac{i}{\rho w_N} \frac{d\hat{p}_N}{dz} [1 - e^{-\lambda y}] \quad (D.31)$$

$$\hat{T} = \hat{T}_N [1 - e^{-\sqrt{\text{Pr}} \lambda y}] = \left( \frac{\bar{y}-1}{\bar{y}} \right) \frac{T_o}{P_o} \hat{p}_N [1 - e^{-\sqrt{\text{Pr}} \lambda y}] \quad (D.32)$$

where  $\hat{u}_N, \hat{T}_N$  are the acoustic solutions far from the wall, given by (D.20) and (D.21) above. The complex quantity  $\lambda$  is

$$\lambda = \frac{1}{\delta} (1 + i) \quad (D.33)$$

where

$$\delta = \sqrt{2\nu/\bar{U}} \quad (D.34)$$

is essentially the thickness of the acoustic boundary layer. The kinematic viscosity of the gas/particle mixture is  $\nu = \mu/\bar{\rho}$ .

For a cylindrical tube having diameter  $D$ , the surface element is  $dS = \pi D dz$ . With (D.31) - (D.33), the integrals in (D.30) are easily carried out to give

$$u \int \frac{d\hat{p}_N}{dz} \left( \frac{\partial \hat{u}(i)}{\partial y} \right)_w dS = \frac{\mu \pi D}{\rho u_N \delta} \int_0^L \left( \frac{d\hat{p}_N}{dz} \right)^2 dz = \frac{v w_N \pi D}{a^2 \delta} \left( \frac{E_N^2}{\pi D^2 / 4} \right)$$

$$k \int \hat{p}_N \left( \frac{\partial \hat{T}(r)}{\partial y} \right)_w dS = \frac{\mu \pi D}{\rho \delta} \left( \frac{k}{\mu} \right) \left( \frac{\bar{Y}-1}{\bar{Y}} \right) \frac{T_o}{P_o} \sqrt{Pr} \left( \frac{E_N^2}{\pi D^2 / 4} \right)$$

Substitution of these results into (D. 30), and use of the relation  $k/\mu = \bar{C}_p / Pr$ , gives eventually

$$\alpha_s = - \frac{2}{D} \sqrt{\frac{w_N v}{2}} \left[ 1 + \frac{\bar{Y}-1}{\sqrt{Pr}} \right]. \quad (D. 35)$$

Note that the kinematic viscosity is based on the density of the mixture,  $v = \mu/\rho$ , which is a function of temperature. The temperature to be used evidently lies between that of the gas and the wall temperature. A brief discussion is given in ref. D-6. The experimental results reported in that work, for un-metallized propellants, suggest that (D. 35) should be used with caution. The dependence of frequency has apparently been verified, but not the variation with diameter. This failure seems to be due to the connections between diameter, heat transfer, amplitude of oscillations, and surface temperature at inert walls, but the matter has not been settled.

The preceding calculations not only provide the two useful formulas (D. 24) and (D. 35) but also show how the general linear analysis described in Appendices E and F can be used to produce the correct forms for the contributions to the constant  $\alpha$ , for both surface and volume processes.

Also, (D. 35) applies only if the inert surface extends the entire length  $L$  of the tube. For a VATB, this is not so, and the integrals over the surface in (D. 30) must be carried out only for the regions on the lateral boundary not covered by burning propellant. Incidentally, it should also be noted that one should not assume a priori that the numerical value of (D. 35) is negligible compared with the decay constant (D. 24) for particle damping.

## REFERENCES

- D-1 Epstein, P.S. and Carhart, R.R. "The Absorption of Sound in Suspensions and Emulsions," J. Acoust. Soc. Amer., V.25, no. 3 (March 1953), pp. 555-565.
- D-2 Dobbins, R. A. and Temkin, S. "Measurement of Particulate Acoustic Attenuation," AIAA J., V.2, no.6 (June 1964), pp. 1106-1111.
- D-3 Temkin, S. and Dobbins, R. A. "Measurements of Attenuation and Dispersion of Sound by an Aerosol," J. Acoust. Soc. Amer., V.40, no.5 (1966), pp. 1016-1024.
- D-4 Temkin, S. and Dobbins, R. A. "Attenuation and Dispersion of Sound by Particulate Relaxation Processes," J. Acoust. Soc. Amer., V.40 (1966), pp. 317-324.
- D-5 Parker, J. G. "Effect of Adsorption on Acoustic Boundary-Layer Losses," J. Chem. Phys., V.36, no.6 (March 1962), pp. 1547-1554.
- D-6 Perry, E.H. "Investigation of the T-burner and Its Role in Combustion Instability Studies," Ph. D. Thesis, California Institute of Technology, Pasadena, Calif. (June 1970).
- D-7 Levine, J. N. and Culick, F. E. C. "Numerical Analysis of Nonlinear Longitudinal Combustion Instability in Metallized Propellant Solid Rocket Motors," 9th JANNAF Combustion Meeting (Sept. 1972).
- D-8 Culick, F. E. C. and Levine, J. N. "Comparison of Approximate and Numerical Analyses of Nonlinear Combustion Instability," AIAA 12th Aerospace Sciences Meeting (Jan. 1974), AIAA Paper No. 74-201; also, subsequent calculations.
- D-9 Lambert, R. F. "A Study of the Factors Influencing the Damping of an Acoustical Cavity Resonator," J. Acoust. Soc. Amer., V.25, no. 6 (November 1953), pp. 1068-1083.

## APPENDIX E

### ONE-DIMENSIONAL STABILITY ANALYSIS

Because the one-dimensional analysis has been discussed in great detail elsewhere, in references (E-1 to E-5) which are readily available, the treatment here will be quite brief.

All linear analyses for unsteady motions in a combustion chamber are based on the idea that the influences of combustion and flow may be represented as perturbations of an acoustics problem in a closed chamber. The accuracy of the results obtained for the problem with combustion and flow -- i. e., the situation one is studying -- depends very much on how much can be incorporated in the unperturbed problem. This is a general feature of perturbation analysis which is particularly important for the case at hand, unsteady motions in a variable-area T-burner used with metallized propellants.

The simplest unperturbed problem is that of purely longitudinal waves in a uniform tube containing only gas. Then the perturbations of this problem include the mean flow, the combustion at the burning surfaces, residual combustion within the volume, the influence of condensed material in the gas, and nonuniform cross-section area. Of these, residual combustion will be represented in the analysis but, owing to the lack of quantitative information, no numerical results will be obtained. The mean flow and surface combustion will be treated entirely as perturbations.

However, the influences of the particulate matter and nonuniform geometry are so large that they must partly be included in unperturbed ("zeroth order") problems. To zeroth order, the particles in the flow affect the speed of sound, causing a reduction which may be as large as 20 per cent or more in realistic cases; and nonuniformities in the cross-section area affect both the frequencies and the spatial structure of the normal modes. Treatment of the nonuniform tubes has been discussed in refs. E-1 to E-4, particularly the last two; but the correct handling of the influence of the condensed phase had not been done until more recently, ref. E-5.

The basis for the computations is the set of conservation equations

for the two-phase flow. As usual, the gas is assumed to be a single average species, obeying the equation of state for a perfect gas. Allowance must be made for combustion of the lateral grains, which is represented as a source of mass, momentum, and energy in the conservation equations. After some rearrangement and combination of the primary conservation equations, discussed in refs. E-3 and E-5, one finds the two equations\* for the velocity parallel to the axis, and the pressure:

$$\rho S_c \frac{\partial u}{\partial t} + \rho u S_c \frac{\partial u}{\partial z} + S_c \frac{\partial p}{\partial z} = S_c (\delta F_p - \sigma) \quad (E.1) \quad (1)$$

$$\frac{\partial}{\partial t} (S_c p) + \left( \frac{\bar{R}}{\bar{C}_v} + 1 \right) p \frac{\partial}{\partial z} (S_c u) + u S_c \frac{\partial p}{\partial z} = \frac{\bar{R}}{\bar{C}_v} \int (h_{os} - e_o + \bar{C}_v T) m_b dq \quad (2) \quad (3)$$

$$+ \frac{\bar{R}}{\bar{C}_v} \int (e_{pos} - e_o) m_b^{(p)} dq + \frac{\bar{R}}{\bar{C}_v} S_c [(u_p - u) F_p + u \sigma] \quad (4)$$

$$+ \frac{\bar{R}}{\bar{C}_v} S_c [(e_{po} - e_o + \bar{C}_v T) w_p + (Q + \delta Q_p)] \quad (E.2)$$

The symbol  $\rho$  stands for the density of the two-phase mixture having specific heat  $\bar{C}_v$  and "gas" constant  $\bar{R}$ . Thus, if  $\rho_g$  is the gas density, and  $\rho_p$  the mass of condensed phase in a unit volume of chamber,

$$\rho = \rho_g + \rho_p = \rho_g (1 + C_m) \quad (E.3)$$

$$\bar{R} = R / (1 + C_m) \quad (E.4)$$

$$\bar{C}_v = \frac{C_v + C_m C}{1 + C_m} \quad (E.5)$$

$$C_m = \rho_p / \rho_g \quad (E.6)$$

It will be assumed that even under unsteady conditions, the mass fraction  $C_m$  is constant and fixed by the original composition of the propellant. The force of interaction  $F_p$  and heat transfer  $Q_p$  between the particles and gas are defined as

\* It is assumed that the flow through the lateral boundary enters or leaves in directions normal to the axis. See ref. E-4 for the general case.

$$F_p = -\rho_p \left[ \frac{\partial u_p}{\partial t} + u_p \frac{\partial u_p}{\partial z} \right], \quad (\text{E. 7})$$

$$Q_p = -\rho_p \left[ \frac{\partial e_p}{\partial t} + u_p \frac{\partial e_p}{\partial z} \right]. \quad (\text{E. 8})$$

With

$$\delta u_p = u_p - u \quad (\text{E. 9})$$

$$\delta T_p = T_p - u, \quad (\text{E. 10})$$

the differential values of  $F_p$  and  $Q_p$  are

$$\delta F_p = -\rho_p \left[ \frac{\partial \delta u_p}{\partial t} + \left( u_p \frac{\partial \delta u_p}{\partial z} \right) \right], \quad (\text{E. 11})$$

$$\delta Q_p = -\rho_p C \left[ \frac{\partial \delta T_p}{\partial t} + \left( u_p \frac{\partial \delta T_p}{\partial z} - u \frac{\partial \delta T_p}{\partial z} \right) \right]. \quad (\text{E. 12})$$

Momentum exchange between the gas in the chamber and the flow entering at the boundary, and between the gas already present and that produced by residual burning, is represented by  $\sigma$ :

$$\sigma = \frac{1}{S_c} \left[ \int u m_b dq + \int u_p m_b^{(p)} dq \right] + (u - u_p) w_p. \quad (\text{E. 13})$$

The four groups of terms on the right hand side of (E. 2) represent respectively:

- 1 energy addition associated with flow of gas through the lateral boundary;
- 2 energy addition associated with flow of particulate material through the lateral boundary;
- 3 dissipation of energy associated with gas/particle interactions and momentum exchange represented by  $\sigma$ ;
- 4 energy addition associated with residual combustion of the condensed phase, homogeneous chemical reactions, and heat transfer between the particles and the gas.

For stability analysis, Eqs. (E. 1) and (E. 2) must first be linearized according to a procedure based on expansion in two small parameters (see Refs. E-1 and E-4, for example). They may then be combined to produce the following wave equation and boundary condition for the pressure fluctuation:

$$\frac{1}{S_c} \frac{\partial}{\partial z} \left( S_c \frac{\partial p'}{\partial z} \right) - \frac{1}{a^2} \frac{\partial^2 p'}{\partial t^2} = h_1 \quad (\text{E. 14})$$

$$\frac{\partial p'}{\partial z} = -f_1 \quad (z = 0, L) \quad (\text{E. 15})$$

where

$$h_1 = -\bar{\rho} \frac{\partial^2}{\partial z^2} (\bar{u}u') + \frac{\bar{u}}{a^2} \frac{\partial^2 p'}{\partial z \partial t} + \frac{\bar{y}}{a^2} \frac{\partial p'}{\partial t} \frac{1}{S_c} \frac{\partial}{\partial z} (S_c \bar{u}) - \bar{\rho} \frac{\partial}{\partial z} (\bar{u}u') \frac{d \ln S_c}{dz} - \frac{1}{a^2} \frac{\partial P'_1}{\partial t} \quad (\text{E. 16})$$

$$f_1 = \bar{\rho} \frac{\partial u'}{\partial t} + \bar{\rho} \frac{\partial}{\partial z} (\bar{u}u') - (\delta F'_p - \sigma' + u') \quad (\text{E. 17})$$

and  $P'_1$  in  $h_1$  is the linearized form of  $P_1$ :

$$S_c P_1 = (1+C_m) \int (\bar{y} \bar{R} T + \bar{y} \bar{R} \Delta T) m_b dq + \frac{\bar{R}}{2C_v} \int [(u_b^2 - u^2) + C_m (u_{ps}^2 - u_p^2)] m_b dq + \frac{\bar{R}}{C_v} S_c [(u_p - u) F_p + u \sigma] + \frac{\bar{R}}{C_v} S_c [(e_{p0} - e_o + (1+C_m) \bar{C}_v T) w_p + (Q + \delta Q_p)] \quad (\text{E. 18})$$

The speed of sound  $\bar{a}$  appearing here is that for the mixture, given by the formula

$$\bar{a}^2 = \frac{\bar{y}}{1+C_m} \frac{p_o}{\rho_g} = \bar{y} \frac{p_o}{\rho} = \bar{y} \bar{R} T_o \quad (\text{E. 19})$$

where

$$\bar{y} = \frac{C_p + C_m C}{C_v + C_m C} \quad (\text{E. 20})$$

and  $p_o, T_o$  are the average values of pressure and temperature. This speed of sound is the rate at which a small disturbance travels when the particles and gas are in both mechanical and thermal equilibrium:  $u = u_p$  and  $T = T_p$  at all times; ref. E-6 contains a good discussion of the behavior of a two-phase flow.

The functions  $h_1$  and  $f_1$  contain the perturbations of the classical acoustics problem of waves in a tube having variable cross-section area  $S_c(z)$ . Thus, the zeroth order problem is governed by the equations

$$\frac{1}{S_c} \frac{\partial}{\partial z} \left( S_c \frac{\partial p'}{\partial z} \right) - \frac{1}{a^2} \frac{\partial^2 p'}{\partial t^2} = 0 \quad (\text{E. 21})$$

$$\partial p' / \partial z = 0 \quad (z = 0, L) \quad (\text{E. 22})$$

Note that the speed of sound in the unperturbed problem is that for the gas/particle mixture.

Now for linear stability analysis, it is unnecessary to solve the general problem of time-dependent behavior. The idea is that an arbitrary disturbance can be decomposed into its Fourier components. For the disturbance to be stable, all of the components must be stable; and if one is unstable, so is any small disturbance containing that component. The Fourier components are the normal modes of the chamber, which by definition vary harmonically in time. In practice, it is almost always the case, particularly in T-burners, that at most only one normal mode is unstable. Thus, if the burner is intrinsically unstable, the pressure record shows a single well-defined frequency. The primary purpose of linear stability analysis is to produce formulas for the growth (or decay) rates of all the normal modes in the presence of combustion and mean flow.

The first step is to assume that all fluctuations vary harmonically in time; thus, the pressure fluctuations in the real flow and for the  $l^{\text{th}}$  unperturbed normal mode are expressed in the form

$$p' = \hat{p} e^{i\bar{a}kt} \quad (\text{E. 23})$$

$$p'_l = \hat{p}_l e^{i\omega_l t} \quad (\text{E. 24})$$

The complex wavenumber  $k$  is related to the frequency  $\omega$  and growth constant  $\alpha$  by

$$\bar{a}k = \omega - i\alpha \quad (\text{E. 25})$$

Consequently,  $p'$  is proportional to  $\exp(\alpha t)$  and increases in time (i. e., is unstable) if  $\alpha$  is positive. The actual mode shape  $\hat{p}$  and that for the normal mode,  $\hat{p}_l$ , are functions only of the axial position  $z$ . They satisfy the equations

$$\frac{1}{S_c} \frac{d}{dz} \left( S_c \frac{d\hat{p}}{dz} \right) + k^2 \hat{p} = \hat{h}_1 \quad (\text{E. 26})$$

$$d\hat{p}/dz = -f_1 \quad (z = 0, 1) \quad (\text{E. 27})$$

$$\frac{1}{S_c} \frac{d}{dz} \left( S_c \frac{d\hat{p}_l}{dz} \right) + k_l^2 \hat{p}_l = 0 \quad (\text{E. 28})$$

$$d\hat{p}_l/dz = 0 \quad (z = 0, L) \quad (\text{E. 29})$$

The wavenumbers for the unperturbed modes are real numbers:

$$k_\ell = \omega_\ell / \bar{a} \quad (\text{E. 30})$$

A formula for  $k^2$  may be deduced, as covered in more detail in the references, by the following method. Multiply (E. 26) by  $\hat{p}_\ell$ , (E. 28) by  $\hat{p}$ , form the difference of the results and integrate over the chamber.

One eventually finds:

$$(k^2 - k_\ell^2)E_\ell^2 = i\bar{\rho}\bar{a}k_\ell \left\{ \left[ \hat{p}_\ell \left( \hat{u}_b + \frac{\bar{u}_b \hat{p}_\ell}{\bar{\rho} \bar{a}} \right) S_c \right]_0^L - \frac{(1+C_m)}{\bar{\rho}} \int_0^L \hat{p}_\ell \int \left[ \hat{m}_b + \bar{m}_b \frac{\Delta \hat{T}}{T_0} \right] dqdz \right.$$

combustion and exhaust nozzle

$$\left. + i \frac{k_\ell}{\bar{a}} \left\{ \frac{(1+C_m)}{\bar{\rho}} \int_0^L \frac{1}{k_\ell^2} \left( \frac{d\hat{p}_\ell}{dz} \right)^2 \int \bar{m}_b dqdz \right\} \right.$$

mean flow/acoustics interactions ("flow turning")

$$\left. - \left\{ \int_0^L \delta \hat{F}_p \frac{d\hat{p}_\ell}{dz} S_c dz + i \frac{k_\ell}{\bar{a}} \frac{\bar{R}}{\bar{C}_v} \int_0^L \delta \hat{Q}_p \hat{p}_\ell S_c dz - \int_0^L \delta \hat{u}_p \frac{d\hat{p}_\ell}{dz} \int \bar{m}_b^{(p)} dqdz \right\} \right.$$

contributions from particulate matter

$$\left. + i \frac{k_\ell}{\bar{a}} \left\{ \frac{(\bar{\gamma}-1)}{\bar{\rho}_g} \int_0^L \hat{p}_\ell^2 \bar{w}_p S_c dz - \int_0^L \delta \hat{u}_p \frac{d\hat{p}_\ell}{dz} \bar{w}_p S_c dz \right. \right.$$

$$\left. - \frac{\bar{R}}{\bar{C}_v} \int_0^L \hat{p}_\ell [(1+C_m)(\hat{e}_p \bar{w}_p + \bar{e}_p \hat{w}_p) - C_m C \delta \hat{T}_p \bar{w}_p + \hat{Q}] S_c dz \right\} \quad (\text{E. 31})$$

residual combustion

For simpler writing, the terms arising from residual combustion will hereafter be dropped. A direct comparison with the three-dimensional calculation (Appendix F, Eq. (F. 17)) shows that those terms and the first two involving the condensed phase are the same in the two computations. However, the one-dimensional calculation produces a new -- and important, both physically and numerically -- term, called "mean flow/acoustics interactions" above. The boundary conditions associated with surface combustion and the exhaust nozzle also appear to be different for the lateral and end surfaces. (It should be noted that it is the form shown for the end surface which arises naturally in the three-dimensional analysis.) The

difference is only apparent, however, for one can show (refs. E-4 and E-5) that

$$\hat{u}_b + \bar{u}_b \frac{\hat{p}}{\rho a^2} = \frac{(1+C_m)}{\bar{\rho}} (\hat{m}_b + \bar{m}_b \frac{\Delta \hat{T}}{T_o}) = \bar{u}_b \left[ \frac{\hat{m}_b}{\bar{m}_b} + \frac{\Delta \hat{T}}{T_o} \right] \quad (\text{E. 32})^*$$

Hence, the two representations have the same form. However, as argued in several places, one should allow for the possibility that the combination (E. 32) will have different values for different elements of burning surface.

The velocity fluctuation  $\hat{u}$  in (E. 32) is in the direction normal to the burning surface and arises because the burning rate fluctuates in response to an external disturbance (pressure or velocity). One must expect that the response of the propellant may be different, for the same unsteady disturbance, if it is exposed to a different steady flow field. For example, particularly for aluminized propellants, the presence of a steady erosive velocity (i. e., parallel to the surface) may well affect the response to unsteady disturbances; and for a given pressure fluctuation, the response may be different for the two extreme cases of acoustic velocity all parallel or all normal to the surface.

Consequently, even though the formal representation of the coupling between the unsteady field and the surfaces -- the first two terms of (E. 31) -- is the same everywhere on the boundary, one must assume that the values will in general be a function of position on the surface. More detailed discussion is given in ref. E-5, particularly related to the question of representing the surface response for a general acoustic field, a problem which arises in application to motors.

The growth constant  $\alpha$  is computed from the imaginary part of (E. 31), because  $\bar{a}^2 k^2 = \omega^2 - 2i\alpha\omega - \alpha^2$ . One eventually finds, with residual combustion ignored\*\*,

---

\*The last form involves the assumption that the density of the mixture leaving the burning surface is the same as the average value  $\bar{\rho}$  in the chamber. Thus,  $\bar{m}_b = \bar{\rho}_g \bar{u}_b = \bar{\rho} \bar{u}_b / (1+C_m)$ .

\*\*The factors  $(1+C_m)$  have been suppressed by making use of the observation appearing in the previous footnote.

$$\alpha = -\frac{\bar{p}a^2}{2E_t} \left\{ \left[ \hat{p}_t \left( \hat{u}^{(r)} + \frac{\bar{u}_b \hat{p}_t}{\bar{p}a^2} \right) S_c \right]_0^L - \int_0^L \hat{p}_t \int \bar{u}_b \left[ \frac{\hat{m}_b}{\bar{m}_b} + \frac{\Delta \hat{T}}{T_o} \right]^{(r)} dq dz \right\}$$

combustion and exhaust nozzle

$$- \frac{1}{2E_t} \int_0^L \frac{1}{k_t} \left( \frac{d\hat{p}_t}{dz} \right)^2 \int \bar{u}_b dq dz$$

mean flow/acoustics interactions ("flow turning")

$$+ \frac{\bar{a}^2}{2\omega_t E_t} \left\{ \int_0^L \delta \hat{F}_p^{(i)} \frac{d\hat{p}_t}{dz} S_c dz + \omega_t \frac{\bar{R}}{\bar{C}_v} \int_0^L \delta \hat{Q}_p^{(r)} \hat{p}_t S_c dz - \int_0^L \delta \hat{u}_p^{(i)} \frac{d\hat{p}_t}{dz} \int \bar{m}_b^{(p)} dq dz \right\}$$

contributions from particulate matter

(E. 33)

It should be noted that in work prior to that reported in ref. E-5, the linearized equations for the two-phase flow were not combined in the manner described here. The result (E. 33) is to be preferred, both for accuracy and rigor; the main points to bear in mind are

- (1) the properties  $\bar{p}$ ,  $\bar{a}$ ,  $\bar{R}$ ,  $\bar{C}_v$  are for the two-phase mixture;
- (2) the representation of the contributions from the particulate matter ( $\delta F_p$ ,  $\delta Q_p$ ) are new.

Recent comparison (ref. E-7) of calculations with exact numerical calculations show that the result (E. 33) is a substantial improvement over earlier work.

When applied to T-burners, the purpose of Eq. (E. 33) is to produce numerical values for some quantity characterizing the coupling between surface combustion and the unsteady flow field. It is useful and conventional to introduce admittance or response functions  $A_b$ ,  $R_b$ , defined by

$$A_b = \frac{\hat{u}_b / \bar{a}}{\hat{p} / \bar{\gamma} p_o} = \bar{M}_b \frac{\hat{u}_b / \bar{u}_b}{\hat{p} / \bar{\gamma} p_o} \quad (\text{E. 34})^*$$

$$R_b = \frac{\hat{m}_b / \bar{m}_b}{\hat{p} / p_o} \quad (\text{E. 35})$$

\* It must be emphasized that  $\bar{M}_b = \bar{u}_b / \bar{a}$  is a convenient definition. While  $\bar{u}_b$  is the average speed of the gases leaving the burning surface,  $\bar{a}$  is the speed of sound in the chamber, not the local value.

Because of the potential dependence of the response function on the position of the surface, and because it is the real part which appears in (E. 33), it is convenient to use the notation

$$B_e = A_b^{(r)} + \bar{M}_b \quad \text{end surface} \quad (\text{E. 36})$$

$$B_s = A_b^{(r)} + \bar{M}_b \quad \text{side (lateral) surface} \quad (\text{E. 37})$$

It is easy to show by using the definitions of  $A_b$  and  $R_b$  that (E. 32) implies the relation

$$\frac{\bar{\gamma} p_o}{\bar{a} \hat{p}} \left( \hat{u}_b + \frac{\bar{u}_b \hat{p}}{\bar{\rho} \bar{a}} \right) = (A_b + \bar{M}_b) = \bar{\gamma} \bar{M}_b \left( R_b + \frac{\Delta \hat{T}/T_o}{\hat{p}/p_o} \right) = \frac{(1+C_m)}{\bar{\rho}} \left( \hat{m}_b + \bar{m}_b \frac{\Delta \hat{T}}{T_o} \right) \frac{\bar{\gamma} p_o}{\bar{a} \hat{p}} \quad (\text{E. 38})$$

Hence, the combustion terms in (E. 33) are readily expressed in terms of  $B_e$  and  $B_s$ .

In ref. E-2, and in more detail in ref. E-8, Eq. (E. 33) has been applied to variable area T-burners. The configurations treated and the definitions of the geometrical variables are shown in Figure C-1 and discussed in Appendix C. A simpler and more explicit form of (E. 33) for practical purposes is obtained in the following way. In the one-dimensional representation, the mode shape  $\hat{p}_t$  for the pressure depends only on axial position. The integral of its square over the volume of the chamber is

$$E_t^2 = \int_0^L \hat{p}_t^2 S_c dz \quad (\text{E. 39})$$

Numerical values for the dimensionless quantity  $\mathcal{E}_t^2$  have been given in Appendix C:

$$\mathcal{E}_t^2 = 2E_t^2 / LS_{c_o} \quad (\text{E. 40})$$

With the definitions (E. 36)-(E. 38), and  $\bar{a}^2 = \bar{\gamma} p_o / \bar{\rho}$ , the combustion terms in (E. 33) can be written

$$\alpha_p = \frac{\bar{a}}{2E_t^2} \left( \int_0^L \hat{p}_t^2 S_c B_e \right) + \int_0^L \hat{p}_t^2 \int B_s dq dS_j \quad (\text{E. 41})$$

Because of symmetry, the terms at the two ends are equal, and because (Appendix C)  $\hat{p}_t = 1$  at  $z = 0, L$ ,

$$\left[ \hat{p}_t^2 S_c B_e \right]_0^L = 2S_{be1} B_e \quad (\text{E. 42})$$

If the ends of the lateral grains are not inhibited, a second contribution to end-burning arises,

$$2 \cos^2(\beta K_\ell) S_{be2} B_e, \quad (E. 43)$$

where the factor  $\cos^2(\beta K_\ell)$  is the value of  $\hat{p}_\ell^2$  at the ends of the lateral grains. If one assumes that the response of the lateral surfaces, and hence  $B_s$ , is independent of position, then

$$\int_0^L \hat{p}_\ell^2 \int B_s dq dz = B_s q \int_0^L \hat{p}_\ell^2 dz = 2 C_\ell S_{bs} B_s, \quad (E. 44)$$

where the area of lateral surface is  $S_{bs} = qL_b$  and the dimensionless function  $C_\ell$  is

$$C_\ell = \frac{1}{L_b} \int_0^{L/2} \hat{p}_\ell^2 dz. \quad (E. 45)$$

For short grains,  $C_\ell \rightarrow 1$ , and for grains extending the entire length of the chamber,  $C_\ell \rightarrow 0.5$ . Numerical values for  $C_\ell$  have been published in ref. E-8; see also Appendix C.

When  $E_\ell^2$  in (E. 41) is replaced by (E. 40), the ratio  $\bar{a}/L$  appears. The speed of sound is not directly measured, so it is common practice to replace this ratio by

$$\frac{\bar{a}}{L} = \frac{\omega_\ell}{L k_\ell} = \frac{\omega_\ell}{2 K_\ell}. \quad (E. 46)$$

Here,  $\omega_\ell$  represents the measured angular frequency, and  $K_\ell$  is the dimensionless wavenumber,  $k_\ell L/2$ , calculated according to the prescription given in Appendix C. With these results, (E. 41) is written

$$\alpha_b = \frac{\omega_\ell}{K_\ell e_\ell^2} \left\{ \left[ \frac{S_{be1}}{S_{co}} + \cos^2(\beta K_\ell) \frac{S_{be2}}{S_c} \right] B_e + C_\ell \frac{S_{bs}}{S_{co}} B_s \right\}. \quad (E. 47)$$

The mean flow/acoustics interactions provide two contributions. First, over the burning surface only, if  $\bar{u}_b$  is assumed independent of position, the integral over the perimeter can be carried out to give

$$\alpha_m^{FT} = - \frac{\bar{u}_b}{L} \frac{S_{bs}}{S_{co}} \frac{g_\ell}{e_\ell^2}, \quad (E. 48)$$

where

$$g_\ell = \frac{1}{L_b} \int_0^L \frac{1}{k_\ell^2} \left( \frac{d\hat{p}_\ell}{dz} \right)^2 dz. \quad (E. 49)$$

Like  $C_{\ell}$  and  $\epsilon_{\ell}^2$ , the function  $g_{\ell}$  depends on the grain configuration. When there are no lateral surfaces,  $g_{\ell} \rightarrow 0$  and  $g_{\ell} = 1$  if the grains extend the entire length of the burner. Some numerical results appear in ref. E-8.

A second contribution arises formally from the center vent. Because the flow is out from the chamber, the sign changes, and the mean flow/acoustics interaction according to the one-dimensional representation provides a gain. The formal result (refs. E-2 and E-8) is

$$\alpha_m^v = 2 \frac{\bar{u}_b}{L} \frac{S_b}{S_{co}} (C_{\ell}^o)^2 \quad (\text{E. 50})$$

where  $S_b$  is the total area of burning surface in one half of the burner, and  $C_{\ell}^o$  is essentially the amplitude of the pressure oscillation at the vent, defined in Appendix C. Equation (E. 50) is valid for a center vent only, and vanishes for the even modes.

Because both (E. 48) and (E. 50) are at best approximations to real processes, it has become fairly common practice when data are correlated to introduce unspecified numerical factors, FT and VF. The values of FT and VF are then determined as part of the statistical analysis of data. The total influence of the mean flow/acoustics interactions is therefore written

$$\alpha_m = (\text{FT})\alpha_m^{\text{FT}} + (\text{VF})\alpha_m^v \quad (\text{E. 51})$$

The last set of terms in (E. 33) are collectively the "particle damping", denoted by  $\alpha_p$ :

$$\alpha_p = \frac{-2}{2\nu_p E_{\ell}} \left\{ \int_0^L \delta F_p^{(i)} \frac{d\hat{p}_{\ell}}{dz} S_c dz + \frac{\bar{R}}{\bar{C}_v} \int_0^L \delta \hat{Q}_p(r) \hat{p}_{\ell} S_c dz \right. \\ \left. - \int_0^L \delta \hat{u}_p^{(i)} \frac{d\hat{p}_{\ell}}{dz} \int \bar{m}_b(p) d\eta dz \right\} \quad (\text{E. 52})$$

It happens that the last term, representing essentially a mean flow/acoustics interaction for the particulate matter entering at the burning surface, is a relatively small contribution. In Appendix D an approximate calculation is given; the result is Eq. (D. 24), an explicit form for the first two terms of (E. 52). That result is restricted to the case when the particles are assumed to be adequately represented by a single particle size.

## REFERENCES

- E-1 Culick, F. E. C. "Stability of Longitudinal Oscillations with Pressure and Velocity Coupling in a Solid Propellant Rocket Motor," Combustion Science and Technology, v. 2, no. 4 (1970), pp. 179-201.
- E-2 Culick, F. E. C., Derr, R. L., and Price, C. F. "Linear Analysis of One-Dimensional Oscillations in a Variable Area T-Burner," 9th JANNAF Combustion Meeting (1972).
- E-3 Derr, R. L., Price, C. F., and Culick, F. E. C. "Analysis of T-burner Data Obtained by AFRPL Workshop Participants for a Metallized Propellant," 9th JANNAF Combustion Meeting (1972).
- E-4 Culick, F. E. C. "The Stability of One-Dimensional Motions in a Rocket Motor," Combustion Science and Technology, v. 7, no. 4 (1973), pp. 165-175.
- E-5 Culick, F. E. C. "Stability of Three-Dimensional Motions in a Combustion Chamber," Combustion Science and Technology, to be published (1975).
- E-6 Marble, F. E. "Dynamics of a Gas Containing Small Solid Particles," in Combustion and Propulsion, 5th AGARDograph Colloquium, Pergamon Press, Oxford (1963), pp. 175-213.
- E-7 Culick, F. E. C. and Levine, J. N. "Comparison of Approximate and Numerical Analyses of Nonlinear Combustion Instability" AIAA Paper No. 74-201, AIAA 12th Aerospace Sciences Meeting (January 1974).
- E-8 Derr, R. L. "Evaluation of a Variable Area T-burner for Metallized Propellants," Lockheed Propulsion Company Technical Report AFRPL-TR-72-97 (Feb. 1973).

## APPENDIX F

### THREE-DIMENSIONAL STABILITY ANALYSIS

The stability of three-dimensional motions has been analyzed in two different ways: by constructing the integral balance for energy in a combustion chamber (refs. F-1 and F-2); and computation of the complex wavenumbers of the normal modes, by using the differential equations of motion (refs. F-3, F-4, and F-5). Both methods will be summarized very briefly here.

#### F.1 Calculation of the Complex Wavenumber

Recent numerical calculations (a preliminary report has appeared in ref. F-6) have shown, by comparison with exact calculations, that for satisfactory accuracy, the equations for the two-phase flow should be combined as described in Appendix E for the one-dimensional problem. If an additional force  $\vec{F}$  (per unit volume) is introduced in the momentum equation, and another source term  $\epsilon$ , is included on the right hand side of the energy equation, then the equations for the velocity and pressure can be written:

$$\rho \frac{\partial \hat{u}}{\partial t} + \bar{u} \cdot \nabla \hat{u} + \nabla p = \delta \vec{F}_p + \vec{F} - \vec{\sigma} \quad (\text{F.1})$$

$$\frac{\partial p}{\partial t} + \bar{u} \cdot \nabla p + \left( \frac{\bar{R}}{\bar{C}_v} + 1 \right) \rho \nabla \cdot \hat{u} = \frac{\bar{R}}{\bar{C}_v} \left[ (\bar{u}_p - \bar{u}) \cdot \vec{F}_p + \bar{u} \cdot (\vec{\sigma} - \vec{F}) + (E_{p0} - c_o) w_p + (Q + Q_p) \right. \\ \left. + (1 + C_{m1}) \bar{C}_v T w_p + \epsilon \right], \quad (\text{F.2})$$

where the properties for the mixture are defined in Appendix E, and corresponding to (E. 9) - (E. 12) one has now:

$$\delta \vec{u}_p = \vec{u}_p - \bar{u} \quad (\text{F.3})$$

$$\delta T_p = T_p - T \quad (\text{F.4})$$

$$\delta \vec{F}_p = -\rho_p \left[ \frac{\partial \delta \vec{u}_p}{\partial t} + (\vec{u}_p \cdot \nabla \vec{u}_p - \bar{u} \cdot \nabla \bar{u}) \right] \quad (\text{F.5})$$

$$\delta Q_p = -\rho_p C_p \left[ \frac{\partial \delta T_p}{\partial t} + (\vec{u}_p \cdot \nabla T_p - \bar{u} \cdot \nabla T) \right] \quad (\text{F.6})$$

---

\* These are included for the calculations discussed in Appendix D.

The momentum exchange represented by  $\vec{\sigma}$  is only that related to residual combustion if the purely three-dimensional problem is treated. If, however, one includes additional source terms  $w$  in the original continuity equation for the gas, and  $w^{(p)}$  in the original equation for the particles, then

$$\vec{\sigma} = (\bar{u} - \bar{u}_p) w_p + \bar{u} w + \bar{u}_p w^{(p)} = -\delta \bar{u}_p w_p + \bar{W}. \quad (\text{F. 7})$$

The linearized forms of (F. 1) and (F. 2) are

$$\bar{\rho} \frac{\partial \vec{u}'}{\partial t} + \nabla p' = -\bar{\rho} (\bar{u} \cdot \nabla \vec{u}' + \vec{u}' \cdot \nabla \bar{u}) + \delta \bar{F}'_p + \bar{F}' - \vec{\sigma}', \quad (\text{F. 8})$$

$$\frac{\partial p'}{\partial t} + \left( \frac{\bar{R}}{\bar{C}_v} + 1 \right) p_o \nabla \cdot \vec{u}' = -\bar{u} \cdot \nabla p' - \left( \frac{\bar{R}}{\bar{C}_v} + 1 \right) p' \nabla \cdot \bar{u} + P', \quad (\text{F. 9})$$

where

$$P' = \frac{\bar{R}}{\bar{C}_v} [(1 + C_m)(e'_p \bar{w}_p + \bar{e}_p w'_p) - C_m C \delta T'_p \bar{w}_p + Q' + \delta Q'_p + \mathcal{E}'] . \quad (\text{F. 10})$$

Upon differentiating (F. 9) with respect to time and substituting (F. 8) for  $\partial \vec{u}' / \partial t$ , one finds the wave equation for the pressure,

$$\nabla^2 p' - \frac{1}{a^2} \frac{\partial^2 p'}{\partial t^2} = h, \quad (\text{F. 11})$$

with the boundary condition

$$\hat{n} \cdot \nabla p' = -f. \quad (\text{F. 12})$$

The functions  $h$  and  $f$  are

$$h = -\bar{\rho} \nabla \cdot (\bar{u} \cdot \nabla \vec{u}' + \vec{u}' \cdot \nabla \bar{u}) + \frac{1}{a^2} \bar{u} \cdot \nabla \frac{\partial p'}{\partial t} + \frac{\bar{Y}}{a^2} \frac{\partial p'}{\partial t} \nabla \cdot \bar{u} + \nabla \cdot (\delta \bar{F}'_p + \bar{F}' - \vec{\sigma}') - \frac{1}{a^2} \frac{\partial P'}{\partial t}, \quad (\text{F. 13})$$

$$f = \bar{\rho} \frac{\partial \vec{u}'}{\partial t} \cdot \hat{n} + \bar{\rho} (\bar{u} \cdot \nabla \vec{u}' \cdot \nabla \bar{u}) \cdot \hat{n} - (\delta \bar{F}'_p + \bar{F}' - \vec{\sigma}') \cdot \hat{n}. \quad (\text{F. 14})$$

The square of the wavenumber for the  $N^{\text{th}}$  perturbed mode is given by the formula

$$k^2 = k_N^2 + \frac{1}{E_N^2} \left\{ \int h \hat{p}_N dV + \oint f \hat{p}_N dS \right\} \quad (\text{F. 15})$$

where

$$E_N^2 = \int \hat{p}_N^2 dV, \quad (\text{F. 16})$$

and  $k_N, \hat{p}_N$  are the wavenumber and mode shape for the  $N^{\text{th}}$  unperturbed (i. e., classical) mode. After some of the integrals are worked out and

combined, (F. 15) becomes

$$\begin{aligned}
 (k^2 - k_N^2) E_N^2 = & i \bar{\rho} \bar{a} k_N \iint \left( \hat{u} \hat{p}_N + \frac{\hat{p}_N^2}{\rho \bar{a}^2} \vec{u} \right) \cdot \hat{n} dS - \left\{ \int \delta \hat{F}_p \cdot \nabla \hat{p}_N dV + \frac{k_N}{\bar{a}} \frac{\bar{R}}{\bar{C}_v} \int \delta \hat{Q}_p \hat{p}_N dV \right\} \\
 & \text{combustion and exhaust nozzle} \qquad \text{contributions from particulate matter} \\
 & + i \frac{k_N}{\bar{a}} \left\{ \frac{\bar{\gamma} - 1}{\rho_g} \int \hat{p}_N^2 \bar{w}_p dV - \int \delta \hat{u}_p \cdot \nabla \hat{p}_N \bar{w}_p dV - \frac{\bar{R}}{\bar{C}_v} \int \hat{p}_N [(1 + C_m)(\hat{e}_p \bar{w}_p + \bar{e}_p \hat{w}_p) \right. \\
 & \qquad \qquad \qquad \text{residual combustion} \\
 & \left. - C_m C \delta \hat{T}_p \bar{w}_p + \hat{Q} ] dV \right\} - \left\{ \int \hat{F} \cdot \nabla \hat{p}_N dV - \int \hat{W} \cdot \nabla \hat{p}_N dV + i \frac{k_N}{\bar{a}} \frac{\bar{R}}{\bar{C}_v} \int \hat{p}_N dV \right\} \\
 & \qquad \qquad \qquad \text{(momentum)} \qquad \text{(mass)} \qquad \qquad \text{(energy)} \\
 & \qquad \qquad \qquad \text{additional source terms}
 \end{aligned}
 \tag{F. 17}$$

Equation (F. 17) is to be compared with the one-dimensional result, eq. (E. 31). First note that in the second combustion term in (E. 31), the integral over the perimeter  $q$ , followed by the integral over the length, can be replaced by the integral over the surface area,  $S$ . Hence, in view of the equality (E. 32), all the combustion terms have the same form. However, the possibility [see remarks following (E. 32)] that the numerical values of the response may be different for surface elements exposed to acoustic velocities having different orientations must be accounted for. This problem has been discussed in refs. F-4 and F-5.

In the one-dimensional problem, the volume element is  $dV = S_c dz$ . Hence, all the volume integrals arising from the presence of the particulate matter and residual combustion are identical in (E. 31) and (F. 17). The "flow-turning" term and the surface term involving  $\delta \hat{u}_p$  in (E. 31) do not appear explicitly in (F. 17). These are the new contributions found in the one-dimensional analysis\*. On the other hand, the last brackets in (F. 17) contain contributions from source terms representing undefined processes.

\* It is worth noting that recent numerical calculations have shown that the term involving  $\delta \hat{u}_p$  is probably negligible under most conditions which prevail in T-burners and motors.

Because the source terms  $\vec{F}$ ,  $\vec{W}$ , and  $\mathcal{E}$  are not defined specifically, one may use them in various ways. If they are taken to represent processes occurring in a thin region near the surface, then it is possible (ref. F-5) to reproduce the one-dimensional terms referred to in the preceding paragraph. As given here, Eq. (E. 31), the one-dimensional contributions apply to the limiting case in which the unperturbed acoustic velocity is entirely parallel to the burning surface. The inviscid three-dimensional analysis produces results which are entirely correct only for a limiting case when there is no component of acoustic velocity parallel to the surface. The way in which the general case is handled rests on a separate argument given in refs. F-4 and F-5.

For the limiting case of acoustic velocity all parallel to the surface, the three-dimensional counterparts of the two one-dimensional terms are:

$$i \frac{(1+C_m)}{\rho a k_N} \iint (\nabla \hat{p}_N)^2 \bar{m}_b dS \quad (\text{flow-turning}) \quad (\text{F. 18})$$

and

$$\iint \delta \hat{u}_p \cdot \nabla \hat{p}_N \bar{m}_b^{(p)} dS \quad (\text{F. 19})$$

The source terms may also be used to represent the influences of baffles and suppression devices, although little has been done in this respect. For example, a baffle may be characterized by a pressure drop, which may be represented by the force  $\vec{F}$  in the momentum equation. Difficulties arise in the representation for unsteady flow conditions.

## F.2 Construction of the Balance of Acoustic Energy

The analysis provided in ref. F-1 was done for gases only; the influence of the particulate matter was subsequently included as an additive term in the formula for the growth constant. This procedure presupposes that one knows how to compute the contribution from particle damping. As shown in Appendix D, the form to be used for accurate results is far from obvious. If the approach of ref. F-1 is followed, the first step is to construct the balance for the total energy,  $C_v T + u^2/2$ , in the chamber. The rate of change of total energy within the entire chamber must equal the rate at which energy flows in due to convection plus the rate at which work is done on the material within the chamber, plus the rate of heat addition:

$$\frac{d}{dt} \int \rho \left( C_v T + \frac{u^2}{2} \right) dV = - \int \nabla \cdot \left[ \rho \vec{u} \left( h + \frac{u^2}{2} \right) \right] dV + \int Q dV . \quad (F.20)$$

If all variables are written as sums of steady and time-varying parts, the time average of (F.20) can eventually be written

$$\begin{aligned} \left\langle \frac{d}{dt} \int dV \left[ \frac{p'^2}{2\rho a^2} + \frac{1}{2} \bar{\rho} \vec{u}'^2 + \frac{(\vec{u} \cdot \vec{u}')}{a^2} p' \right] \right\rangle &= \\ &= - \left\langle \iint dS \hat{n} \cdot \left[ \vec{u}' p' + \frac{\vec{u} p'^2}{\rho a^2} + \bar{\rho} (\vec{u} \cdot \vec{u}') \vec{u}' + \frac{p'}{a} (\vec{u} \cdot \vec{u}') \vec{u} \right] \right\rangle + \langle \int Q' dV \rangle . \end{aligned} \quad (F.21)$$

For simplicity, all other contributions associated with residual combustion and the particulate matter have been ignored.

The reasoning of ref. F-1 is now that the left hand side of (F.21) may be interpreted as the time-averaged rate of change of acoustic energy in the chamber (actually, it is the time average of the time-varying part of the total energy). Hence, if the definition (2.1) of  $\alpha$  is used, the formula is obtained

$$-2\alpha = \frac{\left\langle \iint dS \hat{n} \cdot \left[ p' \vec{u}' + \frac{\vec{u} p'^2}{\rho a^2} + \bar{\rho} (\vec{u} \cdot \vec{u}') \vec{u}' \right] \right\rangle + \langle \int Q' dV \rangle}{\left\langle \int dV \left[ \frac{1}{2} \bar{\rho} \vec{u}'^2 + \frac{p'^2}{2\rho a^2} \right] \right\rangle} . \quad (F.22)$$

Note that two terms have been dropped in passing from (F.21) to (F.22); this approximation restricts all subsequent results to first order in the average Mach number (see refs. F-4 and F-5).

Because all terms in the numerator will be of first order in the average Mach number, zeroth order quantities must be used in the denominator. (If, say, a first order term is retained in the denominator, it will eventually contribute a second order term to  $\alpha$ , which must be dropped.) Hence, one must use unperturbed acoustic values for  $\vec{u}'$  and  $p'$  in the denominator; it is then easy to show (see ref. F-4 among others) that

$$\int dV \left( \frac{1}{2} \bar{\rho} \vec{u}'^2 \right) = \int dV \frac{p'^2}{2\rho a^2} . \quad (F.23)$$

Hence, the denominator of (F.22) is simply  $E_N^2 / \bar{\rho} a^2$ . The term in  $Q'$

vanishes, because  $Q'$  varies harmonically in time and hence has average value equal to zero. This is a consequence of working with the total energy in the chamber rather than the acoustic energy. If the acoustic energy is treated,  $Q'$  is weighted by  $p'$  (see below, and also Eq. (F. 17), for example); in that case, the average value does not vanish. This result is typical of any process occurring completely within the volume, and shows explicitly why in this approach one is forced to add arbitrarily extra terms in  $\alpha$ ; see refs. F-4 and F-5 for further details.

If flow-turning terms are represented by  $\alpha_m$  and other losses (in particular, the attenuation due to condensed material) by  $\alpha_d$ , then (F. 22) can be written

$$\alpha = - \frac{\bar{\rho} \bar{a}^2}{2E_N} \oint \left[ \hat{p} \hat{u}(x) + \frac{\bar{\rho}}{\bar{u}} \frac{\hat{p}^2}{\rho a} + \bar{\rho} (\bar{u} \cdot \hat{u}) \hat{u} \right] \cdot \hat{n} dS + \alpha_m + \alpha_d \quad (F. 24)$$

Although it is not indicated, it is the maximum amplitude in time which should be used for  $\hat{u}$  in the third term under the surface integral: this becomes clear when the time averaging is done.

Following Eq. (2. 3. 4), it is remarked that the third term under the integral also arises in the analysis involving calculation of the wavenumber. It is fairly clear that this must be so, but to show it requires more detailed manipulations than are appropriate here. The demonstration requires carrying further some second-order terms which were dropped early in the calculation outlined in §F. 1.

It has also been shown in ref. F-4 (§8. 2) that if the acoustic energy balance is formed by beginning with the linearized equations (F. 8) and (F. 9), then eventually an expression for  $\alpha$  can be found which is identical with that deduced from the imaginary part of (F. 17). The procedure follows the more traditional path. First, take the scalar product of  $\bar{u}$  with (F. 8); multiply (F. 9) by  $p'/\bar{\rho} \bar{a}^2$ ; and then add the results. The first terms on the left hand sides of (F. 8) and (F. 9) combine to give

$$\bar{\rho} \bar{u}' \cdot \frac{\partial \bar{u}'}{\partial t} + \frac{p'}{\bar{\rho} \bar{a}^2} \frac{\partial p'}{\partial t} \equiv \frac{\partial}{\partial t} \left( \frac{\bar{\rho} \bar{u}'^2}{2} + \frac{1}{2} \frac{p'^2}{\bar{\rho} \bar{a}^2} \right)$$

This is just the rate of change of acoustic energy, as required in the definition of  $\alpha$ . Details of the computation are given in the reference.

#### REFERENCES

- F-1 Cantrell, R.H. and Hart, R.W. "Interaction between Sound and Flow in Acoustic Cavities," J. Acoust. Soc. Amer., V. 36, no. 4 (April 1964), pp. 697-706.
- F-2 Hart, R.W. and McClure, F.T. "Theory of Acoustic Instability in Solid Propellant Rocket Combustion," Tenth Symposium (International) on Combustion, The Combustion Institute (1965), pp. 1047-1065.
- F-3 Culick, F.E.C. "Acoustic Oscillations in Solid Propellant Rocket Chambers," Astronautica Acta, V. 12, no. 2 (1966), pp. 113-126.
- F-4 Culick, F.E.C. "Interaction Between the Flow Field, Combustion, and Wave Motions in Rocket Motors," NWC TP 5349 (June 1972), Naval Weapons Center, China Lake, Calif.
- F-5 Culick, F.E.C. "Stability of Three-Dimensional Motions in a Combustion Chamber," to be published in Combustion Science and Technology (1975).
- F-6 Culick, F.E.C. and Levine, J.N. "Comparison of Approximate and Numerical Analyses of Nonlinear Combustion Instability," AIAA Paper No. 74-201. AIAA 12th Aerospace Sciences Meeting (Jan. 1974).

## APPENDIX G

### REMARKS ON THE PROBLEM OF THE VENT

#### G.1 Analysis

The problem of determining the loss or gain of acoustic energy due to the vent is complicated, because there is an average flow through the vent; and because for much of the work with T-burners, the flow is not choked. At the time of writing, the problem is not only unsolved analytically, but no unambiguous conclusions have been drawn from experimental data (see § G. 2).

There are several sources of energy transfer associated with unsteady flow at a vent. Consider first the case of no average flow. There are two mechanisms causing loss of energy from the acoustic field in the chamber: radiation and internal dissipative processes. Non-zero pressure fluctuations cause the gas in the vent itself to oscillate, and this motion is communicated to the outside world. The result is an acoustic field which, far from the vent or hole, consists only of outgoing waves. As far as the waves in the chamber are concerned, this constitutes a loss of energy by radiation. Viscous stresses and heat transfer cause additional losses, principally in the vicinity of the hole itself.

The simplest case of radiation is that for a hole in a plane wall. A treatment of the radiation from a hole at the end of a duct has been worked out in ref. C-1, based on the acoustical analog to a result of scalar diffraction theory in optics. The starting point is the formula for the oscillating pressure at an observation point P far from the hole:

$$\hat{p}(P) = -\frac{1}{2\pi} \iint_{\text{hole}} \frac{\partial \hat{p}}{\partial n} e^{-ikr_{01}} dS, \quad (\text{G.1})$$

where  $r_{01}$  is the distance from an arbitrary point on the hole to the observation point. The gradient of pressure normal to the plane of the hole, in the outward direction, is  $\partial \hat{p} / \partial n$ . This is equal to  $-i\omega \hat{u}_n$ . However, the acoustic velocity fluctuation  $u'_n$ , through the hole, is unknown except in special cases.

For example, a standard problem discussed in texts on acoustics concerns the energy radiated by a piston in a wall. Then  $u'_n$  is constant over the hole (now a piston), and the integral in (G.1) can be worked out.

But for T-burners, with wave motions parallel to the hole, the velocity  $u_n'$  is unknown and must be found as part of the solution. This amounts, of course, to a calculation of the admittance function  $u_n^{(r)}/p'$  for the hole. An approximate analysis has been reported in ref. G-2 for a T-burner with an annular vent, encircling the entire tube. The result is that for odd modes, the contribution to the decay constant is

$$\alpha_n \approx -\frac{\bar{a}}{L} \frac{\pi^4 (2\ell+1)^2}{(8.44)^2} \frac{d^4}{L^2 D^2} \quad (G.2)$$

where  $d$  is the width of the vent and  $D$  is the diameter of the burner. Suppose  $\bar{a} = 3500$  ft/sec,  $L = 2$  ft,  $D = 1.5$  in,  $d = 1$  in, and take  $\ell = 0$  (the fundamental mode). Then  $\alpha_n \approx 7.4 \text{ sec}^{-1}$ . But this is for an annular opening. If the vent is, say, square, one inch on a side, then the value of  $\alpha_n$  is reduced by the ratio of the area of the square vent to the area of the annulus, i. e., (G.2) is multiplied by  $d^2/d\pi D = d/\pi D$ . For the numbers given above,  $\alpha_n$  is then approximately  $1.6 \text{ sec}^{-1}$ . This is a rather large vent, but even so, the radiation loss is negligible compared with other losses in the system. For the even modes, the pressure of the acoustic field has an anti-node at the vent and the radiation loss is large; numerical values will not be examined here because the question at hand has to do with the influence of the vent on the fundamental mode.

Approximate formulas for the losses associated with sonic and subsonic vents have been given in ref. G-3, based on essentially the same representation as that used here. Both of the analyses covered in Appendix F lead to the general expression for the decay constant due to the vent or exhaust nozzle:

$$\alpha_n = -\frac{\bar{a}}{2E_N} \iint [A_n^{(r)} + \bar{M}_e] \hat{p}_N^2 dS \quad (G.3)$$

where the admittance function  $A_n = (\hat{u}_n/\hat{p})(\gamma p_o/\bar{a})$  has been introduced. For the fundamental mode of a T-burner,  $\hat{p}_N$  vanishes at the center of the burner, so for a vent at that location,  $\alpha_n$  given by (G.3) is negligibly small. It is on this basis that until recently the influence of the vent (either sonic or unchoked) on the fundamental mode has been ignored. The formulas given in ref. G-3 are deduced from Eq. (G.3) and hence show  $\alpha_n = 0$  for the fundamental mode if the vent is at the center of the burner.

What is meant by "the problem of the vent" is the conflict of two non-zero results deduced for a center vent: one is a formal deduction from the one-dimensional analysis; the other is based on Eq. (F.24) for three-dimensional flow, but involves an additional assumption in respect to the interactions between the average flow and the acoustic field at the vent.

It should be noted again that the one-dimensional analysis already incorporates certain assumptions concerning the behavior of the flow. In particular, it is assumed that the flow passing through the boundary has no component of momentum, parallel to the axis of the chamber, when it is outside the boundary. This applies equally to flow entering and leaving.

To see the difficulty, write equations for the real part of (F.17) with the flow-turning term (F.18) included, and (F.24),

$$\alpha = \alpha_b + \alpha_d + \alpha_m \quad (3\text{- plus 1-dimensional analysis, §F.1}) \quad (G.4)$$

$$\alpha = \alpha_b + \alpha_d + \alpha_v \quad (3\text{-dimensional analysis, §F.2}) \quad (G.5)$$

where  $\alpha_b$  represents the contribution from surface combustion;  $\alpha_d$  stands for energy losses, mainly particle damping and viscous losses at inert surfaces; and

$$\alpha_m = -(1+C_m) \frac{1}{2\rho E_N^2 k_N^2} \oint (\nabla \hat{p}_N)^2 \bar{m}_b dS \approx \frac{-\bar{u}_b}{2E_N^2 k_N^2} \oint (\nabla \hat{p}_N)^2 dS, \quad (G.6)$$

$$\alpha_v = -\frac{\bar{\rho} a^2}{2E_N} \oint (\vec{u} \cdot \hat{n}) \vec{u} \cdot \hat{n} dS. \quad (G.7)^{\#}$$

First, a remark on sign conventions:

- (i)  $\bar{m}_b$  is positive for flow into the chamber at the boundary,
- (ii) the normal vector  $\hat{n}$  points outward, so  $\vec{u} \cdot \hat{n}$  is positive for flow outward through the boundary.

Because of the convention (i),  $\alpha_m$  given by (G.6) is negative at a burning surface and hence represents a loss of energy, the "flow-turning"

---

\* As noted in §F, this term also arises in the three-dimensional analysis covered in §F.1, but in the original work it was always dropped as a higher order term. Hence, the term is identified as part of the analysis (§F.2) in which it has not been omitted.

loss, denoted  $\alpha_m^{FT}$ . But at the vent,  $\bar{m}_b$  is negative, so  $\alpha_m$  is positive and represents a process causing the waves in the chamber to gain energy, denoted  $\alpha_m^v$ . A more explicit formula can be obtained; suppose that the outward flow is approximately uniform over the vent. Then, because for the longitudinal modes

$$(\nabla \hat{p}_N)^2 = (k_\ell \sin k_\ell z)^2 \approx k_\ell^2 \quad (\text{center vent})$$

and

$$E_N^2 = \int \hat{p}_N^2 dV = S_c \int_0^L \cos^2 k_N z dz = \frac{LS_c}{2},$$

so (G.6) applied to the vent gives

$$\alpha_m^v = \frac{(1+C_m)}{L} \frac{1}{\bar{\rho} S_c} \left[ \iint_{\text{vent}} \bar{m}_v dS \right].$$

The term in brackets is the total time-averaged mass flow through the vent, which must equal  $\bar{m}_b S_b \equiv \bar{\rho} \bar{u}_b S_b$ , the total average mass flow in from the burning surfaces. Hence, the contribution from the vent is\*

$$\alpha_m^v = \frac{\bar{u}_b}{L} \frac{S_b}{S_c} \quad (\text{center vent, odd harmonics}) \quad (C.8)$$

It must be understood clearly that this is a formal consequence of the one-dimensional analysis. Because the flow is strongly three-dimensional in the vicinity of the vent, the approximations used in the one-dimensional analysis may be very poor. In particular, viscous effects (including separation) may be so important that the approximate analysis is simply not applicable. The factor VF in (G.14) below is a crude means of incorporating viscous effects.

If the T-burner is operated with short lateral grains at the ends (or only end grains), then the flow-turning loss is negligibly small and  $\alpha_m$  consists only of the positive contribution from the vent, the "vent gain."

Now consider the term  $\alpha_v$ , Eq. (G-7). Over the burning surface, the mean flow is in the formal direction, so the velocities in the integrand become

$$(\bar{u} \cdot \hat{u}) \hat{u} \cdot \hat{n} \equiv -\bar{u}_b (\hat{u}_n)^2, \quad (G.9)$$

---

\* See also Eq. (E.50) and remarks there.

where  $\bar{u}_b$  and  $\hat{u}_n$  are both positive inward. Because  $\hat{u}$  is non-zero at a burning surface only because of the combustion response, it is of the order of the mean flow speed; thus, (G. 9) is of the order of the cube of the mean flow speed and is negligible -- indeed, it must be dropped.

At an exhaust vent,  $\bar{u}_b = -\bar{u}_v$  because the flow is outward, and (G.7) is

$$\alpha_v = \frac{\rho a^2}{2E_N} \iint \bar{u}_v (\hat{u}_n)^2 dS \quad (G. 10)$$

Consider first a center vent. If the unperturbed acoustic field is a longitudinal mode, the quantity  $\hat{u}_n$  represents a perturbation due to the opening in the lateral boundary. It is the fluctuating velocity causing the radiation of acoustic energy from the chamber.

If, in addition, there is an average flow through the vent, there will be a further contribution to the perturbation  $\hat{u}_n$ . The position taken in refs. G-4 and G-5 is that this additional perturbation (which has never been calculated) must be at most first order in the average speed, and the right hand side is therefore negligible, being of second (or higher) order in small quantities. The acoustic and mean flow streamlines appear roughly as sketched in Figure G-1(a).

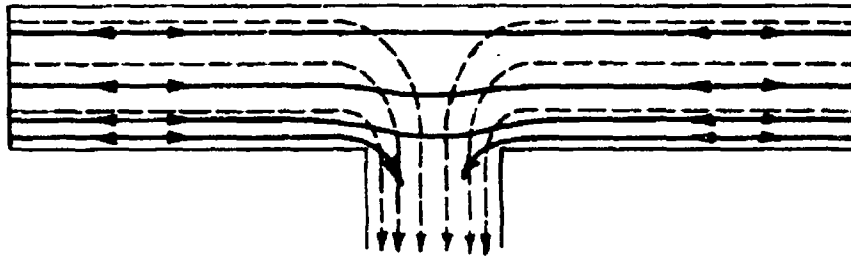
On the other hand, the authors of refs. G-6 and G-7 assume that the component of acoustic velocity parallel to the mean flow leaving the vent has the full value appropriate to the unperturbed acoustic field at the center of the chamber. That is, if  $\hat{p}_N = \cos k_L z$ , then from the momentum equation for the acoustic field, the unperturbed velocity parallel to the axis is

$$\hat{u}_N = \frac{1}{i\rho\omega_N} \frac{d\hat{p}_N}{dz} = \frac{-k_L}{i\rho\omega_N} \sin k_L z = \frac{i}{\rho a} \sin k_L z$$

The factor  $i$  is dropped for use in (G. 10) because time-averaging has already been done. Hence, because  $\sin k_L z = L/2$ , (G. 10) becomes

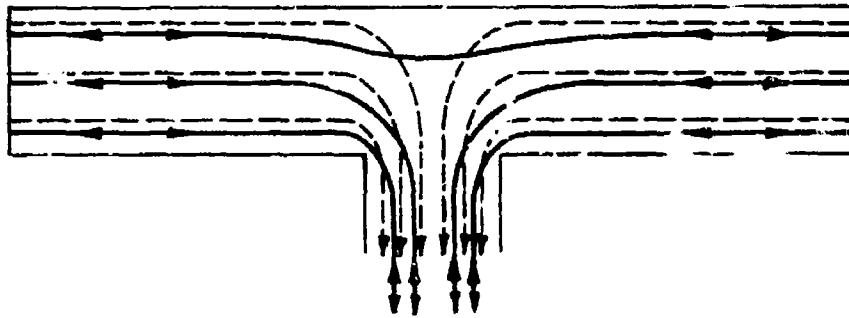
$$\alpha_v = \frac{\rho a^2}{2 \cdot LS_c/2} \frac{\bar{u}_v S_v}{\rho a^2} = \frac{\bar{u}_b}{L} \left( \frac{S_b}{S_c} \right) \quad (G. 11)$$

If  $\hat{u}_n$  has the large value implied by this substitution, then the acoustic streamlines would look something like those sketched in Figure G-1(b).



(a) STREAMLINES SHOWING PERTURBATIONS  
DUE TO THE VENT. (REFS. G-4 AND G-5)

—— ACOUSTIC STREAMLINES  
 - - - - STREAMLINES FOR THE AVERAGE FLOW



(b) STREAMLINES ACCORDING TO THE  
ASSUMPTIONS PROPOSED IN REFS.  
G-6 AND G-7

Figure C-1 Sketches of Two Interpretations of the Influence of a  
Center Vent

supported by the data; and a loss as large as that given by  $FV = -1$  is also not shown by the data.

Some tests, referred to in §G.2, have been done with burners having no center vent but one end open to the atmosphere. Without a sonic exhaust nozzle, the unperturbed acoustic field is that for an open organ pipe; the burner is approximately a quarter-wave tube. In that case, the acoustic velocity is a maximum at the open end, and the integral in (G. 7) is correctly of first order in the mean flow speed. The contribution to  $\alpha$  is then, with no other assumptions, correctly given by (G. 11).

### G.2 Experimental Results

As noted in §G. 1, there is uncertainty concerning the proper treatment of some acoustic/mean flow interactions in the T-burner, particularly those associated with flow through the vent. Neither the use of formal analysis nor the use of pressure-coupled T-burner data has satisfactorily resolved the difficulty. Therefore, special tests have been performed to obtain results that would assist in the selection of the correct representation. The following pages contain a summary of the useful equations, a description of the tests, a summary of the results, and the conclusions reached.

The equations used to describe unsteady motions in a T-burner, refs. G-4 and G-8, include mean flow terms that combine in such a way as to prevent one from evaluating their magnitude from pressure-coupled T-burner data. Special T-burner configurations have therefore been selected to obtain appropriate data and to resolve uncertainty.

Figure G-2 shows one burner used with the test variable being the amount of propellant surface area near the vent. The grains are relatively short and, for the conditions under which data are taken, essentially flush with the wall. The contribution to the flow-turning loss at the end grains is negligibly small, because the local acoustic velocity goes to zero at the ends. At the center of the burner, the acoustic velocity is a maximum for the fundamental mode; the flow-turning loss,  $\alpha_m^{FT}$ , due to the sample grains near the vent, exactly cancels the "vent gain" contribution in Eq. (G. 12) if the formal results are assumed to be valid. Hence, the change in growth constant due to a small change of surface

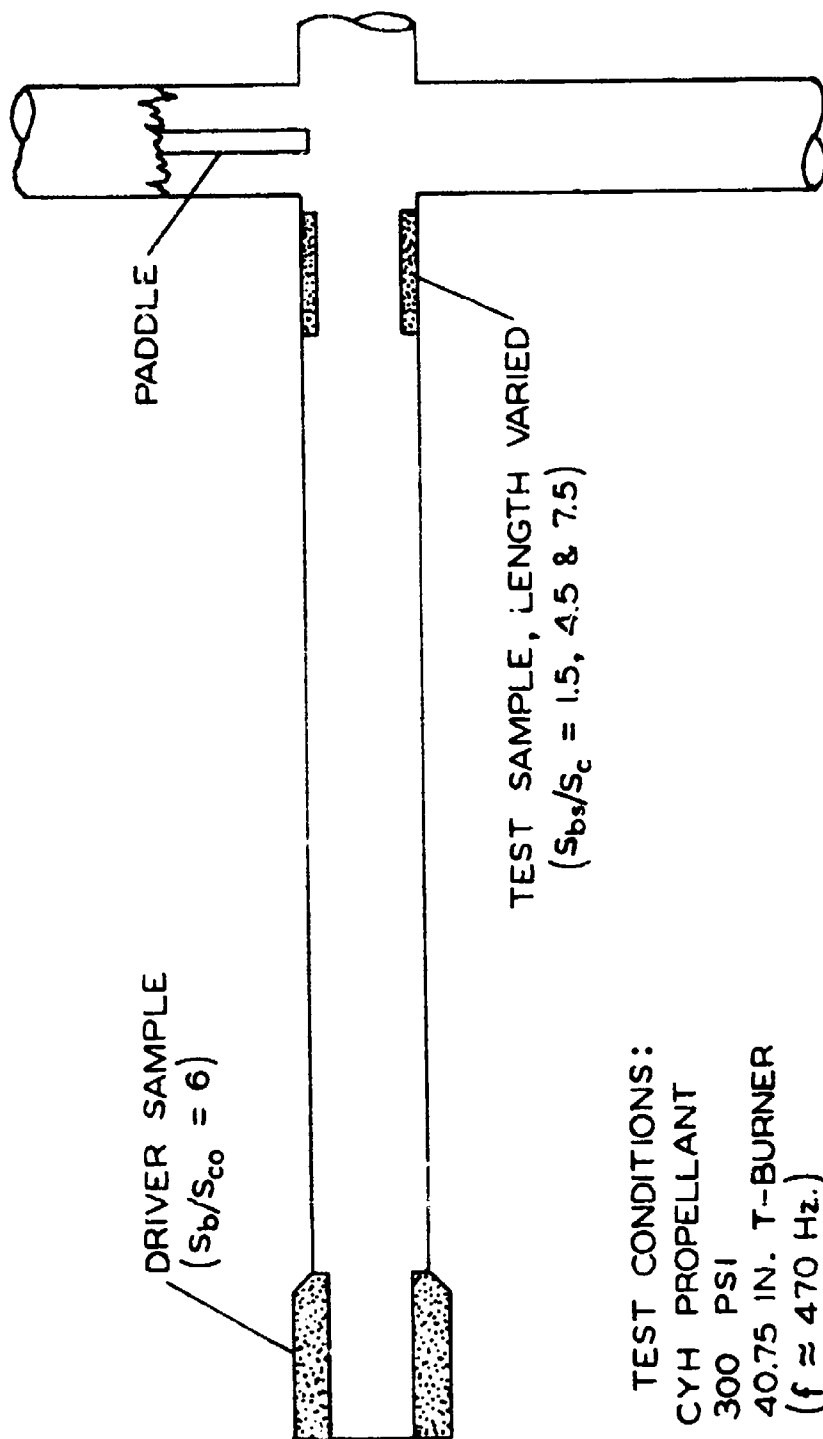


Figure G-2 Configuration of a T-Burner for Studies of the Influence of the Vent

But in Figure G-1(b), much of the acoustic field has a node at the center of the burner, so the half-wavelength  $\lambda/2$  approaches  $L/2$ ; and because the frequency is always equal to the speed of sound divided by the wavelength, the frequency associated with the field suggested by Figure G-1(b) is much less than  $\bar{a}/L$ . The frequency for the field sketched in Figure G-1(a) is approximately  $2\bar{a}/L$ , which is essentially that observed value for the fundamental mode in T-burner tests.

However, (G. 11) has been proposed as a representation of losses for the fundamental mode, and a number of tests have been done in attempts to determine the true influence of the vent. To summarize, the formal application of (G. 4) and (G. 6) to the vent leads to

$$\alpha = \alpha_b + \alpha_d + \alpha_m^{FT} + \frac{\bar{u}_b}{L} \frac{S_b}{S_c}, \quad (\text{G. 12})$$

(vent)

where  $\alpha_m^{FT}$  represents only the "flow-turning" loss associated with the flow at the burning surface. Equations (G. 5) and (G. 7) plus the crucial assumption noted above give

$$\alpha = \alpha_b + \alpha_d - \frac{\bar{u}_b}{L} \frac{S_b}{S_c}. \quad (\text{G. 13})$$

(vent)

Equations (G. 12) and (G. 13) can be written together as

$$\alpha = \alpha_b + \alpha_d - (FT) \frac{\bar{u}_b}{L} \frac{S_b}{S_c} \frac{g_1}{\epsilon_1^2} + (VF) \frac{\bar{u}_b}{L} \frac{S_b}{S_c}, \quad (\text{G. 14})$$

where VF is the "vent factor" and FT is the "flow-turning factor." Equation (E. 49) has been used for  $\alpha_m^{FT}$ .

Obviously, VF = +1 if the vent provides maximum gain of energy, and VF = -1 if the loss is that expressed in (G. 13). Because of the doubts concerning the true value of VF, this has often been treated as a floating parameter in the interpretation of experimental data. To date, the results are not conclusive (§G.2), primarily because it is not possible to separate totally the influence of the vent from other contributions. However, it does seem that a vent "gain" (i. e., VF positive) is not strongly

area of the sample grain vanishes.

$$\frac{d\alpha}{d(S_{bs}/S_c)} = 0 \quad (G. 15)$$

Equation (G. 15) is based on the purely one-dimensional analysis. On the other hand, if the flow-turning loss is ignored, and the vent is assumed to contribute the loss shown in Eq. (G. 13), one finds

$$\frac{d\alpha}{d(S_{bs}/S_c)} = -2 \frac{\bar{u}_b}{L} \quad (G. 16)$$

Here, and in the following,  $S_{bs}$  denotes the burning surface area of the sample grains on the lateral boundary in one half of the T-burner.

Other tests have been done with a special combustor called the quarter-wave burner, shown in Figure G-3(a). The acoustic velocity reaches a maximum at the open end, and the contribution defined by Eq. (G. 7) must be retained. The flow-turning loss is negligible for the grains at the closed end, and because there is now no side vent, both approaches described in §G. 1 produce the same result,

$$\frac{d\alpha}{d(S_{bs}/S_c)} = -2 \frac{\bar{u}_b}{L} \quad (G. 17)$$

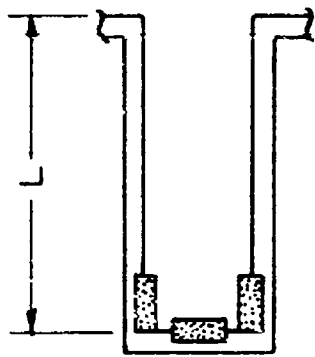
Finally, some tests have been done with sample grains displaced from the ends, shown in Figure G-3(b). The two approaches then lead to

$$\frac{d\alpha}{d(S_{bs}/S_c)} = 2 \frac{\bar{u}_b}{L} \left[ R_b^{(r)} \left( \frac{\hat{p}}{\bar{p}} \right)_s^2 - 1 \right] \quad (G. 18)$$

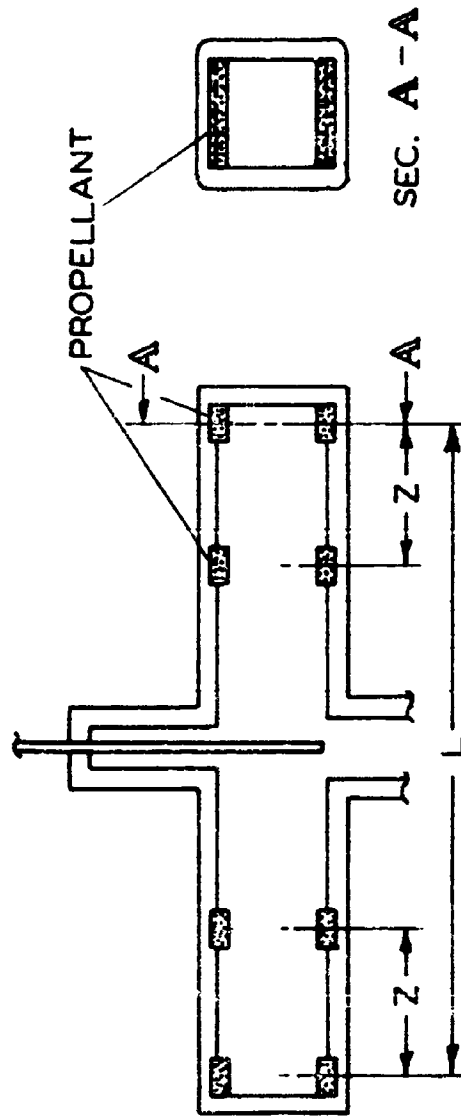
$$\frac{d\alpha}{d(S_{bs}/S_c)} = 2 \frac{\bar{u}_b}{L} \left[ R_b^{(r)} + 1 \right] \left( \frac{\hat{p}}{\bar{p}} \right)_s^2 \quad (G. 19)$$

The first is based on the three-dimensional analysis, and the second on the one-dimensional analysis described above and summarized as Eq. (G. 14). It has been assumed that the grains are short, so that the pressure fluctuation is essentially uniform over the samples, and represented by  $(\hat{p}/\bar{p})_s$ .

Equations (G. 15) - (G. 19) have been used as the basis for several series of tests. One series of tests was conducted in the burner shown in



(a) QUARTER WAVE BURNER



(b) T-BURNER WITH DISPLACED GRAINS

Figure G-3 A Quarter-Wave Burner and a T-Burner with Displaced Grains

Figure G-2, with the test samples being located as near the vent as physically possible. The hardware and instrumentation systems used were the same as those used in variable-area T-burner testing (ref. C-9) and for velocity-coupled T-burner testing (refs. G-10 and G-11). The tests were performed with CYH propellant at 300 psi and 450 Hz. Because of the proximity of the test sample to the vent, the normal propellant sample holder could not be used. Therefore, the test sample was located one inch away from the centerline of the burner, and was machined to fit into the 1.5-inch ID of the T-burner wall (e. g. the sample had a 1.25-inch ID and 1.5-inch OD). The test sample near the vent therefore had a smaller web than the driver sample. Consequently, the test sample burned out while the driver sample continued to burn, showing an instantaneous effect of the test sample. The driver sample was chosen large enough to drive the T-burner spontaneously unstable with a growth constant of roughly  $80 \text{ sec}^{-1}$  and a limiting amplitude of  $\sim 80$  psi peak-to-peak.

Another group of tests, ref. G-7, was conducted at a test pressure of 215 psia in the T-burner shown in Figure G-3(b), which differed from those commonly used. First, it was smaller than most described in the literature, having a cross-sectional area of approximately one square inch. Second, the cross section was nearly square rather than circular. Third, there were recesses machined in the internal walls of the burner into which flat slab-shaped propellant samples could be placed. For some tests, additional propellant samples were placed at various positions between the ends and the vent. In different runs, the additional samples were placed at different positions and thus the instability determined as a function of sample position.

The quarter-wave burner shown in Figure G-3(a) was constructed with the same square tube material and the same type of sample holders as were used in the square T-burner. To simulate an opening attached to an infinite flange, the open end of this burner was attached to a two-foot square plate of steel. The metal plate had a hole in the center that matched the hole in the burner.

Both square burners were equipped with a retractable air-driven paddle located at the vent. The propellant was ignited with the paddle in-

serted into the burner, so that unstable motions were suppressed. When steady burning had been established and the propellant samples had burned to the point where the burning surface was very nearly flush with the tube walls, the paddle was rapidly (within approximately 20 msec) retracted and oscillations were permitted to grow.

Another series of tests was conducted in a T-burner that had no vent pipe but simply a hole in the side of the burner. This burner was fired at atmospheric pressure and the plume behavior studied through the use of high speed photography.

The results of the first series of tests were rather dramatic and showed that after the test sample burned out, both the limiting pressure amplitude and the measured growth constant were larger than while the test sample was burning, indicating that the test sample at the vent caused a loss in the system. The test records also showed that the change in both  $\alpha$  and amplitude become greater for larger test samples.

Figure G-4 shows a plot of  $\alpha$  versus the test sample area ratio (because the data were taken at very nearly flush conditions, the corrections for nonuniformities are negligible at all area ratios). Calculated curves are superimposed using values of  $B_s$ ,  $\alpha_d$ , and  $R_{vi}$  determined from extensive testing with CYH propellant at these conditions (refs. G-10 and G-11). The results are striking. The only curves that fit the data are those resulting from an arbitrary use of a large mean flow damping that has no theoretical basis. The damping is not only larger than that predicted as the flow turning or vent loss alone, but also larger than their sum. It should be noted that there is considerable curvature in the predicted curves, whereas Eq. (C.14) suggests a linear variation. The reason is that the samples were not located precisely at the center of the burner, as Figure G-2 shows. Moreover, the large samples ( $S_b/S_{co} = 7$ ) were 2.75 inches long, extending a significant distance along the burner. The pressure varies over the sample, so that both  $\alpha_b$  due to combustion and  $g_t$  depend on the length of the grain.

The equations for a different series of tests, ref. G-7, were used to compute response function values for two PBAA-AP propellants (refs. G-17 and G-18) tested in the T-burner and also in the quarter-wave

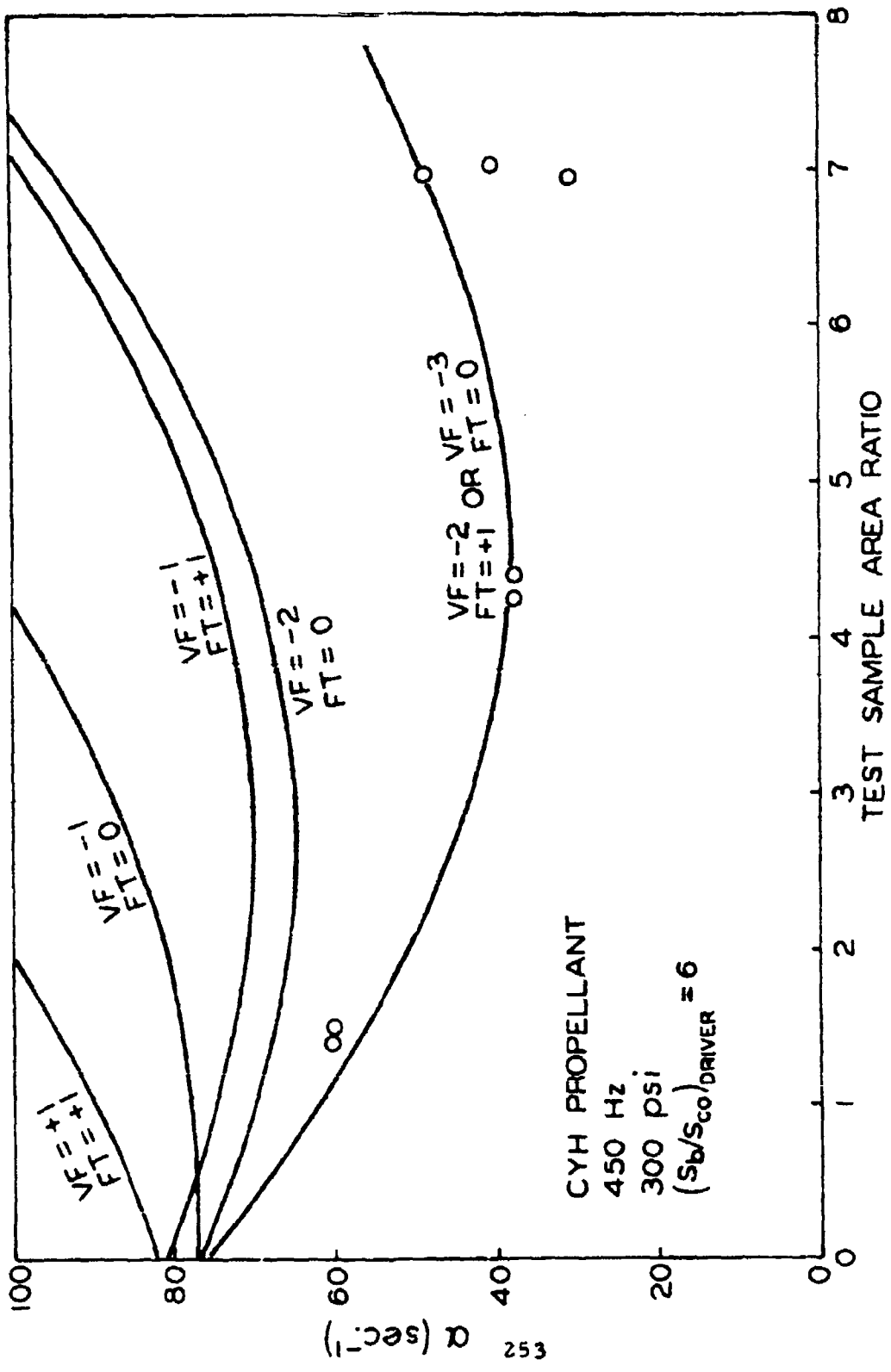


Figure C-4 Comparison of Test Data for the Vent with Calculations Using Several Combinations of VF and FT

burner. This was done from the least-squares, best-fit slopes for the  $\alpha$  versus  $S_b/S_{CO}$  data plots. The computed response functions are tabulated in Table G-1. It is apparent that the use of a vent loss term yields more consistent response function values from the two different burner configurations.

TABLE G-1. Experimental Values of the Response Function

<u>Theory</u>	$R_b$	
	<u>A-17</u>	<u>A-18</u>
Three-dimensional		
T-burner	1.6	2.1
Quarter-wave burner	1.5	2.9
One-Dimensional		
T-burner	-0.4	0.1
Quarter-wave burner	1.5	2.9

Finally, data have been taken in the T-burner shown in Figure G-3(a), in which the position of the test sample was varied. In reducing the data, it was assumed that the mode shape was a simple cosine. Then the incremental growth constant caused by the additional propellant samples was determined by using the appropriately simplified form of Eq. (G. 14).

Figure G-5 shows the data from these tests plotted as  $\alpha - \alpha_0$  versus  $Z/L$ , where  $Z$  represents the average distance of the variable position samples from the ends of the burner and  $L$  is the burner length.  $\alpha$  is the growth rate with samples present only in the extreme ends of the burner.

The least-squares best-fit values of  $R_b$  for the data are listed in Table G-2. The combination of  $R_b = 2.64$ ,  $VF = -2$  and  $FT = +1$  resulted in an amazingly good correlation of the data, substantially better than the other combinations that were tried and better than could be expected from the precision of the data. As with the other data, these values for  $VF$  and  $FT$  indicate a large magnitude of mean flow damping and also a flow-turning loss.

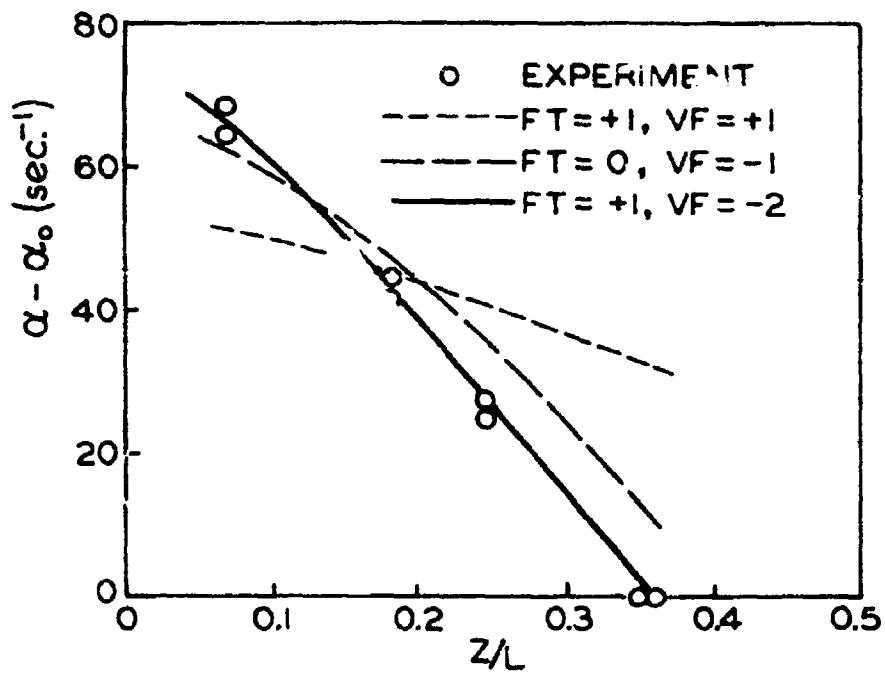


Figure C-5 Comparison of Experimental Results and Calculations for a Smokeless Propellant Tested in the T-Burner Shown in Figure C-3(b)

TABLE G-2. Statistical Comparison of Theory and Data\*

FT	Theory	VF	Best $R_b$	$\Sigma(\alpha - \alpha_i)^2$
0		-1	2.46	831 sec <sup>-1</sup>
+1		+1	.02	3201 sec <sup>-1</sup>
+1		-2	2.64	25 sec <sup>-1</sup>

\*  $\Sigma(\alpha - \alpha_i)^2$  is the sum of the squares of the deviations between the best-fit theoretical line and the individual data points.

Part of the theoretical description of the vent involves the question of whether or not there is a "convection" of acoustic energy out of the vent of a T-burner. In a brief study (ref. G-12) of this problem, high-speed motion pictures were taken of the flow exhausting through a hole cut at the center of a T-burner. The flow exhausted directly to the atmosphere, and there was no vent pipe attached to the burner. When oscillatory combustion began, the exhaust was perpendicular to the T-burner. Later, oscillations began to grow, and the exhaust began to vibrate. As the oscillations grew to large amplitude, so also did the vibrations in the exhaust. Ultimately the vibrations, whose frequency matched that inside the burner, became quite violent. These visual observations suggest that, at least for the geometry used, the oscillatory motion parallel to the burner is indeed communicated to the exhaust flow.

One interpretation is that the acoustic energy is convected from the burner even though the acoustic and mean flow vectors are perpendicular. Such a convective loss cannot be formally described by Eq. (G. 7), but the following intuitive approach to its use is proposed. First, note that a loss term of the magnitude  $4fMb S_b/S_c$  results formally if the mean flow and acoustic flow vectors are parallel at the vent. Physically, this means that all of the local acoustic kinetic energy is convected from the chamber by the exiting gases. It is suggested that in a T-burner, all of the local acoustic kinetic energy is carried from the burner into the vent pipe. Thus, even though the vectors are perpendicular, there is a loss term whose magnitude is  $4fMb S_b/S_c$ . The result is that one artificially treats the flow problem as if the two velocities are parallel and the term

Eq. (C. 7) is retained in the analysis of the T-burner and treated as being

$$\frac{\rho a^2 \hat{u}^2}{\rho a^2 \hat{u}^2}$$

rather than

$$\frac{\rho a^2 (\vec{u} \cdot \hat{u}) \hat{u}}{\rho a^2 (\vec{u} \cdot \hat{u}) \hat{u}}$$

### C. 3 Summary

Taken as a whole, the results seem to support the conclusion that both a flow-turning and vent-loss term ought to be used in the analysis of T-burner data. However, for various reasons, this is only a tentative conclusion. One reason is that the experimental work is incomplete, and is continuing. Another is that many of the tests were carried out at atmospheric pressure where conditions are far removed from those encountered at the higher pressures used in motors. Lastly, many of the results were obtained in burners and geometries which have seen very limited use. It is possible that these systems may not behave as one would expect based on experience with other T-burners. The best procedure to follow for interpreting experimental results is to allow the coefficients VF and FT to vary, and determine those values producing best correlation of the data.

## REFERENCES

- G-1 Candel, S. M. "Analytical Studies of Some Acoustic Problems of Jet Engines" (Appendix 5-B), Ph. D. Thesis, California Institute of Technology, Pasadena, Calif. (November 1971).
- G-2 Hart, R. W. and Cantrell, R. H. "Acoustic Radiation from Pressure - Antisymmetric Modes of a Centrally Vented Cylindrical Cavity," J. Acoust. Soc. Amer., V. 35, no. 1 (January 1963), pp. 18-24.
- G-3 Hart, R. W. and McClure, F. T. "Theory of Acoustic Instability in Solid-Propellant Rocket Combustion," Tenth Symposium (International) on Combustion,
- G-4 Culick, F. E. C. "Interaction Between the Flow Field, Combustion, and Wave Motions in a Rocket Motor," NWC TP 5344, Naval Weapons Center, China Lake, Calif. (June 1972).
- G-5 Culick, F. E. C. "The Stability of One-Dimensional Motions in a Rocket Motor," Combustion Science and Technology, V. 7, no. 4 (1973), pp. 165-175.
- G-6 Coates, R. L. and Horton, M. D. "Further Consideration on the Interaction of Sound and Flow in Rocket Motors and T-Burners," to be published in Combustion Science and Technology (1974).
- G-7 Horton, M. D. and Coates, R. L. "T-burner Experiments Compared with Theory," J. Spacecraft and Rockets, V. 11, no. 1 (Jan. 1974), pp. 48-51.
- G-8 "Velocity Coupling Analysis," Technical Report AFRPL-TR-72-12 (January 1972), Hercules, Inc., Magna, Utah.
- G-9 Beckstead, M. W., Bennion, D. U., Butcher, A. G., and Peterson, N. L. "Variable Area T-Burner Investigation," Technical Report AFRPL-TR-72-85 (December 1972), Hercules, Inc., Magna, Utah.
- G-10 Beckstead, M. W., Peterson, N. L., Butcher, A. G., and Horton, M. D. "A Technique for Evaluating Velocity Coupled Combustion Instability," 10th JANNAF Combustion Meeting (August 1973).
- G-11 Beckstead, M. W., Butcher, A. G., and Peterson, N. L. "A Study of Velocity Coupling in Solid Propellant Combustion Instability," AFRPL-TR-73-73 (September 1973), Hercules, Inc., Magna, Utah.